Investigation of miR-652 in Host Immunity Against Intracellular Bacterial Pathogens

by Maxwell T. Stevens

Thesis submitted in fulfilment of the requirements for the degree of

Doctor of Philosophy

under the supervision of Associate Professor Bernadette Saunders and Dr Matthew Padula

University of Technology Sydney
Faculty of Science

July 2022

CERTIFICATE OF ORIGINAL AUTHORSHIP

I, Maxwell Stevens, declare that this thesis is submitted in fulfilment of the requirements for the award of Doctor of Philosophy, in the Faculty of Science at the University of Technology Sydney.

This thesis is wholly my own work unless otherwise referenced or acknowledged. In addition, I certify that all information sources and literature used are indicated in the thesis. This document has not been submitted for qualifications at any other academic institution. This research is supported by the Australian Government Research Training Program.

Signature:

Production Note:
Signature removed prior to publication.

Date: 30 July 2022

Acknowledgments

The last 4 years have been an endurance event, and there are many people who I need to thank for helping me through.

Firstly, I would like to acknowledge and thank my supervisor Associate Professor Bernadette Saunders and my co-supervisor Dr Matthew Padula. Your support and guidance throughout my PhD have instilled me with the ethical and scientific base I needed to really delve into my study, continually learning and developing as a research scientist. You provided sound advice when I needed it most, but also gave me the reigns to drive my project and make the most of this opportunity. Also, thank you to Dr Nilesh Bokil for the technical introduction to kick off the whole project.

A big thank you to everyone who has been a part of the Saunders lab with me, with special thanks to Dr Jessica Pedersen and Giang Le. Your physical assistance and effervescent characters were the essential ingredients to get through arduous days in the PC3, toiling for hours through flow cytometry data, or carefully deciphering my most perplexing results. So much of this work would not have been accomplished without you all.

Thank you to Professor Warwick Britton and all the members of the mycobacteria group at the Centenary Institute. The technical expertise you've all shared has been amazing, and the opportunity to regularly present my work to you all has been invaluable. Presentation opportunities have been few and far between these 2 years, and I am very grateful. Your fresh perspectives and weekly discussion fostered my scientific thinking, which really made this thesis what it has finally become.

My parents, family, and friends have been a constant, not just through my PhD, but through all my work and education. Thank you so much for all your encouragement and support. To Matthew Hamlyn, thank you for your constant positivity, it is a very welcome light when things feel rough. To Dr Marley Pulbrook, thanks for your wit, humour, and encouragement as we've both been slogging through what feels like endless study.

And most importantly, thank you to my wife Emily. These years have been hard and I could not have done it without you. There were many months where you were literally the only person I saw, which is lucky because you are the best support I could wish for. Your love, friendship, and encouragement have kept me sane through long nights in the lab and prolonged weeks writing. Thank you so, so much; I love you!

Thesis format

This is a thesis by compilation, consisting of two published peer-reviewed papers, two results chapters, and a general discussion chapter.

Publications associated with this thesis

Stevens, M. T., B. D. Nagaria, W. J. Britton, and B. M. Saunders. 2021. Macrophages of different tissue origin exhibit distinct inflammatory responses to mycobacterial infection. *Immunol. Cell Biol.* 99: 1085-1092.

Stevens, M. T., and B. M. Saunders. 2021. Targets and regulation of microRNA-652-3p in homoeostasis and disease. *J. Mol. Med.* 99: 755-769.

Table of Contents

List of figures

Chapter 5

Appendices xvi

List of tables

Abbreviations

3'UTR	3' untranslated region
ADC	Albumin dextrose catalase
ANOVA	Analysis of variance
BMDM	Bone marrow-derived macrophage
BSA	Bovine serum albumin
CBA	Cytometric bead array
cDNA	Complementary deoxyribonucleic acid
CFU	Colony forming unit
cGAMP	Cyclic GMP-AMP
CNS	Central nervous system
CVD	Cardiovascular disease
DC	Dendritic cell
DNA	Deoxyribonucleic acid
dsDNA	Double stranded deoxyribonucleic acid
DTT	Dithiothreitol
EDTA	Ethylenediaminetetraacetic acid
ET	Ethical threshold
FBS	Foetal bovine serum
LB	Lysogeny broth
LPS	Lipopolysaccharide
MDR TB	Multidrug-resistant
miRNA	microRNA
MLN	Mediastinal lymph node
MOI	Multiplicity of infection
NK cell	Natural killer cell
NP	Nanoparticle
OADC	Oleic acid albumin dextrose catalase
PAMP	Pathogen-associated molecular pattern

PBMC	Peripheral blood mononuclear cell
PBS	Phosphate buffered saline
PC3	Physical containment level 3
PEG	Polyethylene glycol
PEI	Polyethylenimine
Pre-miR	Pre-microRNA
Pri-miR	Primary microRNA
RISC	RNA-induced silencing complex
RNA	Ribonucleic acid
ROC curve	Receiver operating characteristic curve
RT-qPCR	Real time quantitative polymerase chain reaction
SD	Standard deviation
SDS-PAGE	Sodium dodecyl sulphate polyacrylamide gel electrophoresis
SEM	Standard error of the mean
siRNA	Small interfering ribonucleic acid
SNP	Single nucleotide polymorphism
TBST	Tris-buffered saline Tween 20
TCA cycle	Tricarboxylic acid cycle
TCEP	Tris(2-carboxyethyl)phosphine
TFA	Trifluoroacetic acid
TLR	Toll-like receptor
TP	Time point

Abstract

Tuberculosis (TB) is an infectious respiratory disease caused by the bacterial pathogen *Mycobacterium tuberculosis*. Each year, 1.5 million deaths are attributable to TB and survivors are prone to increased all-cause mortality, due to excessive TB-associated pulmonary inflammation. Recent literature indicated the microRNA hsa-miR-652-3p (miR-652) was downregulated in plasma of Chinese TB patients, and further decreased in patients who failed to clear the bacteria after antibiotic therapy. This thesis investigated the activities of miR-652 during *in vitro* and *in vivo* infections with intracellular bacterial pathogens, with a special focus on the macrophage response to infection.

My initial study aimed to characterise the phenotypic differences between murine alveolar (AMJ2-C11) and peritoneal (IC-21) macrophage cell lines during *in vitro* mycobacterial infections, in order to illustrate the influence of tissue origin on macrophage function. Both cell lines were able to control *M. bovis* BCG and *M. tuberculosis* H37Rv bacterial loads. However, AMJ2-C11 cells exhibited a more inflammatory phenotype, with significantly increased cytokine release and nitric oxide generation. Additionally, expression of inflammatory cell surface markers was increased on AMJ2-C11 cells relative to IC-21 cells. These data suggest that whilst tissue origin can influence macrophage phenotype, cell plasticity ensures diverse macrophages can respond to invading pathogens.

Chapter 4 investigated the impact of miR-652 on the murine immune response to *M. tuberculosis.* Bone marrow macrophages from miR-652$^{-/-}$ C57BL/6 mice were able to control bacterial growth over 6 days *in vitro*, though IL-6, TNF, MIP-1α, and KC expression was significantly lower than in their wild type counterparts. Western blot results indicated AKT and mTOR activation was attenuated in miR-652$^{-/-}$ macrophages. miR-652$^{-/-}$ mice infected aerogenically with *M. tuberculosis* were able to control the bacterial load in the lungs and spleen equal to wild type mice over 13 weeks. Leukocyte populations were comparable between mouse strains, however, early CD8$^+$ effector T cell numbers were elevated in the lung and lymph node miR-652$^{-/-}$ mice, suggesting miR-652 may have some impact on T cell differentiation during bacterial infection.

Chapter 5 investigated this question in a CD8$^+$ T cell-focused infection model; intraperitoneal *Listeria monocytogenes* infection. miR-652$^{-/-}$ mice were highly susceptible to a low-dose infection of 2000 CFU/mouse, exhibiting significantly increased weight loss and high morbidity. The early onset of morbidity indicated a deficiency in the innate immune response. Highly necrotic liver lesions in miR-652$^{-/-}$ mice displayed intense recruitment of neutrophils and macrophages, but bacterial load was uncontrolled in these mice. To investigate the antimicrobial phenotype of miR-652$^{-/-}$ macrophages, primary peritoneal macrophages were infected with *L. monocytogenes in vitro*. A proteomic analysis highlighted dysregulation of key immune pathways, including the lysosome pathway and the pentose phosphate pathway. Also downregulated was the *in silico*-predicted miR-652 target CAPZB. Transfection experiments using luciferase reporter constructs indicated miR-652 does not target a predicted sequence in the CAPZB 3'UTR. Further, CAPZB mRNA and protein were unaffected by transfection with a miR-652 mimic in IC-21 mouse peritoneal macrophage cells, indicating CAPZB expression is unaffected by miR-652.

This thesis demonstrates miR-652 plays clear roles in the proper innate immune response to acute infection with an intracellular bacterial pathogen. The pathways impacted in miR-652$^{-/-}$ macrophages position miR-652 as an important regulator of immune function, potentially regulating inflammation and cell metabolism. Host-directed therapies possess amazing potential as a complement to existing antimicrobial drugs. microRNA-based therapeutics for infectious diseases are progressing well through clinical trials. Analysis of the genes validated as targets for miR-652 underscores the promise for a miR-652 mimic as a therapeutic in chronic TB, particular when administered with a cell-targeted delivery mechanism. Additional holistic research is needed to evaluate the impacts of miR-652 in macrophages to realise the potential of miR-652 as a therapeutic miRNA.

CHAPTER 1

Targets and regulation of microRNA-652-3p in homeostasis and disease

Chapter 1. Targets and regulation of microRNA-652-3p in homeostasis and disease

1.1.   Preamble to Chapter 1

MicroRNAs (miRNA) are short non-coding RNA which modulate gene translation in mammalian cells. The list of cellular pathways and processes regulated by miRNA is extensive, from cell fate determination and embryonic development, to cell apoptosis and many disease states (1, 2). miRNA regulatory networks continue to grow as new miRNA are discovered and further miRNA targets are validated.

As part of the canonical miRNA biogenesis pathway, long single-stranded primary-miRNA (pri-miR) are transcribed by RNA polymerase II (3). Pri-miRs, often containing multiple miRNAs, are cleaved into pre-miRNA (pre-miR) stem-loops by Drosha and are exported to the cytoplasm by Exportin-5 (4, 5). Alternatively, miRNA located within the introns of translated genes can be processed to pre-miRs by the spliceosome before exportation (6). Cytoplasmic pre-miR stem-loops are further processed by the RNase enzyme Dicer to give a double stranded RNA molecule (7). The strands are denominated 5p and 3p based on their position in the pre-miR stem loop, and both strands can possess gene silencing activity (8). The double stranded miRNA is incorporated with an Argonaute protein to form the RNA-induced silencing complex (RISC), where one strand is degraded (9), and the remaining guide strand binds its target mRNA through binding of miRNA nucleotides 2-7 (10). RISC typically inhibits translation of the target mRNA and promotes its decay (11). However, in some contexts gene translation is enhanced by miRNA binding (12).

Individual miRNAs can each target and regulate multiple mRNA, creating dense networks of interacting genes and miRNA. The diversity of disease-related genes in these networks prompts investigation into the use of miRNA as biomarkers and therapeutic targets. miRNA-based biomarker panels are already available for diagnosis of osteoporosis, cardiovascular disease, and several cancers (13). Whilst no miRNA therapeutic has yet received FDA approval, several are in phase 1 and 2 clinical trials for both infectious and non-infectious diseases (1, 13). Phase 1 trials for mir-17 inhibitor

RGLS4326 in polycystic kidney syndrome are completed (14), and phase 2 trials for mir-16 replacement therapy Mesomir/TargomiRs in late-stage mesothelioma are ongoing (13, 15). Multiple molecules antagonising mir-122 to treat chronic hepatitis C infection have entered or completed phase 2 trials (16, 17). miR-122 is known to bind and stabilise the hepatitis RNA genome (18). A recent *in silico* analysis has suggested that miR-122 could bind and stabilise the genome of SARS-CoV-2 by a similar mechanism (19). Further research into miRNA regulated cell pathways could present novel opportunities for miRNA-targeted therapeutics, particularly in the field of infectious disease.

The object of this thesis is to describe cellular pathways and activities associated with the mammalian miRNA miR-652-3p. Dysregulation of this miRNA was recently associated with tuberculosis (TB) disease and poor response to treatment (20). There are persistent issues with TB diagnosis and treatment, leading to over one million TB-related deaths each year (21), with an unequal proportion occurring in lower income countries (22). TB is caused by infection with the bacterium *Mycobacterium tuberculosis*, an evasive pathogen which can survive and replicate within host cells, subverting many host defence mechanisms.

Antibiotic regimes are effective at treating the majority of TB cases, however, the 3-6 month duration of the necessary antibiotic course can lead to poor adherence and relapsing infections (23). Because of this, the development of antibiotic resistance is a growing concern. For example, the incidence of multi-drug resistant (MDR) TB in Papua New Guinea ranges from 2-20% of new TB cases, depending on geographic location (24, 25), and in several eastern European countries as many as 30% of TB cases are estimated to be MDR (26).

Pulmonary TB induces severe inflammation to accumulate in the lungs, and can permanently impair lung function (27). Patients successfully treated for TB continue to have increased mortality (28). Development of adjunct therapies to control inflammation during TB antibiotic treatment is of real importance, and the modulation of miRNA pathways presents an intriguing opportunity.

The growing threat of drug-resistant TB highlights the need for novel diagnostics and treatments, both antimicrobial and anti-inflammatory. Investigation of TB-associated miRNA like miR-652 could uncover anti-TB treatments, or conjunctive therapies to control TB-associated inflammation. My investigations utilised two intracellular pathogens, *M. tuberculosis* and *Listeria monocytogenes*, to investigate the relationship between miR-652 dysregulation and intracellular bacterial infection. Identifying these relationships and categorizing potential miR-652 target genes in inflammatory antibacterial pathways will guide future research into miR-652 as a diagnostic or treatment.

The aims of this study are:

(i) To investigate the relationship between macrophage tissue origin and the response to mycobacterial infection.

(ii) To identify the impacts of miR-652 expression during *in vitro* and *in vivo* *Mycobacterium tuberculosis* infection.

(iii) To characterise the impacts of miR-652 during *Listeria monocytogenes* infection in mice and mouse macrophages.

The hypotheses of the study are:

(i) The alveolar macrophage cell line AMJ2-C11 will exhibit a more proinflammatory response to mycobacterial infection, compared to the peritoneal macrophage cell line IC-21.

(ii) Absent miR-652 expression in mouse macrophages will hinder their inflammatory response to *M. tuberculosis*, and prevent control of bacterial growth.

(iii) The inflammatory immune response to *in vivo* aerosol *M. tuberculosis* infection will be diminished in miR-652-deficient mice.

(iv) The absence of miR-652 expression will inhibit proinflammatory pathways and make mice vulnerable to *Listeria monocytogenes* infection.

1.2. Chapter 1 – Declaration

I declare that the below publication meets the requirements for inclusion as a chapter in this thesis.

- I have contributed more than 50% of work for the publication below. I performed the literature search, complied all relevant data, and performed all described sequence alignments. I wrote the complete draft of manuscript and prepared all figures. BS edited and approved the manuscript.
- The below publication has been peer reviewed.
- Permission is not required by the publisher for inclusion of this publication in this thesis for non-commercial purposes.

Stevens, M. T., and B. M. Saunders. 2021. Targets and regulation of microRNA-652-3p in homoeostasis and disease. *Journal of Molecular Medicine.* 99: 755-769.

Publication status: published.

The published version of the manuscript can be found in Appendix 1.

Signature: Production Note:
               Signature removed prior to publication.

Date: 30 July 2022

1.3.   Abstract

microRNA are small non-coding RNA molecules which inhibit gene expression by binding mRNA, preventing its translation. As important regulators of gene expression, there is increasing interest in microRNAs as potential diagnostic biomarkers and therapeutic targets. Studies investigating the role of one of the miRNA – miR-652-3p – detail diverse roles for this miRNA in normal cell homeostasis and disease states, including cancers, cardiovascular disease, mental health, and central nervous system diseases. Here we review recent literature surrounding miR-652-3p, discussing its known target genes and their relevance to disease progression. These studies demonstrate that miR-652-3p targets *LLGL1* and *ZEB1* to modulate cell polarity mechanisms, with impacts on cancer metastasis and asymmetric cell division. Inhibition of the NOTCH ligand *JAG1* by miR-652-3p can have diverse effects on angiogenesis and immune cell regulation. Investigation of miR-652-3p and other dysregulated miRNAs identified a number of pathways potentially regulated by miR-652-3p. This review demonstrates that miR-652-3p has great promise as a diagnostic or therapeutic target due to its activity across multiple cellular systems.

Key Words: miR-652, cancer, cardiovascular disease, Notch signalling, mental health

1.4.   Introduction

microRNAs (miRNA) are short 20-24 nucleotide non-coding RNA molecules which modulate gene expression. In the 27 years since the biomodulatory function of miRNA was first described in *C. elegans* (29), miRNA have been identified as a key element in eukaryotic cell regulation (30, 31). Diverse networks of activity are being characterised for many miRNAs, including miR-652-3p, already known to modulate cell differentiation, proliferation, polarity, and apoptosis pathways (32-35).

In this review, we focus on miR-652-3p in cardiovascular disease, cancer, and other diseases. We describe the utilisation of miR-652-3p in biomarker panels, and we detail the validated gene targets of miR-652-3p and their conservation in humans and mice.

Ever developing knowledge in the field has made miRNA very interesting candidates for use as therapeutics and diagnostic tools. miRNA-based biomarker panels are already

available for diagnosis of osteoporosis, cardiovascular disease, and several cancers (13). Whilst no miRNA therapeutic has yet received FDA approval, several are in phase 1 and 2 clinical trials for both infectious and non-infectious diseases (1, 13). As the literature surrounding miR-652-3p and its target genes continues to expand, its diverse cellular activities provide great potential as a diagnostic or therapeutic target.

1.5. Characteristics of miR-652

Human gene *MIR652* is located on the X chromosome, within an intron of *TMEM164*, encoding transmembrane protein 164 (36, 37). As yet no publications have provided evidence that *TMEM164* is translated in humans. *MIR652* expression is controlled under the *TMEM164* promoter (38), and the pre-miR hsa-miR-652 may be generated by the spliceosome (6). A second miRNA encoding gene *MIR3978* is also located on a *TMEM164* intron (39). The encoded miRNA, miR-3978, has been associated with peritoneal gastric cancer metastasis (40), but has not been linked with miR-652-3p.

Expression of miR-652-3p is highest in human myeloid-lineage leukocytes, including circulating monocytes, neutrophils, and eosinophils (41-43). Deep sequencing data from the FANTOM5 project suggests comparatively low expression of the pre-miR hsa-miR-652 in human lymphocytes (38), though the mouse homologue mmu-miR-652-3p has been shown to affect the differentiation of CD4$^+$ T cells (44). Mature miR-652-3p is also expressed in human epithelial cells and dysregulation of miR-652 in epithelial cells has been associated with several cancers (35, 45, 46). Extracellular miR-652-3p has been identified in circulating exosomes (47, 48), and numerous studies have quantitated miR-652-3p from human serum and plasma (20, 49-54).

Dysregulated expression of the passenger strand miR-652-5p has been associated with diabetes and gastrointestinal cancers, and with a model of ischaemia (55-59). However, deep sequencing data indicates expression of miR-652-5p is much lower than miR-652-3p (38), suggesting miR-652-3p is preferentially bound to Argonaute proteins during biogenesis (60).

Numerous studies are reporting an association or role of miR-652-3p in cardiovascular disease, cancers, mental health and the central nervous system (CNS), and immune regulation. The association of miR-652-3p with these diseases and known targets of miR-652-3p are reviewed here.

1.6.   miR-652-3p in cardiovascular disease

Cardiovascular disease (CVD) is the leading cause of death globally, responsible for 17.8 million deaths in 2017 (61). miR-652-3p has been implicated in multiple studies of CVD with roles in pathways including atherosclerosis, and myocardial infarction.

Numerous studies have analysed the association of circulating miR-652-3p with CVD, focusing on heart failure. An early study found miR-652-3p upregulated in the plasma of 200 acute coronary syndrome patients (62). When analysed in combination with existing prognostic markers NT-proBP and LVEF, low miR-652-3p concentration at initial admission was strongly predictive of readmission for heart failure. Ovchinnikova et al. found miR-652-3p expression was significantly downregulated in plasma of heart failure patients (63). Expression was negatively correlated with heart failure severity and low miR-652-3p concentration was predictive of poor 180-day survival. A follow-up study found miR-652-3p downregulated in heart failure patients, though not significantly (64). Further, this study noted a correlation between lower miR-652-3p expression and increased incidence of atherosclerotic lesions (64). With this evidence suggesting a role for miR-652-3p in human heart failure, studies were conducted in a rat hypertension model and a mouse ischaemic heart failure model (65). In the rodent models, hypertension and heart failure did not induce significant changes in expression of the miRNAs previously reported to be differentially expressed in humans.

Recent studies have also suggested miR-652-3p as a biomarker of acute kidney injury in heart failure patients. Upregulated miR-652-3p, in conjunction with increased neutrophil gelatinase-associated lipocalin (NGAL), in both serum and urine of patients with heart failure was predictive of acute kidney injury onset (66). Though, this finding was not seen in a separate study that did not find any correlation between miR-652-3p and NGAL (49). These differences may be due to the population sampled, methods used to measure miRNA levels or other, as yet unidentified factors.

It has been suggested that miR-652-3p may play a role in regulating coagulation (48). Low miR-652-3p expression in plasma was found to correlate with low platelet count in venous thromboembolism patients (67). Low platelet count has been associated with an increased risk of recurrent embolisms (67, 68). Additionally, low plasma miR-652-3p was associated with increased risk of adverse cardiac and cerebral events in end-stage kidney disease patients, suggesting an increased risk of thrombotic events (69).

Research is ongoing to investigate the involvement of miR-652 in CVD. The most prominent CVD is atherosclerosis, a narrowing of blood vessels caused by a build-up of lipid plaque in the endothelium (70). Early plaque generation is driven by phagocytosis of low-density lipoproteins by macrophages in the subendothelial space (71). These macrophages promote atherosclerotic lesion formation through secretion of IL-1α (72). Huang et al. observed miR-652-3p was upregulated in atherosclerotic plaque of both humans and mice (73). miR-652-3p was found to target Cyclin D2 (*CCND2*) in human umbilical vein endothelial cells, inhibiting endothelial cell proliferation and enhancing atherosclerotic lesion formation. Cyclin family proteins are cell cycle regulators, and Cyclin D2 was shown to promote cardiac muscle repair in a mouse myocardial infarction model (74). *In vivo* administration of an anti-miR-652-3p antagomir in mice decreased aortic lesion area, suggesting miR-652-3p inhibition as a therapeutic in atherosclerotic disease (73). A further study from the same group found miR-652-3p upregulation was associated with dyslipidaemia (75). Dyslipidaemia predisposes patients to atherosclerosis by lowering nitric oxide (NO) generation from endothelial cells (76). The transcription factor, insulin gene enhancer protein (ISL1) increases NO production and stimulates vasodilation (77, 78). miR-652-3p is overexpressed under hyperlipidaemic conditions and targets ISL1, decreasing NO production (75). Administration of simvastatin, commonly given to treat dyslipidaemia, led to decreased miR-652-3p expression and rescued NO levels in hyperlipidaemic mice (75).

In vivo inhibition of miR-652-3p also limited cardiomyocyte hypertrophy and apoptosis in a mouse myocardial infarction model (79). Hypertrophic cardiomyocytes upregulated miR-652-3p, inhibiting expression of NOTCH ligand JAG1 (Figure 1.1). Administration of a miR-652- 3p inhibitor in mice with cardiac hypertrophy resulted in increased cardiac

angiogenesis, with no obvious organ toxicity (79). Notch signalling plays diverse roles in cardiac development and repair, but it is also influential in the immune response (80-82). *In vitro* Jag1-mediated Notch signalling was found to inhibit apoptosis of rat cardiomyocytes, and promote their proliferation (83). Furthermore, *Mycobacterium bovis* BCG infection of mouse macrophages increased Notch signalling and inhibited macrophage apoptosis (84). Additional research investigating the role of miR-652-3p in regulating the NOTCH pathway will be required to elucidate these mechanisms.

In an *in vitro* myocardial infarction model using primary mouse cardiomyocytes, downregulation of miR-652-3p allowed increased expression of MTP18, a controller of mitochondrial fission and apoptosis (33, 85). This study determined miR-652-3p activity was regulated by the circular-RNA MFACR, which contains numerous miR-652-3p binding sites and acted as a miR-652-3p sponge. This circular-RNA has not been further investigated and as will be discussed later in this review, it is not clear whether miR-652-3p target sites are present in human *MTP18* mRNA transcripts. Together these studies indicate that miR-652-3p may have multiple roles to play in regulating CVD and further research in this area is warranted.
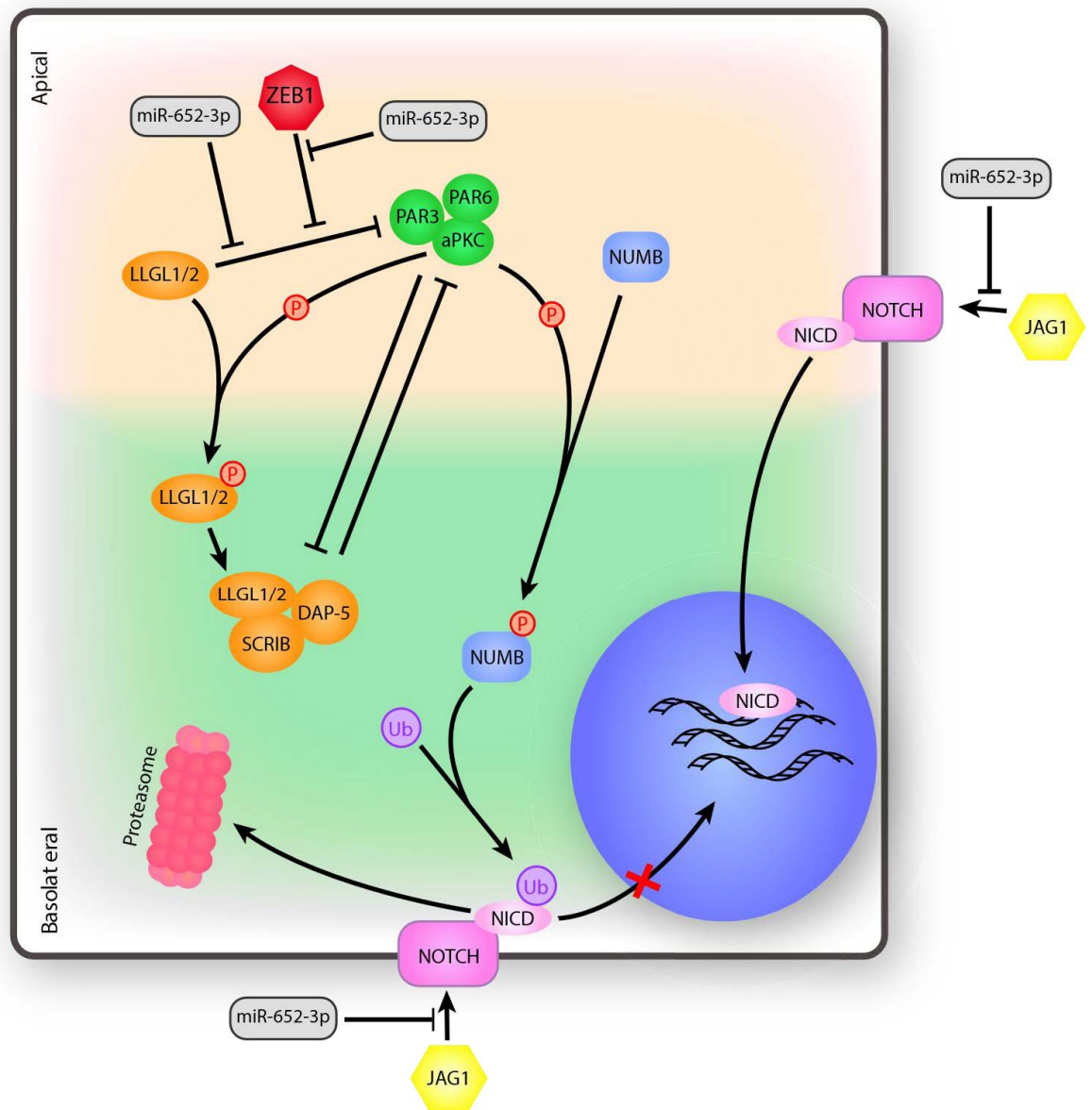
Figure 1.1. Regulation of cell polarity and Notch signalling by miR-652-3p. Organisation of cytoplasmic components in epithelial cells and mitotic cells is regulated by the co-inhibitory activity of the PAR complex (composed of PAR3, PAR6, and aPKC) and the Scribble complex (composed of Scribble (SCRIB), DAP-5, and LLGL1 or LLGL2). LLGL1/2 competes with PAR3 to bind aPKC in the apical zone. PAR3 binds and activates aPKC, initiating phosphorylation of LLGL1/2, deactivating LLGL1/2 and transporting it to the basolateral zone. Phosphorylated LLGL1/2 is reactivated and binds the scribble complex in the basolateral zone. ZEB1 prevents the expression of LLGL2, interfering with the regulation of the PAR complex. NOTCH-ligand JAG1 activates NOTCH, causing cleavage of the Notch intracellular domain (NICD) which translocates to the nucleus and activates transcription factors. NUMB inhibits Notch signalling by ubiquitinating NICD, directing it to the proteasome for degradation. During asymmetric cell division, active aPKC phosphorylates NUMB in the apical zone, driving transport of NUMB to basolateral zone. Asymmetric distribution of NUMB during mitosis influences daughter cell phenotype. miR-652-3p inhibits the activity of both ZEB1 and LLGL1, which can either promote or inhibit cell polarity and differentiation of dividing cells depending on cell type, tissue location, and disease. miR-652-3p also inhibits expression of JAG1, controlling Notch signalling activity.

1.7.   miR-652-3p in cancer

Given the wide range of critical cellular pathways controlled by miRNA, it is unsurprising that many miRNAs, including miR-652-3p, are dysregulated in cancer (Figure 1.2). For example, the miR-34 family is known to downregulate more than 30 oncogenes, and downregulation of miR-34 is associated with multiple cancer subtypes (86, 87). This very broad influence makes miR-34 a prime target for drug development, though unfortunately no miR-34-based therapeutics have passed clinical trials to date (13). Cancer is the most studied disease context of hsa-miR-652-3p expression, with miR-652-3p reported to possess both protective and oncogenic roles in different cancer types. These seemingly contradictory activities may be due to the types of tumours, the gene(s) targeted by miR-652-3p, or other as yet undetermined factors. The validation of numerous miR-652-3p target genes in different cancer settings illustrates the regulatory function miR-652-3p plays in key cell processes (34, 35, 45, 46, 88, 89).

1.7.1   Lung cancer

A four-miRNA diagnostic biomarker panel containing miR-652-3p was identified by Andersen et al., differentiating malignant pleural mesothelioma tumour tissue from non-neoplastic tissue (90). The biomarker classifier analysed the downregulation of miR-126-3p, miR-143-3p, miR-145-5p, and miR-652-3p in tumour tissue, categorising tissue samples with an accuracy of 94% (90). Another study found miR-652-3p was similarly downregulated in squamous cell lung carcinoma tumour tissue (91). Conversely, two other studies found miR-652-3p expression was upregulated in non-small cell lung cancer patient serum and tumour tissue, respectively (35, 54). These expression differences may be influenced by differences in the study size, subject ethnicity or the host response to different lung cancer subtypes. One major issue with measuring miRNA expression is data normalisation. These studies each used different housekeeper RNA to normalise qRT-PCR data, which can lead to conflicting results. A study analysing plasma miRNA of Chinese and Australian tuberculosis patients found the expression of several commonly used housekeeper miRNAs varied significantly between geographical cohorts (92). Further studies are needed to determine an appropriate housekeeper in these lung cancers.

A 3-marker panel analysing increased serum expression of mir-660-5p, miR-652-3p, and a known lung-cancer biomarker protein Cyfra21-1 was developed for diagnosis of non-small cell lung cancer (54). A receiver operating characteristic (ROC) curve for this panel had an area under the curve of 0.94 for distinguishing non-small cell lung cancer patients from controls.

The potential that miR-652-3p possesses as a biomarker in a number of cancers suggests this miR is important in cancer biology. How miR-652-3p influences cancer development is now starting to be elucidated.

miR-652-3p was found to be upregulated in tumour tissue of non-small cell lung cancer patients, and promoted tumour metastasis by targeting Lethal(2) giant larvae protein homologue 1 (*LLGL1*) (35). LLGL1 is considered a tumour suppressor, largely because its activity in cell polarity maintenance prevents metastasis of cancerous epithelial cells (Figure 1.1) (93). Upregulation of miR-652-3p in lung tumour cells, and the subsequent inhibition of LLGL1 expression led to an epithelial-to-mesenchymal transition in tumour cells, promoting cell migration and invasion (35). Interestingly, downregulation of miR-652-3p in pancreatic cancer lines was also found to promote cancer cell proliferation and invasion. In this case miR-652-3p acted by targeting the tumour promoting expression of transcription factor zinc finger E-box-binding homeobox 1 (*ZEB1)* (45). Increased ZEB1 expression promotes epithelial-to-mesenchymal transition and cell migration by inhibiting translation of *LLGL2*, which performs a similar function to *LLGL1* in many cell types (94-96). These studies, indicate that *LLGL1* and *ZEB1* targeting by miR-652 can both promote or inhibit cell polarity maintenance. These differences may depend on cell type, tissue location, or disease state and clearly this subject requires further research.

Cell polarity maintained by LLGL activity also influences the polar distribution of NOTCH regulator protein NUMB during cell division (Figure 1.1), controlling Notch signalling in daughter cells (97). Considering it also targets a NOTCH ligand, JAG1, miR-652-3p may be an influential regulator of the Notch signalling pathway.
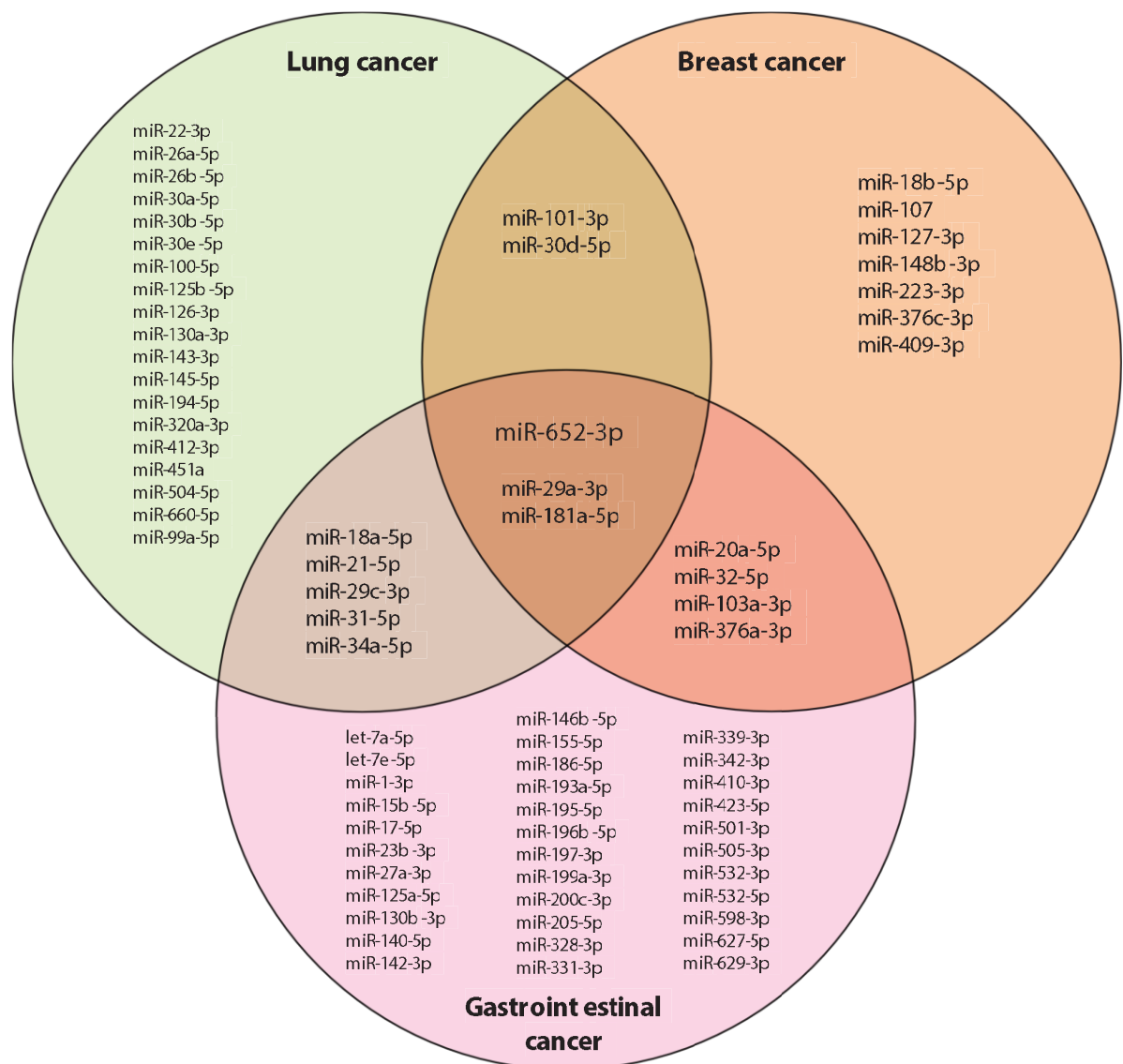
Figure 1.2. Human miRNAs reported dysregulated with hsa-miR-652-3p in lung cancer, breast cancer, and gastrointestinal cancers. Lung cancers include non-small cell lung cancer and plural mesothelioma. Gastrointestinal cancer includes oesophageal cancer, gastric cancer, and colorectal cancer.

1.7.2   Breast cancer

Along with lung cancers, several studies have identified dysregulated expression of miR-652-3p in breast cancer patients, though no specific target genes have yet been identified. Cuk et al. found that miR-652-3p was upregulated in the plasma of 150 breast cancer patients (98). miR-652-3p was part of a 7-miRNA panel identified which distinguished benign and malignant breast cancer (98). The panel was particularly effective in young women (<50 years old), with an area under the ROC curve of 0.86.

This study also found miR-652-3p levels correlated with tumour suppressor p53 expression, which is interestingly a predicted target of miR-652-3p on the TargetScan v7.2 database (99). An additional study established a 4-miRNA serum signature including miR-652-3p which could also identify triple-negative breast cancer patients likely to relapse (53). Increased expression of the 4 miRNAs was predictive of relapse within 36 months post-surgery.

Interestingly two studies found circulating miR-652-3p expression reduced in Luminal A type breast cancer patients (100, 101). A biomarker panel analysing decreased miR-652-3p, miR-29a-3p, and miR-181a-5p concentrations in whole blood was able to identify Luminal A breast cancer, with an area under the ROC curve of 0.80 (101). Indeed, low serum levels of miR-652-3p alone was able to identify both Luminal A and non-Luminal A breast cancers (100).

Discrepancies in circulating miR-652-3p expression reported in breast cancer may be due to the variation between serum and plasma, particularly considering miR-652-3p was identified in circulating exosomes, which are depleted in serum (47). Alternatively, differences could be attributed to use of different reference controls in miRNA data normalisation. These studies used either small nuclear RNA U6 (53, 98) or miR-16-5p (101) as a housekeeping control, or no housekeeper at all in a ddPCR method (100). Data normalisation methods can cause significant difference in experiment outcomes, and the use of U6 as a circulating housekeeping RNA has been questioned (102, 103). A further consideration is the varying sizes the cohorts used. Studies reporting miR-652-3p overexpression in breast cancer used larger cohorts (n=110 and n=210) than those reporting miR-652-3p underexpression (n=59 and n=90). Other factors such as stage of disease at diagnosis, ethnicity, and age may all influence miR-652-3p expression. It may also be that miR-652-3p functions differently in different cancers due to other biological factors.

1.7.3   Gastrointestinal cancers

Gastrointestinal cancers make up 26% of all cancers globally with 5-year survival rates of 24-65%, depending on cancer subtype, and miRNA are already of major interest as diagnostic biomarkers in this field (104-106). Recent studies have reported dysregulated

miR-652-3p in multiple gastrointestinal cancers including oesophageal, gastric, and colorectal cancers.

A small study of two oesophageal cancer patients found high miR-652-3p levels in fixed tumour tissue correlated with poor prognosis (107). Conversely, a later study by Zhen et al. found miR-652-3p was downregulated in oesophageal tumour tissue (89). Whilst both studies analysed squamous cell carcinoma tissues and used similar RNA quantification and data normalisation methods, tissue collection and processing varied significantly (89, 107). Larger studies accounting for comorbidities and environmental factors are warranted to investigate the role of miR-652-3p in oesophageal cancer. Zehn et al. found that transfection of a miR-652-3p mimic in oesophageal cancer cell lines decreased cell proliferation and invasion by targeting fibroblast growth factor receptor 1 (*FGFR1*) (89). Overexpression of FGFR1 is associated with poor prognosis in several cancer types (108-110), and miR-652-3p appears to play a protective role in this context.

In addition to oesophageal cancer, miR-652 has also been associated with gastric cancer. miR-652-3p was upregulated in the serum of gastric cancer patients, determined through whole-genome sequencing (111). Shin et al. also found miR-652-3p upregulated in plasma of 50 gastric cancer patients using qRT-PCR. This study identified miR-627-5p, miR-629-5p, and miR-652-3p as an effective diagnostic/prognostic biomarker panel for identification of gastric cancer (112).

Several other studies have found circulating miR-652-3p is increased in serum and plasma of colorectal cancer patients (113, 114). Pre-cancerous colorectal adenoma could be identified using increased plasma miR-652-3p concentration (114), and an *in silico* analysis of microarray data found increased miR-652-3p concentration in colorectal tumour tissue was associated with poor prognosis (115). Additionally, a conference abstract reported upregulated miR-652-3p in serum was also associated with poor prognosis in 43 colorectal cancer patients (113). Interestingly, a further study found low serum miR-652-3p levels were associated with poor prognosis in 322 patients with stage I-III colorectal cancer (52).

These apparently conflicting results in colorectal cancer again highlight important issues with miRNA as biomarkers. miRNA expression can be influenced by many factors including diet, ethnicity, cancer subtype, and environmental factors (116, 117). In this instance, miR-652-3p was upregulated in American cancer patients compared to healthy controls (114), but no difference was observed in a Chinese population (52). Differences may also be dependent on the experimental method, as each study used differing sample matrices and methodologies (ddPCR versus qRT-PCR, versus microarray), each with their own miRNA normalisation strategy. Further studies including uniform approaches to normalise biomarker analysis are clearly required.

1.7.4 Other cancers

Dysregulation of miR-652-3p expression has been associated with numerous other cancers, and in many cases a miR-652-3p target gene has been experimentally validated.

miR-652-3p was found to be upregulated in urothelial cells in the urine of bladder cancer patients (118). This study developed a large and specific 25-miR biomarker panel which included miR-652-3p for non-invasive bladder cancer diagnosis (118). The role of miR-652-3p in this context is not yet clear. miR-652-3p has been shown to target *KCNN3*, encoding small conductance calcium-activated potassium channel 3 (SK3). Treatment of the bladder cancer cell lines T24 and J83 with miR-652-3p mimics inhibited SK3 expression and promoted cancer cell invasion (34). One study found that low SK3 expression in ovarian tumours was associated with poor patient survival (119). However, a number of other studies have shown SK3 is overexpressed in primary tumours, and that high SK3 expression by cancer cells caused tumour cell invasion and metastasis (120-122). SK3 expression in these T24 and J83 cell lines is low, compared to primary bladder cancer tissue (121) and this may account for the differences seen between the cell lines and primary cells. Whilst the activity of miR-652-3p in the T24 and J28 cell lines suggests that miR-652-3p does target *KCNN3* in bladder cancer, the in vivo effects of miR-652-3p on bladder cancer require further investigation.

Along with targeting SK3, miR-652-3p has been shown to directly target retinoic acid receptor-related orphan receptor alpha (*RORA*) in endometrial cancer cells (46). Transfection of the Ishikawa human endometrial cancer cell line with a miR-652-3p

mimic decreased RORA expression, leading to increased cell migration and proliferation. RORA was also targeted by miR-652-3p in gastric cancer, where miR-652-3p overexpression was associated with decreased survival (123). RORA is commonly downregulated in cancers and is reportedly a regulator of p53 anti-tumour activity (124-126).

Downregulated miR-652-3p has also been seen in primary glioblastoma tissues with low miR-652-3p expression associated with poor overall survival (34). Here miR-652-3p was acting as a tumour suppressor in glioblastoma cell lines, targeting the transcription factor forkhead-box k1 (*FOXK1*), inhibiting cell migration and promoting apoptosis. FOXK1 regulates a variety of cell processes, including aerobic glycolysis and cell differentiation, and is upregulated in many cancers (127). Transfection of a glioblastoma cell line with a miR-652-3p mimic caused decreased tumour growth when xenografted into nude mice (34).

While downregulation of miR-652-3p has been associated with poor survival in a number of cancers, overexpression of miR-652-3p has also been associated with increased tumour growth. Overexpression of mir-652-3p has been demonstrated in uveal melanoma tissues and in uveal melanoma cell lines (88). Transfection of these cell lines with a miR-652-3p inhibitor led to decreased cell migration and increased expression of the validated miR-652-3p-target homeobox A9 (*HOXA9*). HOXA9 is a transcription factor regulating diverse processes, including embryonic development and haematopoiesis, and HOXA9 dysregulation is associated with several cancers (128-130). Increased miR-652-3p expression in uveal melanoma promoted metastatic cell behaviour through modulating HOXA9 activity (88). mir-652-3p has also been shown to target HOXA9 in human trophoblast cells (32), with inhibition of mir-652-3p leading to decreased trophoblast proliferation and migration.

Upregulated miR-652-3p has been seen in osteosarcoma tissue and osteosarcoma cell lines compared to osteoblast cell lines (131). Jin et al. suggested miR-652-3p overexpression in osteosarcoma tissue may drive tumour malignancy by targeting the transcription factor Krueppel like factor 9 (KLF9) (132). Dysregulation of KLF9 has been associated with development of several cancers (133, 134). Increased miR-652-3p

expression in osteosarcoma cell lines inhibited KLF9 expression and promoted cancer cell invasion (132).

These recent studies highlight the diverse role of miR-652-3p, with both up- and downregulation of this miRNA associated with increased tumour growth and reduced survival. This apparent contradiction in function of miR-652-3p as both a tumour suppressor and tumour promoter is likely due to the multiple targets of miR-652-3p and how it acts on specific tumour or immune cells. Further research is required to fully understand how miR-652-3p is functioning in these different cancers and to determine the therapeutic potential of inhibiting or overexpressing miR-652-3p on tumour function.

1.8. miR-652-3p in mental illnesses and the central nervous system

Along with multiple roles in numerous cancers, miRNAs, including miR-652-3p, are also being recognised for their roles in mental illnesses and CNS diseases. Knowledge of how neuron function is regulated by miRNA is developing rapidly, with miRNA regulation, including that of miR-652-3p, being described in control systems in the central nervous system, through to neuronal diseases and mental illness (135-137).

A study of miRNA expression in post-mortem schizophrenia patient brain tissue found 6 miRNAs upregulated, including miR-652-3p (138). A similar analysis found miR-652-3p noticeably upregulated in the frontal cortex of alcoholic patients (139). In order to develop a non-invasive molecular method of schizophrenia diagnosis, Lai et al. measured miRNA levels in patients' peripheral blood mononuclear cells (PBMCs) (140). miR-652-3p was upregulated in schizophrenia patients compared to controls, and formed part of a 7-miR biomarker panel able to robustly identify schizophrenia patients. However, a follow-up study found miR-652-3p was notably, but not significantly, upregulated in PBMCs of hospitalised schizophrenia patients (141). Differing results between the 2 studies may be due a number of factors including recruitment methods, ethnicity, age, cohort size, concurrent medications or other comorbidities, and further studies in this area are required.

miR-652-3p has also been associated with a number of other mental illnesses and CNS conditions. miR-652-3p levels were elevated in the blood of bipolar disorder patients, while plasma miR-652-3p was decreased in patients diagnosed with the recently described internet gaming disorder (142, 143). Both studies implicated miR-652-3p in dysregulation of the gamma-aminobutyric acid signalling pathway, associated with schizophrenia, bipolar disorder, and alcoholism (144). The potential use of circulating cells and molecules as accessible markers of mental illness has been under investigation for some time (145), and the mechanisms by which psychiatric conditions interact with circulating leukocytes continue to be elucidated (146).

Studies have also shown an association between upregulated miR-652-3p and the onset of multiple sclerosis in both paediatric and adult patients (147). Pleckstrin-2 (*PLEK2)*, an *in silico* predicted target of miR-652-3p, was downregulated in the paediatric multiple sclerosis patients (147). PLEK2 expression is associated with T cell movement and metastasis of numerous cancers (148, 149), potentially deepening the already discussed role of miR-652-3p as a regulator of cell migration.

Whilst no genes have yet been validated as miR-652-3p targets in nervous diseases, targets validated in other studies have implications in CNS disorders. SK3, targeted by miR-652-3p in bladder cancer (34), has been linked with schizophrenia and bipolar disorder (150, 151). Additionally, changes in SK3 expression have been associated with myotonic dystrophy (152) and miR-652-3p was also reported to be upregulated in the serum of myotonic dystrophy patients (51).

Cardiovascular disease

Cancer

let-7c-5p
let-7i-5p
miR-27b-3p
miR-106a-5p
miR-122-5p
miR-126-5p
miR-218-5p
miR-323a-3p
miR-361-5p
miR-375-3p
miR-625-5p
miR-642a-5p

miR-22-3p
miR-27a-3p
miR-30e-5p
miR-143-3p
miR-146b-5p
miR-197-3p
miR-199a-3p
miR-222-3p
miR-223-3p
miR-324-3p
miR-331-3p
miR-532-5p

let-7e-5p   miR-106b-5p
miR-18b-5p   miR-125b-5p
miR-19a-3p   miR-126-3p
miR-19b-3p   miR-127-3p
miR-20a-5p   miR-130a-3p
miR-20b-5p   miR-130b-3p
miR-23b-3p   miR-140-3p
miR-26a-5p   miR-142-3p
miR-29c-3p   miR-142-5p
miR-30a-5p   miR-145-5p
miR-30b-5p   miR-150-5p
miR-30d-5p   miR-151a-3p
miR-31-5p   miR-155-5p
miR-32-5p   miR-186-5p
miR-93-5p   miR-191-5p
miR-96-5p   miR-193a-5p
miR-99a-5p   miR-195-5p
miR-100-5p   miR-200a-3p
                       miR-205-5p
                       miR-224-5p
                       miR-339-3p
                       miR-342-3p
                       miR-376a-3p

miR-409-3p
miR-410-3p
miR-412-3p
miR-429
miR-451a
miR-491-5p
miR-501-3p
miR-504-5p
miR-505-3p
miR-532-3p
miR-542-5p
miR-573
miR-598-3p
miR-627-5p
miR-629-3p
miR-660-5p
miR-1305

miR-652-3p
miR-15b-5p
miR-18a-5p
miR-21-5p
miR-26b-5p
miR-99b-5p
miR-103a-3p
miR-423-5p

miR-30c-5p
miR-92a-3p
miR-185-5p

miR-29a-3p
miR-34a-5p
miR-101-3p
miR-107
miR-125a-5p miR-194-5p
miR-135b-5p miR-196b-5p
miR-140-5p   miR-200c-3p
let-7a-5p   miR-146a-5p miR-221-3p
miR-1-3p   miR-148b-3p miR-320a-3p
miR-17-5p   miR-181a-5p miR-328-3p
            miR-182-5p   miR-376c-3p

let-7b-5p
let-7f-5p
let-7g-5p
miR-7-5p
miR-25-3p
miR-34c-5p
miR-132-3p
miR-134-5p
miR-144-3p
miR-152-3p
miR-153-3p

miR-196a-5p
miR-203a-3p
miR-301a-3p
miR-339-5p
miR-369-3p
miR-374b-5p
miR-380-3p
miR-382-5p
miR-432-5p
miR-449a
miR-454-3p

miR-515-3p
miR-519b-3p
miR-548d-3p
miR-553
miR-564
miR-572
miR-580-3p
miR-586
miR-665
miR-802
miR-942-5p

**Mental health and
CNS disease**

Figure 1.3. Human miRNAs reported dysregulated with hsa-miR-652-3p in cardiovascular disease, cancer, and mental health and central nervous system diseases. Cardiovascular disease includes acute coronary syndrome, heart failure, venous thromboembolism, and obesity. Cancer includes bladder cancer, breast cancer, oesophageal cancer, gastric cancer, mesothelioma, non-small cell lung cancer, and osteosarcoma. CNS and mental health disease includes alcoholism, bipolar disorder, internet gaming disorder, multiple sclerosis, myotonic dystrophy, and schizophrenia.

1.9.   miR-652-3p in other indications

The multifactorial actions of miR-652-3p also extend to reported roles in a number of other diseases. miR-652-3p was upregulated in PBMCs of paediatric patients with type 1 diabetes (59) and downregulated in plasma of pregnant women with pregestational

and gestational obesity (50). Low plasma miR-652-3p levels correlated with high blood glucose and increased weight gain during pregnancy. Similarly, downregulation of miR-652-3p in white adipose tissue was associated with insulin resistance in obese women (153). Transfection of primary white adipose cells with a miR-652-3p mimic decreased expression of ectonucleotide pyrophosphatase/phosphodiesterase 1 (ENPP1) and increased glucose incorporation into lipids. ENPP1 is a regulator of bone and soft tissue mineralisation, and has been associated with obesity, type 2 diabetes, and pathological calcification of soft tissues (154, 155). Several additional studies have linked *in silico*-predicted miR-652-3p targets with fatty acid metabolism pathways (139, 147), suggesting further investigation into the involvement of miR-652-3p in cell metabolism is warranted.

Downregulation of serum miR-652-3p in liver cirrhosis patients was shown to be highly predictive of cirrhosis disease, but not the aetiology or stage of cirrhosis (43). In a mouse model of fibrosis, miR-652-3p levels were decreased in the liver tissue suggesting a role for miR-652-3p in immune regulation (44). Mouse CD4$^+$ T cells transfected with a miR-652-3p mimic expressed significantly lower levels of the Th17 cytokines, IL-17A and IL-22 (44). In host immunity, down regulation of miR-652-3p may aid this early response to infection. These transfected CD4$^+$ T cells also displayed significantly lower levels of β-arrestin 1 (*ARRB1*), and a luciferase reporter assay confirmed ARRB1 was a target of miR-652-3p (44). ARRB1 is ubiquitously expressed, and has known functions in T cell regulation (156), TLR signalling (157), and colorectal cancer progression (158), underpinning the role of miR-652-3p in immunoregulation and cancer metastasis (35, 45, 79).

To date, the only communicable disease associated with miR-652-3p is *Mycobacterium tuberculosis* infection. Barry et al. found plasma miR-652-3p levels were lower in active tuberculosis patients compared to healthy controls, and that concentrations remained downregulated throughout the standard 6-month antibiotic treatment (20). If the patient group was further stratified based on the success or failure of antibiotic treatment, pre-treatment miR-652-3p levels were significantly lower in treatment failures compared to treatment successes. Additionally, the human monocyte cell line

U937 downregulated miR-652-3p following lentiviral-transduction to express *M. tuberculosis* protein Hsp16.3 (42). Whether the downregulation of miR-652-3p is part of the host immune response or bacterial pathogenesis remains to be elucidated. The expression of proinflammatory cytokines by *Mycobacterium bovis* BCG-infected macrophages is mediated by JAG1/NOTCH signalling (159), further suggesting a role for miR-652-3p in immune regulation (79).

1.10. miRNAs regularly associated with dysregulated miR-652-3p

To complement analysis of individual miRNA, investigation of miRNA commonly identified as dysregulated together can give insight into which pathways these miRNAs may regulate and can give insight into the physiological pathways altered in specific diseases.

Online Resource 1 details all miRNAs reported as either up- or downregulated where dysregulated miR-652-3p was also reported. Additionally, all studies identifying miR-652-3p as part of a disease biomarker signature are listed in Online Resource 2. Many miRNAs have been identified as dysregulated with miR-652-3p across multiple cancer types (Figure 1.2), and more still are dysregulated with miR-652-3p across cancer, CVD, and mental health and CNS disorders (Figure 1.3).

The miRNA most commonly associated with dysregulated miR-652-3p is mir-223-3p. Both were reported as dysregulated in breast cancer, bladder cancer, heart failure, and tuberculosis patients (20, 53, 64, 101, 118). miR-223-3p regulates myeloid leukocyte differentiation and function (160), with reported functions as either a tumour promotor or suppressor in different cancers (161). Similar to miR-652-3p, miR-223-3p can inhibit metastasis of cancer cells by targeting ZEB1 (162).

Multiple studies have also reported an association between significant changes in circulating mir-143-3p levels with miR-652-3p, with both miRNAs highly expressed in myeloid leukocytes (41). Both miR-143-3p and miR-652-3p were reported to be upregulated in non-small cell lung cancer, mesothelioma, and CVD patients, and both downregulated in bladder cancer patients (48, 90, 91, 118). miR-143-3p regulates the cell cycle by targeting MAPK7, and downregulation of miR-143-3p is associated with

progression of several cancers (163, 164). In a murine model, miR-143-3p expression was controlled by the Jag1/Notch1 pathway in vascular smooth muscle cells (165). As miR-652-3p inhibits JAG1, this suggests miR-652-3p may regulate expression of miR-143-3p, through inhibition of JAG1 (79).

Similarly, miR-18a-5p has reported protective or pathogenic roles in different cancers (166), and dysregulated expression of miR-18a-5p has been reported with dysregulated miR-652-3p in lung, gastric, and bladder cancers (91, 112, 118). Both miR-18a-5p and miR-652-3p are overexpressed in non-small cell lung cancer (35, 167). Moreover, miR-18a-3p and miR-652-3p target RORA in glioma and endometrial cancer, respectively (46, 168), suggesting both miRNAs may regulate similar pathways.

Additional studies have suggested that miR-29a-3p dysregulation may be linked with both miR-181a-5p and miR-652-3p in breast, lung, and gastrointestinal cancers (Figure 1.2). Studies have shown both miR-181a-5p and miR-29a-3p target VEGF-A to supress angiogenesis in tumours (169, 170). This is intriguing considering miR-652-3p has been associated with VEGF signalling in colorectal cancer (115), and suggests miR-652-3p could play a protective role in these tumours.

Another miRNA associated with miR-652-3p in multiple conditions is miR-107. Both have been reported to be upregulated in parallel in breast cancer, schizophrenia, and myotonic dystrophy (51, 53, 138). miR-107 prevents cell cycle arrest and cancer progression by inhibiting CDK6 expression (171). CDK6 itself is regulated by CCND2, a validated miR-652-3p-target, illustrating the involvement of miR-652-3p cell cycle maintenance (73). In a similar fashion, a study in glioma cells showed hsa-miR-107 targets NOTCH2 (172), itself a receptor for the miR-652-3p target JAG1 (79). Expression of miR-107 in macrophages is TLR and NF-κB dependant, and miR-107 was downregulated is response to LPS in mouse macrophages (173, 174). Moreover, miR-107 and miR-652-3p were both downregulated in human macrophages expressing the recombinant mycobacterial antigen Hsp16.3 (42).These co-dysregulation analyses highlight the diversity of pathways influenced by miR-652-3p and present interesting avenues for further investigation of miR-652-3p activity.

1.11. Interspecies conservation of miR-652-3p and its validated target genes

Common practical and ethical limitations associated with obtaining human samples make animal models an attractive alternative for scientific experimentation. Mice are among the most commonly used laboratory animals due to ease of colony maintenance and relatively short breeding cycle. Whilst mouse and human genomes are largely homologous (175), genetic differences between the species can greatly affect phenotypic and experimental outcomes (176).

In order to assess the use of mice as a model of miR-652-3p activity, we performed sequence alignments using the EMBOSS Needle global alignment tool (https://www.ebi.ac.uk/Tools/psa/) for all miR-652-3p targets validated in humans or mice: *ARRB1* (44), *CCND2* (73), *ENPP1* (153), *FGFR1* (89), *FOXK1* (34), *HOXA9* (32, 88), *ISL1* (75), *JAG1* (79), *KCNN3* (34), *KLF9* (132), *LLGL1* (35), *MTP18* (33), *RORA* (46, 123), and *ZEB1* (45).

mRNA sequences used in this analysis are detailed in Table S2. The mature miRNAs, hsa-miR-652-3p and mmu-miR-652-3p are 100% homologous (177). However, the target sequences in the genes they are predicted to bind are not all conserved between humans and mice. For instance, the *RORA* 3'-UTR is conserved in mice, with only a single base difference in the binding region (Figure 1.4A). Target sequences in *ISL1*, *KLF9*, *ZEB1*, and *JAG1* are also well conserved in mice. However, single base differences are present in each gene corresponding to the miR-652-3p 5' seed sequence, known to be influential in miRNA-mRNA targeting (10). The hsa-miR-652-3p target sites in human *LLGL1* and *ENPP1*, and the mmu-miR-652-3p target site in mouse *Arrb1* are all moderately conserved between the two species, however, binding of the miR-652-3p seed sequence may be significantly impacted by 3' changes in the target genes. Conservation of 3'-UTR target sites in human *FGFR1* and *FOXK1* in mice is poor, and miR-652-3p is not expected to bind these sites. The validated target site for *Mtp18* in mice is not present in humans.

Two separate studies have validated human *HOXA9* as a hsa-miR-652-3p target. Both studies listed the target sequence predicted by the TargetScan v7.2 database (99). However, this target sequence is not present within any *HOXA9* mRNA transcripts in the

Refseq database for either human or mouse (32, 88). Rather, it is in a non-transcribed region over 600 bp downstream of *HOXA9* (Figure 1.4B). This non-transcribed region is also well conserved in mice. The predicted target sequence was validated in both studies using recombinant luciferase reporter constructs (32, 88). miR-652-3p mimics and inhibitors modulated HOXA9 expression, as determined by western blot, suggesting there may be a second miR-652-3p target site in the *HOXA9* mRNA transcript, or that miR-652-3p could be targeting another protein upstream of HOXA9. Similar to the *HOXA9* target site, the validated miR-652-3p target site in the human *KCNN3* 3'-UTR is not present in known mouse *Kcnn3* mRNA transcripts (Figure 1.4C), but it is well conserved in the mouse genomic sequence downstream of *Kcnn3* (data not shown).

Though some validated 3'-UTR target sequences are not conserved between humans and mice, this does not necessarily mean miR-652-3p does not target these genes, as some miRNA are known to have several target sites within a single gene. Huang et al. predicted different miR-652-3p target sequences in human and mouse *CCND2*. Two predicted target sites in the human *CCND2* 3'-UTR are not well conserved in mice (Figure 1.4D), however a predicted target site in the mouse *Cnnd2* coding sequence is well conserved in humans (73). Western blot data confirmed miR-652-3p targeted both human *CCND2* and mouse *Ccnd2* and the predicted target site in the mouse *Ccnd2* coding sequence was validated by a standard recombinant-gene luciferase assay (73).

Mouse models remain a valuable tool for the elucidation of miR-652-3p activity. The interspecies conservation of miRNA binding sites should be considered when developing investigative models of miRNA activity.

```
Human RORA 1740 ATGGCCCTGCACAGACCTGGAGCGCCA--CA 1769    Human ARRB1 3200 ------CCAGCACCTCCTGGGG-------3206
                |||||||||||.|.|||||||||||||||||.|               ||.||..||.|||||
Mouse Rora 1712 ATGGCCCTGCACAGCCCTGGAGCGCCAACAA 1742    Mouse Arrb1 3330 CATGCCCCTGCCACTGCTGGCGCCATGCTG 3360

Human MTP18 1124 -----------------------------1133       Human ENPP1 5055 TCAGCATTTGCTGGTATGGGTGGGGCCATG 5085
                                                                         .|   ||.||||||.||||.|| |
Mouse Mtp18 1353 AATCACAACCCAAGTGCTAACCTAATAAAAG 1383     Mouse Enpp1 4866 CC----TTGGCTGGTGTGGGAGG------4885

Human LLGL1 4134 TTGTTAAAATTAG-CGCCATTTTAATATTAA 4163     Human ZEB1 4506 GCCTTAAGCAAGACCTGTGTGCTGTAAGTG 4536
                |.|.|||||.||| .| |||||||||||||                   ||||||||||||||||||||||||||||||
Mouse Llgl1 4246 TTTTAAAAACTAGTTG---TTTTAATATTAA 4273     Mouse Zeb1 4180 GCCTTAAGCAAGACC--TGTGCTCTAAGTG 4208

Human JAG1 4119 CGTATAGCAGACCGCGGGCACTGCCGCCGCT 4150       Human FOXK1 6017 -----ACTGGCTTCACGCTAGAGGGCGCCA 6043
                |||||||||||||.|.|||||||||||.|                   ||||  ||  ||.||
Mouse Jag1 3913 CGTATAGCAGACAGTGGG--CTGCCGCC-A 3941        Mouse Foxk1 4774 TCCGAACTG----CAC-----AGTGC---4790

Human FGFR1 4701 GGAGGTTGCAGTGAGCCGAGATTGCGCCCA 4732       Human ISL1 2317 AAATCAAAGCGCCATATGTAGAATTATATC 2347
                                         ||||                    ||||||||||||||||||||||||||||
Mouse Fgfr1 4394 --------------------------CATG 4398        Mouse Isl1 2445 AAATCAAAGCGCCATATGTAGAATTATATC 2475

Human KLF9 2607 -----CGCCATAGCACAGCTGTC-TTTATG 2629
                |.||||||||||||||||| |||||                 3'UTR sequence:
Mouse Klf9 1826 CCAACCCTCCATAGCACAGCTGTCTTTTATG 1856      Human CCND2 5686 ATTCTAAACAACCCAGAATGGTCAT--TTC 5714
                                                                         |||.|.|||||.|.||.||.||||.|.|.
Human HOXA9 8715 GCAATTGACGAGCCCCTAAGCGCCATAAAA 8745       Mouse Ccnd2 5475 ATTTTCAACAGCACAAAAGAGTCCTCGAGC 5505
                .|.|||.|||||||.||||||
Mouse Hoxa9 17181 -CAACCGACAAGCCCCGAAGCGCCATAAAA 17149    Human CCND2 6000 ATCCCCAGCAAATCATCGGGCCATTGGATT 6030
                                                                         ||.|||..|.|| ||..|
Human KCNN3 10889 GACGTGAATTCTGATATTGGCGCCATAACT 10918    Mouse Ccnd2 5755 A-----AGAAAAAAACG-----TTAAA--5772
                                     ||.|||..|.||
Mouse Kcnn3 7619 -----------------------------7618        CDS sequence:
                                                          Human CCND2 1040 TCCTCAATAGCCTGCAGCAGTACCGTCAGGA 1070
                                                                         |.||.||.||||||||||||.||||||.||
                                                          Mouse Ccnd2 1033 TGCTGAACAGCCTGCAGCAGTTCCGTCAAGA 1063
```

Figure 1.4. mir-652-3p target sequences are conserved between humans and mice. Yellow indicates bases bound by miR-652-3p, as described in published literature. a The 3'-UTR of validated miR-652-3p target genes in humans and mice. b The in silico predicted miR-652-3p target site in HOXA9 reported in the literature is downstream of the transcribed mRNA. c The miR-652-3p target sequence in human KCNN3 is conserved in the mouse genome, but is not included in known mouse mRNA transcripts. d The predicted miR-652-3p binding sites in the human CCND2 3'-UTR are moderately conserved in mice. The predicted miR-652-3p binding site in the mouse Ccnd2 CDS is well conserved in humans.

1.12. Conclusion

The current literature illustrates the diverse roles miR-652-3p plays in maintaining cellular processes, and its contributions to disease pathogenesis. Validated gene targets have implicated miR-652-3p in regulation of cell differentiation, metabolism, proliferation, and apoptosis, and aberrant miR-652-3p expression in these systems can lead to oesophageal, lung, uveal, bladder, endometrial, and pancreatic cancers. Dysregulation of miR-652-3p has been associated with several cardiovascular diseases, with a number of cardiac repair genes confirmed as miR-652-3p targets. The ability of miR-652-3p to target *JAG1*, *LLGL1*, and *ZEB1*, could profoundly influence cell polarity maintenance, cell fate determination, generation of inflammatory immune responses, and initiation or repression of cancer metastasis.

Although miR-652-3p has been identified as a potential biomarker in a number of mental health and central nervous system diseases, the mechanisms by which miR-652-3p is

associated with these conditions are yet to be uncovered. The activity of miR-652-3p in infectious disease also remains poorly understood and its association with mycobacterial infection provides an excellent opportunity for further investigation. Continued investigation into the actions of miR-652-3p offers considerable opportunity to develop new diagnostic and therapeutic targets to treat a range of human diseases.

1.13. Declarations

1.14. Acknowledgements

1.15. Online resources

Online resources are included in Appendix 2.

Online Resource 1 miRNAs dysregulated with miR-652-3p

Online Resource 2 Identified disease biomarker signatures utilising miR-652-3p

Online Resource 3 Sequences used for inter-species alignment analysis of validated miR-652-3p target genes

CHAPTER 2

Macrophages of different tissue origin exhibit distinct inflammatory responses to mycobacterial infection

Chapter 2. Macrophages of different tissue origin exhibit distinct inflammatory responses to mycobacterial infection

2.1.   Chapter 2 – Declaration

I declare that the below publication meets the requirements for inclusion as a chapter in this thesis.

- I have contributed more than 50% of work for the publication below. I designed and conducted all experiments, performed all data analysis. I prepared the complete manuscript and generated all figures. BN, WB, and BS assisted in study conceptualisation. WB and BS edited and approved the manuscript.
- The below publication has been peer reviewed.
- Permission is not required by the publisher for inclusion of this publication in this thesis for non-commercial purposes.

Stevens, M. T., B. D. Nagaria, W. J. Britton, and B. M. Saunders. 2021. Macrophages of different tissue origin exhibit distinct inflammatory responses to mycobacterial infection. *Immunology and Cell Biology*. 99: 1085-1092.

Publication status: published.

The published version of the manuscript can be found in Appendix 3.

Signature: Production Note:
Signature removed prior to publication.

Date: 30 July 2022

2.2.   Abstract

Macrophages display marked plasticity with functions in both inflammation and tissue repair. Evidence demonstrates that this spectrum of macrophage phenotypes is influenced by their local microenvironment and tissue origin. However, *in vitro* macrophage experiments often do not or cannot readily use macrophages from the most relevant tissue of origin. In this study we investigated if the origin of two C57BL/6 mouse macrophage cell lines of alveolar (AMJ2-C11) and peritoneal (IC-21) origin may influence their response to mycobacterial infection.

Both cell lines equally controlled growth of *Mycobacterium bovis* BCG and *Mycobacterium tuberculosis*, although expression of all proinflammatory cytokines and chemokines measured (TNF, IL-6, MCP-1, MIP-1α, MIP-1β, and RANTES) was significantly higher in AMJ2-C11 cells than IC-21 cells. During *M. tuberculosis* infection, IL-6, MCP-1, and RANTES expression increased 5-fold, and MIP-1β expression increased 30-fold. Additionally, AMJ2-C11 cells exhibited significantly higher iNOS activity than IC-21 cells, indicative of a more polarised M1 response. Expression of multiple surface markers were also assessed by flow cytometry. CD80 and CD86 were significantly upregulated in AMJ2-C11 cells and downregulated in IC-21 cells during *M. tuberculosis* infection.

Our results support the notion that the origin of tissue-resident macrophages influences their phenotype and antimicrobial response and demonstrate hereto unrecognised potential for these cell lines in *in vitro* studies.

2.3.   Introduction

Macrophages are often the first leukocytes to interact with invading pathogens and form an integral part of the innate and adaptive immune systems. Macrophage activity is influenced by environmental stimuli and macrophage phenotype is often lineated into two categories. M1 macrophages are produced *in vitro* by stimulation with pathogen-associated molecules such as LPS, with or without GM-CSF or IFN-γ, and express proinflammatory cytokines including IL-1β, IL-6, IL-12, and TNF (178, 179). By contrast, Th2-related or anti-inflammatory cytokines such as IL-4, IL-13, IL-10, and TGF-β stimulate M2 macrophages, expressing ARG1 and the anti-inflammatory cytokine IL-10 (180). Macrophage plasticity allows switching between the M1 and M2 phenotypes as stimuli change (181). Recent studies have demonstrated that a binary M1-M2 phenotype classification does not universally apply to many tissue-resident macrophage subtypes, and that macrophage phenotype is strongly influenced by tissue of origin (182).

Local tissue microenvironments and disease states generate gene expression profiles unique to tissue-resident macrophage subtypes, modulating the gene enhancer landscape of transplanted macrophages to produce a spectrum of M1-M2 phenotypes (183). Retinoic acid produced in the mouse peritoneal cavity induces expression of the peritoneal macrophage-specific transcription factor GATA6, which in turn induces TGF-β and ARG1 production, both M2 markers (184). GATA6 is downregulated when peritoneal macrophages are transplanted to the lung (183). Peritoneal macrophages express typical M2 macrophage markers, including CD206 and TGF-β (182, 185). In comparison, alveolar macrophages commonly express both M2 marker CD206 as well as M1 marker CD86 in steady state (186). The percentage of alveolar macrophages expressing CD206 and M1-activation associated enzyme, inducible nitrogen oxide synthase (iNOS), is increased in smokers and chronic obstructive pulmonary disease patients (187). Acute *Mycobacterium tuberculosis* infection drives mouse alveolar macrophages toward an iNOS$^+$ M1 phenotype, before switching to an ARG1$^+$ M2 phenotype as chronic infection persists (188).

Many *in vitro* studies utilise immortalised phagocyte cell lines, such as human THP-1 or murine RAW 264.7 cells, or commonly differentiate macrophages from circulating

human monocytes or mouse bone marrow progenitors. The polarity of mouse bone marrow-derived macrophages (BMDM) depends heavily on the cytokines used in their differentiation (189). BMDMs differentiated with GM-CSF and M-CSF are phenotypically M1 and M2, respectively, the former expressing TNF and IL-6, whilst the latter secrete IL-10 and CCL2 (190). Studies in M-CSF deficient mice identified that M-CSF was essential for *in vivo* development of peritoneal macrophages, but not alveolar macrophages (191). Secreted cytokine levels may vary markedly between macrophage cell lines and change during extended culture (192). Variability in steady state phenotype of model cells may influence the cell's response to *M. tuberculosis* infection.

Here we examine the response to mycobacterial infection by two immortalised C57BL/6 mouse macrophage cell lines of peritoneal and alveolar origin. We compare the ability of each cell line to control bacterial growth, demonstrating distinct proinflammatory cytokine expression patterns and differing iNOS activity in macrophage cell lines of different tissue origin. We demonstrate a more M1 phenotypic profile in the AMJ2-C11 cells compared to the IC-21 cells, and this also influences the surface receptor expression patterns associated with mycobacterial infection.

2.4.   Results
2.4.1 Macrophages from distinct origins retain control of mycobacterial growth

In order to assess the effect of tissue origin on the ability of macrophages to control mycobacteria, bacterial growth in AMJ2-C11 and IC-21 cultures were measured over time. Bacterial loads in *Mycobacterium bovis* Bacillus Calmette-Guérin (BCG)-infected macrophages remained stable up to 24 hours post-infection (hpi), with both cell lines showing mycobacterial killing by 48 hours ($P < 0.05$, Figure 2.1a). Macrophages infected with *M. tuberculosis* exhibited stable bacterial load over the 48 hour infection, and there was no significant difference in capacity to control bacterial growth between the two cell lines (Figure 2.2b).
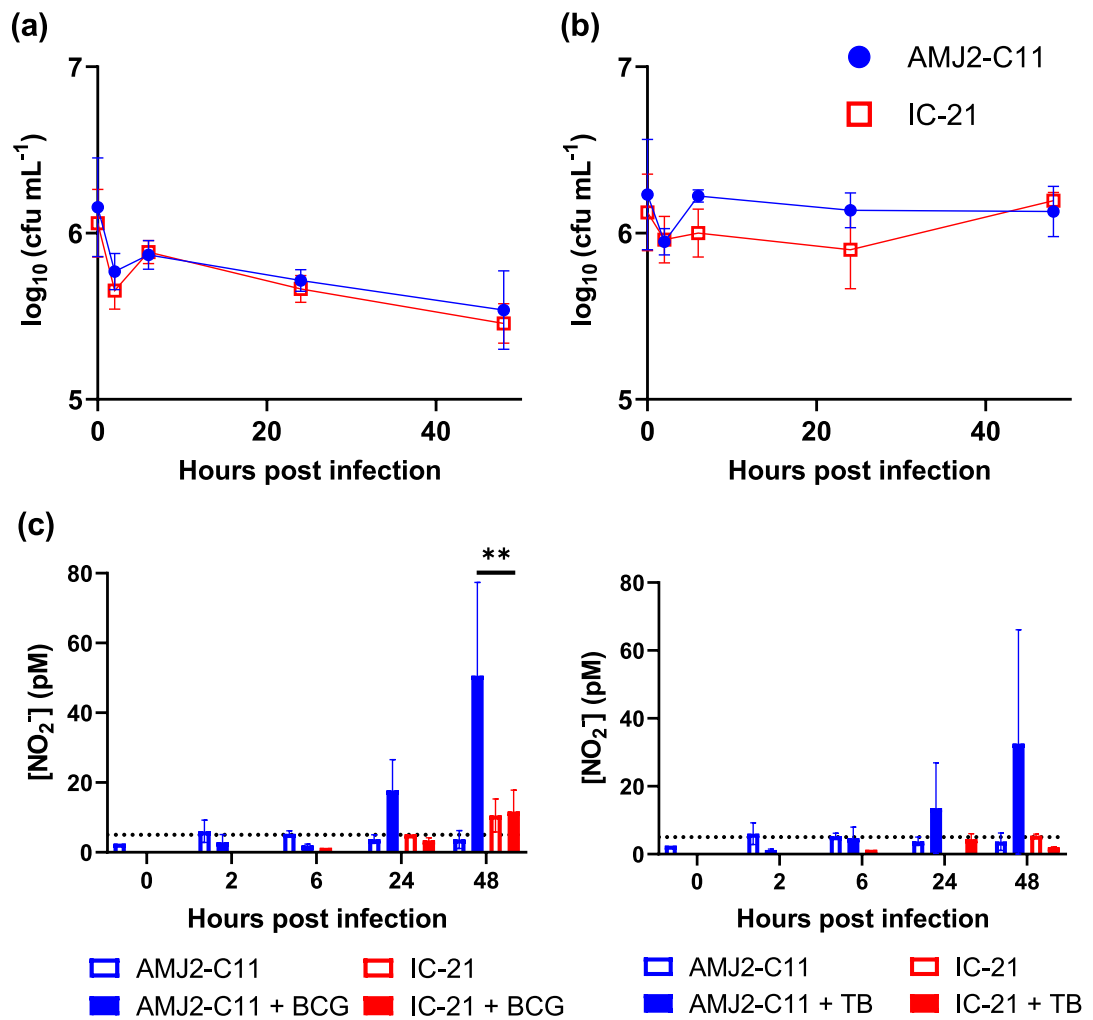
Figure 2.1 Bacterial growth in alveolar AMJ2-C11 and peritoneal IC-21 macrophage cultures infected with (a) BCG and (b) *Mycobacterium tuberculosis*. Data are the mean ± s.e.m. of nine replicates, from three repeat experiments. (c) Supernatant nitrite concentration of AMJ2-C11 and IC-21 macrophage cultures during BCG and *M. tuberculosis* infection. Data are the mean ± s.d. of nine replicate wells, from three repeat experiments. Dotted lines represent the assay's lower limit of quantitation. **$P < 0.01$, by the Student's t-test, Holm-Šidák method corrected.

2.4.2 iNOS activity is influenced by macrophage tissue origin

The proinflammatory iNOS activity of the macrophage cell lines was compared through quantification of nitrite, a downstream product of NO. AMJ2-C11 macrophages exhibited more iNOS activity than IC-21 macrophages (Figure 2.1c). BCG infection of AMJ2-C11 cells induced significantly more nitrite than BCG infection of IC-21 cells. AMJ2-C11 cells produced similar nitrite levels during BCG and *M. tuberculosis* infection. No nitrite production by IC-21 cells was detected following *M. tuberculosis* infection.

2.4.3 Increased proinflammatory cytokines expression in alveolar macrophages

The inflammatory response of these macrophages during mycobacterial infection were investigated by measuring the cell lines' proinflammatory cytokine expression during BCG and *M. tuberculosis* infection. Infection with the less virulent BCG induced more cytokine and chemokine expression in both cell lines compared to infection with the more virulent *M. tuberculosis*. In particular, production of the chemokines IL-6, TNF, MCP-1, and MIP-1β was considerably increased during BCG infection (Figure 2.2).

BCG infection induced a similar cytokine response from both cell lines (Figure 2.2a), although the production of the chemokines MIP-1α and MIP-1β was increased in IC-21 cells at 6 and 24 hpi, respectively, whilst RANTES production in AMJ2-C11 cells was almost 9-fold higher at 24 hpi (Figure 2.2a). Late IL-6 and MCP-1 expression was significantly higher at 48 hpi in AMJ2-C11 cells. A significant decrease in bacterial load at 24-48 hpi (Figure 2.1a) coincided with increases in cytokine expression, particularly MIP-1β, MCP-1, and IL-6.

However, *M. tuberculosis* infection induced differential responses between the cell lines. AMJ2-C11 cells expressed over 5-fold more IL-6, MCP-1, and RANTES, and more than 30-fold more MIP-1β at 48 hpi compared to IC-21 cells (Figure 2.2b).
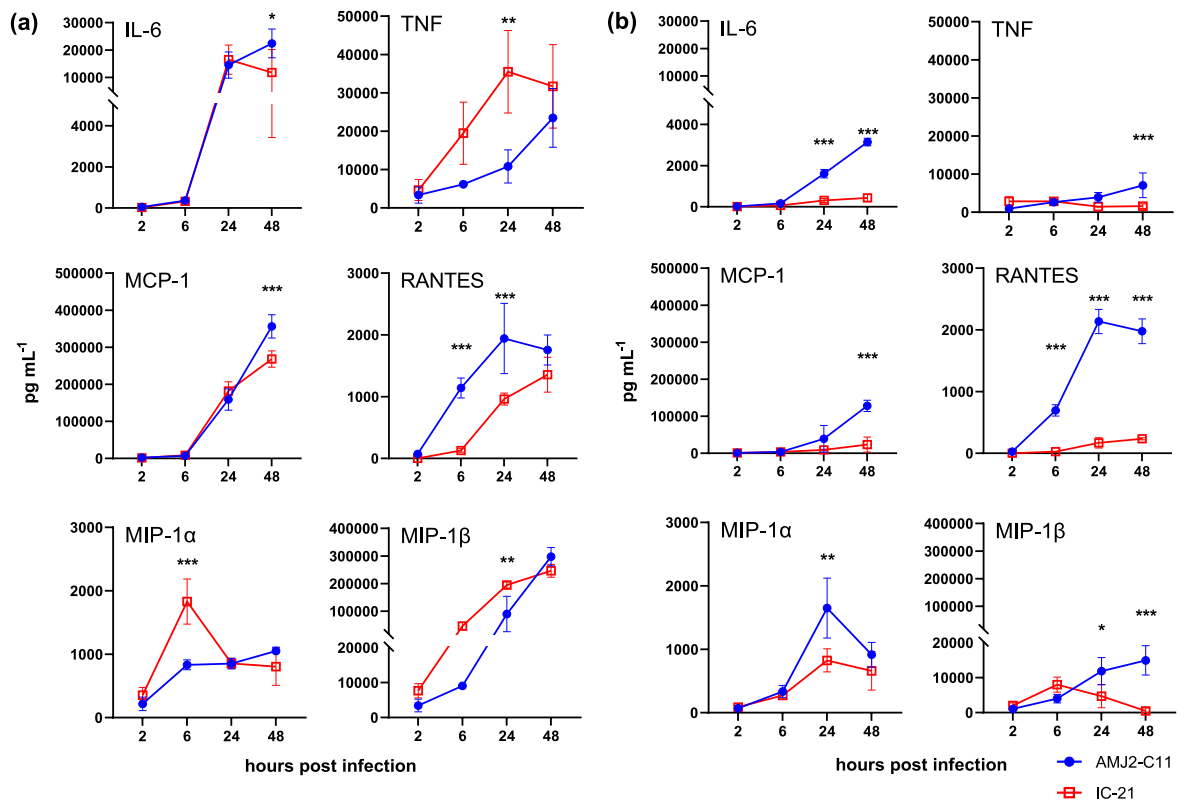
Figure 2.2 Increased cytokine expression by AMJ2-C11 alveolar macrophages compared with IC-21 peritoneal macrophages following infection with (a) BCG or (b) *M. tuberculosis*, relative to uninfected cells. Data are the mean ± s.d. of triplicate wells, representative of three repeat experiments. Repeat experiment data are shown in Supplementary figures 3 and 4. Asterisks represent significant difference between AMJ2-C11 and IC-21 expression by 2-way ANOVA with multiple comparisons post-test, Šidák method corrected. *$P < 0.05$, **$P < 0.01$, ***$P < 0.001$.

2.4.4 Surface phenotype of alveolar macrophages indicates stronger proinflammatory response to mycobacterial infection

Cell surface marker expression is an indicator of macrophage subtype and inflammatory state. We quantitated the expression of 12 cell-surface proteins on AMJ2-C11 and IC-21 cells by flow cytometry, comparing median fluorescence intensity (MFI) between cells lines, uninfected and after infection with BCG and *M. tuberculosis*. A resazurin fluorescence assay confirmed no decrease in mitochondrial activity following mycobacterial infection, indicating cells remain viable at 24 hpi (Supplementary figure 1).

The expression of most markers was greater in uninfected IC-21 cells compared to uninfected AMJ2-C11 cells (Figure 2.3a). Only Ly6C expression was skewed towards AMJ2-C11 cells, and this difference was exaggerated upon mycobacterial infection. Expression of the M1 marker CD86 was higher in IC-21 peritoneal macrophages prior to infection, though AMJ2-C11 alveolar macrophages showed significantly higher expression after infection. Furthermore, uninfected IC-21 cells expressed more of the M2 marker CD206, as well as CD11b, CD24, and Siglec-F. Expression of these markers was not significantly different between cells lines during BCG infection, and was similar during *M. tuberculosis* infection. Expression of MHC-II was equivalent on the uninfected cell lines, however, this rose significantly on AMJ2-C11 cells following BCG infection. Expression of the M1 marker CD80, as well as CD11c, Ly6G, and immunoglobulin receptor, CD64, was greater on IC-21 cells under all conditions.

Infection with BCG and *M. tuberculosis* induced comparable responses in AMJ2-C11 macrophages, with increased expression of all tested markers (Figure 2.3). This activation was also reflected in the strong iNOS (Figure 2.1c) and cytokine response (Figure 2.2) from AMJ2-C11 cells to both bacterial species. In contrast, IC-21 cells downregulated Ly-6C upon BCG infection, and downregulated multiple inflammatory markers upon *M. tuberculosis* infection, including CD80 and CD86 (Figure 2.3). Moreover, downregulation of CD64 and CD11b by *M. tuberculosis* infected IC-21 cells could indicate a shift towards an anti-inflammatory phenotype. The comparable marker upregulation seen in AMJ2-C11 and IC-21 cells following BCG infection reflects the similar cytokine responses by both cell lines (Figure 2.2a). In contrast, the downregulation of inflammatory surface markers by IC-21 cells upon *M. tuberculosis* infection coincides with lower cytokine expression (Figure 2.2b) and undetectable iNOS activity (Figure 2.1c).
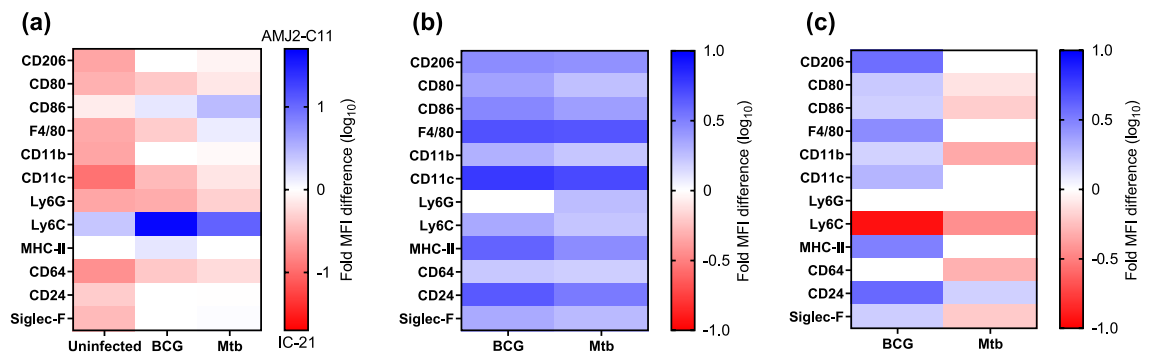
Figure 2.3 Expression of surface markers on AMJ2-C11 alveolar macrophages and IC-21 peritoneal macrophages during BCG and *Mycobacterium tuberculosis* infection, as determined by flow cytometry. (a) Fold MFI difference for surface markers expressed on AMJ2-C11 and IC-21 cells, uninfected, and 24 h after BCG and *M. tuberculosis* infection. Fold difference is a ratio of AMJ2-C11 MFI to IC-21 MFI. (b) Fold change in surface marker expression of AMJ2-C11 cells following 24 h mycobacterial infection, compared with uninfected cells. (c) Fold change in surface marker expression of IC-21 cells following 24-h mycobacterial infection, compared to uninfected cells. Data are the mean of triplicate wells. All coloured rectangles represent *P* < 0.05, the Student's t-test, Holm-Šidák method corrected.

2.5.   Discussion

Mice are the most commonly used animal model of mycobacterial infection, with C57BL/6 the most common genetic background used. In this study we compared two C57BL/6 mouse macrophage cell lines of differing tissue origin, in response to *in vitro* mycobacterial infection. Whilst both the AMJ2-C11 alveolar macrophages and IC-21 peritoneal macrophages controlled the growth of BCG and *M. tuberculosis* to the same extent, AMJ2-C11 cells exhibited significantly greater proinflammatory cytokine expression and iNOS activity in response to the bacterial species. Additionally, AMJ2-C11 cells presented a more inflammatory surface phenotype during *M. tuberculosis* infection. The response to infection may be influenced by the tissue origin of the two cell lines.

When using primary macrophages or macrophage-derived cell lines for *in vitro* models of infection, it is important to consider both the site of *in vivo* infection and the origin of the macrophage cells. The IC-21 line was prepared from mouse peritoneal macrophages virally transduced *in vitro* (193). In contrast, the AMJ2-C11 line was virally immortalised from characterised primary mouse alveolar macrophages(194) and readily expresses proinflammatory cytokines when activated (195).

Development of a cell-based model of *M. tuberculosis* infection should take into account the basal alveolar macrophage phenotype and cellular changes associated with chronic disease (187, 188). Here we illustrated the polarity and anti-microbial response of the alveolar and peritoneal macrophage cell lines, AMJ2-C11 and IC-21, during acute mycobacterial infection.

During acute *M. tuberculosis* infection *in vitro*, control of bacterial replication does not appear to be influenced by macrophage origin. THP-1 monocytic cells controlled *M. tuberculosis* load as efficiently as primary human alveolar macrophages over 4 days (196), and MPI cells, a recently derived murine alveolar macrophage line, exhibit a similar infection pattern to THP-1, RAW 264.7, and BMDM cells (197). Likewise, this study shows both AMJ2-C11 and IC-21 cells demonstrated comparable control of BCG and *M. tuberculosis* growth during a 48-hour infection. However, this may not replicate *in vivo* infection completely, as following intranasal infection in mice, alveolar macrophages were more permissive to intracellular *M. tuberculosis* replication than pulmonary interstitial macrophages (198). *Ex vivo* lung and peritoneal macrophages comparably controlled *M. tuberculosis* H37Rv bacterial load up to 3 days, before bacterial growth accelerated in lung macrophages (199). Extended *M. tuberculosis* infection of AMJ2-C11 cells may present similar results.

Cytokine secretion is central to macrophage antimicrobial and anti-inflammatory functions (179), and pro-inflammatory M1 macrophages release cytokines, including TNF and IL-6, that are critical for anti-mycobacterial protection (200). We observed significantly greater IL-6 expression from AMJ2-C11 cells, indicative of the M1-primed polarity seen in alveolar macrophages (186). The alveolar cell line MPI also displays an M1 dominant phenotype, expressing high levels of TNF and IL-6 compared to BMDMs, when infected with *M. tuberculosis* (197). Like AMJ2-C11 cells, human alveolar macrophages are known to express chemokines associated with an M1 phenotype, including MIP-1α, MIP-1β, and RANTES, following *M. tuberculosis* infection (201). Although peritoneal macrophage-derived cell lines can also express these chemokines (192), our results indicate infection-induced chemokine upregulation is delayed (Figure 2.2).

Alveolar macrophage-expressed MCP-1 recruits circulating monocytes during *M. tuberculosis* infection, aiding in bacterial dissemination(202, 203). In the current study avirulent BCG induced higher MCP-1 expression on AMJ2-C11 cells than virulent *M. tuberculosis* H37Rv. Similarly, primary human alveolar macrophages expressed more MCP-1 when infected with avirulent *M. tuberculosis* H37Ra, compared to H37Rv (201). We observed IC-21 cells expressed comparable MCP-1 to AMJ2-C11 cells during BCG infection, but significantly less during *M. tuberculosis* infection. In turn, IC-21 cells expressed more MCP-1 than BMDMs differentiated with M-CSF-containing L929 supernatant (192). Tissue-resident macrophages are difficult to obtain in large numbers from small laboratory animals and mouse bone marrow is commonly used as a source of macrophages *in vitro* due to the quantity of cells generated. Although BMDMs may be a more practical for many laboratories than primary tissue-resident macrophages, basal phenotypic differences like chemokine expression should be considered when planning experimentation.

A number of surface protein markers are regularly used to characterise macrophage polarity, including CD206, CD80, and CD86 (179). The M2 marker CD206 is the mannose receptor, involved in post-infection remediation of inflammation, binding bacterial glycoproteins and heavily glycosylated anti-bacterial proteins such as myeloperoxidase (204). CD206 also facilitates mycobacterial colonisation of macrophages (205). CD80 and CD86 are inflammatory co-receptors required for antigen presentation and T-cell activation (206). Pro-inflammatory M1 macrophages are known to express high levels of CD80 and CD86 (179), whereas only a subset of M2 macrophages express CD86 (207). We found that CD206, CD80, and CD86 levels were all higher for uninfected IC-21 compared to AMJ2-C11. However, whilst IC-21 upregulation of CD206 was notably higher during BCG infection, AMJ2-C11 cells showed significantly more upregulation of CD80 and CD86 during BCG and TB infection. Studies have shown that during acute *M. tuberculosis* infection, alveolar macrophages present an inflammatory phenotype, with high CD86 expression and strong iNOS activity (188), similar to what was shown here with AMJ2-C11 alveolar macrophages. Yet, as the granuloma structures typical of chronic tuberculosis develop, macrophages decrease iNOS activity and upregulate the anti-inflammatory cytokine IL-10 (188). The subdued cytokine expression and weak iNOS

activity of IC-21 cells during *M. tuberculosis* infection suggests these cells may not be an appropriate model of acute macrophage infection in the lung.

Our findings demonstrate that macrophage cell lines of different tissue-origin display marked differences in their response to infection, and this should be considered when utilising cell lines in *in vitro* assays. Mycobacterial infection induced significantly increased cytokine expression and iNOS activity in AMJ2-C11 cells, highlighting the M1/M2 phenotype of their alveolar macrophage origin. In contrast, IC-21 cells, whilst still controlling mycobacterial infection over the time frame of this experiment, displayed a more M2 phenotype, with lower cytokine expression and downregulation of proinflammatory markers. Our work supports the idea that acute *M. tuberculosis* infection models should consider using M1-like macrophages, particularly when using polarity-dependent readouts, such as cytokine expression and surface markers. The development of more alveolar macrophage-representative cell models, like the MPI cell line (197), may also aid future tuberculosis research.

2.6.   Methods
2.6.1 Cell culture

Murine AMJ2-C11 cells of C57BL/6 origin (ATCC, Manassas, VA, USA) were maintained in DMEM (Thermo Fisher Scientific, Waltham, MA, USA) supplemented with 25 mM HEPES, 100 U mL^{-1} penicillin, 100 μg mL^{-1} streptomycin, and 10% foetal bovine serum. Murine IC-21 cells of C57BL/6 origin (ATCC) were maintained in RPMI 1640 medium (Thermo Fisher Scientific) supplemented with 25 mM HEPES, 100 U mL^{-1} penicillin, 100 μg mL^{-1} streptomycin, and 10% foetal bovine serum.

2.6.2 Bacterial cultures

Mycobacterium bovis Bacillus Calmette-Guérin (BCG) Pasteur and *M. tuberculosis* H37Rv were grown in Middlebrook 7H9 broth (BD Biosciences, Franklin Lakes, NJ, USA) supplemented with 5 g L^{-1} bovine serum albumin (BSA), 2 g L^{-1} glucose, 4 mg L^{-1} catalase, 0.2% glycerol, and 0.05% Tween 20. Cell concentration was routinely determined by OD at 600 nm. CFU was determined by plating serial dilutions on Middlebrook 7H11 agar

(BD Biosciences) supplemented with 5 g L^{-1} BSA, 2 g L^{-1} glucose, 4 mg L^{-1} catalase, 500 mg L^{-1} oleic acid, and 0.5% glycerol, and incubating for 3 weeks at 37 °C.

2.6.3 Macrophage infections with mycobacteria

AMJ2-C11 and IC-21 cells were stimulated with 100 U mL^{-1} IFN-γ (R&D Systems, Minneapolis, MN, USA) and infected with BCG or *M. tuberculosi*s at a multiplicity of infection of 5 or 1, respectively. Cells were washed after 4-6 hours to remove extracellular bacteria. At time points from 0-48 h post-infection, supernatant was removed for cytokine and nitrite quantification. Cells were lysed with 0.1% Triton X-100 solution for CFU determination. Lysates were plated on 7H11 agar and incubated at 37 °C for 21 days to determine CFU.

2.6.4 Cytometric bead array

The concentrations of IL-6, TNF, MCP-1, MIP-1α, MIP-1β, and RANTES in supernatants were determined by cytometric bead array (BD Biosciences) according to the manufacturer's protocol. Data were analysed using FCAP Array software (BD Biosciences).

2.6.5 Nitrite assay

Nitrite concentrations of supernatant samples were determined using Griess reagent, consisting of 3.85 mM *N*-(naphthyl)ethylenediamine dihydrochloride (Sigma-Aldrich, St. Louis, MO, USA), 58 mM sulphanilamide (Sigma-Aldrich), and 0.4 M phosphoric acid (Sigma-Aldrich) in water. Nitrite standards were prepared using Sodium nitrite (Sigma-Aldrich). Griess reagent was added to supernatant samples at a ratio of 1:1, and the immediate colour change was quantified by measuring absorbance at 550 nm using a FLUOstar plate reader (BMG Labtech, Ortenberg, Germany).

2.6.6 Flow cytometry

AMJ2-C11 and IC-21 cells were assessed by flow cytometry before infection and 24 hours after infection with BCG or *M. tuberculosis*. Cells were incubated with Fc Block (BD Biosciences) for 30 minutes and then stained with fluorochrome-labelled antibodies (see Supplementary table 1 for a list of antibodies, clones, fluorochromes, and manufacturers) for 30 minutes at room temperature in the dark. Stained samples were fixed with 10% neutral buffered formalin (Fronine, NSW, Australia). Data acquisition was

performed on a BD Fortessa X20 using the BD FACS Diva software (BD Biosciences). Compensation and data analysis were performed in FlowJo v10 software (BD Biosciences). Cells were gated using forward scatter and side scatter to remove debris and dead cells (see Supplementary figure 2 for an example dot-plot). The expression of surface markers is presented as fold MFI difference. This is calculated as a ratio of individual surface marker expression on infected cells (BCG or *M. tuberculosis*) compared to uninfected cells, or on AMJ2-C11 cells compared to IC-21 cells, both infected (BCG and *M. tuberculosis*) and uninfected.

2.6.7 Cell viability

Macrophage viability was confirmed using a resazurin assay for mitochondrial activity. Macrophages were incubated with 5.5 mM resazurin (Sigma Aldrich) for 3 h at 37 °C. Conversion of resazurin to resorufin was evaluated by measuring fluorescence using a FLUOstar plate reader, excitation at 550 nm, emission at 590 nm.

2.6.8 Statistical analysis

GraphPad Prism (GraphPad Software, San Diego, CA, USA) was used for statistical analyses. CFU and cytokine concentration over time were compared by two-way analysis of variance with multiple comparisons post-test, corrected using the Šidák method. Nitrate concentration and flow cytometry MFI were compared using Student's *t*-test, corrected for multiple comparisons using the Holm-Šidák method.

2.7. Acknowledgements

CHAPTER 3

General materials and methods

Chapter 3. General materials and methods

3.1.   Materials

3.1.1 General solutions

- **Phosphate buffered saline (PBS):** Prepared in deionised water from 10X DPBS solution (Gibco).

- **PBS/Heparin**: PBS with 20 U/ml Heparin (Sigma).

- **FACS wash**: PBS supplemented with 2% foetal bovine serum (FBS) (Hyclone), and 2 mM EDTA (Sigma).

- **ACK lysis buffer**: 15 nM NH_4Cl (Biochemicals), 10 mM $KHCO_3$ (Sigma), and 127 µM EDTA dissolved in deionised water, adjusted to pH 7.4.

- **0.1% Triton solution**: 0.1% v/v Triton^{TM} X-100 (Sigma) dissolved in water.

- **Resazurin solution**: 2 mM resazurin sodium salt (Sigma), dissolved in PBS and sterilised by 0.2 µm filtration.

- **Polyethenimine (PEI) solution**: 1 g/L polyethylenimine (linear, average M_n 20000) hydrochloride salt (Sigma) dissolved in deionised water, adjusted to pH 7.4.

3.1.2 Bacterial culture media

- **Oleic acid albumin dextrose catalase (OADC) enrichment**: 50 g/L bovine serum albumin (BSA) (Moregate Biotech), 20 g/L dextrose (Sigma), 40 mg/L catalase (Sigma), 150 mM NaCl (Sigma), and 1.6 mM oleic acid (Sigma) in water. Solution was sterilised by 0.2 µm filtration.

- **Albumin dextrose catalase (ADC) enrichment**: 50 g/L BSA, 2 g/L dextrose, and 4 mg/L catalase in water. Solution was sterilised by 0.2 µm filtration.

- **7H9 media**: 4.7 g/L Middlebrook 7H9 broth powder (BD Biosciences), 0.2% v/v glycerol (Sigma), 0.05% v/v Tween 80 (Sigma) in water. Media is then autoclaved before the addition of 10% v/v ADC. When culturing *M. avium*, 7H9 media can also be supplemented with 0.05% v/v Tyloxapol (Sigma) to prevent bacteria clumping.

- **7H10 agar**: 19 g/L 7H10 agar base (BD Biosciences), 0.5% v/v glycerol in water. Media was autoclaved before the addition of 10% v/v OADC.

- **7H11 agar**: 19 g/L Seven H11 agar base (BD Biosciences), 0.5% v/v glycerol in water. Media was autoclaved before the addition of 10% v/v OADC.

- **Lysogeny broth (LB)**: 20 g/L LB Broth, Lennox (Beckton Dickinson), dissolved in water and sterilised by autoclaving.

- **LB agar**: 35 g/L LB Broth with agar, Lennox (Sigma), dissolved in water and sterilised by autoclaving.

3.1.3 Bacteria

Mycobacterium tuberculosis H37Rv was supplied by BEI Resources (USA). *Mycobacterium avium* 104 lab strain obtained from Dr Luiz Bermudez, The Kuzell Institute, San Francisco. *Listeria monocytogenes* was obtained from Christina Cheers, University of Melbourne.

To prepare the Heat-killed Listeria, *L. monocytogenes* culture in LB was incubated at 80 °C for 1 h. Heat-killed Listeria was stored at -80 °C, and resuspended in PBS or tissue media before use.

3.1.4 Animals

Wild type C57BL/6 mice were obtained from Australian BioResources (Mossvale). The tuberculosis model in C57BL/6 mice has been thoroughly investigated in published literature, providing a good platform for novel investigations of miRNA in this infection. The wealth of antibody reagents available for C57BL/6 mice allows for in depth flow cytometric analysis of the immune response to both *M. tuberculosis* and *L. monocytogenes*.

The miR-652$^{-/-}$ mouse line was generated on a C57BL/6 background, under a commercial arrangement with the Garvan Institute. The gene *Mir652* was deleted by CRISPR/Cas9 mutagenesis and the deletion validated by genomic sequencing. All mice were housed in the Centenary Institute Animal House according to standard husbandry conditions, as stated in animal ethics protocols 2018-001 and 2021-001.

3.1.5 Cell lines

The IC-21 murine peritoneal macrophage cell line was obtained from ATCC (Manassas, USA). The HEK-293T human embryonic kidney cell line was a generous gift from Edward Ni.

3.1.6 Plasmids

pIS0 was a gift from David Bartel (Addgene plasmid # 12178; http://n2t.net/addgene:12178; RRID:Addgene_12178). pIS0 is a reporter plasmid containing firefly luciferase under an SV40 promoter (Figure A 1), with restriction sites upstream of the SV40 poly(A) signal sequence for insertion of a 3' untranslated region (3'UTR) of interest (208). Oligonucleotides containing the *Mus musculus Capzb* 3'UTR were purchased from IDT DNA with added 5' and 3' restriction sites for SacI and XbaI, respectively (Table 3.1). The *Capzb* 3'UTR wild type fragment was inserted into pIS0 to generate pIS0-Capzb-WT (Figure A 2). The *Capzb* 3'UTR mutant fragment, with a mutant sequence in place of an *in silico*-predicted miR-652 binding site, was inserted into pIS0 to generate pIS0-Capzb-mut (Figure A 3).

Table 3.1. Oligonucleotide gene fragments for insertion into pIS0. Gene fragments contain the murine Capzb 3' untranslated region with 5' and 3' restriction sites (underlined) and a wild type or mutant miR 652 predicted target sequence (bold and underlined).

Oligonucleotide	Sequence
Capzb 3'UTR wild type	GTA <u>GAG CTC</u> GTC TGT GCA GAC GTT TGC AGA CAA ATC AAA GCA AGA AGC GCT TAA GAA CGA CCT GGT GGA GGC CTT GAA GAG AAA GCA GCA GTG TTG AAG ACC TCT GCT TCA CGC TAA CCG GAC ACG CCA TGC ACT CGT TAG GTT CCT TTC TTT AGA AAA CTC GTT TTC TGC TCC TTT TCC CTC TTC CTT TCC CGC CCT GAC AGG TCA CAT AAC AGT TTG CAT CGA CCA CGC A**<u>GC GCC AT</u>**C TCT CCC CCA AAA TAA AGT CCG ATA ACC ACC CTC CTC TGG CTC CAA GGC CTG CTT CCC ACG ACG TTT CCA TAG AGA CCG TGT GGT TTT GTT CGC CTG TCC CCC TTC CTT CCC TTG CCC ATT TAT AGG CAC AGA TAC ACT GTC TGA CAC CGC TCC CTC CAT CTT TTT GTT ACA TTG GTG TAA AAA ATG TAA AAC AAA AAA TTT TAT GAA CTA ACT GGT GTG TGA GAG AAG AAA CTG GAG ATC TGA TCC GTG TGT GTG TGG GAG TTG CTT GGA GTC AGG GCT GGG GAC AGG GGA CAG CAG TGG AGG AAG GAG TGA TGT CCT CAG CAC TGT CCT GCA CAG GTG GAC CCT TGT CCC AAG GAG ACC ATG CTG GGG TGG GGT GGG GCT GGC GAC CGG CTG CTC TTC AGG CCA GGT GCT TTT CTG TCA ATT TTT ATG GAA TGC AAA AGG AGT TTT TTG TTT TAT TTT GGT TTT TTT TTG TAA AGC TTA AAC AGA CAA AAA AAT CTA CAT CTT CTA CTT GAG CCT CCA TAC TTA <u>TCT AGA</u> CGT TA
Capzb 3'UTR mutant	TAA GTA <u>GAG CTC</u> GTC TGT GCA GAC GTT TGC AGA CAA ATC AAA GCA AGA AGC GCT TAA GAA CGA CCT GGT GGA GGC CTT GAA GAG AAA GCA GCA GTG TTG AAG ACC TCT GCT TCA CGC TAA CCG GAC ACG CCA TGC ACT CGT TAG GTT CCT TTC TTT AGA AAA CTC GTT TTC TGC TCC TTT TCC CTC TTC CTT TCC CGC CCT GAC AGG TCA CAT AAC AGT TTG CAT CGA CCA CGC A**<u>CG CGG TA</u>**C TCT CCC CCA AAA TAA AGT CCG ATA ACC ACC CTC CTC TGG CTC CAA GGC CTG CTT CCC ACG ACG TTT CCA TAG AGA CCG TGT GGT TTT GTT CGC CTG TCC CCC TTC CTT CCC TTG CCC ATT TAT AGG CAC AGA TAC ACT GTC TGA CAC CGC TCC CTC CAT CTT TTT GTT ACA TTG GTG TAA AAA ATG TAA AAC AAA AAA TTT TAT GAA CTA ACT GGT GTG TGA GAG AAG AAA CTG GAG ATC TGA TCC GTG TGT GTG TGG GAG TTG CTT GGA GTC AGG GCT GGG GAC AGG GGA CAG CAG TGG AGG AAG GAG TGA TGT CCT CAG CAC TGT CCT GCA CAG GTG GAC CCT TGT CCC AAG GAG ACC ATG CTG GGG TGG GGT GGG GCT GGC GAC CGG CTG CTC TTC AGG CCA GGT GCT TTT CTG TCA ATT TTT ATG GAA TGC AAA AGG AGT TTT TTG TTT TAT TTT GGT TTT TTT TTG TAA AGC TTA AAC AGA CAA AAA AAT CTA CAT CTT CTA CTT GAG CCT CCA TAC TTA <u>TCT AGA</u> CGT TA

3.1.7 miRNA mimics

mirVana mmu-miR-652 and mmu-miR-146a mimic nucleotides were purchased from Thermo Fisher. A mirVana miRNA mimic negative control #1 was also purchased from Thermo Fisher. Lyophilised mimics were resuspended in nuclease-free water at 100 µM and stored at -30 °C in small aliquots. Thawed aliquots were discarded after use.

3.1.8 Tissue culture media

- **Bone marrow-derived macrophage (BMDM) media**: RPMI 1640 media (Gibco) supplemented with 10% v/v FBS, and 46 µM 2-mercaptoethanol (Sigma).

- **BMDM differentiation media**: RPMI 1640 media supplemented with 10% v/v FBS, and 46 µM 2-mercaptoethanol, 110 pM recombinant mouse GM-CSF (Peprotech), 100 U/ml penicillin (Gibco), and 100 µg/ml streptomycin (Gibco).

- **Tissue media**: RPMI 1640 supplemented with 10% v/v FBS, 100 U/ml penicillin, and 100 µg/ml streptomycin, and 46 µM 2-mercaptoethanol.

- **IC-21 media**: RPMI-1640 media supplemented with 10% v/v FBS.

- **HEK-293T media**: DMEM media (Gibco) supplemented with 10% v/v FBS.

3.1.9 Western blotting solutions

- **Tris-buffered saline tween (TBST)**: 10 mM Tris (ChemSupply Australia), 150 mM NaCl (ChemSupply Australia), and 0.05% v/v Tween 20 (Sigma) dissolved in deionised water, adjusted to pH 8.0.

- **Transfer buffer**: 25 mM Tris, 192 mM glycine (ChemSupply Australia), 10% v/v methanol (Sigma) in deionised water.

- **Blocking buffer**: 10 mM Tris, 150 mM NaCl, 0.05% v/v Tween 20, and 50 g/L BSA dissolved in deionised water, adjusted to pH 8.0.

- **Stripping buffer**: 200 mM glycine, 3.45 mM sodium dodecyl sulphate (SDS) (Oxoid), and 0.5% v/v Tween 20 dissolved in deionised water, adjusted to pH 2.2.

3.1.10 Western blot staining antibodies

All western blot staining antibodies listed in Table 3.2 were diluted 2000-fold in blocking

buffer before use.

Table 3.2. Antibodies used in western blot staining procedure.

Target protein	Antibody	Manufacturer	Catalogue #
GAPDH	GAPDH (D16H11) XP® Rabbit mAb	Cell signalling technology	5174S
p-AKT	Phospho-Akt (Ser473) (D9E) XP® Rabbit mAb	Cell signalling technology	4060S
p-mTOR	Phospho-mTOR (Ser2448) (D9C2) XP® Rabbit mAb	Cell signalling technology	5536S
AKT	Akt Antibody	Cell signalling technology	9272S
mTOR	mTOR (7C10) Rabbit mAb	Cell signalling technology	2983S
β-Actin	Beta-Actin (13E5) Rabbit mAb	Cell signalling technology	4970S
CAPZB	CAPZB Rabbit PolyAb	Proteintech	25043-1-AP
Rabbit IgG	Anti-rabbit IgG, HRP-linked Antibody	Cell signalling technology	7074S

3.1.11 Primer oligonucleotides for RT-qPCR

All mRNA primer oligonucleotides listed in Table 3.3, and all miRNA primer
oligonucleotides listed in Table 3.4, were purchased from Integrated DNA Technologies
(Carolville, IO, US) and stored in nuclease-free water at -20 °C. The mmu-miR-652-3p
qPCR primer was purchased from GeneCopoeia.

Table 3.3. Primers sequences used in mRNA qPCR reactions.

Target gene	Primer	Sequence
Capzb	Forward	ACA AAA TCC GAA GCA CGC TG
	Reverse	GTG GTT GTC GGG GAT AGC AT
Ctsz	Forward	TGT CAA CTA TGC CAG CGT CA
	Reverse	TTG ATG TTG ATT CGG TCT GCC
Ctsd	Forward	CTT GTG AGA AGG TGT CCA GC
	Reverse	CAC CCT GCG ATA CCT TGA GTA
Ctsb	Forward	GAA GCC ATT TCT GAC CGA ACC
	Reverse	CAC CAT TAC AGC CGT CCC
Pgd	Forward	CAT GCC CGT CAC CCT CAT T
	Reverse	GGA CCC TTC AGC TTT TGG CT
G6pdx	Forward	CAA GAG ACC TGC ATG AGT CAG A
	Reverse	TGT GGT TCG ACA GTT GAT TGG A
Gpi1	Forward	TTG TCG CCC TGT CTA CGA AC
	Reverse	AGT CCA ATG GCT GAC CAC AG
Pfkl	Forward	CTA CGT GAA GGA TCT GGT GGT
	Reverse	GGA TTC GGT CGA AGG CTG AA
Tkt	Forward	CCC TGA AGG ACA CAG CCA AT
	Reverse	ACA GGA CAG CCA TGA TCT CG
Taldo1	Forward	GCC GAC ACG GGT GAT TTC AA
	Reverse	CTT GGT AGG CAG GCA TCT GG
Isg15	Forward	TCT GAC TGT GAG AGC AAG CAG
	Reverse	ACC TTT AGG TCC AGG CCC ATT
Ifnb1	Forward	TGG GAG ATG TCC TCA ACT GC
	Reverse	CCA GGC GTA GCT GTT GTA CT
Stx5a	Forward	GAA ACA GCA GAG GAA CCG TC
	Reverse	AAT TAT GGG ACC ACC TCC AAG G
Jag1	Forward	CCT GCG AGC CAA GGT GTG
	Reverse	CTC CAC CAC AAC AGT TCC CA
Notch1	Forward	AAG TGG GAC CTG CCT GAA TG
	Reverse	GAT TGG AGT CCT GGC ATC GT
Notch2	Forward	GCC GTG GGG CTG AAA AAT CT
	Reverse	GGC TGG GGT CCT TCA TCA TC

Table 3.4. Forward primer sequences used in miRNA qPCR reactions.

Target miRNA	Sequence
RNU6	CGC AAG GAT GAC ACG CAA AT
miR-146a-5p	GCA GTG AGA ACT GAA TTC CA
miR-652-3p	Unknown, proprietary

3.1.12 Flow cytometry staining antibodies

The antibodies listed in Table 3.5 were used for extracellular and intracellular cell staining, for flow cytometry experiments. Live/Dead differential staining was performed using LIVE/DEAD Fixable Blue Dead Cell Stain (Invitrogen).

Table 3.5. Fluorescent antibodies for flow cytometry staining.

Target marker	Fluorophore conjugate	Antibody clone	Manufacturer
CD103	APC	M290	BD Biosciences
CD11b	AF700	M1/70	Biolegend
CD11b	BB515	M1/70	BD Biosciences
CD11c	BV421	N418	BD Biosciences
CD11c	PE/Cy7	HL3	BD Biosciences
CD24	PE-CF594	M1/69	BD Biosciences
CD4	APC	GK1.5	eBioscience
CD4	BV510	RM4-5	BD Biosciences
CD44	FITC	IM7	BD Biosciences
CD44	FITC	IM7	BD Biosciences
CD45	AF700	30-F11	BD Biosciences
CD45.2	Pacific Blue	104	Biolegend
CD45.2	PerCP-Cy5.5	104	Biolegend
CD45.2	V450	104	BD Biosciences
CD45R/B220	FITC	RA3-6B2	BD Biosciences
CD45R/B220	PerCP-CyTM5.5	RA3-6B2	BD Biosciences
CD62L	APC/Cy7	MEL-14	Biolegend
CD62L	BV786	MEL-14	BD Biosciences
CD69	BV605	H1.2F3	BD Biosciences
CD69	BV786	H1.2F3	BD Biosciences
CD69	PE	H1.2F3	BD Biosciences
CD8	AF700	53-6.7	Biolegend
CD8	PE	53-6.7	BD Biosciences
CD8	PECy5	53-6.7	Biolegend
CD8	PerCP-Cy5.5	53-6.7	BD Biosciences
IFN-y	PE	XMG1.2	BD Biosciences
IL-17A	PE-CF594	TC11-18H10	BD Biosciences
IL-2	BV421	JES6-5H4	BD Biosciences
KLRG1	APC	2F1	BD Biosciences
Ly-6C	BV605	AL-21	BD Biosciences
Ly-6C	PerCP-Cy5.5	O4-46	BD Biosciences
Ly-6G	APC	RB6-8C5	Biolegend
Ly-6G	BV786	1A8	BD Biosciences
Ly-6G	PerCP-Cy5.5	1A8	Biolegend
MHC-II	APC	M5/114.15.2	Biolegend
MHC-II	BV510	2G9	BD Biosciences
MHC-II	PE	M5/114.15.2	Biolegend
Siglec-F	PE	E50-2440	BD Biosciences
TNF	APC	MP6-XT22	BD Biosciences

3.1.13 Flow cytometer

Flow cytometry data acquisition was performed on a Fortessa X20 instrument (Becton Dickinson). The lasers and detectors of the Fortessa X20 instrument are detailed in Table 3.6.

Table 3.6. Fortessa X20 lasers and detectors.

Laser colour	Laser wavelength (nm)	Detector	Detector wavelength (nm)	Detector bandwidth (nm)	Typical fluorophore
UV	355	UV379_C	379	28	BUV395
		UV450_B	450	50	Hoescht
		UV740_A	740	41	BUV737
Violet	405	V450_F	450	50	BV421
		V525_E	525	50	BV510
		V605_D	605	12	BV605
		V655_C	655	8	BV650
		V710_B	710	50	BV711
		V810_A	810	60	BV786
Blue	488	SSC	488	10	-
		B530_B	530	30	FITC
		B695_A	695	30	PerCP-Cy5.5
Yellow/Green	561	YG582_D	582	15	PerCP-Cy5.5
		YG610_C	610	20	PE-AF610
		YG670_B	670	30	PE-AF647
		YG780_A	780	60	PE-Cy7
Red	640	R670_C	670	15	APC
		R730_B	730	45	AF700
		R780_A	780	60	APC-Cy7

3.1.14 Reagents for protein isolation and processing

- **Reconstitution buffer**: 1% SDS, 0.1 M HEPES (Gibco), 1X c0mplete protease inhibitors (Thermo Fisher), 34 U/ml benzonase endonuclease (Sigma), in deionised water, adjusted to pH 8.0.

- **Tris(2-carboxyethyl)phosphine (TCEP) solution**: 250 mM TCEP-HCl (Sigma) in deionised water, adjusted to pH 7.0.

- **Acrylamide solution**: 1 M acrylamide monomers (Sigma) in deionised water.

- **Dithiothreitol (DTT) solution**: 1M DTT (Sigma) in water.

- **AMBIC**: 200 mM Ammonium bicarbonate (Sigma) in water.

- **SP3 bead mixtures**: 25 mg/ml hydrophilic and 25 mg/ml hydrophobic SpeedBead™ Magnetic Carboxylate Modified Particles (GE Healthcare).

- **10% trifluoroacetic acid (TFA):** 10% v/v TFA (Honeywell) in deionised water.

- **Isopropanol/1% TFA:** 1% v/v TFA in isopropanol (Honeywell).

- **Elution solvent**: 1M NH_4OH (Sigma), 70% acetonitrile (Honeywell), dissolved in deionised water.

- **MS loading solvent**: 2% v/v acetonitrile, 0.2% v/v formic acid (Honeywell), in deionised water.

To generate STAGE-Tips for protein clean-up procedures, a blunt needle is used to punch an SDB-RPS (Sigma) disk, which is forced into a standard plastic 200 µl pipette tip. A hole is formed in the lid of a 2 ml tube, for the tube to act as a holder and filtrate reservoir for the STAGE-tip during centrifugation steps.

3.2.   Methods
3.2.1 Mammalian cell line tissue culture

IC-21 adherent cultures were maintained in IC-21 media and incubated at 37 °C, 5% CO_2. Cultures were passaged twice weekly and kept below 1 x 10^6 cells/ml. To passage, adherent cultures were washed twice with PBS and treated with trypsin-EDTA solution (Sigma), incubating at 37 °C for 10 min. IC-21 media was added to deactivate trypsin before cells were counted and passaged at the desired concentration. For long term storage, IC-21 cells were resuspended in RPMI-1640 media supplemented with 10% v/v FBS, and 5% v/v dimethyl sulphoxide (Amresco). Cells were frozen at -80 °C overnight in a CoolCell controlled cooling apparatus (BioCision) before transfer to vapour phase liquid nitrogen storage.

HEK-293T adherent cultures were maintained in HEK-293T media and incubated at 37 °C, 5% CO_2. Cultures were passaged 2-3 times weekly and kept below 2 x 10^6 cells/ml. To passage, adherent cultures were washed twice with PBS and treated with

trypsin-EDTA solution (Sigma), incubating at 37 °C for 10 min. HEK-293T media was added to deactivate trypsin before cells were counted and passaged at the desired concentration. For long term storage, HEK-293T cells were resuspended in DMEM media supplemented with 10% v/v FBS, and 5% v/v dimethyl sulphoxide. Cells were frozen at -80 °C overnight in a CoolCell controlled cooling apparatus before transfer to vapour phase liquid nitrogen storage.

3.2.2 Bacterial culture

Mycobacterial suspension cultures were maintained in 7H9 medium and incubated at 37 °C, 5% CO_2. Static cultures were prepared in T25 or T75 tissue culture flasks. Culture optical density was measured using the Biophotometer spectrophotometer (Eppendrof), and sustained at less than 0.8 OD through dilution with 7H9. For long term storage, mycobacterial cultures were centrifuged and resuspended in 30% v/v glycerol/PBS, and stored at -80 °C.

Listeria monocytogenes suspension cultures were maintained in LB medium and incubated at 37 °C. Static cultures were prepared in T25 or T75 tissue culture flasks. Cultures were split daily, by dilution with additional LB medium. For long term storage, *L. monocytogenes* cultures were centrifuged and resuspended in 30% v/v glycerol/LB, and stored at -80 °C.

3.2.3 Enumeration of bacterial colony forming units

M. tuberculosis or *M. avium* colony forming units (CFU) were enumerated in supernatant, tissue homogenates, or other suspensions. Samples were serially diluted in sterile deionised water, and 100 µl aliquots plated on 7H10 or 7H11 agar. Solid agar cultures were wrapped in plastic food wrap to minimise contamination, and incubated for 14-21 days at 37 °C with 5% CO_2. After this time, bacterial colonies were counted to calculate the bacterial load in original solutions and homogenised tissues.

L. monocytogenes CFU were enumerated in supernatant, tissue homogenates, or other suspensions. Samples were serially diluted in sterile deionised water, and 100 µl aliquots plated on LB agar. Solid agar cultures were incubated for 24-48 hours at 37 °C in aerobic culture. After this time, bacterial colonies were counted to calculate the bacterial load in original solutions and homogenised tissues.

3.2.4 Tissue homogenisation to determine bacterial load

Liver, spleen, and lung tissues were collected into sterile water and homogenised using an IKA T10 basic ULTRA-TURRAX (IKA-Works) or Polytron (Kinematica) homogeniser. The bacterial load of tissue homogenates was determined as detailed in section 3.2.3. Homogenates were clarified by centrifugation at 2500 rcf for 5 min. Clarified homogenates were stored at -80 °C for later cytokine quantitation.

3.2.5 Histology

Tissue was perfused with 10% neutral buffered formalin and fixed by submersion in 10% neutral buffered formalin for 6 months. Tissue segments were paraffin embedded and 5 µm sections stained with haematoxylin and eosin by Veterinary Pathology Diagnostic Services, Sydney School of Veterinary Science, University of Sydney. Stained sections were imaged using the Axioscan (Zeiss) slide-scanning bright field microscope and the BX51 (Olympus) bright field inverted microscope.

3.2.6 Tissue dissociation to single cells for flow cytometry

Lung tissue from *M. tuberculosis*-infected mice was dissociated to single cells using the gentleMACS Dissociator (Miltenyi). Initial dissociation was performed using the LUNG_01 setting. Dissociated tissue was supplemented with 13 µg/ml DNase (Sigma) and 50 U/ml collagenase IV (Sigma), and then incubated for 30 min at 37 °C with rolling agitation. A second dissociation was performed with the gentleMACS LUNG_02 setting. The cell suspension was passed through a 70 µm cell strainer. Cells were centrifuged at 500 rcf for 5 min. The cell pellet was resuspended in 1 ml ACK lysis buffer for 1 min to lyse red blood cells. Cells were immediately diluted 10-fold with tissue media to halt cell lysis. Cells were centrifuged at 500 rcf for 5 min, and the cell pellet resuspended in 1 ml tissue media. Cells were counted and diluted in tissue media as required for flow cytometry staining.

The mediastinal lymph node of *M. tuberculosis*-infected mice was forced through a 70 µm cell strainer using a syringe plunger, generating a single-cell suspension for flow cytometry staining. Cells were centrifuged at 500 rcf for 5 min, and the cell pellet resuspended in 1 ml tissue media. Cells were counted and diluted in tissue media as required for flow cytometry staining.

Spleen tissue from *L. monocytogenes*-infected mice was perfused with tissue media to dislodge cells. All suspended cells and remaining tissue were forced through a 70 μm cell strainer using a syringe plunger, generating a single-cell suspension for flow cytometry staining. Cells were centrifuged at 500 rcf for 5 min. The cell pellet was resuspended in 1 ml ACK lysis buffer for 1 min to lyse red blood cells. Cells were immediately diluted 10-fold with tissue media to halt cell lysis. Cells were centrifuged at 500 rcf for 5 min, and the cell pellet resuspended in 1 ml tissue media. Cells were counted and diluted in tissue media as required for flow cytometry staining.

3.2.7   Flow Cytometry
3.2.7.1   Surface antigen staining

Single cell suspensions of 5×10^5-1×10^6 mouse cells were added to a 96-well round-bottom assay plate (Corning) and centrifuged at 500 rcf for 5 min. Pelleted cells were resuspended in 50 μl Mouse Fc Block^{TM} (Becton Dickinson, diluted 300-fold in FACS wash), and incubated at room temperature in the dark for 30 min with shaking. Fluorescent antibody stains in FACS wash were added to each well (50 μl/well) and incubated at room temperature in the dark for 30 min with shaking. Stained cells were centrifuged at 500 rcf for 5 min. The cell pellet was resuspended in 100 μl 10% neutral buffered formalin to fix cells. *M. tuberculosis*-infected cells were incubated in formalin at room temperature in the dark for at least one hour to kill any remaining bacteria before removal from the physical containment level 3 (PC3) facility. Flow cytometry analysis was performed on the Fortessa X20 instrument. Collected FCS data was analysed using FlowJo software version 10.5.0 (Becton Dickinson).

3.2.7.2   Intracellular staining

Mouse spleen cells from *L. monocytogenes*-infected mice were plated in a 24-well flat-bottom plate (Corning) in tissue media. Each well was stimulated with 2×10^7 CFU/ml heat-killed Listeria for 2 h at 37 °C, 5% CO_2. Brefeldin A (Sigma) was added to each well at 10 μg/ml and the plate incubated at 37 °C overnight. Cells were pelleted by centrifugation at 500 rcf for 5 min, resuspended in 200 μl FACS wash, and transferred to a 96-well round bottom plate.

Cells were pelleted and resuspended in 50 μl Mouse Fc Block™ (diluted 300-fold in FACS wash), and then incubated at room temperature in the dark for 30 min with shaking. Cell surface markers were stained with a surface marker antibody panel (50 μl/well), shaking at room temperature in the dark for 30 min. Cells were pelleted by centrifugation at 500 rcf for 5 min, and resuspended in 100 μl Cytofix/Cytoperm buffer (BD Biosciences). Cells were incubated at room temperature in the dark for 30 min with shaking, before cells were washed twice with 200 μl Perm/Wash buffer (BD Biosciences), centrifuging at 500 rcf for 5 min each wash. Intracellular markers were stained with an intracellular marker antibody panel (50 μl/well), shaking at room temperature in the dark for 30 min. Stained cells were washed twice with 200 μl Perm/Wash buffer, centrifuging at 500 rcf for 5 min each wash, then resuspended in 150 μl 10% neutral buffered formalin for fixation. Flow cytometry analysis was performed on the Fortessa X20 instrument. Collected FCS data was analysed using FlowJo software version 10.5.0.

3.2.8 Resazurin metabolic activity assay

A resazurin assay was run to determine the metabolic activity of *in vitro* mammalian and bacterial cultures in a 96-well flat-bottom culture plate. All culture supernatant was removed and replaced with 200 μl BMDM media. Resazurin solution was added to each well to a final 50 μM concentration, and the plate incubated at 37 °C for 3 h. A 150 μl aliquot was then taken from each well and transferred to a new 96-well flat-bottom plate. Fluorescence was read using the FLUOstar plate reader (BMG Labtech); excitation at 550 nm, emission at 590 nm.

3.2.9 Cytometric bead array cytokine assay

Supernatant from infected macrophages was collected to analyse cytokine concentrations. Quantitation of IL-6, TNF, MIP-1α, and KC concentration was performed by cytometric bead array (CBA) (Becton Dickinson).

Clarified liver and spleen homogenates from infected mice were analysed for IL-6 and TNF concentration by CBA. All tissue homogenate samples were diluted 1:1 with CBA assay diluent (Beckton Dickinson). Cytokine standard titrations were prepared in control 50% tissue homogenate solutions, generated from the relevant tissues of uninfected mice.

All CBA assays were run according to the manufacturer's protocol, detailed briefly here. Required fluorescent capture beads were combined and diluted 100-fold in CBA Capture Bead Diluent (Becton Dickinson). Required fluorescent detection antibody reagents were combined and diluted 100-fold in CBA Detection Reagent Diluent (Becton Dickinson). Kit recombinant cytokine standards were reconstituted in CBA Assay Diluent (Becton Dickinson), giving a stock concentration of 25 ng/ml. Required cytokine standards were combined and diluted 10-fold in CBA Assay Diluent, before serial dilution in CBA Assay Diluent to generate the standard titration.

The wells of a round-bottom 96-well plate were pre-wet by addition and removal of 100 µl CBA Wash Buffer (Becton Dickinson). Standard titration samples and all unknown samples were added to the assay plate (10 µl/well). Capture beads were mixed well by aspiration and 10 µl added to each well. The plate was incubated for 1 hour at room temperature in the dark with shaking. The detection reagent mixture was mixed well by aspiration and 10 µl added to each well. The plate was incubated for 1 hour at room temperature in the dark with shaking. The plate was centrifuged at 2000 rcf for 5 min, and the pelleted beads resuspended in 200 µl 10% neutral buffered formalin to fix samples. *M. tuberculosis*-containing samples were incubated in formalin at room temperature in the dark for at least one hour to kill any remaining bacteria before removal from the PC3 facility.

Flow cytometry analysis was performed on the Fortessa X20 instrument. Unknown cytokine concentrations were determined by interpolation into the standard titration curves using FCAP Array software version 3.0 (Becton Dickinson).

3.2.10 Western blot for protein phosphorylation
3.2.10.1 Assessing protein concentration
Cellular protein was collected from infected BMDMs following lysis with RIPA buffer (Thermo Fisher), supplemented with Halt™ Protease and Phosphatase Inhibitor Single-Use Cocktail (Thermo Fisher). *M. tuberculosis*-containing protein samples were sterilised by 30 min incubation in an 80 °C water bath before removal from the PC3 facility. Sample protein concentrations were determined using a Pierce™ BCA Protein Assay Kit (Thermo Fisher) according to the manufacturer's protocol, detailed briefly here. The kit BSA

standard was serially diluted in deionised water to prepare the standard titration. A 10 µl volume of each unknown protein sample and each standard titration sample was added to the wells of a flat-bottom 96-well plate. The kit BCA reagent, consisting of 1 part kit Reagent A and 50 parts kit Reagent B, was added to each well of the assay plate (100 µl/well). The plate was incubated for 1 hour at 37 °C, before the 562 nm absorbance was measured using the Spark 10M plate reader (Tecan). Unknown protein concentrations were determined by interpolation into the standard titration curve using Prism software version 9.3.1 (Graphpad Software).

3.2.10.2 Separation by gel electrophoresis

In preparation for sodium dodecyl sulphate polyacrylamide gel electrophoresis (SDS-PAGE), 5 µg of each protein sample was diluted in deionised water to a maximum volume of 13 µl, and the supplemented with 5 µl 4X NuPAGE LDS sample loading buffer (Invitrogen) and 2 µl 10X NuPAGE sample reducing agent (Invitrogen). Samples were incubated at 70 °C for 10 min before each 20 µl sample was loaded onto Bolt 10% Bis-Tris Plus gels (Invitrogen), and electrophoresis run at 200 V for 30 min using MOPS SDS running buffer (Invitrogen). The completed SDS-PAGE gel was moved into TBST.

3.2.10.3 Western blot membrane transfer

Western blot transfer was conducted using the Mini Blot Module (Invitrogen), with the transfer stack assembled as indicated in Figure 3.1. Placed on the Mini Blot Module cathode were one sponge soaked in transfer buffer, 3MM Chr blotting paper (GE) soaked in transfer buffer, the SDS-PAGE gel in TBST, a PVDF western blotting membrane (Roche) activated by briefly soaking in methanol (Honeywell), another 3MM Chr blotting paper soaked in transfer buffer, and one sponge soaked in transfer buffer. The anode cover was added, and then the blotting module filled with transfer buffer and run at 10 V for 70 min.
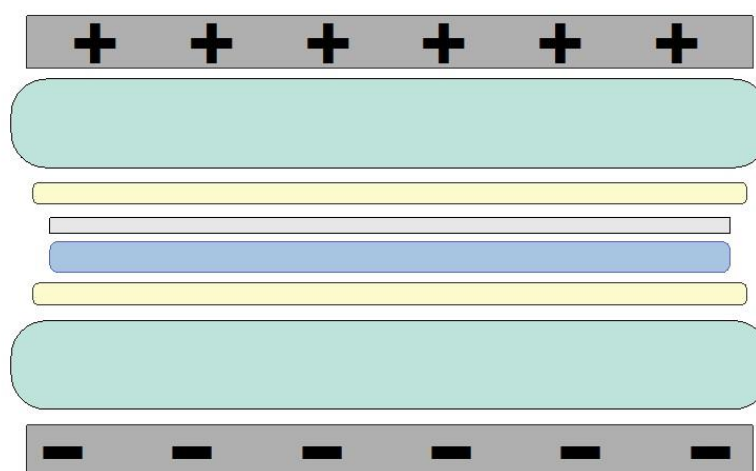
Figure 3.1. The western blot transfer stack. Components of the stack are assembled in ascending order: the Mini Blot Module cathode, sponge soaked in transfer buffer (green), blotting paper soaked in transfer buffer (yellow), SDS-PAGE gel in TBST (blue), PVDF membrane in methanol (grey), blotting paper soaked in transfer buffer, sponge soaked in transfer buffer, and the Mini Blot module anode.

3.2.10.4 Antibody staining and stripping

Before antibody staining, blot membranes were blocked by 3 h room temperature incubation in blocking buffer. Rabbit primary antibodies (Table 3.2) were diluted 2000-fold in blocking buffer and incubated with the blot for 16 h at 4 °C, with constant rolling agitation. The primary antibodies were removed and the blots washed 3 times with TBST, 5 min each wash with constant rolling agitation. The horse radish peroxidase-conjugated anti-rabbit IgG secondary antibody (Table 3.2) was diluted 2000-fold in blocking buffer and incubated with the blots for 1 h at room temperature, with constant rolling agitation. The secondary antibody was removed and the blots washed twice with TBST, 10 min each wash with constant rolling agitation. Blots were imaged using the Amersham Imager 600 (GE Healthcare) and Pierce™ ECL Western Blotting Substrate (Thermo Fisher).

Staining antibodies were stripped from blots by two 5 min washes with stripping buffer, followed by two 5 min washes with PBS, and then two 5 min washes with TBST. Stripped blots were re-blocked by 3 h room temperature incubation in blocking buffer, before antibody re-staining.

All blots stained for AKT and mTOR activation were initially stained for phosphorylated AKT (p-AKT), phosphorylated mTOR (p-mTOR), and the housekeeper protein GAPDH. Each blot was then stripped, and stained for total AKT, total mTOR, and GAPDH.

3.2.10.5 Western blot band quantitation

Amersham Imager 600 output blot images were converted from 16-bit TIFF to 8-bit TIFF format using ImageJ software version 2.3.0 (209). Band quantitation was performed using GelAnalyzer software version 19.1 (www.gelanalyzer.com) by Istvan Lazar Jr., PhD and Istvan Lazar Sr., PhD, CSc. Lane background was subtracted using the rolling ball technique, with peak width tolerance 10% of lane length. Peaks were detected automatically or drawn manually when required. To normalise for protein loading, all AKT and mTOR band volumes were divided by the respective GAPDH band volume. Protein activation results for AKT and mTOR were calculated as phosphorylated protein divided by total protein. To normalise for CAPZB protein loading, all CAPZB band volumes were divided by the respective β-Actin band volume.

3.2.11 RNA purification

Infected mouse cells were lysed with TRIzol reagent (Bioline) and snap frozen at -80 °C. RNA was purified from TRIzol samples using Direct-zol RNA Miniprep Plus kits (Zymo Research) and the manufacturer's protocol, detailed briefly here.

The TRIzol samples were diluted 1:1 with 100% ethanol (Sigma) and mixed thoroughly. Samples were transferred into the kit's Zymo-spin IIC column (Zymo Research) and centrifuged at 16000 rcf for 30 s. Centrifugation was repeated with remaining sample volume for samples larger than 350 µl. Then 400 µl RNA Wash Buffer (Zymo Research) was added and the column centrifuged at 16000 rcf for 30 s. DNase treatment was performed to remove any DNA contaminant. Lyophilised DNase I (Zymo Research) was reconstituted in deionised water to 6 U/µl. A 5 µl aliquot of DNase I solution was added to 75 µl DNA Digestion Buffer (Zymo Research), and the entire mixture added to the spin column for 15 min at room temperature to digest DNA. A 400 µl volume of RNA PreWash (Zymo Research) was added to the column and centrifuged at 16000 rcf for 30 s. This wash was repeated. Afterwards 700 µl RNA Wash Buffer was added to the column and centrifuged at 16000 rcf for 2 min. The spin column was transferred to a new 1.5 ml

Eppendorf tube. 30 μl DNase/RNase-Free Water (Zymo Research) was added directly to the column membrane, and the column centrifuged at 16000 rcf for 30 s to elute purified RNA.

3.2.12 Determining mRNA expression by quantitative PCR
3.2.12.1 RNA purification and cDNA synthesis from mRNA template

RNA was purified from lysed cells as described in section 3.2.11. Sample RNA concentrations were determined using the NanoDrop One spectrophotometer (Thermo Fisher). Synthesis of cDNA from mRNA was performed using the Superscript™ III Reverse Transcriptase system. To prepare for cDNA synthesis, the RNA sample, dNTP mix, and oligo(dT) primer were mixed (Table 3.7). Mixtures were incubated in the Mastercycler thermocycler (Eppendorf) for 5 min at 65 °C, then for 1 min at 4 °C. The First Strand buffer, DTT and Superscript™ III Reverse Transcriptase were then added to the mixture (Table 3.7). The cDNA synthesis reaction was performed in the Mastercycler thermocycler, incubating at 37 °C for 60 min, 85 °C for 5 min, and then held at 4 °C.

Table 3.7. cDNA synthesis reaction for messenger RNA template.

Reagent	Manufacturer	Final concentration	Volume (μl)
RNA sample	-	20 ng/μl	0-5
Nuclease-free Water	-	-	0-5
dNTP mix	Invitrogen	0.5 mM dTTP 0.5 mM dATP 0.5 mM dCTP 0.5 mM dGTP	0.5
Superscript III	Invitrogen	2.5 U/μl	0.125
DTT	Invitrogen	5 mM	0.5
Oligo(dT) primer	Integrated DNA technologies	5 μM	0.5
First Strand Buffer	Invitrogen	1X	2
Total			**10**

3.2.12.2 Quantitative real-time quantitative polymerase chain reaction (RT-qPCR)

RT-qPCR assays were run using the SYBR Green intercalation system to quantitate the relative gene expression. Reagents were mixed as detailed in Table 3.8. Reactions were setup in MicroAmp Optical 384-well reaction plates (Applied Biosystems), and plates sealed with MicroAmp Optical Adhesive Film (Applied Biosystems). All primer pairs are listed in Table 3.3. Assays were performed using the QuantStudio 12K Flex instrument (Applied Biosystems). PCR reactions were initiated with 2 min incubation at 50 °C, and a 10 min incubation at 95 °C, followed by 40 PCR cycles of 95 °C for 15 s and 60 °C for 1 min. Melting curve analysis was performed at the end of amplification.

Table 3.8. mRNA qPCR reaction reagent volumes.

Reagent	Manufacturer	Final concentration	Volume (µl)
cDNA sample	-	0.8 ng/µl	2
PowerUp SYBR Green Master Mix	Applied Biosystems	1X	5
Forward primer	Integrated DNA technologies	400 nM	1
Reverse primer	Integrated DNA technologies	400 nM	1
Nuclease-free Water	-	-	1
Total			**10**

3.2.12.3 Relative expression calculation

Gene expression was quantified using the ΔΔCt method. Sample *Stx5a* Ct was subtracted from target gene Ct to give ΔCt. Mean ΔCt of the uninfected control was subtracted from the infected sample ΔCt to give ΔΔCt. Fold change expression was calculated by $2^{-\Delta\Delta Ct}$. *Stx5a* has been validated as a suitable housekeeper gene for *in vitro* analysis of murine macrophages following stimulation with bacterial antigens (210).

3.2.13 Determining miRNA expression by quantitative PCR
3.2.13.1 cDNA synthesis from miRNA template

RNA was purified from lysed cells as described in section 3.2.11. Sample miRNA concentrations were determined using the Qubit 2.0 Fluorometer (Invitrogen) and Qubit microRNA Assay Kit (Invitrogen), according to the manufacturer's protocol. Briefly, the Qubit microRNA Reagent was diluted 200-fold in Qubit miRNA Buffer to prepare the Qubit Working Solution. Each unknown RNA sample was diluted 200-fold in Qubit Working solution, then vortexed for 2-3 s and incubated at room temperature for 2 min, before analysis.

Synthesis of cDNA from miRNA was performed using All-in-One miRNA First-Strand cDNA Synthesis Kit (GeneCopoeia). To prepare for cDNA synthesis, the RNA sample, Poly A polymerase, RT mix, and PAP/RT Buffer were mixed (Table 3.9). The cDNA synthesis reaction was performed in the Mastercycler thermocycler, incubating at 37 °C for 60 min, 85 °C for 5 min, and then held at 4 °C.

Table 3.9. cDNA synthesis reaction for microRNA template.

Reagent	Manufacturer	Final concentration	Volume (μl)
RNA sample	-	16 ng/μl small molecule RNA	0-9
Nuclease-free Water	-	-	0-9
Poly A Polymerase	GeneCopoeia	0.1 U/μl	0.5
RTase Mix	GeneCopoeia	1X	0.5
5X PAP/RT Buffer	GeneCopoeia	1X	2.5
Total			**12.5**

3.2.13.2 Quantitative RT-qPCR for miRNA expression

RT-qPCR assays for miRNA were run using the All-in-One™ miRNA qRT-PCR Detection Kit (GeneCopoeia), according to the manufacturer's protocol, modified to utilise the PowerUp SYBR Green Master Mix. Reagents were mixed as detailed in Table 3.10. Reactions were setup in MicroAmp Optical 384-well reaction plates, and plates sealed with MicroAmp Optical Adhesive Film. All forward primers are listed in Table 3.4; the kit uses a universal reverse primer. Assays were performed using the QuantStudio 12K Flex instrument. PCR reactions were initiated with a 10 min incubation at 95 °C, followed by 40 PCR cycles of 95 °C for 10 s, 60 °C for 20 s, and 72 °C for 10 s. Melting curve analysis was performed at the end of amplification.

Table 3.10. miRNA qPCR reaction reagent volumes.

Reagent	Manufacturer	Final concentration	Volume (µl)
cDNA sample	-	0.64 ng/µl	2
PowerUp SYBR Green Master Mix	Applied Biosystems	1X	5
Forward primer	Integrated DNA technologies	200 nM	1
Universal Adaptor PCR Primer	GeneCopoeia	200 nM	1
Nuclease-free Water	-	-	1
Total			**10**

3.2.13.3 Relative miRNA expression calculation

miRNA expression was quantified using the ΔΔCt method. Sample *RNU6* Ct was subtracted from target gene Ct to give ΔCt. Mean ΔCt of the uninfected control was subtracted from the infected sample ΔCt to give ΔΔCt. Fold change expression was calculated by $2^{-\Delta\Delta Ct}$.

3.2.14 Statistical analyses

All statistical comparisons were made using Prism software version 9.3.1. Bacterial load (CFU/ml) values were $\log_{10}$ transformed and compared using 2-way analysis of variance (ANOVA) with multiple comparisons post-test, corrected for multiple comparisons using the Šidák method.

Cytokine expression, resazurin fluorescence, protein phosphorylation, and qPCR-quantified mRNA expression were compared using 2-way analysis of variance (ANOVA) with multiple comparisons post-test, corrected for multiple comparisons using the Šidák method.

miR-652-3p miRNA, *Capzb* mRNA, and CAPZB protein expression by transfected IC-21 cells were compared by 2-tailed student's t test.

CHAPTER 4

The impact of miR-652 during mycobacterial infection

Chapter 4. The impact of miR-652 during mycobacterial infection

4.1. Introduction

Tuberculosis (TB) is an ancient disease and continues to be one of the deadliest infectious diseases on the planet. The causative pathogen, *Mycobacterium tuberculosis*, infects almost 10 million people annually, leading to 1.5 million fatalities in 2020 (21). TB infections and deaths are overrepresented in low- and lower middle-income countries (22). Furthermore, the emergence of the SARS-CoV-2 virus and its effect on global medical systems has led to decreased notifications of new TB cases, fewer patients successfully treated, and increased TB-related deaths (21).

M. tuberculosis infection occurs primarily through inhalation of aerosol droplets, transferred between people through coughing. Once in the alveolar space, the bacteria are phagocytised by tissue-resident alveolar macrophages, which migrate into the lung interstitial space (211). *M. tuberculosis* can persist and replicate inside the macrophage phagosome, ultimately leading to cell death and bacterial release (212, 213). Free *M. tuberculosis* bacilli in the lung interstitium are phagocytised by dendritic cells (DC) and transported to the draining lymph node, initiating CD4$^+$ helper T cell activation (214, 215). Activation of the adaptive immune response triggers formation of the TB granuloma, consisting of live *M. tuberculosis* bacilli and infected macrophages at its core, surrounded by epithelioid macrophages, multi-nuclear giant cells, and foamy macrophages, and with outer layers of NK cells, DCs, B cells, and T lymphocytes (216). From this point the infection can proceed on three possible paths; the clearance of all bacteria, long-term bacterial containment in a latent infection state, or continued progression into TB disease (200, 217, 218). An estimated 1.7 billion people are latently infected with *M. tuberculosis* (219), each with the potential of reactivation and progression to active TB (218, 220).

Standard TB treatment is a 6-month regimen of multiple antibiotics, with an 85% success rate globally (21). Infection with drug-resistant *M. tuberculosis* strains requires 9-24 months treatment with additional antibiotics (221). This is problematic for patients in

lower-income settings due to the high cost and low availability of these medications in an extended regimen (222). Poor adherence is not uncommon, largely due to severe adverse side effects, high pill burden, and poor education about regimen requirements (23, 222-224). Even following successful treatment of active TB, disease-associated host inflammation can lead to permanent lung damage. Cured TB patients are prone to airway obstruction and chronic obstructive pulmonary disease (27), up to half can have persistent pulmonary dysfunction, and TB patients present increased all-cause mortality rates (28, 225, 226).

The World Health Organisation-recommended diagnosis method is GeneXpert rapid nucleotide-based testing for both *M. tuberculosis* presence and rifampicin resistance (227). However, the most common method of diagnosis remains microscopic evaluation of sputum smears, largely due to technology availability (228). Microscopic diagnosis requires specialised staff experience and is less sensitive than molecular techniques (228, 229). Additionally, both microscopy and GeneXpert require the generation of sputum, something difficult or impossible in paediatric, latently-infected, or extrapulmonary patients (230).

In this TB landscape, urgent development of point of care, non-sputum-based diagnostics, and host-directed therapies to combat excessive inflammation and antimicrobial resistance is required. Host miRNAs continue to garner interest as diagnostic and therapeutic targets in infectious disease settings. Several studies have identified promising miRNA biomarker panels for the diagnosis of pulmonary TB (231), and a number of miRNA, including miRNA-155, provide protective roles during TB (232). However, as yet no miRNA has been nominated as a target in TB treatment.

The miRNA hsa-miR-652-3p (from here termed miR-652) was downregulated in a cohort of Chinese TB patients, and low miR-652 expression correlated with poor response to antibiotic treatment (20). As detailed in Chapter 1, miR-652 regulates multiple processes in cell differentiation and maintenance, with interesting implications in the immune response to infectious disease.

This chapter describes an exploratory study into the activity of miR-652 during *M. tuberculosis* infection. With a focus in macrophage phenotype, the responses to mycobacterial infection are assessed *in vitro* and *in vivo*. This study describes the effect of miR-652 expression on macrophage cytokine secretion and the involvement of miR-652 in the NOTCH and mTOR signalling pathways. The absence of miR-652 expression in mice and mouse macrophages has important impacts on macrophage inflammatory activation, and on CD8+ T cell differentiation. These changes may critically influence the control of *M. tuberculosis* and TB disease progression.

4.2. Methods
4.2.1 Isolation and culture of primary mouse bone marrow cells

Mice were euthanised by CO_2 asphyxiation and the tibia and femur collected into tissue media. Bone marrow was flushed out using a 27G needle (Terumo) and passed through a 70 µm cell strainer (Corning). Cells were centrifuged at 500 rcf for 5 min at 4 °C, and then resuspended in ACK lysis buffer for 1 min to lyse red blood cells. Cells were immediately diluted 10-fold in BMDM differentiation media to halt cell lysis, before centrifugation at 500 rcf for 5 min at 4 °C, in order to remove ACK lysis buffer ingredients. Remaining cells were resuspended in BMDM differentiation media, counted, and diluted as required. Cells were cultured in BMDM differentiation media, containing GM-CSF, for 6 days at 37 °C with 5% CO_2, with media replenished after 3 days. BMDM cells were selected by adherence to tissue culture plates. Non-adherent cells were washed away with BMDM media before *in vitro* infection assays.

4.2.2 *In vitro* mycobacterial infection

BMDMs were seeded in flat-bottom tissue culture plates (Corning Costar) at 5×10^5 cells/ml or 1.5×10^6 cells/ml in BMDM media. *M. tuberculosis* or *M. avium* cultures were centrifuged and resuspended in BMDM media, before sonication in the Digital Sonifier 250 (Branson) cup sonicator (amplitude 30%, 10 s) to separate clumped bacteria. BMDMs were infected with *M. tuberculosis* at a multiplicity-of-infection (MOI) of 1 (low-dose) or 5 (high-dose), or with *M. avium* at an MOI of 2 (low-dose) or 10 (high-dose).

Infected cultures were washed with BMDM media after 4 h to remove extracellular bacteria.

To determine the bacterial load of infected wells, all supernatant was removed and cells lysed with 200 µl 0.1% Triton solution for 15 min at 37 °C. Lysates were serially diluted in water and plated to determine the CFU concentration. Plates were incubated at 37 °C for 14-20 days before CFU counts.

4.2.3 *In vivo* mycobacterial infection

Mice were infected with *M. tuberculosis* by aerosol administration. A 10 ml volume of *M. tuberculosis* culture was centrifuged at 3270 rcf for 10 min, and the bacteria resuspended in 4 ml PBS with 0.05% v/v Tween 20. The resuspended bacteria were centrifuged at a low-speed of 230 rcf for 10 min to collect the single cell suspension in the supernatant. Bacteria were again centrifuged at 3270 rcf for 10 min and resuspended in water, then sonicated before aerosol infection using the Digital Sonifier 250 cup sonicator (amplitude 30%, 10 s). Aerosol infection was conducted using the Glascol Inhalation Exposure Chamber (vacuum 60, nebuliser 8-9).

On day 1 post-infection, two mice were euthanised for CFU dose check. Lungs were homogenised in sterile deionised water, the entire volume plated on 7H11 agar, and incubated for 14-21 days before CFU check. Each mouse was infected with a dose of 81 ± 17 CFU.

Mice were housed for up to 13-weeks post infection and at predetermined time points, were euthanised by CO_2 asphyxiation for organ collection. Prior to lung dissection, the lungs were perfused with PBS/Heparin by injection into the heart. The middle right lung lobe and the left liver lobe were removed into 10% neutral-buffered formalin (Fronine) for histology. The left lung and spleen were each collected into sterile water for CFU determination. Superior and inferior lung lobes were collected into tissue media for dissociation to single cells.

4.2.4 Flow cytometry gating

Lung and MLN leukocytes of *M. tuberculosis*-infected mice were stained and analysed according to section 3.2.7. Gating was performed using FlowJo v10 software.

<u>Myeloid cell subsets</u>

A gating strategy was developed to analyse myeloid lineage leukocytes (Figure 4.1), based on a previously published strategy (233). Cell debris was excluded by gating for high FSC-A and low-high SSC-A. Single cells were gated in the linear portion of the FSC-A vs FSC-H plot, eliminating cell aggregates. This gating was repeated using SSC-A and SCC-H to exclude further aggregates. Live cells were gated based on Live-Dead dye exclusion. All leukocytes were gated based on CD45 expression. From the total CD45$^+$ population, events were plotted on CD11b vs CD11c to gate CD11c$^+$ CD11b^{mid} alveolar macrophages. An MHC-II vs CD11b plot was used to gate CD11b$^+$ cells apart from CD11b$^-$ cells, which includes some MHC-II$^-$ CD11b^{mid} cells. The CD11b$^-$ population was plot on MHC-II vs B220 in order to gate MHC-II$^+$ B220$^+$ B cells. CD11b$^+$ cells were plot on CD11b vs Ly6G to gate Ly6G$^+$ neutrophils. The remaining Ly6G$^-$ population was gated on MHC-II vs CD11c to gate MHC-II$^+$ CD11c$^{low-mid}$ interstitial macrophages and MHC-II^{low} CD11c$^-$ monocytes.

<u>T cell subsets</u>

A gating strategy was developed to analyse T cell leukocytes, and the activation status of particular T cell subsets (Figure 4.2). Cell debris was excluded by gating for high FSC-A and low-high SSC-A. Single cells were gated in the linear portion of the FSC-A vs FSC-H plot, eliminating cell aggregates. This gating was repeated using SSC-A and SCC-H to exclude further aggregates. Live cells were gated based on Live-Dead dye exclusion. All leukocytes were gated based on CD45 expression, and then CD4$^+$ helper T cells and CD8$^+$ cytotoxic T cells were gated on a CD4 vs CD8 plot. Under each of the CD4$^+$ and CD8$^+$ gates, the effector T cells were gated as CD44^{hi} CD62L^{lo}, memory T cells were gated as CD44^{hi} CD62L^{hi}, and naïve T cells were gated as CD44^{lo} CD62L^{hi}. Effector CD4$^+$ T cells and effector CD8$^+$ T cells were identified as activated based on CD69 expression.

Figure 4.1. Flow cytometry gating strategy for the analysis of myeloid lineage cells in tissue of *M. tuberculosis*-infected mice. Cells are gated to remove cell debris, before selection of singles cells. Live cells are selected based on dye exclusion. Leukocytes are isolated by CD45.2 expression. Alveolar macrophages are gated as CD11b^{mid} and CD11c^{hi}. Remaining cells were separated into CD11b$^+$ cells and CD11b$^-$ cells, containing B220$^+$ B cells. Neutrophils were gated as CD11b$^+$ Ly6G$^+$. Ly6G$^-$ cells were separated into MHC-II$^-$ monocytes and MHC-II$^+$ interstitial macrophages.
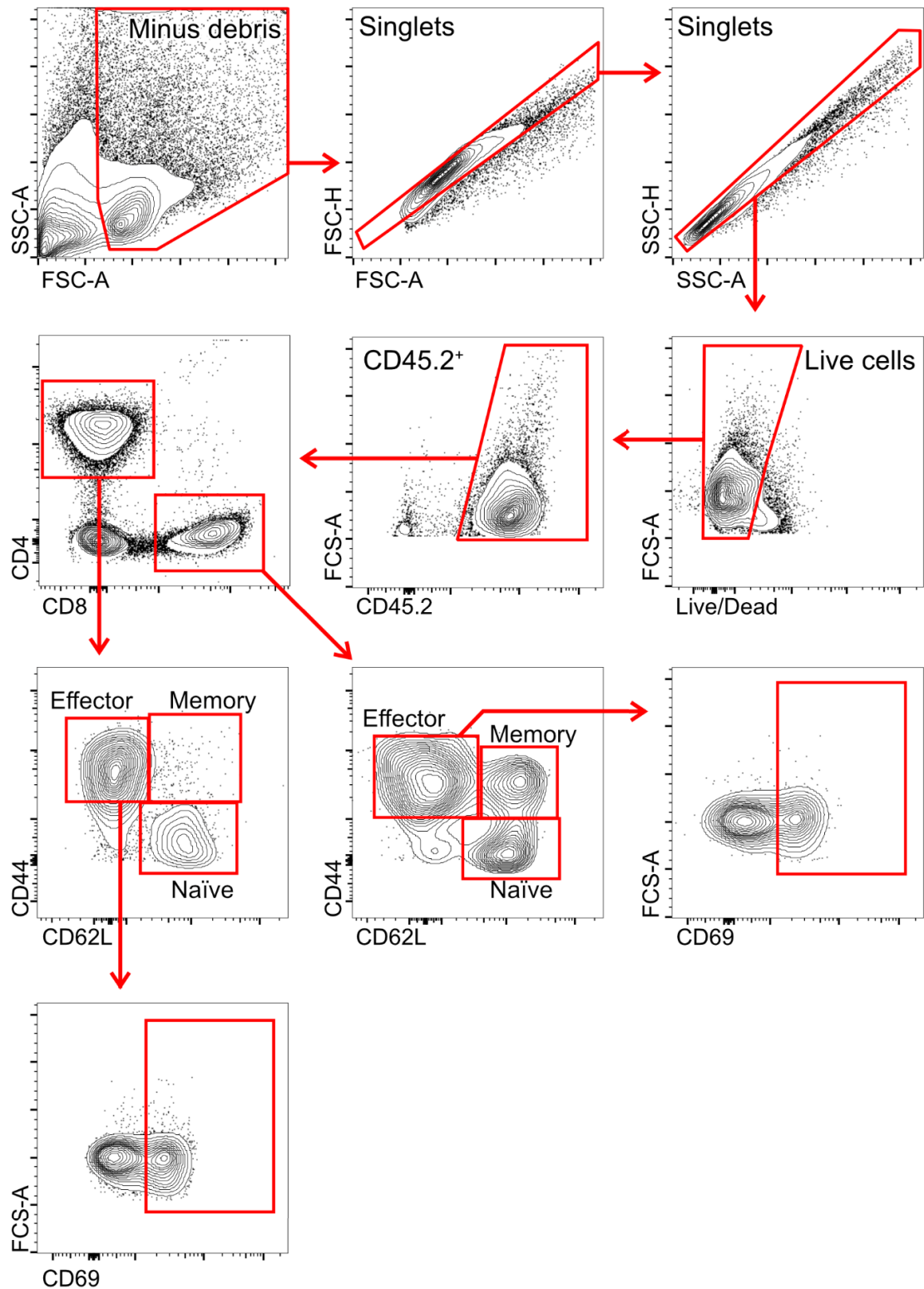
Figure 4.2. Flow cytometry gating strategy for the analysis of T cells in tissue from *M. tuberculosis*-infected mice. Cells are gated to remove cell debris, before selection of singles cells. Live cells are selected based on dye exclusion. Leukocytes are isolated by CD45.2 expression. CD4+ and CD8+ T cell populations are gated, and individually separated into effector, memory, and naïve subsets based on CD44 and CD62L expression. Effector T cell subsets are gated on CD69 expression as a marker of activation.

4.3.   Results

4.3.1 *In vitro* cytokine expression by infected macrophages is impaired by miR-652 knockout

No previous studies have investigated the roles of miR-652 in an infectious disease setting. To characterise miR-652 activities *in vitro* and *in vivo*, a miR-652$^{-/-}$ mouse line was generated on a C57BL/6 background. The *M. tuberculosis* aerosol infection in mice is well studied (234). As macrophages are the first immune cells exposed to *M. tuberculosis* in the lung, bone-marrow macrophages were infected with two mycobacterial species, *M. tuberculosis* and *M. avium*.

BMDMs from wild type C57BL/6 and miR-652$^{-/-}$ mice were infected *in vitro* with *M. tuberculosis* or *M. avium*, and cultured for up to 6 days. Macrophage cytokine expression is essential for the control of mycobacteria in the lung (200). The concentrations of proinflammatory cytokines IL-6, TNF, MIP-1α, and KC in culture supernatant were analysed by CBA. Cytokine levels in all uninfected wells were at or below the lower limit of detection for the CBA assay method (data not shown). Expression of all cytokines was increased within 6 hours of infection, under all infection conditions (Figure 4.3). Generally, cytokine levels increased up to 24 hours post-infection, where they trended to plateau.

Expression of key cytokines IL-6 and TNF were significantly decreased in miR-652$^{-/-}$ cells following high-dose *M. tuberculosis* (MOI of 5) and *M. avium* (MOI of 10) infections (Figure 4.3b and d), suggesting the inflammatory response in these miR-652$^{-/-}$ macrophages is much weaker. Down regulation occurred early at 24 hours post-*M. tuberculosis* infection and 48 hours post-*M. avium* infection, and remained downregulated at 144 hours post-infection. Furthermore, the neutrophil-attracting chemokine MIP-1α was downregulated in miR-652$^{-/-}$ cells at early time points during both infections, and expression of chemokine KC was noticeably lower in miR-652$^{-/-}$ cells, though differences were not significant.

Cytokine expression was lower in all cells following low-dose mycobacterial infections. Wild type BMDMs expressed significantly more of all four cytokines 144 hour after *M. tuberculosis* infection at an MOI of 1 (Figure 4.3a). However, cytokine expression was

comparable between wild type and miR-652^{-/-} BMDMs after *M. avium* infection at an MOI of 2 (Figure 4.3c).
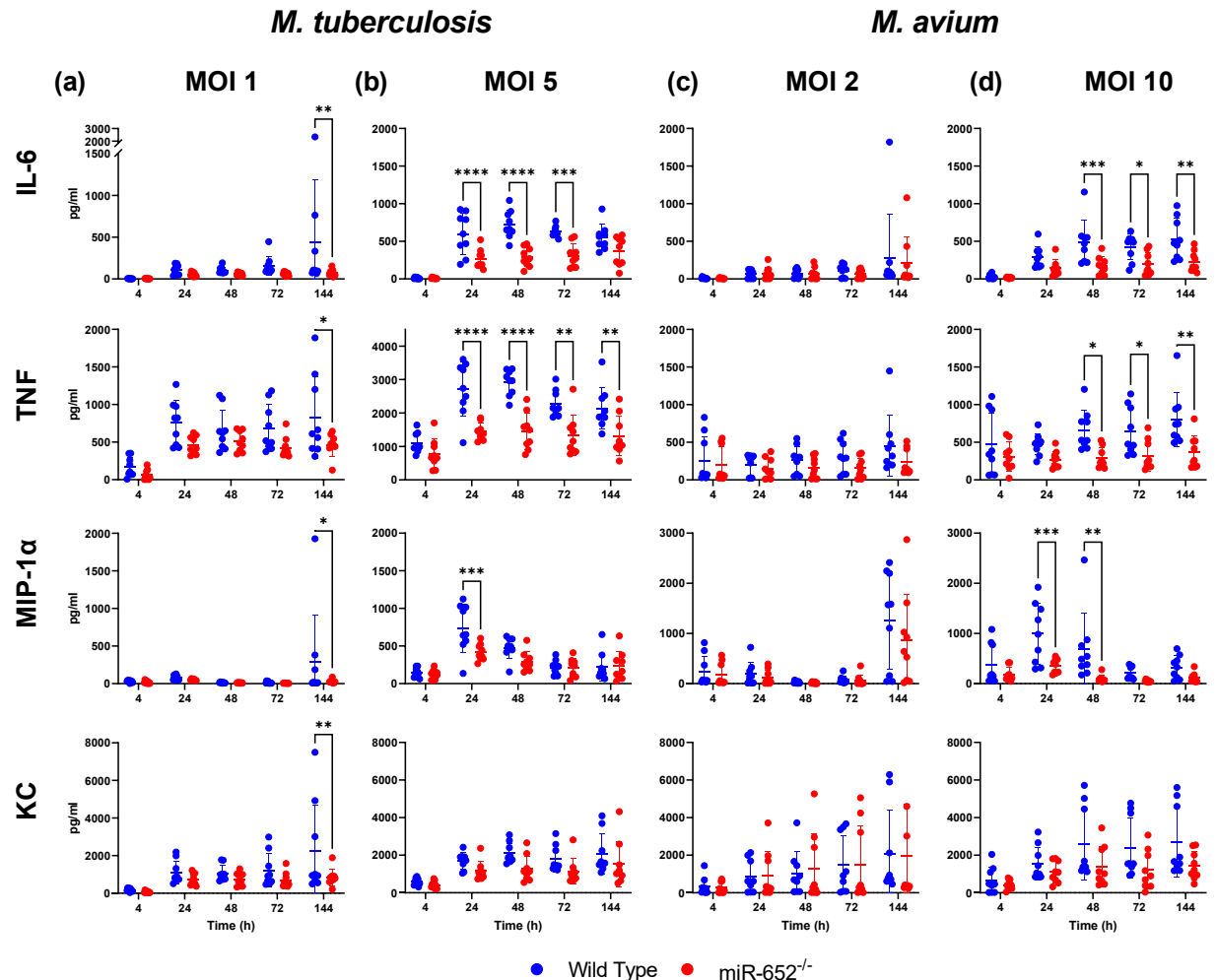
Figure 4.3. Proinflammatory cytokine expression is reduced in miR-652^{-/-} macrophages after mycobacterial infection. Wild type and miR-652^{-/-} mouse BMDMs were infected *in vitro* with *M. tuberculosis* at an MOI of (a) 1 or (b) 5, or with *M. avium* at an MOI of (c) 2 or (d) 10. Cytokine concentrations in supernatant were quantified by CBA. Data are the mean ± SD of 9 biological replicates, from 3 separate experiments. *$P < 0.05$, **$P < 0.01$, ***$P < 0.001$, ****$P < 0.0001$, by 2-way ANOVA with multiple comparisons post-test, Šidák method corrected.

4.3.2 Inflammatory pathways are downregulated in infected miR-652^{-/-} macrophages

Decreased cytokine expression in miR-652^{-/-} macrophages could be regulated by a number of inflammatory pathways. It was hypothesised that activation of the AKT/mTOR pathway may be dysregulated in miR-652^{-/-} cells. The AKT/mTOR pathway is known to regulate the inflammatory phenotype of macrophages, including cytokine

expression (235). BMDMs were infected with *M. tuberculosis* and *M. avium*, and lysed for western blot analysis of AKT and mTOR phosphorylation, indicating protein activation. Activation of both proteins was significantly upregulated in wild type BMDMs, compared to miR-652$^{-/-}$ cells (Figure 4.4). AKT phosphorylation was increased 90 min after high-dose *M. tuberculosis* infection (Figure 4.4c). Moreover, low-dose *M. avium* infection also induced increased AKT and mTOR activation in wild type cells at 90 min post-infection (Figure 4.4d). High-dose *M. avium* infection induced a similar trend, whereas AKT activation was notably, though not significantly, increased in wild type cells (Figure 4.4e).

Regulation of AKT activation can be mediated through NOTCH signalling (236), shown to be regulated by miR-652 targeting of a NOTCH ligand JAG1 (79). RT-qPCR analysis of infected BMDMs monitored expression of receptors *Notch1* and *Notch2*, and the *Jag1* ligand. Mycobacterial infection did not elicit differential expression of *Notch1, Notch2, or Jag1* mRNA in wild type or miR-652$^{-/-}$ BMDMs (Figure 4.5). This suggests that the sustained increase in cytokine expression by wild type BMDMs may not be stimulated through the NOTCH signalling pathway, and the observed AKT activation in wild type macrophages may occur through an alternative mechanism.

4.3.3   miR-652 knockout in macrophages does not impair control of mycobacterial growth

TNF is required for macrophage activation during TB (200, 237). It was hypothesised that decreased TNF expression *in vitro* could negatively impact bacterial killing and impair control of the bacterial load. To address the impact of decreased cytokine expression and AKT activation on the antibacterial activity of miR-652$^{-/-}$ BMDMs, bacterial CFU concentrations were determined from cell lysates of infected BMDMs. The *M. tuberculosis* bacterial load was comparable between wild type and miR-652$^{-/-}$ BMDMs (Figure 4.6a and b). Though significantly higher CFU were present in wild type BMDMs 72 and 24 hours after low- and high-dose infection, respectively, in both cases, CFU equalised at later time points. Conversely, *M. avium* bacterial load was significantly higher in miR-652$^{-/-}$ cells 48 hours after low-dose infection (Figure 4.6c), but again, this difference was transient.
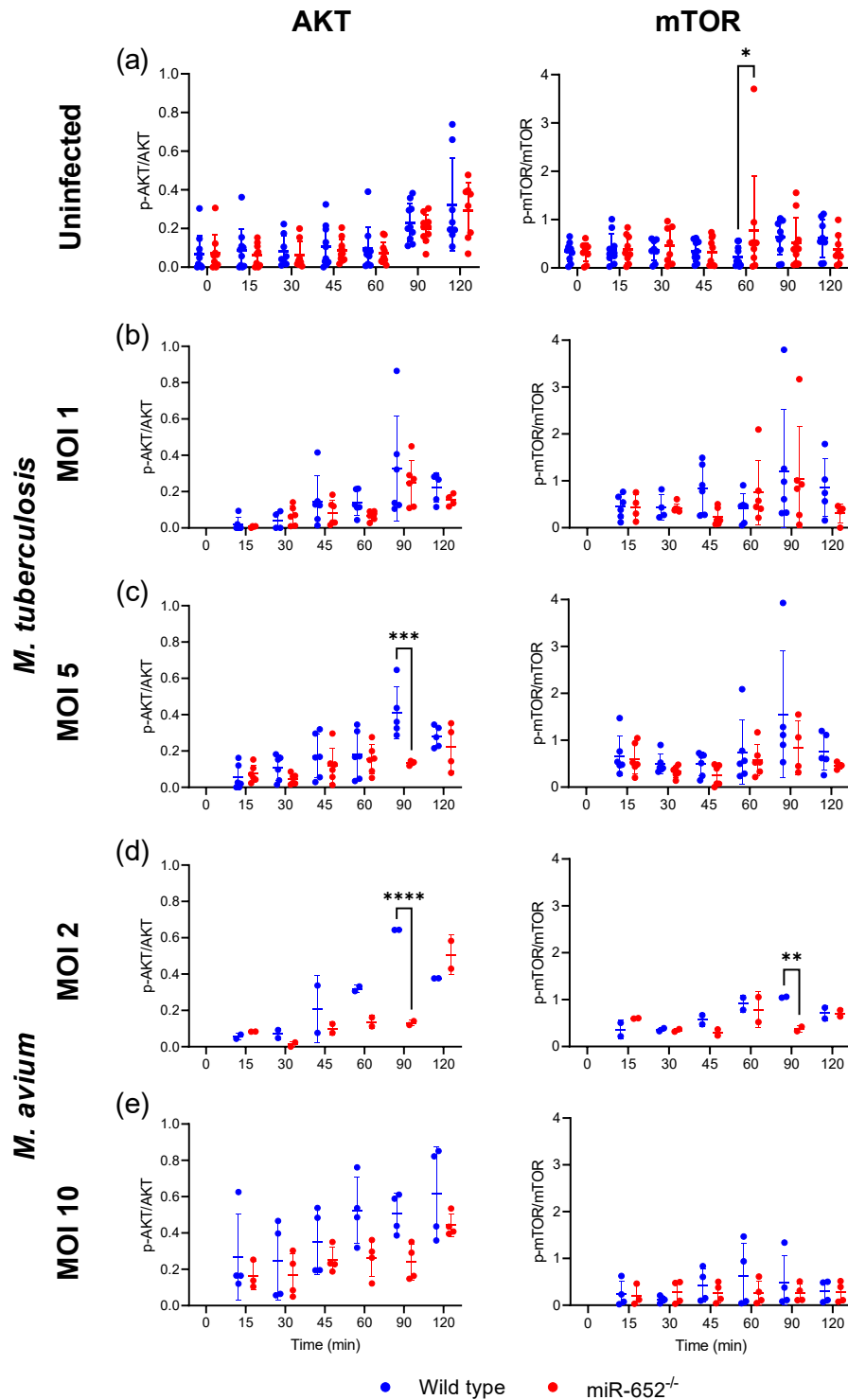
Figure 4.4. Activation of the AKT-mTOR pathway is decreased in miR-652^{-/-} macrophages following mycobacterial infection. Mouse BMDMs were infected as in Figure 4.3. Protein samples were collected from (a) uninfected cells, cells infected with *M. tuberculosis* at (b) MOI 1 or (c) MOI 5, and cells infected with *M. avium* at (d) MOI 2 or (e) MOI 10. Phosphorylated and total AKT, and phosphorylated and total mTOR were detected, normalised to GAPDH. Activation is expressed as phosphorylated protein divided by total protein. Data are the mean ± SD of biological replicates, from 3 separate experiments. *$P < 0.05$, **$P < 0.01$, ***$P < 0.001$, ****$P < 0.0001$, by 2-way ANOVA with multiple comparisons post-test, Šidák method corrected.
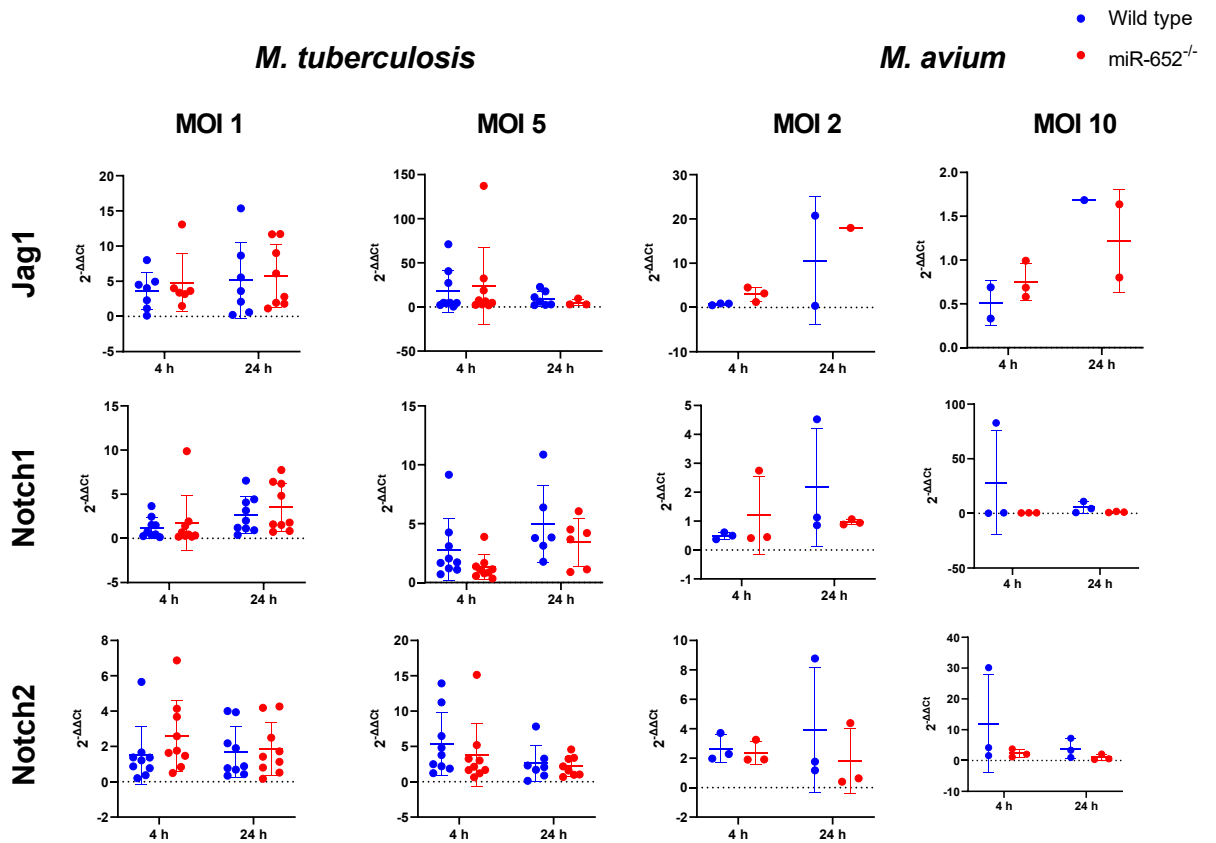
Figure 4.5. Notch receptor expression is not impaired in miR-652$^{-/-}$ cells after mycobacterial infection. Mouse BMDMs were infected as in Figure 4.3. Cells were lysed with TRIsure reagent and mRNA was purified. *Jag1*, *Notch1*, and *Notch2* transcripts were quantified by RT-qPCR, and normalised against *Stx5a*. Data are the mean ± SD of biological replicates, from 1-3 separate experiments. Comparisons were made using 2-way ANOVA with multiple comparisons post-test, Šidák method corrected.
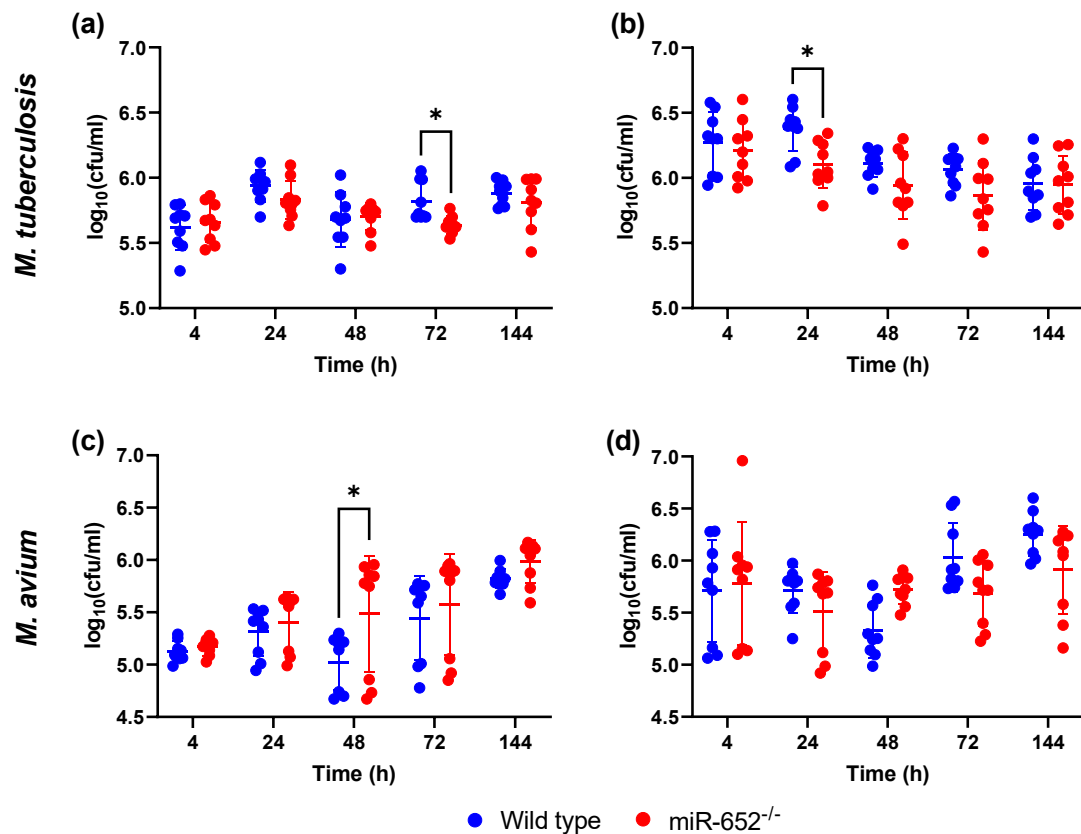
Figure 4.6. Wild type and miR-652$^{-/-}$ BMDMs control *M. tuberculosis* growth. Mouse BMDMs were infected *in vitro* with *M. tuberculosis* at an MOI of (a) 1 or (b) 5, or with *M. avium* at an MOI of (c) 2 or (d) 10, as in Figure 4.3. Supernatant was removed and BMDMs were lysed with Triton-X100 for enumeration of internalised bacteria. Data are the mean ± SD of 9 biological replicates, from 3 separate experiments. *$P < 0.05$, by 2-way ANOVA with multiple comparisons post-test, Šidák method corrected.
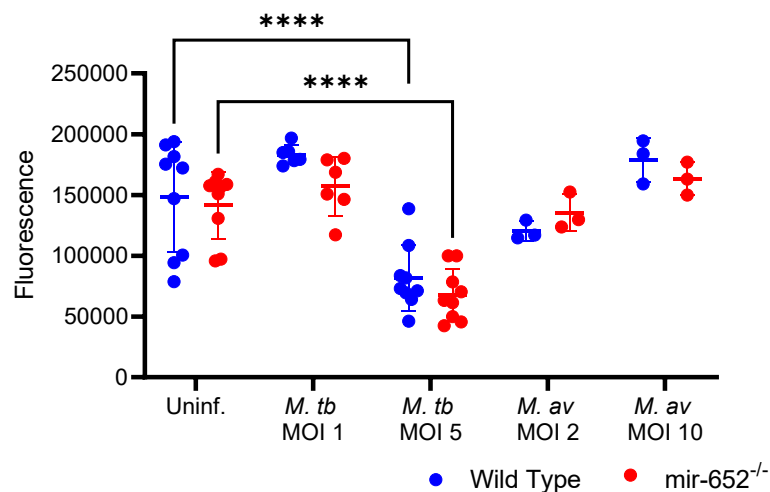
Figure 4.7. Wild type and miR-652$^{-/-}$ macrophages are metabolically active 24 hours after mycobacterial infection. Mouse BMDMs were infected as in Figure 4.3. Resazurin metabolic activity fluorescence assay was performed 24 hours post-infection. Data are the mean ± SD of biological replicates, from 3 separate experiments. ****$P < 0.0001$, by 2-way ANOVA with multiple comparisons post-test, Šidák method corrected.

Notably, high-dose *M. tuberculosis* (Figure 4.6b) and *M. avium* (Figure 4.6d) infections did not lead to extensive bacterial overgrowth at 72- or 144-hours post-infection. To confirm bacteria were not lost in culture supernatant before macrophage lysis, supernatant bacterial load was analysed. Culture supernatants removed before cell lysis contained a small and consistent proportion of the bacterial CFU count (Figure A 4). The percent of bacteria in solution was not significantly different between mouse strains or with time.

Though bacterial loads were similar between wild type and miR-652$^{-/-}$ BMDMs, it remained unclear whether macrophages from each mouse strain could equally engulf and control the same number of bacteria, or whether large quantities of bacteria were outnumbering dying macrophages. Resazurin fluorescence assays were run to determine the cells metabolic activity as a measure of cell number and cell viability. There were no significant differences in metabolic activity between wild type and miR-652$^{-/-}$ cells 24 hours after any infection (Figure 4.7). Metabolic activity was significantly lower in both cell types following high-dose *M. tuberculosis* infection, suggesting the significant burden of pathogenic bacteria was causing macrophage cell death. Observed by light microscopy, macrophage numbers were markedly lower by 72 hours post-infection (data not shown). Nevertheless, any macrophage death at late time points did not allow for a significant increase in bacterial burden (Figure 4.6b). During all other infections, macrophage metabolic activity did not change significantly.

To determine the effect of bacterial metabolism on the resazurin assay, infected BMDMs were lysed with Triton-X100 and bacterial metabolism assayed alone. The metabolic activity of the bacteria alone was far lower than that of the macrophages (Figure A 5a and b), and in many cases the fluorescent signal generated by the mycobacteria was not significantly greater than that of lysed uninfected macrophages (Figure A 5c).

4.3.4 miR-652$^{-/-}$ mice capably control *M. tuberculosis* bacterial load

From the *in vitro* experiments detailed above, miR-652$^{-/-}$ macrophages could not produce the cytokine levels of their wild type counterparts, and yet they controlled bacterial growth equally well over the 6-day infection. The cytokines and chemokines

assayed have important roles in recruiting and activating other leukocytes at the site of infection, including T cells and neutrophils (200, 217). These experiments raised the question of how decreased cytokine expression in macrophages may impact the immune response to chronic *M. tuberculosis* infection. An *in vivo* infection model was used to explore these interactions. Lung alveolar macrophages are the first immune cells to come into contact with *M. tuberculosis* following *in vivo* infection. To establish whether the downregulated cytokine response from miR-652$^{-/-}$ macrophages *in vitro* would translate into a delayed *in vivo* response to infection, mice were infected with *M. tuberculosis* by aerosol administration (Figure 4.8).

The bacterial load in the lungs and the spleen is an indicator of tuberculosis development in mice. The *M. tuberculosis* bacterial load increased in the spleen of both mouse strains between 4 and 13 weeks post-infection (Figure 4.9b). A significant increase in lung bacterial load was only seen in wild type mice (Figure 4.9a), however, there was no significant difference in bacterial load in either organ between wild type and miR-652$^{-/-}$ mice at any time point.

Lung tissue of infected mice was analysed by histology to identify whether similar bacterial loads in mice would be reflected in equivalent levels of inflammation. Fixed tissue sections were stained with haematoxylin and eosin, and then imaged by light microscopy. Moderate lung inflammation was seen in both wild type and miR-652$^{-/-}$ mice at 4 weeks post-infection (Figure 4.10a and b). At 13 weeks, inflammation in both mouse strains had increased, with inflammatory lesions growing markedly denser (Figure 4.10c and d). Nevertheless, the level of lung inflammation was comparable between wild type and knockout mice, with inflammatory involvement increasing in line with bacterial load (Figure 4.9).
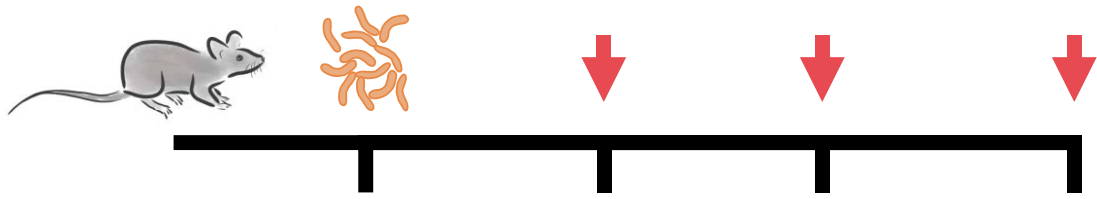
Figure 4.8. *In vivo Mycobacterium tuberculosis* **infection in mice.** Mice were infected with 81 ± 17 CFU by aerosol administration. At 4, 8, and 13-weeks post-infection, mice were euthanised for organ collection and analysis.
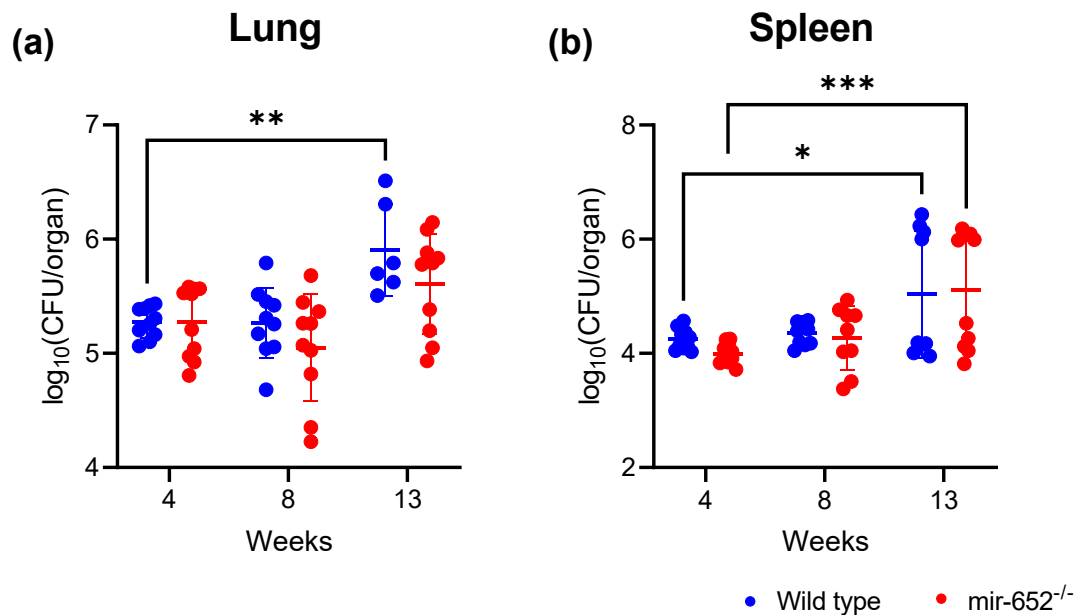
Figure 4.9. Wild type and miR-652$^{-/-}$ mice control *M. tuberculosis* bacterial load. Mice were infected with *M. tuberculosis* by aerosol administration. The bacterial load in the (a) lung and (b) spleen homogenates was enumerated over 13 weeks. Data are the mean ± SD, of 6-10 mice from two experiments. *$P < 0.05$, **$P < 0.01$, ***$P < 0.001$, by 2-way ANOVA with multiple comparisons post-test, Šidák method corrected.
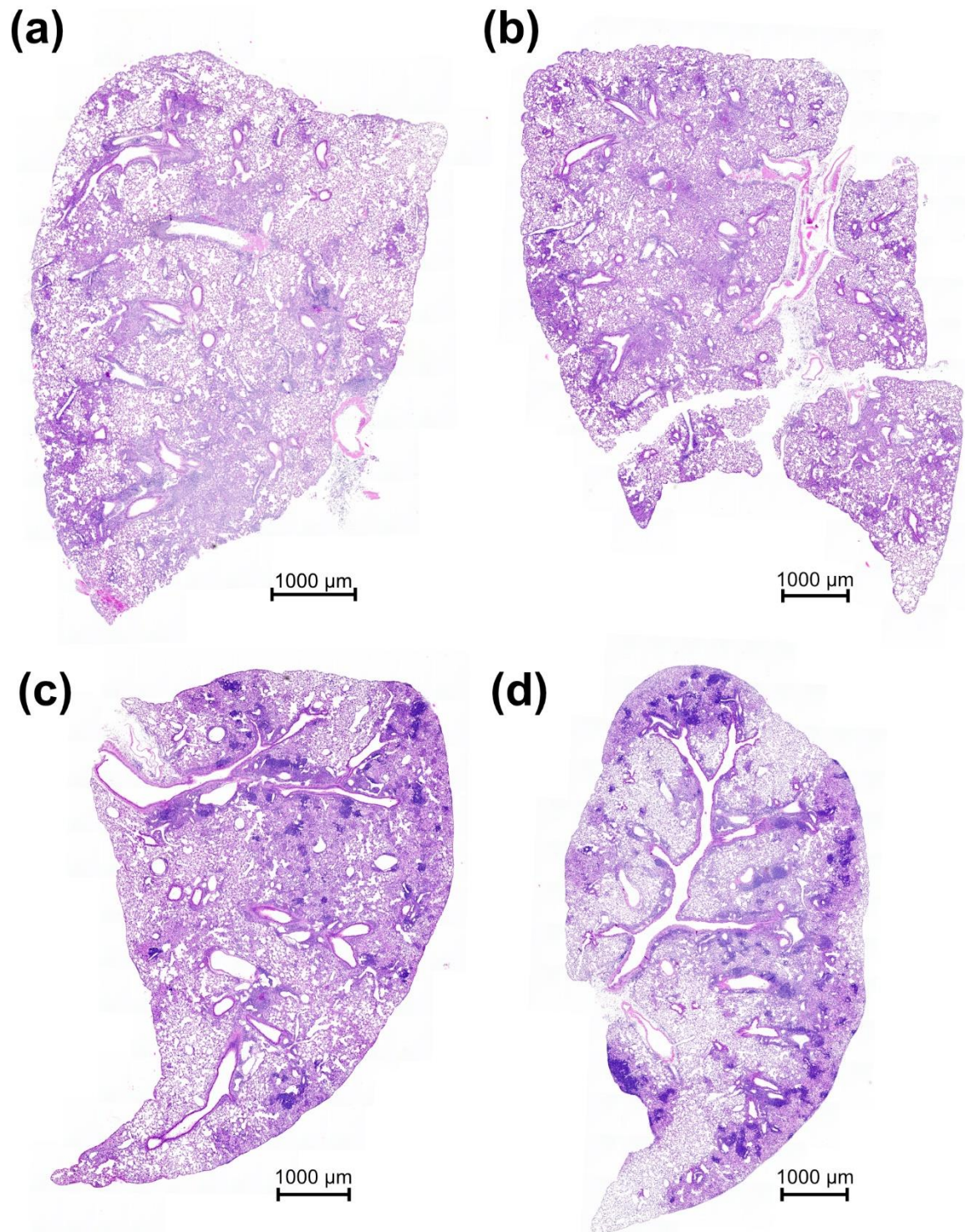
Figure 4.10. Lung inflammation progresses in both wild type and miR-652$^{-/-}$ mice following *M. tuberculosis* infection. Mice were infected as in Figure 4.9. Lungs were formalin fixed and paraffin embedded. Sections were stained with haematoxylin and eosin and images under bright field microscopy. Images show lungs from wild type mice at (a) 4 and (c) 13 weeks post-infection, and mir-652$^{-/-}$ mice at (b) 4 and (d) 13 weeks post-infection. Images are brightness and contrast adjusted.

4.3.5 Lung immune cell populations are not affected by miR-652 knockout

The anti-mycobacterial defence response relies on recruitment of diverse immune cells to the lung. The leukocyte composition of lung inflammation was analysed by flow cytometry, as was the mediastinal lymph node (MLN), the draining lymph node of the lung. Gating strategies were developed for analysis of myeloid lineage cell types (Figure 4.1) and T cell subtypes (Figure 4.2). There were no significant differences in macrophage or monocyte populations in the lungs of wild type and miR-652$^{-/-}$ mice (Figure 4.11a). Phagocytic cell populations decreased at 8 weeks, though monocyte numbers rebounded at 13 weeks post-infection. Chemokines MIP-1α and KC are key for attracting neutrophils to sites of inflammation during infection (238). Whilst significant decreases in chemokine expression were observed in *in vitro*-infected miR-652$^{-/-}$ macrophages (Figure 4.3), neutrophil populations were not significantly decreased *in vivo* (Figure 4.11).

Similar to myeloid phagocyte cell types, lymphocyte populations were comparable between wild type and miR-652$^{-/-}$ mice, in both the lung and MLN. However, a late decrease in miR-652$^{-/-}$ lung B cell numbers at 13 weeks corresponded with a significant increase in CD4 T cell numbers (Figure 4.12a). Lung B cell populations expanded significantly at 8 weeks in both wild type ($P < 0.0001$) and miR-652$^{-/-}$ ($P < 0.001$) mice. The lung T cell proportion duly decreased over the same period ($P < 0.0001$ for both mouse strains).

Whilst comparable lymphocyte populations in the lungs suggest T cell recruitment to the lung is not hampered in miR-652$^{-/-}$ mice, dramatic decreases in IL-6 expression by lung phagocytes may affect T cell activation (239). CD69 expression was used as a marker of effector T cell activation. CD8 effector T cell activation was notably increased at 13 weeks in both the lung and MLN of miR-652$^{-/-}$ mice (Figure 4.13). However, there were no significant differences in CD4$^+$ or CD8$^+$ T cell activation between wild type and miR-652$^{-/-}$ mice.

Though effector T cell populations in both mouse strains were equally activated, decreased effector T cell numbers could adversely affect the ability of mice to respond

to new pathogens and acute infections. There was no difference in CD4$^+$ effector T cell (CD44^{hi} CD62L^{lo}), memory (CD44^{hi} CD62L^{hi}), or naïve (CD44^{lo} CD62L^{hi}) populations between wild type and miR-652$^{-/-}$ mice at any time point. The large majority of CD4$^+$ T cells in the lungs of infected mice were effector cells. This high percentage remained for the entire 13-week study.

Converse to stable CD4$^+$ populations, significant changes were seen in CD8$^+$ T cell populations of miR-652$^{-/-}$ mice. CD8$^+$ memory T cells formed a significantly larger proportion of CD8$^+$ cells in wild type mouse lungs at 4 weeks (Figure 4.15a). Lung naïve T cells were increased at 4 weeks in wild type mice (P = 0.07), and a corresponding reduction in effector CD8$^+$ T cells was observed at the same time point (P = 0.12). CD8$^+$ populations in the MLN were comparable between wild type and miR-652$^{-/-}$ mice (Figure 4.15b), and did not change significantly over time.

Figure 4.11 to Figure 4.15 display populations as a percentage of live cells, and these same population comparisons were also made with total cell numbers. The trends observed in total cell numbers and the resulting conclusions reflected those seen in population percentages.
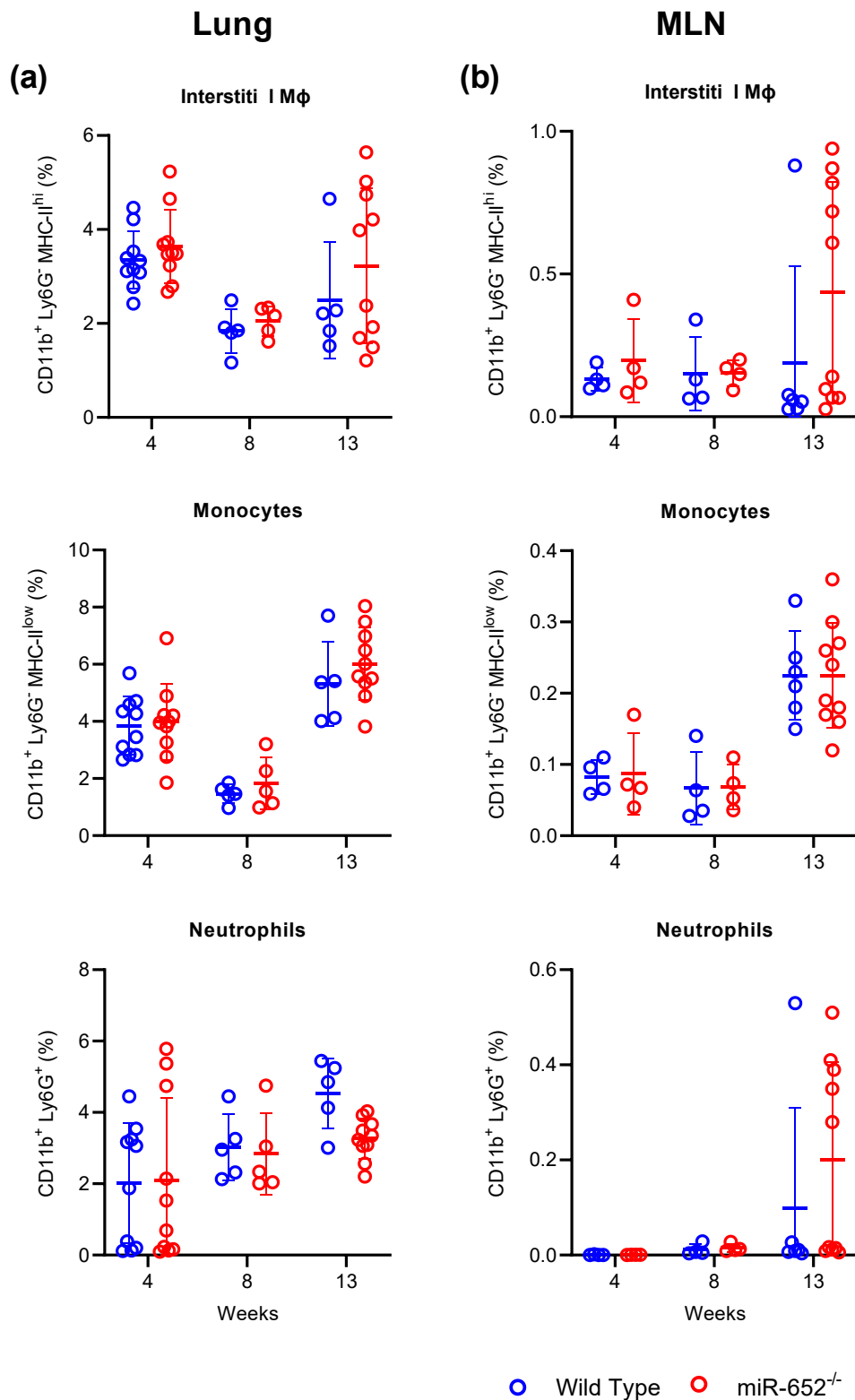
Figure 4.11. Myeloid leukocyte populations are not affected by miR-652 expression in *M. tuberculosis*-infected mice. Mice were infected as in Figure 4.9. The lungs and mediastinal lymph nodes of infected mice were dissociated to single cells, and stained for flow cytometry. Plots present (a) lung and (b) mediastinal lymph node myeloid lineage leukocytes. Populations are presented as a percentage of all CD45+ leukocytes. Data are the mean ± SD of 5-10 animals, from two experiments. Comparisons were made using 2-way ANOVA with multiple comparisons post-test, Šidák method corrected.
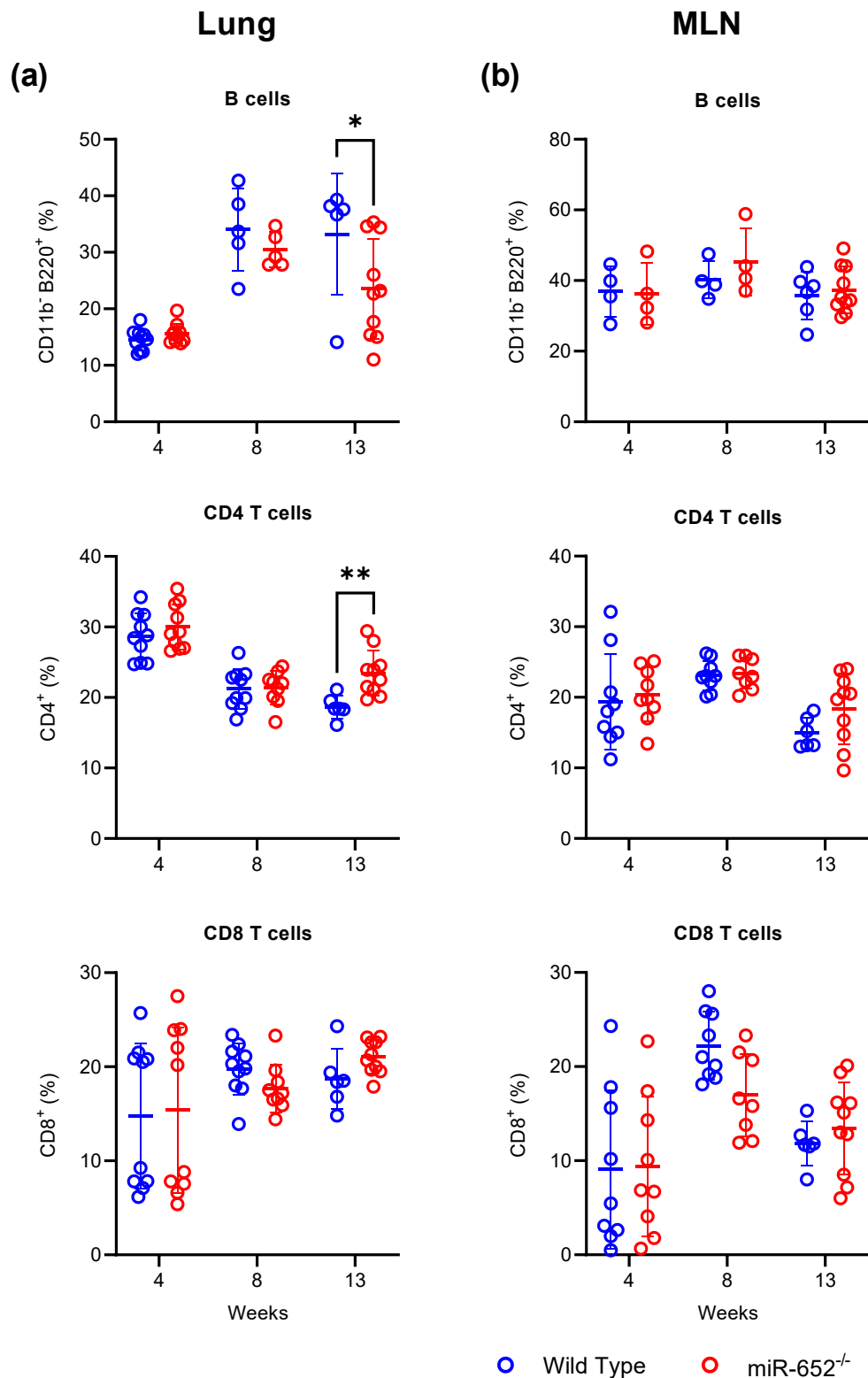
Figure 4.12. Lymphocyte populations are altered during chromic *M. tuberculosis* infection of miR-652^{-/-} mice. Mice were infected as in Figure 4.9. The lungs and mediastinal lymph nodes of infected mice were dissociated to single cells, and stained for flow cytometry. Plots present lymphocyte populations of the (a) lung and (b) mediastinal lymph node. Populations are presented as a percentage of all CD45^{+} leukocytes. Data are the mean ± SD of 5-10 animals, from two experiments. * $P < 0.05$, ** $P < 0.01$, by 2-way ANOVA with multiple comparisons post-test, Šidák method corrected.
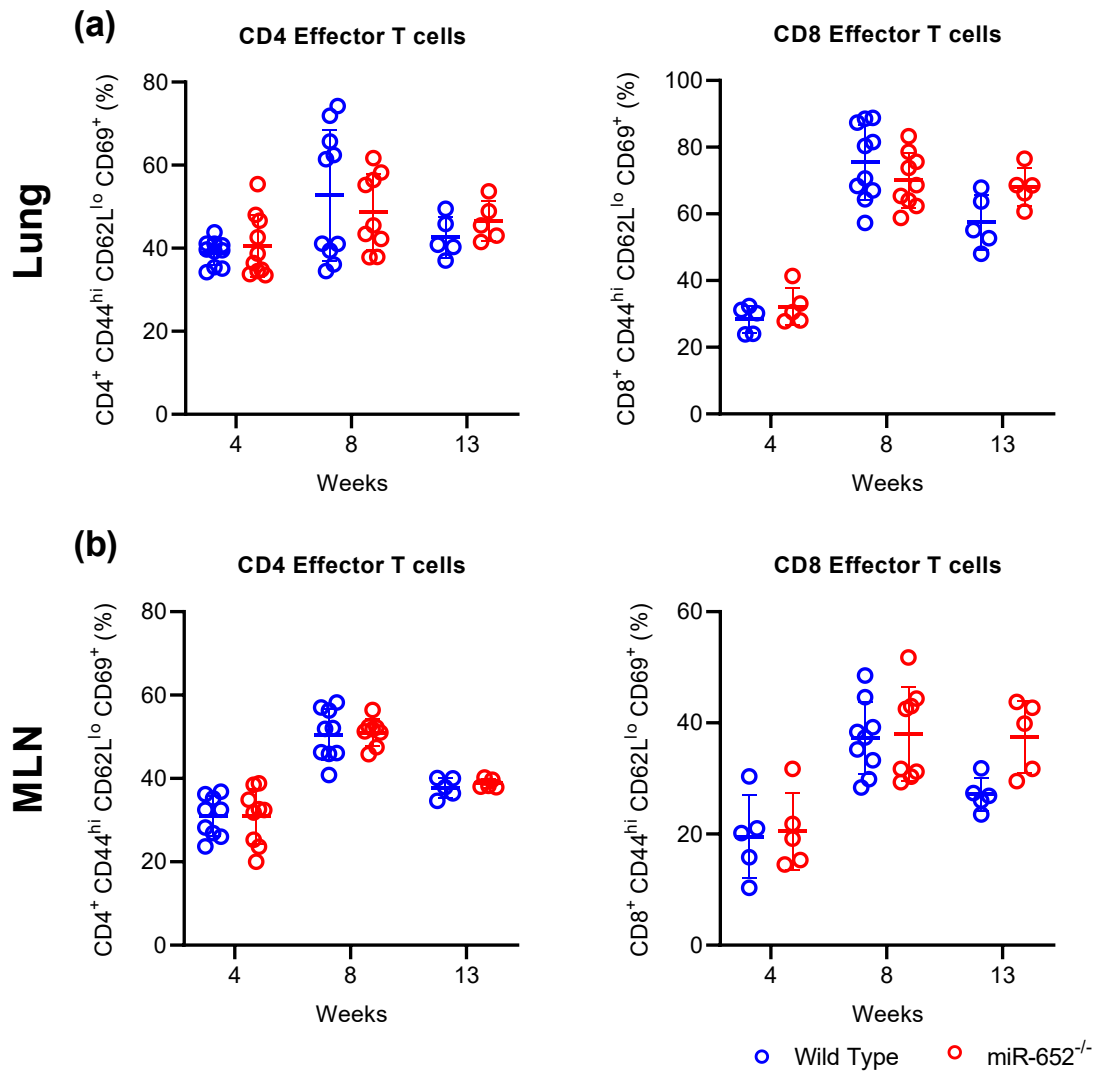
Figure 4.13. miR-652 deficiency does not affect activation of effector T cell populations in _M. tuberculosis_-infected mice. Mice were infected as in Figure 4.9. The (a) lungs and (b) mediastinal lymph nodes of infected mice were dissociated to single cells, and stained for flow cytometry. The activation of effector T cells is indicated by expression of CD69. Activated cell numbers are presented as a percentage of all CD4+ or CD8+ effector T cells. Data are the mean ± SD of 5-10 animals, from two experiments. Comparisons were made using 2-way ANOVA with multiple comparisons post-test, Šidák method corrected.
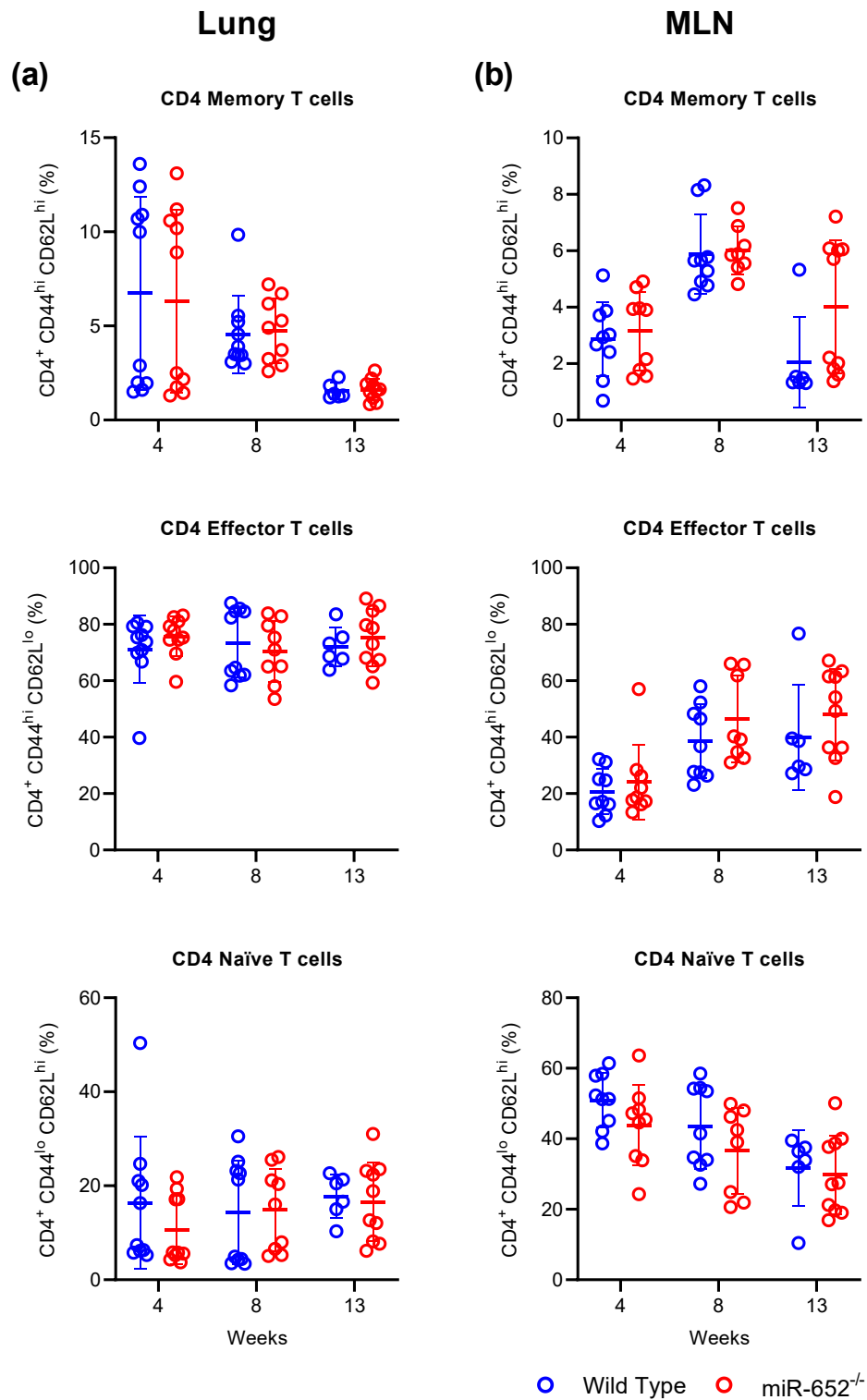
Figure 4.14. Helper T cell populations are similar in wild type and miR-652$^{-/-}$ mice during *M. tuberculosis* infection. Mice were infected as in Figure 4.9. The (a) lungs and (b) mediastinal lymph nodes of infected mice were dissociated to single cells, and stained for flow cytometry. The T cell subsets are expressed as a percentage of all CD4$^+$ cells. Data are the mean ± SD of 5-10 animals, from two experiments. Comparisons were made using 2-way ANOVA with multiple comparisons post-test, Šidák method corrected.
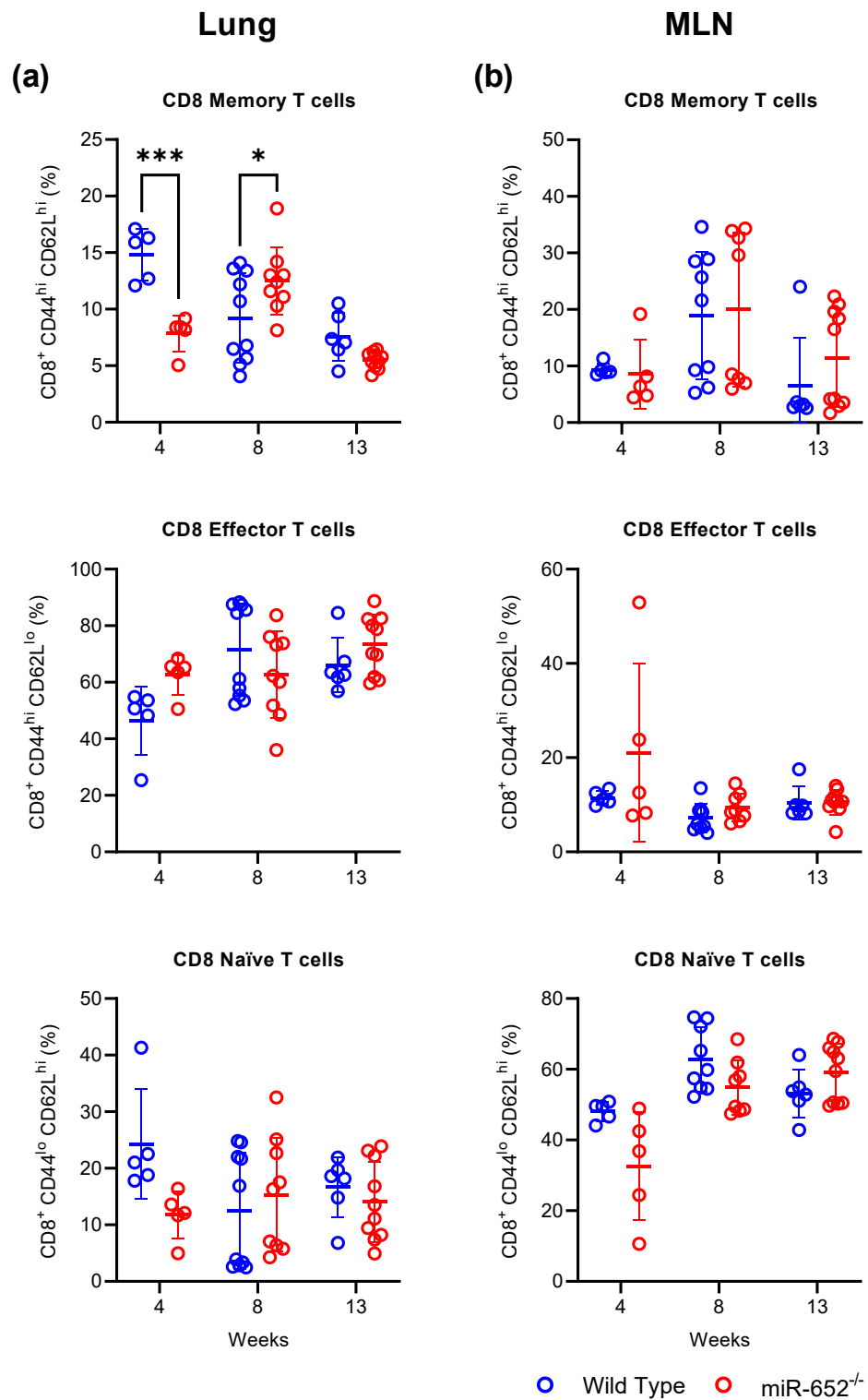
Figure 4.15. Memory cytotoxic T cell populations are decreased during acute *M. tuberculosis* infection of miR-652⁻/⁻ mice. Mice were infected as in Figure 4.9. The (a) lungs and (b) mediastinal lymph nodes of infected mice were dissociated to single cells, and stained for flow cytometry. The T cell subsets are expressed as a percentage of all CD8⁺ cells. Data are the mean ± SD of 5-10 animals, from two experiments. *$P < 0.05$, ***$P < 0.001$, by 2-way ANOVA with multiple comparisons post-test, Šidák method corrected.

4.4.   Discussion

An investigation quantifying plasma miRNA in a cohort of Chinese TB patients found that decreased circulating miR-652 was associated with severe TB disease, and also with TB treatment failure (20). The current investigation endeavoured to characterise the actions of miR-652 during mycobacterial infection in miR-652$^{-/-}$ mice. This chapter showed that miR-652 deficiency in mouse macrophages greatly impaired the expression of cytokines TNF, IL-6, MIP-1α, and KC, all critical for the activation of anti-mycobacterial defences. Activation of the AKT-mTOR signalling pathway was dysregulated in miR-652$^{-/-}$ cells, indicating a potential pathway by which miR-652 may regulate cytokine expression. However, during *in vivo* aerosol *M. tuberculosis* infection, miR-652$^{-/-}$ mice controlled the bacterial load comparably with their wild type counterparts. Considering the less inflammatory phenotype of miR-652$^{-/-}$ macrophages, the competent *in vivo* control suggests these mice rely on compensatory mechanisms from other immune compartments, which will be discussed here.

Alveolar tissue resident macrophages are the first leukocytes to encounter mycobacteria following a pulmonary infection, and their reaction to the invading pathogen is instrumental in shaping the immune response, including granuloma formation. *In vitro* macrophage infections with *M. tuberculosis* and *M. avium* highlight the differential macrophage response to mycobacteria of differing virulence. Both *Mycobacterium* species are important human pathogens, known to induce distinctive immune responses (200, 217, 240). After infection with *M. tuberculosis*, around 10% of patients will develop active tuberculosis disease, whilst the remainder clear the bacteria or contain the pathogen in a latent infection (217). In comparison, *M. avium* is a non-tuberculoid mycobacteria common in the environment. The majority of the population are not susceptible to *M. avium* infection, however, immunosuppression and severe pulmonary disease predispose patients to *M. avium* colonisation (240). Global TB incidence has slowly decreased between 2000-2020 (21), whilst *M. avium* infection rates have recently increased in several reporting regions, including Australia (241). Better understanding the impact of miR-652 in both infections could have important implications for anti-microbial treatments or conjunctive inflammation management.

Macrophage cytokine expression is key for leukocyte recruitment to the lung, and assists in activation and programming of arriving cells. An efficient cytokine response is required for an organised immune response to *M. tuberculosis* infection, and mice lacking key cytokines including TNF, IFNγ, and IL-12 are susceptible to low-dose infection (200). TNF is primarily produced by macrophages and functions to regulate cell apoptosis and cytokine expression (242). TNF^{-/-} mice fail to form structured granulomas and cannot control bacterial spread, resulting in a high bacterial burden in the lung (243-245). Similar results are observed in human patients receiving anti-TNF therapies (220). TNF expression in miR-652^{-/-} macrophages was significantly decreased *in vitro* compared to wild type cells, despite both wild type and miR-652^{-/-} macrophages controlling the bacterial growth in a similar fashion. Previous studies have demonstrated mice lacking macrophage-derived TNF struggle to control bacterial load up to 4 weeks post-infection, however bacterial load is subsequently reduced with TNF expression from T cells (246). The data presented here demonstrated that the lungs of *M. tuberculosis*-infected miR-652^{-/-} mice displayed an unaffected histological phenotype, with contained inflammatory lesions, even though macrophage TNF expression was significantly decreased *in vitro*. Whilst macrophage TNF expression is decreased in miR-652^{-/-} mice, compensatory TNF may be expressed by other cell types. *In vivo* TNF expression in the lung was not analysed in this study, and determination of TNF concentration in mouse lung homogenates could shed light on any compensatory mechanisms. For example, the *in vitro* macrophage infection in this study has limitations due to the lack of T cell interactions, in particular T cell IFNγ release. IFNγ is essential for proinflammatory activation of macrophages, stimulating cytokine release and bacterial killing (217, 247). Future studies should investigate the contribution of IFNγ towards activation of miR-652^{-/-} macrophages. Additionally, intracellular staining for TNF expression in miR-652^{-/-} primary lung leukocytes could clarify if decreased TNF expression is macrophage- or myeloid lineage-restricted.

And so, while the susceptibility of TNF^{-/-} mice to *M. tuberculosis* is well established (244, 248, 249), the effect of low-level macrophage TNF expression in *M. tuberculosis*-infected miR-652^{-/-} mice is less clear. Studies have shown transmembrane TNF-restricted mice, which cannot produce soluble TNF, can control *M. tuberculosis* in the lung for more than

16 weeks, but lesions degenerate by 25 weeks post-infection and mice become moribund (245). Similarly, diminished TNF expression in miR-652$^{-/-}$ mice could be sufficient to attract leukocytes to the lung and initially restrict *M. tuberculosis* growth, but may not be sufficient to maintain long-term control. As previously stated, future studies should assess actual soluble TNF concentrations in the lung.

This chapter demonstrated decreased expression of the cytokine IL-6 in mycobacteria-infected miR-652$^{-/-}$ macrophages. IL-6 is not essential for the early control of low-dose aerosol *M. tuberculosis* infection (250), however, IL-6$^{-/-}$ mice are more susceptible to intravenous *M. tuberculosis* infection (250, 251). Furthermore, decreased IL-6 levels in the bronchoalveolar lavage fluid of human TB patients is associated with increased cavitary lung lesions (252). Both TNF and CXCL1, the human KC analogue, induce IL-6 expression in macrophages (242, 253), and TNF itself can induce CXCL1 expression. The decreased cytokine expression observed in miR-652$^{-/-}$ mice may be a downstream impact of TNF downregulation.

The chemokines MIP-1α and CXCL1 recruit T cells and neutrophils to the *M. tuberculosis*-infected lung (242, 254). Both chemokines are elevated in the plasma of TB patients, and higher concentrations are associated with increased disease severity (255). Moreover, high plasma MIP-1α prior to antibiotic treatment is associated with poorer treatment outcomes, whilst increased plasma CXCL1 correlates with improved outcomes (255, 256). This study showed decreased expression of both MIP-1α and KC in miR-652$^{-/-}$ cells. Considering higher miR-652$^{-/-}$ concentration in serum is associated with better treatment outcomes (20), these results suggest miR-652 might play a more direct role in regulating KC expression in macrophages.

As dysregulated cytokine expression in miR-652$^{-/-}$ mice could lead to impaired chronic *M. tuberculosis* tolerance, it is necessary to investigate the miR-652-dependent mechanisms of cytokine regulation. Ideally, this would provide an opportunity to therapeutically augment *M. tuberculosis* control in miR-652-low individuals. With this aim, it was hypothesised that the AKT-mTOR pathway would regulate cytokine release in miR-652$^{-/-}$ mouse macrophages. The highly conserved kinase mTOR is a central regulator of cell growth, differentiation, metabolism, and proliferation, with important

impacts on the immune response. mTOR forms two separate complexes, mTORC1 and mTORC2, depending on whether it associates with Raptor or Rictor, respectively (257, 258). mTORC1 is regulated by the serine/threonine kinase AKT via phosphorylation of the TSC1/TSC2 complex (235). mTORC2 is not regulated by AKT kinase activity, but rather mTORC2 phosphorylates and activates AKT (257, 259). There are three AKT isoforms present in humans and mice, AKT1, AKT2, and AKT3, each transcribed from separate genes and each with varying activities (260-262).

In this study AKT phosphorylation was decreased in miR-652$^{-/-}$ macrophages 90 min after infection with both *M. tuberculosis* and *M. avium*. This only translated into increased mTOR phosphorylation during low-dose *M. avium* infection, however, these results suggest miR-652 could regulate cytokine expression through AKT. This complex mTOR regulatory pathway is very relevant to *M. tuberculosis* infection, as mycobacterial antigens can modulate diverse leukocyte phenotypes via AKT-mTOR pathway activation, affecting the progression of TB disease. Mannose-capped lipoarabinomannan, a characteristic component of the *M. tuberculosis* cell wall, interferes with CD3 activation on CD4$^+$ T cells (263). This leads to decreased AKT and mTOR phosphorylation and subsequent inhibition of T cell proliferation and cytokine expression (264, 265), functions both essential to the containment of the bacteria (217).

M. tuberculosis is also known to influence macrophage phenotype via AKT-mTOR modulation. Rv1987, a protein secreted by pathogenic mycobacteria, induces a Th2 response and M2 macrophage phenotypes *in vivo* (266). Alveolar macrophages decreased CD86 expression and increased CD206 in response to Rv1987-expressing *M. smegmatis,* changes not induced by wild type *M. smegmatis*. Rv1987 binds macrophages through an unknown mechanism, causing phosphorylation of AKT1 and mTORC1, thus inhibiting NF-κB activation (267) and impairing control of bacterial load (266). In contrast, phosphorylation of AKT2 induces NF-κB activation in macrophages, potentially through kinase HK2 (268). AKT2 activation switches macrophages towards an M1 inflammatory phenotype and induces TNF and IL-6 expression (260, 262). The AKT3 isotype inhibits development of macrophages into foam cells (269), and whilst

foam cells have a role in the tuberculosis granuloma (216), the involvement of AKT3 in bacterial control is uncertain.

These conflicting activities of the AKT isotypes are interesting, as the methods described in this chapter do not differentiate which AKT isotype was phosphorylated during infection. The western blot antibodies used here to evaluate AKT expression and phosphorylation are not specific for a particular AKT isotype. Thus, it remains unclear whether decreased AKT activation may be responsible for low cytokine expression in miR-652$^{-/-}$ macrophages. Similarly, the antibodies used to measure mTOR expression and phosphorylation by western blot bind mTOR alone, and it is not possible from these results to determine its activity within the mTORC1 or mTORC2 complexes. Western blot antibodies targeting specific AKT isotypes are commercially available, and should be applied in future studies to accurately characterise miR-652-dependent AKT activation.

Macrophage metabolism is heavily regulated by the AKT-mTOR pathway (257), further manipulated by *M. tuberculosis* antigens (270, 271). *In vitro M. tuberculosis* infection of PBMCs causes metabolic switching towards glycolysis via TLR2 and AKT-mTOR, increasing IL-1β expression (270, 272). Glycolytic interstitial macrophages are more adept at controlling *M. tuberculosis* bacterial load, compared to alveolar macrophages which utilise oxidative phosphorylation (273). Furthermore, macrophage glycolysis allows for increased generation of NADPH via the pentose phosphate pathway shunt, providing necessary substrates for generating reactive oxygen and nitrogen species (274). Modulated AKT activation in miR-652$^{-/-}$ macrophages could regulate their inflammatory phenotype and downstream cytokine secretion. The relevance of macrophage immunometabolism and glycolytic activity in miR-652$^{-/-}$ mice will be discussed further in chapters 5 and 6.

In order to identify the upstream activators of AKT, or indeed parallel pathways for miR-652-dependent cytokine regulation, this study investigated the impacts of miR-652 deficiency on Notch signalling. The Notch pathway was a hypothesised target of miR-652 regulation in macrophages because the NOTCH ligand JAG1 is a validated target of miR-652 in cardiomyocytes (79). Furthermore, the Notch signalling pathway regulates a diverse range of cellular systems, including key anti-mycobacterial defence pathways.

Notch signalling heavily impacts T cell development (275-278) and macrophage inflammatory phenotypes (279-282). Infection with *M. bovis* BCG activates NOTCH signalling via TLR2 (159, 283), stimulating IL-6 and TNF expression (280, 284-286). In turn, NOTCH1 activation by JAG1 further increases JAG1 expression in an auto-activation feedback loop to enhance inflammatory macrophage phenotype (84, 285). This study saw no change in NOTCH1, NOTCH2, or JAG1 mRNA transcription during mycobacterial infection of miR-652$^{-/-}$ macrophages. No change in the NOTCH-JAG1 auto-amplification loop suggests that the NOTCH signalling in macrophages is not impacted by miR-652 expression. Considering JAG1 was validated as a miR-652 target in mouse cardiac tissue (79), other redundant regulatory mechanisms may influence NOTCH activation in the macrophage context, including alternative NOTCH ligands JAG2 and DLL1, 3, and 4. For example, DLL4 activation of NOTCH in human macrophages promotes an inflammatory phenotype, including increased IL-1β secretion, and increased apoptosis of M2 macrophages (287). Thus, the effects of competing ligands could compensate for or augment any modified JAG1 signalling in miR-652$^{-/-}$ cells. Further studies are necessary to investigate these additional ligands in miR-652-deficient mice.

Although miR-652 expression has a clear impact on cytokine expression during an acute mycobacterial infection *in vitro*, it remained unclear how this might influence the immune response in a chronic *in vivo* infection. Considering that a high MOI *in vitro* induced more cytokine release than a low MOI, this suggests the aerosol bacterial dose administered *in vivo* could also impact the disease phenotype. When a moderate dose of approximately 100 bacilli is administered to the lungs of C57BL/6 mice, each animal will typically control the infection for more than 6 months (245). However, lung granulomas in C57BL/6 mice are often considered disorganised and diffuse compared to those in the human lung (288-290). Interestingly, a very recent study suggests this may have more to do with the bacterial load administered than the species infected. Mice receiving approximately one *M. tuberculosis* bacterium by aerosol infection present very human-like granulomas, with lymphocytes and macrophages densely associated around the granuloma, rather than throughout adjacent lung tissue (291). Low miR-652 expression is associated with TB disease in the human context (20), where patients are probably receiving a similarly low infectious dose. Reflecting this, perhaps the *in vivo*

impact of miR-652-deficiency would be more apparent in mice with a much lower dose administered. Whilst there are unavoidable practical obstacles associated with conducting such ultra-low dose infection experiments in mice, such protocols may give a more accurate picture of the immune response in miR-652-low patients.

When imaging lung inflammation in *M. tuberculosis* infected mice, this study found that miR-652$^{-/-}$ mice presented with very similar lung inflammation to their wild type counterparts over a 13-week infection. Histology showed progression of inflammatory lung lesions was comparable in both mouse strains, and this was reflected in the ability of both strains to control bacterial growth. Histological data was further validated by flow cytometry data. Neutrophil and T cell populations recruited to the infected lungs were largely similar, suggesting that differences in *in vitro* chemokine expression may be compensated for *in vivo*, either through expression by other cell types or by stimulation of macrophages with IFNγ to optimise activation. Furthermore, the comparable CD69 expression observed in effector T cells suggests that T cell activation was not adversely affected by any potential downregulation of TNF expression. A similar result was observed in mice lacking soluble TNF (245). These mice effectively recruited and activated T cells, and yet could not control the *M. tuberculosis* infection beyond 25 weeks. An assessment of cytokine concentration in lung homogenates may shed light on *in vivo* TNF regulation in the miR-652$^{-/-}$ mouse, and extended time points may be necessary to capture any late-stage capitulation of lung granulomas lacking sufficient TNF.

Whilst CD4$^+$ T cell subpopulations were comparable between wild type and miR-652$^{-/-}$ mice analysed at each time point, the proportion of CD8$^+$ effector T cells increased at 4 weeks post-infection, with fewer memory CD8$^+$ T cells present in the lungs of miR-652$^{-/-}$ mice. This is of particular interest because the differentiation of CD8$^+$ memory and effector subsets is regulated by LGL1 (292, 293), another confirmed gene target of miR-652 (35). The proper expansion of memory CD8$^+$ cytotoxic T cells is necessary for the long-term control of latent *M. tuberculosis* infection and guards against potential reinfection (294, 295). CD8$^+$ T cell-depleted mice die earlier than wild type mice (296). Furthermore, CD8$^+$ T cell depletion prior to *M. tuberculosis* infection of non-human

primates removes the protection provided by *M. bovis* BCG vaccination or previous *M. tuberculosis* infection (294). In this context, dysregulation of the CD8⁺ T cell response in miR-652$^{-/-}$ mice suggests low miR-652 expression could impair bacterial control during chronic infection, or during the long antibiotic course required for TB treatment. Further studies could investigate the impact on differentiation of CD8⁺ effecter T cells into terminally differentiated effector cells versus long-lived effector memory precursors, a process also modulated by LGL1 complexes (292, 297, 298). These phenotypes can be distinguished by KLRG1 and IL-7Rα expression.

There are notable differences in the activities of human and murine CD8⁺ T cells against mycobacteria, particularly the expression of granulysin. The pore-forming protein granulysin enters infected cells through perforin pores, and can attack the mycobacterial cell wall directly (299). CD8⁺ T cell granulysin expression is increased in patients with latent versus active TB (300), suggesting this direct antimicrobial activity may play an important role in bacterial control. These activities are not present in the mouse model, as there is no granulysin homologue in rodent species. Additionally, transgenic expression of human granulysin in mice aids in *M. tuberculosis* clearance (301). That said, murine CD8⁺ T cells do possess other cytotoxic proteins including perforin and granzymes, and granulysin is not essential for the control of other intracellular bacterial pathogens (302, 303). To better characterise the impact of miR-652 expression on CD8⁺ T cell differentiation and phenotype, miR-652$^{-/-}$ mice were studied in a CD8⁺ T cell-focused infection model; acute infection with the *Listeria monocytogenes* bacterium. This study is described in Chapter 5.

This chapter described the importance of miR-652 expression in the proinflammatory macrophage response to *M. tuberculosis*. Cells deficient in miR-652 showed decreased expression of key cytokines, and although the direct mechanism of miR-652 in cytokine regulation remains unclear, these data suggest activation of the AKT-mTOR axis is necessary. Data from *M. tuberculosis*-infected miR-652$^{-/-}$ mice suggest that, in addition to macrophages, CD8⁺ T cell phenotypes may be modulated by miR-652 expression. This could have important implications in control of latent and chronic TB disease.

CHAPTER 5

The impact of miR-652 during *Listeria monocytogenes* infection

Chapter 5. The impact of miR-652 during *Listeria monocytogenes* infection

5.1. Introduction

Listeria monocytogenes is a gram-positive bacillus ubiquitous in the environment. It is the causative agent of the disease listeriosis in animals and humans, typically contracted following ingestion of contaminated plant matter or processed foods (304, 305). In the past few decades, murine listeriosis has become an important laboratory model for analysis of the cytotoxic T cell response, as well as the interactions between the innate and adaptive immune systems. *L. monocytogenes* is notably able to colonise an intracellular niche, spreading from cell-to-cell without passing through the intercellular space, and thus evading much of the innate immune system. This is accomplished through the actions of several essential virulence factors.

The listerial receptors InlA and InlB bind mammalian E-cadherin and cMet, respectively, to gain entry to non-phagocytic cells via endocytosis (306, 307). Phagocytic cells quickly engulf free bacteria into a phagosome, and the majority are destroyed following lysosome-phagosome fusion (308). The secreted pore-forming protein Listeriolysin O cooperates with two secreted phospholipases PlcA and PlcB to destabilise the phagosome, and allow escape of the bacteria into the host cell cytosol (309-311). *Listeria* do not form flagella at mammalian corporal temperatures, and instead rely on sequestration and polymerisation of host cell actin to generate characteristic comet tails (312). The listerial membrane protein ActA, localised on one end of the bacillus, binds host ARP2/3 to initiate actin filament extension (313). Continuous filament extension propels the bacteria within the cytosol, enabling nutrient access and autophagy evasion (314, 315). Cytosolic *Listeria* sense the metabolic state of the host cell and regulate their metabolic activity in response (316). At the cell membrane, actin filament propulsion protrudes the bacteria into neighbouring cells, which engulf *Listeria* in a double-membraned endosome (313). Endosome escape continues, and the bacteria disseminate without exposure to the extracellular space and the humoral immune system.

Following gastric infection, *L. monocytogenes* targets goblet cells to invade the intestinal lumen, where it is phagocytised by resident intestinal macrophages (317). Macrophages and CD103⁺ DCs carry live bacteria to the mesenteric lymph node and spleen for antigen presentation (318, 319). *Listeria* colonising the intestines can also transit through the peritoneal cavity and invade the liver capsule directly (320). Though gastric infection is the most common clinical presentation, intravenous and intraperitoneal system infection methods are commonly used in mice. This was initially to overcome an apparent murine resistance to gastric listeriosis, later attributed to an amino acid difference in E-cadherin which affected affinity to InlA (321).

In systemically infected mice, *L. monocytogenes* is quickly phagocytised by spleen macrophages, liver Kupffer cells, and circulating monocytes (317, 322-324). Infected macrophages express IL-12 and TNF to activate local natural killer (NK) cells, inducing IFNγ expression to activate the antibacterial functions of the macrophage in turn (325). Neutrophils and monocytes are recruited from the bone marrow to contain the infection in the spleen and the liver (326-328). If bacterial growth is not contained, disseminated infection can cross the blood-brain barrier and the placental-foetal barrier (329).

Whilst the innate immune system can contain the initial infection for more than 10 days, a cytotoxic T cell response is required for *Listeria* clearance (330, 331). The splenic naïve T cell population begins to change within 24 hours of infection before rapid expansion of antigen specific cells at days 4-5 post-infection (332). The T cell response peaks at days 7-8 (333, 334), before swift population contraction by day 10, by which time most bacteria have been cleared (330, 335). Memory T cell populations begin differentiation from day 5 and capably protect animals from secondary infection (334, 336).

Constant interaction between these innate and adaptive immune systems are necessary in defence against intracellular bacterial pathogens, including *L. monocytogenes* and *M. tuberculosis*. Regulation of these interactions is multifaceted, and the contributions of miRNA to this immunoregulation are yet to be fully uncovered. Chapter 4 described the effects of miR-652 deficiency to murine antimycobacterial responses. Cytokine expression by infected macrophages was diminished in the absence of miR-652, and data suggested that CD8⁺ T cell development may also be impacted. In this chapter, the

CD8$^+$ T cell-focused *Listeria* infection model was used to ascertain the impacts of miR-652 on both macrophage and T cell function. *In vivo* mouse infections demonstrated that miR-652 has a vital role in immunoregulation during the response to acute *Listeria* infection. Further, the proteomes of *in vitro* infected macrophages indicate that multiple key antibacterial pathways can be regulated by miR-652.

5.2. Methods

5.2.1 Isolation and culture of primary mouse peritoneal macrophages

Mice were euthanised by CO_2 asphyxiation and the skin removed to reveal the peritoneum. A 27G needle was used to inject the peritoneal cavity with 10 ml PBS/Heparin. The cavity was gently massaged to suspend peritoneal cells, and the fluid removed using an 18G needle and held on ice. Collected peritoneal cells were pelleted by centrifugation at 500 rcf for 5 min at 4 °C. Cells were resuspended in tissue media, counted, and diluted as required. Peritoneal macrophage cultures were incubated in adherent static culture at 37 °C, with 5% CO_2. Non-adherent cells were washed away with BMDM media before infection assays, leaving remaining adherent macrophages.

5.2.2 *In vitro L. monocytogenes* infection

Mouse peritoneal macrophages in BMDM media were seeded on 6-well, 24-well, and 96-well flat-bottom culture plates (Corning) and incubated overnight for macrophages to adhere to the plate surface. Wells were washed twice with BMDM media to remove non-adherent cells.

L. monocytogenes culture in LB was centrifuged at 10000 rcf for 5 min. The bacteria pellet was resuspended in BMDM media, the OD_{600} determined using a spectrophotometer (Eppendorf), and then the bacteria were diluted in BMDM media as required. Peritoneal macrophages were infected with *L. monocytogenes* at an MOI of 1 and incubated for 1 h. Wells were then washed with BMDM media to remove extracellular bacteria. BMDM media supplemented with 50 µg/ml gentamicin (Gibco) was added to each well and the plate incubated for 1 h, to kill any remaining extracellular

bacteria. Wells were washed twice with BMDM media to remove gentamicin and replacement BMDM media was added. Infected cells were incubated for up to 8 h.

To determine the bacterial load of infected wells, all supernatant was removed and cells lysed with 200 μl 0.1% Triton solution for 10 min at 37 °C. Lysates were serially diluted in sterile water and plated on LB agar to determine the CFU concentration. Plates were incubated at 37 °C for 20-30 h before CFU counts.

5.2.3 *In vivo L. monocytogenes* infection

Mice were infected with a low dose of *L. monocytogenes* by intraperitoneal injection. *L. monocytogenes* suspension culture was revived from frozen stock and grown overnight at 37 °C in LB. The bacterial culture was centrifuged at 6000 rcf for 5 min, and the bacterial pellet resuspended in PBS at 5×10^4 CFU/ml. Each mouse was administered 200 μl bacterial suspension into the peritoneal cavity. To confirm infection dose, the injection suspension was serially diluted in sterile water, plated on LB agar, and incubated at 37 °C for 24 h before CFU were counted. Mice were administered 2000-4800 CFU/mouse.

Mice were weighed prior to infection, and then once or twice daily from 2-10 days post-infection. At regular timepoints, mice were euthanised by CO_2 asphyxiation for organ collection.

The right median liver lobe was removed into 10% neutral-buffered formalin for histology. The left liver lobe was collected into sterile water for CFU enumeration. The spleen was cut in half and each half weighed; half was placed in sterile water for CFU enumeration, and half was placed in tissue media for flow cytometry analysis.

5.2.4 Flow cytometry gating

Spleen leukocytes of *L. monocytogenes*-infected mice were stained and analysed according to section 3.2.7. Gating was performed using FlowJo v10 software.

<u>T cell subsets</u>

A gating strategy was developed to analyse T cell leukocytes, and the activation status of particular T cell subsets (Figure 5.1). Cell debris was excluded by gating for high FSC-A and low-high SSC-A. Single cells were gated in the linear portion of the FSC-A vs FSC-H plot, eliminating cell aggregates. This gating was repeated using SSC-A and SCC-H to exclude further aggregates. All leukocytes were gated based on CD45 expression, and then CD4$^+$ helper T cells and CD8$^+$ cytotoxic T cells were gated on a CD4 vs CD8 plot. Under each of the CD4$^+$ and CD8$^+$ gates, the effector T cells were gated as CD44^{hi} CD62L^{lo}, memory T cells were gated as CD44^{hi} CD62L^{hi}, and naïve T cells were gated as CD44^{lo} CD62L^{hi}. Effector CD4$^+$ T cells and effector CD8$^+$ T cells were identified as activated based on CD69 expression, and as terminally differentiated effector T cells based on KLRG1 expression.

<u>Myeloid subsets</u>

A gating strategy was developed to analyse myeloid lineage leukocytes (Figure 5.2), based on a previously published strategy (233). Cell debris was excluded by gating for high FSC-A and low-high SSC-A. Single cells were gated in the linear portion of the FSC-A vs FSC-H plot, eliminating cell aggregates. This gating was repeated using SSC-A and SCC-H to exclude further aggregates. All leukocytes were gated based on CD45 expression. From the total CD45$^+$ population, a CD103$^+$ DC subset was gated based on CD103 expression. CD103$^-$ cells were plotted on CD11b vs Ly6G to gate Ly6G$^+$ neutrophils. Ly6G$^-$ cells were plotted on CD11c vs Siglec F to gate CD11c$^-$ Siglec-F$^+$ eosinophils. An MHC-II vs CD11b plot was used to gate CD11b$^+$ cells from CD11b$^-$ cells, and the CD11b$^-$ population includes some MHC-II$^-$ CD11b^{mid} cells. The CD11b$^-$ population was plot on MHC-II vs B220 in order to gate MHC-II$^+$ B220$^+$ B cells. The CD11b$^+$ population was plot on MHC-II vs CD24, gating for MHC-II$^+$ CD24$^-$ interstitial macrophages, an MHC-II$^+$ CD24$^+$ CD11b$^+$ DC subset, and remaining MHC-II^{lo} cells. These MHC-II^{lo} cells were separated based on Ly6C expression into Ly6C$^+$ monocytes and Ly6C$^-$ monocytes.

Intracellular cytokine expression

A gating strategy was developed to analyse cytokine expression by T cell leukocytes (Figure 5.3), following intracellular staining of cytokines. Cell debris was excluded by gating for high FSC-A and low-high SSC-A. Single cells were gated in the linear portion of the FSC-A vs FSC-H plot, eliminating cell aggregates. This gating was repeated using SSC-A and SCC-H to exclude further aggregates. All leukocytes were gated based on CD45 expression, and then CD4$^+$ helper T cells and CD8$^+$ cytotoxic T cells were gated on a CD4 vs CD8 plot. Under each of the CD4$^+$ and CD8$^+$ gates, cells were gated for expression of four cytokines; IFNγ, IL-2, IL-17a, and TNF.
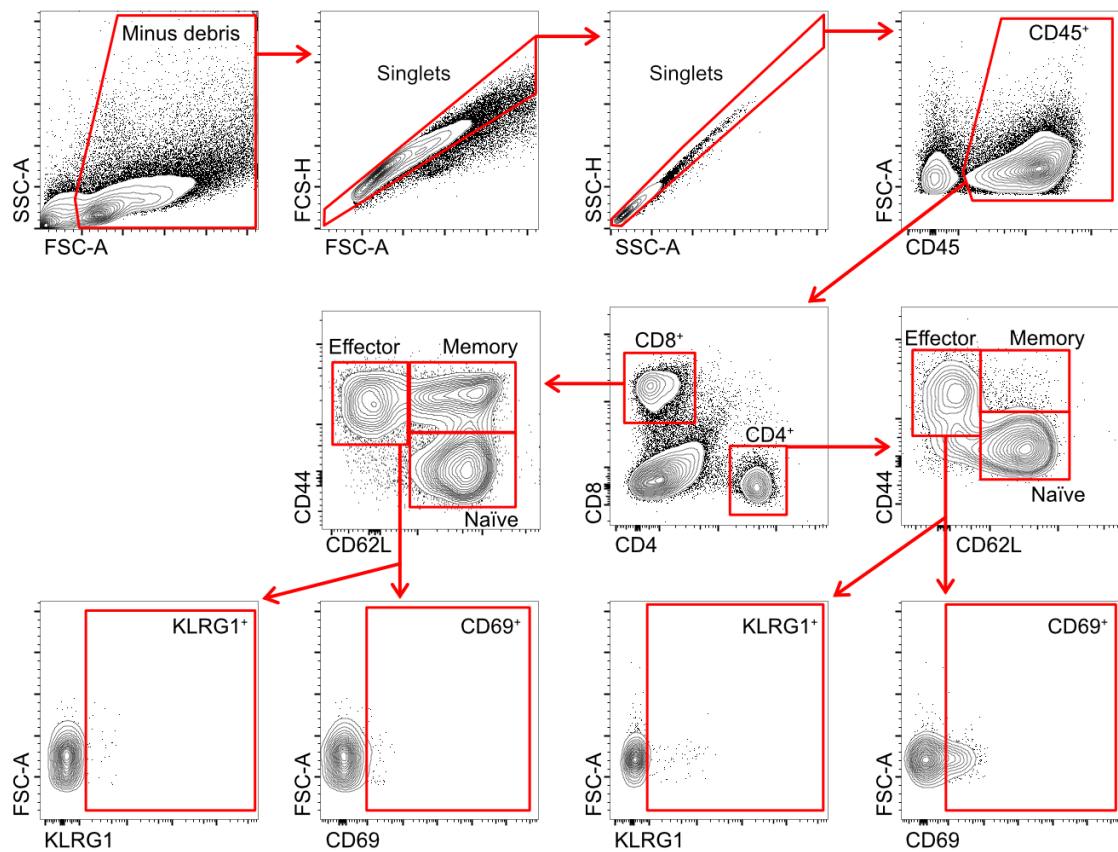
Figure 5.1. Flow cytometry gating strategy for analysis of T cell populations in the spleen of _L. monocytogenes_-infected mice. Cells are isolated from debris and single cells selected. CD45$^+$ leukocytes are isolated into CD4$^+$ and CD8$^+$ T cell populations, and both are gated for effector, memory, and naïve T cell subsets. The expression of early activation marker CD69 and terminal differentiation marker KLRG1 are analysed within the effector T cell subsets.
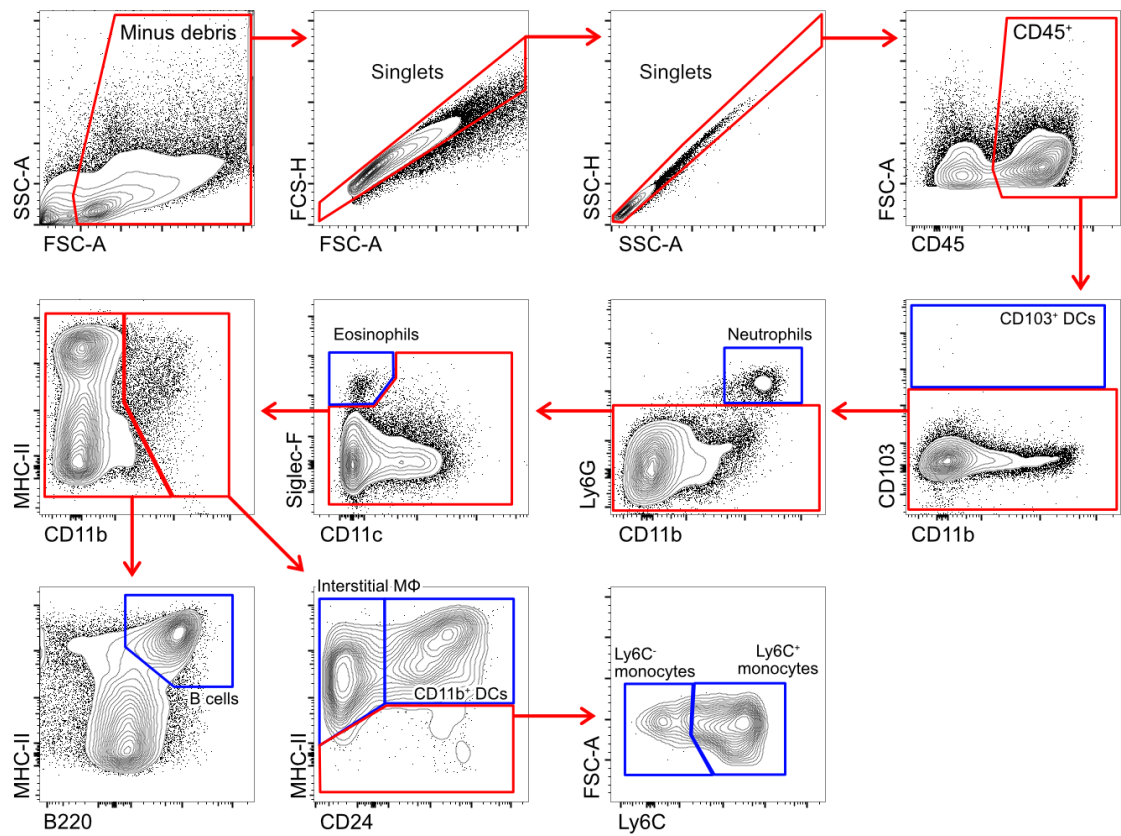
Figure 5.2. Flow cytometry gating strategy for analysis of myeloid lineage cell populations in the spleen of *L. monocytogenes*-infected mice. Cells are isolated from debris and single cells selected. CD45^{+} leukocytes are isolated from remaining cells. Dendritic cell, neutrophil, and eosinophil populations are sequentially isolated using CD103^{+}, Ly6G^{+}, and Siglec-F^{+} selection, respectively. CD11b expression separates B220^{+} B cells, from phagocytic populations. MHC-II and CD24 expression isolates CD11b^{+} dendritic cells and interstitial tissue macrophages from monocytes and monocyte-derived macrophages, which can themselves be separated into subsets based on Ly6C expression
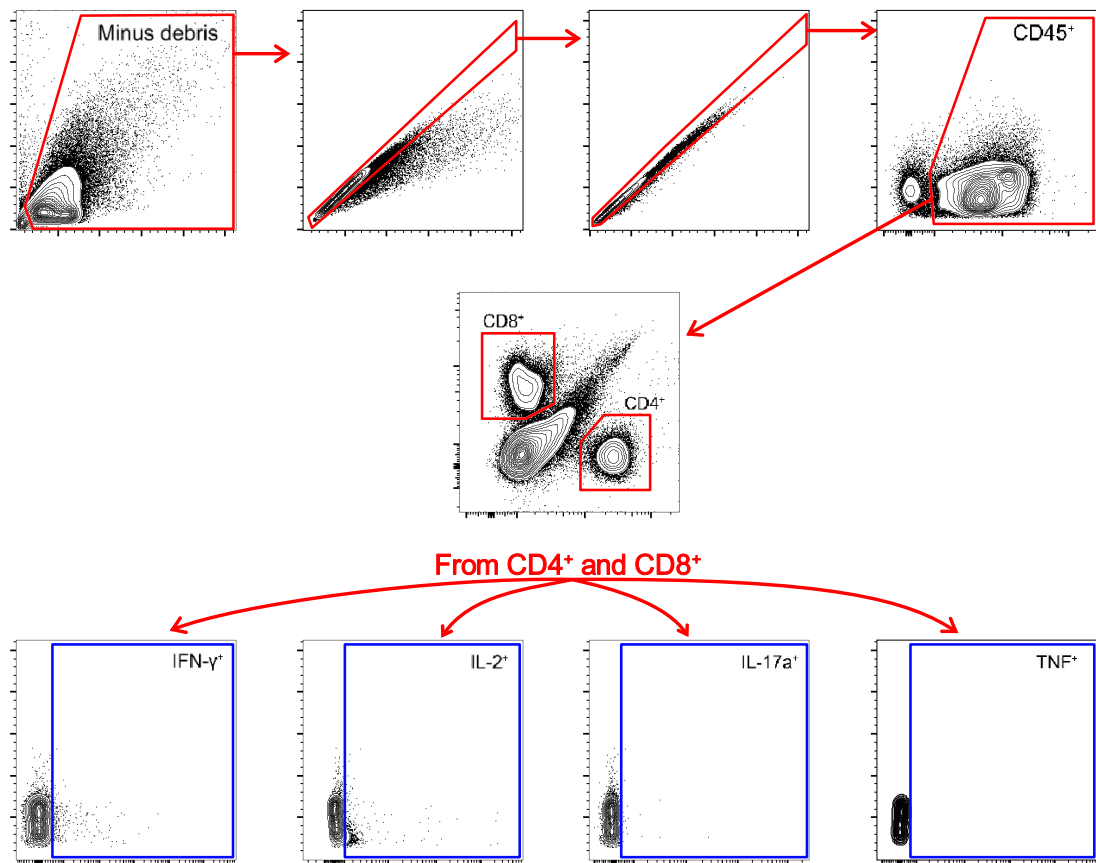
Figure 5.3. Flow cytometry gating strategy for analysis of T cell cytokine expression, following intracellular staining of spleen cells from *L. monocytogenes*-infected mice. Cells are isolated from debris and single cells selected. CD45+ leukocytes are isolated into CD4+ and CD8+ T cell populations. Each of the CD4+ and CD8+ populations is then gated for expression of IL-2, IL17a, IFNγ, and TNF.

5.2.1 Proteomics analysis of protein expression
5.2.1.1   Protein isolation and alkylation

Peritoneal macrophages were infected with *L. monocytogenes* in a 6-well flat-bottom plate. Cells were washed 3 times with PBS before lysis with 200 µl reconstitution buffer. Samples in reconstitution buffer were incubated for 30 min at 37 °C in order for benzonase to digest DNA. Samples were heated to 60 °C for 60 min, and cooled to room temperature. Samples were supplemented with TCEP to 5 mM and acrylamide to 20 mM, and then incubated at room temperature for 60 min in order to reduce and alkylate protein disulphide bonds. Alkylation was quenched with the addition of DTT to 20 mM.

5.2.1.2   Protein digestion and clean-up

Alkylated proteins were prepared for proteomics according to the SP3 method (337). Briefly, 180 µl alkylated protein sample was mixed with 2 µl SP3 beads, giving a final 55 µg/ml bead concentration. To induce protein binding to beads, 180 µl 100% ethanol was added and mixed for 5 min. Beads were washed 3 times with 80 % ethanol to remove surfactants. Using a magnetic rack, protein-saturated beads were isolated and suspended in 100 µl AMBIC solution, before addition of 1 µg Trypsin Gold, Mass Spectrometry Grade (Promega). Beads were disaggregated by brief sonication, and incubated at 37 °C overnight to digest proteins. The sample was then centrifuged at 20000 rcf to pellet beads and recover peptides in solution.

5.2.1.3   Protein normalisation by STAGE-tip desalting

STAGE-tips and all solutions were prepared as detailed in section 3.1.13. A standard STAGE-tip typically binds 10 µg of peptides under acidic conditions. Peptide concentrations were normalised by saturating each STAGE-tip with protein sample, and eluting peptides into a constant volume.

Digested peptides were acidified with TFA (final 1% concentration). 50 µl acetonitrile was added to the STAGE-tip and the tip centrifuged at 2300 rcf for 5 min, thus activating the STAGE-tip. The STAGE-tip was then equilibrated with 50 µl 1% TFA, and centrifuged at 2300 rcf for 5 min. Peptide samples were loaded onto the STAGE-tip, passed into the filter disc by brief centrifugation, incubated for 1 min at room temperature, and then centrifuged at 2300 rcf for 5 min. The STAGE-tip was washed with 60 µl isopropanol/1%

TFA, then with 60 µl 1% TFA, centrifuging at 2300 rcf for 2 min each wash. 60 µl elution solvent was passed into the STAGE-tip disc by brief centrifugation, and incubated for 10 min at room temperature. The tip was then centrifuged at 2300 rcf for 5 min to elute peptides. Samples were dried in the Speed Vac Concentrator DNA 120 (Thermo Fisher) and resuspended in 25 µl MS loading solvent, ready for LC/MS/MS sampling.

5.2.1.4   LC/MS/MS

Using an Acquity M-class nanoLC system (Waters), 5 µl of the sample was loaded at 15 µl/min for 3 min onto a nanoEase Symmetry C18 trapping column (180 µm x 20 mm) before being washed onto a PicoFrit column (75 µmID x 350 mm; New Objective) packed with SP-120-1.7-ODS-BIO resin (1.7 µm; Osaka Soda Co) heated to 45 °C. Peptides were eluted from the column and into the source of a Q Exactive Plus mass spectrometer (Thermo Scientific) using the following program: 5-30% MS buffer B (98% Acetonitrile + 0.2% Formic Acid) over 90 minutes, 30-80% MS buffer B over 3 minutes, 80% MS buffer B for 2 minutes, 80-5% for 3 min. The eluting peptides were ionised at 2400 V. A Data Dependant MS/MS (dd-MS2) experiment was performed, with a survey scan of 350-1500 Da performed at 70,000 resolution for peptides of charge state 2+ or higher with an AGC target of 3e6 and maximum Injection Time of 50 ms. The Top 12 peptides were selected fragmented in the HCD cell using an isolation window of 1.4 m/z, an AGC target of 1e5 and maximum injection time of 100 ms. Fragments were scanned in the Orbitrap analyser at 17,500 resolution and the product ion fragment masses measured over a mass range of 120-2000 Da. The mass of the precursor peptide was then excluded for 30 s.

5.2.1.5   Data analysis

The MS/MS data files produced by the Q Exactive Plus were searched using PEAKS Studio version 10.6 (Bioinformatics Solutions Inc.) against a combined C57BL/6 mouse and *L. monocytogenes* database (based on the reference sequence database Uniprot) with the following parameter settings. Variable modifications: propionamide, oxidised methionine, deamidated asparagine. Enzyme: trypsin. Number of allowed missed cleavages: 3. Parent mass error tolerance: 10 ppm. Fragment mass error tolerance: 0.05 Da. The results of the search were then filtered to include peptides with a -log10P

score that was determined by the False Discovery Rate (FDR) of <1%, the score being that where decoy database search matches were <1% of the total matches.

Expression comparisons were performed using PEAKS label-free quantitation with the following settings. Mass error tolerance: 20.0 ppm. Retention time shift tolerance: 3.0 min. The results were filtered by including only proteins with ≥5 unique peptides, significance ≥20, and fold change ≥2.

Protein network analysis was performed using the STRING database (string-db.org) (338), inputting proteins differentially expressed between infected wild type and infected miR652$^{-/-}$ peritoneal macrophages, filtered as detailed above. KEGG pathway analysis was performed as part of STRING network generation (339).

5.2.2 Mammalian cell transient transfection

A modified transient transfection protocol was adapted from Longo et al. (340). IC-21 murine peritoneal macrophage cells were seeded in 12-well tissue culture plates at 2 x 10^5 cells/ml, 1 ml/well, and allowed 24 hours to adhere. The miR-652 and negative control miRNA mimics were diluted to 600 nM in RPMI-1640. PEI was diluted to 17 µg/ml in RPMI-1640. miRNA and PEI solutions were combined in a 1:1 ratio and held at room temperature for 15 min. This approximates to a 1:1 µg ratio of PEI:RNA. IC-21 culture supernatant was removed and replaced with 900 µl RPMI-1640 media, supplemented with 0.5% FBS. To each culture well, 100 µl PEI-RNA solution was added, resulting in 1.7 µg/ml PEI and 30 nM RNA. After 24 hours, transfected cells were lysed with 400 µl TRIsure reagent for collection of RNA, or with 200 µl RIPA buffer supplemented with protease and phosphatase inhibitors. Collected RNA and protein samples were stored at -80 °C.

HEK-293T cells were seeded in a solid-white 96-well tissue culture plates at 2 x 10^5 cells/well, 200 µl/well, and allowed 24 hours to adhere. The miR-652 or miR-146a mimic was diluted to 200 nM in DMEM together with luciferase reporter plasmids pIS0, pIS0-Capzb-WT, or pIS0-Capzb-mut at 20 ng/µl. PEI was diluted to 70 µg/ml in DMEM. RNA-DNA and PEI solutions were combined in a 1:1 ratio and incubated at room temperature for 15 min. This approximates to a 3:1 µg ratio of PEI:nucleotide. HEK-293T

culture supernatant was removed and replaced with 900 µl DMEM media, supplemented with 0.5% FBS. To each culture well, 100 µl PEI-RNA-DNA solution was added, resulting in 3.5 ng/µl PEI, 10 nM miRNA, and 1 ng/µl plasmid DNA. After 24 hours, luciferase expression was quantified by luminescence assay.

5.2.3   Firefly luciferase luminescence assay

The luminescence assay was run to quantify firefly luciferase expression after pIS0 transfection. The ONE-Glo luciferase assay system (Promega) was run according to the manufacturer's specifications. Lyophilised ONE-Glo luciferase substrate was reconstituted in ONE-Glo luciferase assay buffer to prepare the luciferase reagent.

Luciferase reagent was equilibrated to room temperature. All supernatant was removed from the solid-white 96-well plate containing transfected cells. 100 µl DMEM was added to each well. 100 µl luciferase reagent was added to each well and incubated at room temperature for 5 min to allow for cell lysis. Luminescence was measured using the Infinity M200 Pro plate reader (Tecan). Luminescence measurements for miRNA mimic-transfected wells were normalised against wells transfected with pIS0 only.

5.3. Results

5.3.1 miR-652^{-/-} mice are highly susceptible to *L. monocytogenes* infection

In order to assess the impact of miR-652 expression on the development of the CD8$^+$ T cell response, wild type and miR-652$^{-/-}$ mice were infected with *L. monocytogenes*. Mice were administered a low dose (approximately 2000-4000 CFU/mouse) by IP injection (Figure 5.4) and weighed twice daily from 3 days post-infection. At each weighing, the physical condition of each mouse was assessed. Evidence of poor condition included a rough coat, a scrunched nose, hunching, and inability to move freely or access food and water. Any mice in poor condition and any mice whose mass fell below 20% of their starting mass were euthanised. Mice which met ethical thresholds for euthanasia were designated ET mice, whilst mice euthanised at preassigned time points were designated TP mice.
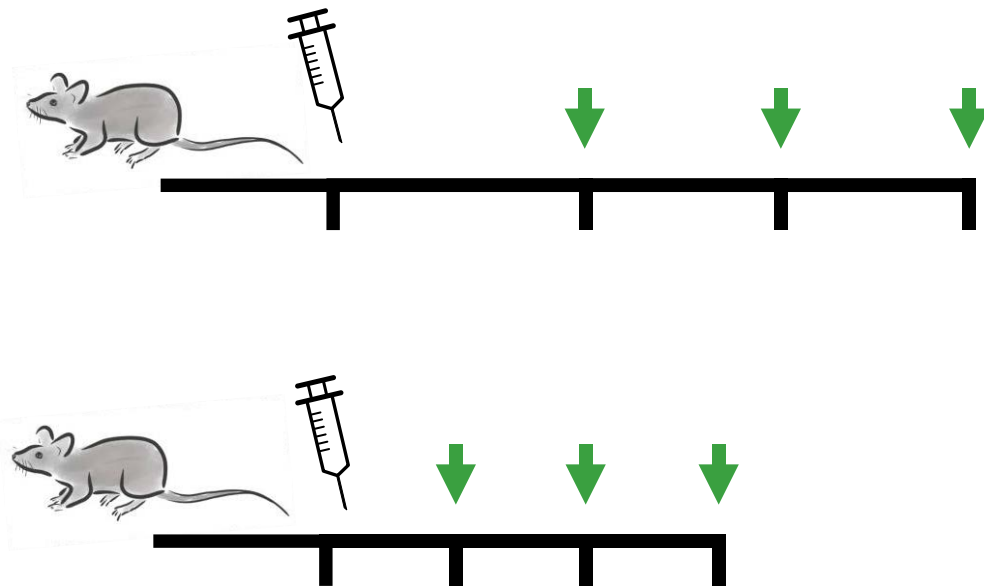
Figure 5.4. *In vivo Listeria monocytogenes* infection in mice. Mice were infected with 2000-4800 CFU of *L. monocytogenes* by intraperitoneal injection, and euthanised at predetermined time points (green arrows) for organ collection and analysis. (a) Experiment 1 timeline; mice euthanised on days 4, 7, and 10 post-infection. (b) Experiment 2 timeline; mice euthanised on days 2, 4, and 6 post-infection.

The miR-652$^{-/-}$ mice were more susceptible to low-dose *L. monocytogenes* infection. A Kaplan-Meier analysis demonstrated miR-652$^{-/-}$ mice had a significantly lower rate of survival compared to wild type mice (Figure 5.5). The condition of miR-652 mice deteriorated early during infection, with several mice euthanised on days 3 and 4 post-infection. In comparison, only a single wild type mouse was euthanised due to excessive weight loss, at 6 days post-infection. The early-stage vulnerability necessitated a shorter experimental timeline for a repeat infection experiment (Figure 5.4).

Weight measurements taken for wild type and miR-652$^{-/-}$ groups are presented in Figure 5.6. miR-652$^{-/-}$ TP mice lost significantly more weight compared to wild type TP mice (Figure 5.6). Furthermore, by 10 days post-infection, wild type TP mice had regained and surpassed their starting weight, whilst miR-652$^{-/-}$ TP mice did not recover to their starting weight.

Significant weight loss was a feature of both the one wild type mouse and all miR-652$^{-/-}$ mice that met an ET (Figure 5.6), suggesting that the path to morbidity in the two groups is similar. However, as significantly more miR-652$^{-/-}$ mice were moribund compared with wild type mice, and their weight loss occurred earlier, it was clear that the loss of miR-652 expression impairs the ability of the mice to control the *Listeria* infection in the acute phase.

Unlike the ET mice, both wild type TP and miR-652$^{-/-}$ TP mice controlled the *Listeria* infection over 10 days. The bacterial load in the spleen was stable in both TP groups up to 4 days post-infection, and decreased by day 7 (Figure 5.7a). By day 10, all 7 wild type TP mice had cleared the infection in the spleen, as had all 3 miR-652$^{-/-}$ TP mice. Additionally, both wild type TP and miR-652$^{-/-}$ TP groups controlled the bacterial load in the liver up to day 7 (Figure 5.7b). Similar to the spleen, 5 of 7 wild type TP and 3 of 3 miR-652$^{-/-}$ TP mice had cleared the infection in the liver by day 10.

Whilst the majority of mice controlled the *Listeria* infection, the one wild type ET mouse and all miR-652$^{-/-}$ ET mice controlled the infection poorly in the acute phase. Bacterial load in the miR-652$^{-/-}$ ET spleen was 10-100-fold higher than in corresponding miR-652$^{-/-}$ TP mice (Figure 5.7a). The single wild type ET mouse also showed a 100-fold

increase in spleen CFU compared to wild type TP mice, when euthanised at day 6. The bacterial load in the spleens of miR-652$^{-/-}$ ET mice decreased from days 3-6, suggesting these mice began to control the infection. However, by that time, the condition of these mice had already deteriorated and they met the threshold for euthanasia.

Liver bacterial loads presented a similar trend. The livers of moribund wild type ET and miR-652$^{-/-}$ ET mice contained 10-100-fold more CFU than those from wild type TP and miR-652$^{-/-}$ TP mice (Figure 5.7b). The bacterial load in livers of miR-652$^{-/-}$ ET mice was stable between days 3-6. However, mice were moribund before the infection was controlled. In summary, these data suggest that the path to morbidity was similar in *L. monocytogenes*-infected wild type and miR-652$^{-/-}$ mice, but miR-652$^{-/-}$ mice were more likely lose control of the infection. A failure to control the bacterial load before day 3 led to mouse morbidity.
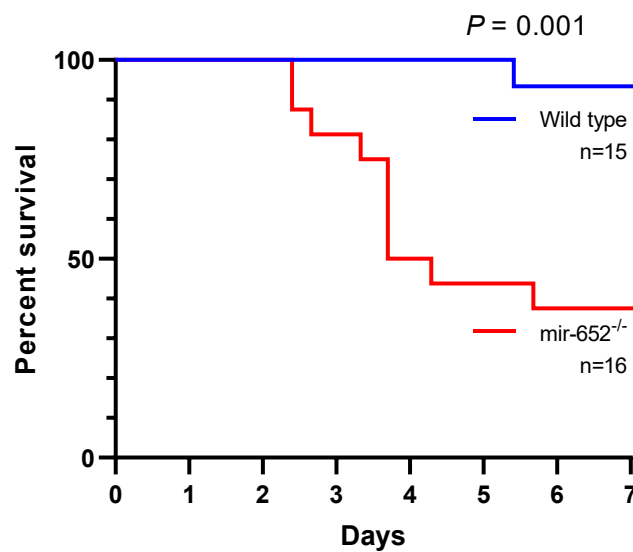
Figure 5.5. miR-652$^{-/-}$ are mortally susceptible to *Listeria* infection. Mice were infected with a low dose of *L. monocytogenes* by IP injection. Kaplan-Meier survival analysis between wild type and miR-652$^{-/-}$ mice. Comparison by log-rank test.
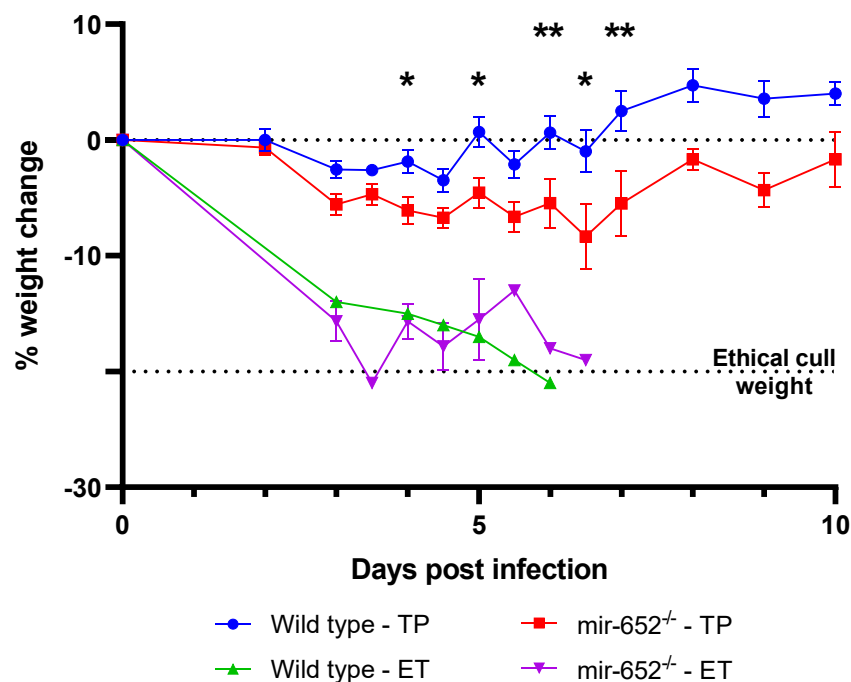
Figure 5.6. Infection-induced weight loss is increased and prolonged in miR-652$^{-/-}$ mice. Relative weight change in mice infected with *L. monocytogenes*. Mice were infected with a low dose of *L. monocytogenes* by IP injection. Infected mice were euthanised at a predetermined time point (TP) or upon meeting an ethical threshold (ET). Moribund ET wild type and miR-652$^{-/-}$ mice lost considerably more weight than their TP counterparts. Data are mean ± SEM from two replicate experiments (cohorts; n=34 wild type TP, n=26 miR-652$^{-/-}$ TP, n=1 wild type EP, n=9 miR-652$^{-/-}$ EP). Comparisons were made between wild type TP and miR-652$^{-/-}$ TP groups only. *$P < 0.05$, **$P < 0.01$, by 2-way ANOVA with multiple comparisons posttest, Šidák method corrected.

Table 5.1. Euthanasia times for *L. monocytogenes*-infected mice. Mice infected as in Figure 5.6.

Day	Wild type TP	Wild type ET	miR-652-/- TP	miR-652-/- ET
2	5	0	5	0
3	0	0	0	3
4	10	0	10	4
5	0	0	0	1
6	5	1	5	1
7	7	0	3	0
8	0	0	0	0
9	0	0	0	0
10	7	0	3	0
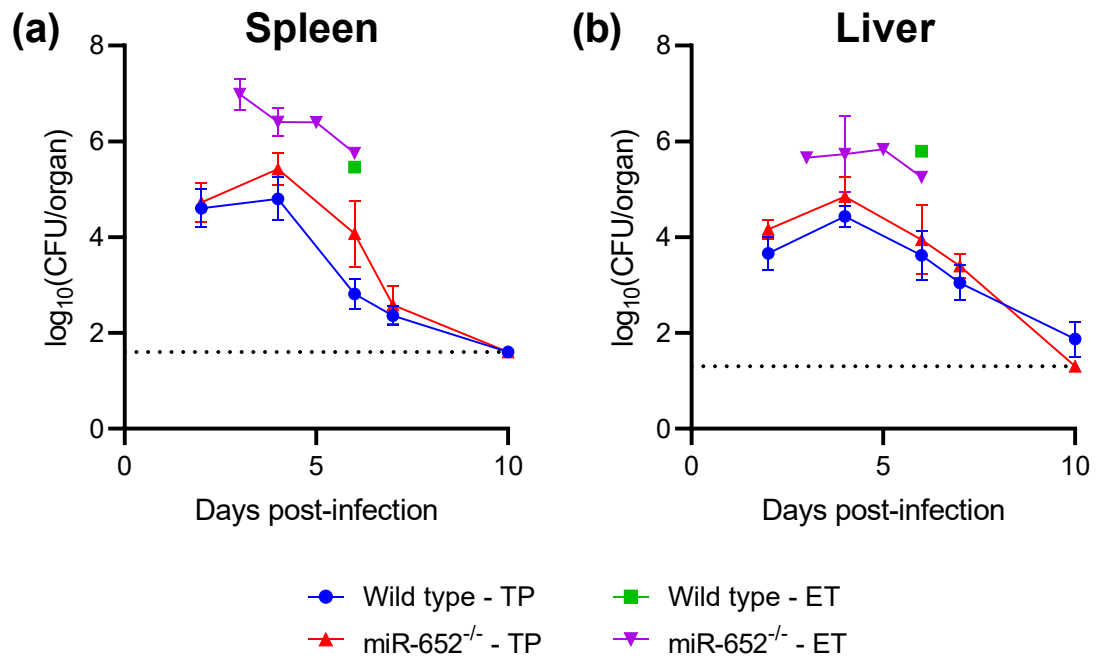
Figure 5.7. Bacterial growth was uncontrolled in moribund ET mice. The bacterial load in the (a) spleen and (b) liver of *Listeria*-infected mice. Mice were infected as in Figure 5.6. *L. monocytogenes* CFU were enumerated from tissue homogenates. Bacterial growth was comparable between TP groups, but much higher in EP mice. Dotted lines depict the lower limit of quantitation; 40 and 20 CFU/organ for the spleen and liver, respectively. Data are mean ± SEM from two replicate experiments (cohorts; n=34 wild type TP, n=26 miR-652^{-/-} TP, n=1 wild type EP, n=9 miR-652^{-/-} EP). Comparisons were made between wild type TP and miR-652^{-/-} TP groups only, by 2-way ANOVA with multiple comparisons post-test, Šidák method corrected.

5.3.2 Liver inflammation is increased in susceptible miR-652$^{-/-}$ mice

We endeavoured to assess whether the significant weight loss and increased bacterial load observed in miR-652$^{-/-}$ mice was associated with dysregulated inflammation in the spleen and liver, the organs most affected by *L. monocytogenes* infection. IL-6 and TNF concentrations in spleen and liver homogenates were assessed by CBA.

Inflammatory cytokine concentrations in the tissues were increased in miR-652$^{-/-}$ TP mice over wild type TP mice, and all ET mice presented still higher concentrations in the liver (Figure 5.8). Day 4 IL-6 levels in the miR-652$^{-/-}$ TP liver were much higher than in wild type TP mice (Figure 5.8a), and liver TNF levels were increased in miR-652$^{-/-}$ mice from days 2-6 post-infection (Figure 5.8c). Furthermore, both wild type and miR-652$^{-/-}$ ET mice presented 2-fold higher liver IL-6 and almost 10-fold higher liver TNF at day 6. In the spleen, both IL-6 and TNF were elevated in miR-652$^{-/-}$ TP mice compared to wild type TP mice (Figure 5.8b and d). Spleen TNF levels were particularly high in moribund miR-652$^{-/-}$ ET mice (Figure 5.8d), however they decreased sharply in mice euthanised after day 4, as the mice gradually controlled the bacterial growth within the spleen (Figure 5.7a).

IL-6 and TNF expression is associated with recruitment and proliferation of inflammatory leukocytes (239, 341), and it was not clear whether this cytokine elevation was a result of, or associated with, increased inflammation. To investigate this, fixed liver sections from infected wild type and miR-652$^{-/-}$ mice were stained with haematoxylin and eosin, and viewed by bright field microscopy. From the early stages of infection, lesions in wild type livers were predominantly small and contained (Figure 5.9a). They consisted of polymorphonuclear cells (PMNs) and macrophages at their core, with macrophages at the lesion periphery in the surrounding hepatic parenchyma (Figure 5.9b). Although a single wild type mouse presented one large lesion, it remained contained. At day 7, lesions were smaller than seen at day 4. At day 7, wild type lesions were composed of lymphocytes and some macrophages (Figure 5.9d), and by day 10 liver inflammation was largely resolved in wild type mice.

In contrast, miR-652$^{-/-}$ liver lesions were larger and more numerous, suggesting a failure to control bacterial spread. Whilst small contained lesions were common from 3 days post-infection, large necrotic lesions were also present (Figure 5.10a) with a dense PMN core surrounded by necrotic hepatocytes (Figure 5.10b). Macrophages were present, but lesions were dominated by PMNs. By day 4, some lymphocyte migration into the lesions was evident, but lesions in both TP and ET miR-652$^{-/-}$ mice were large and diffuse (Figure 5.10c). These large lesions held dense concentrations of PMNs at their centre, and were surrounded by several smaller lesions, also dominated by PMNs (Figure 5.10d). These smaller satellite lesions suggest *L. monocytogenes* was spreading effectively in miR-652$^{-/-}$ mice, either inside infected motile phagocytes, or directly between infected hepatocytes. PMNs and macrophages spread broadly through the liver parenchyma, and furthermore, areas of broad hepatocyte necrosis were evident, with no discernible organisation in lesion structure. By contrast, only the single moribund wild type mouse presented such disorganised and necrotic lesions (Figure 5.9c). miR-652$^{-/-}$ mice began to resolve inflammation by day 7 as lymphocyte recruitment increased (Figure 5.10e). However, regions of intense necrosis were still present at day 10, by then encased in recruited lymphocytes (Figure 5.10f).
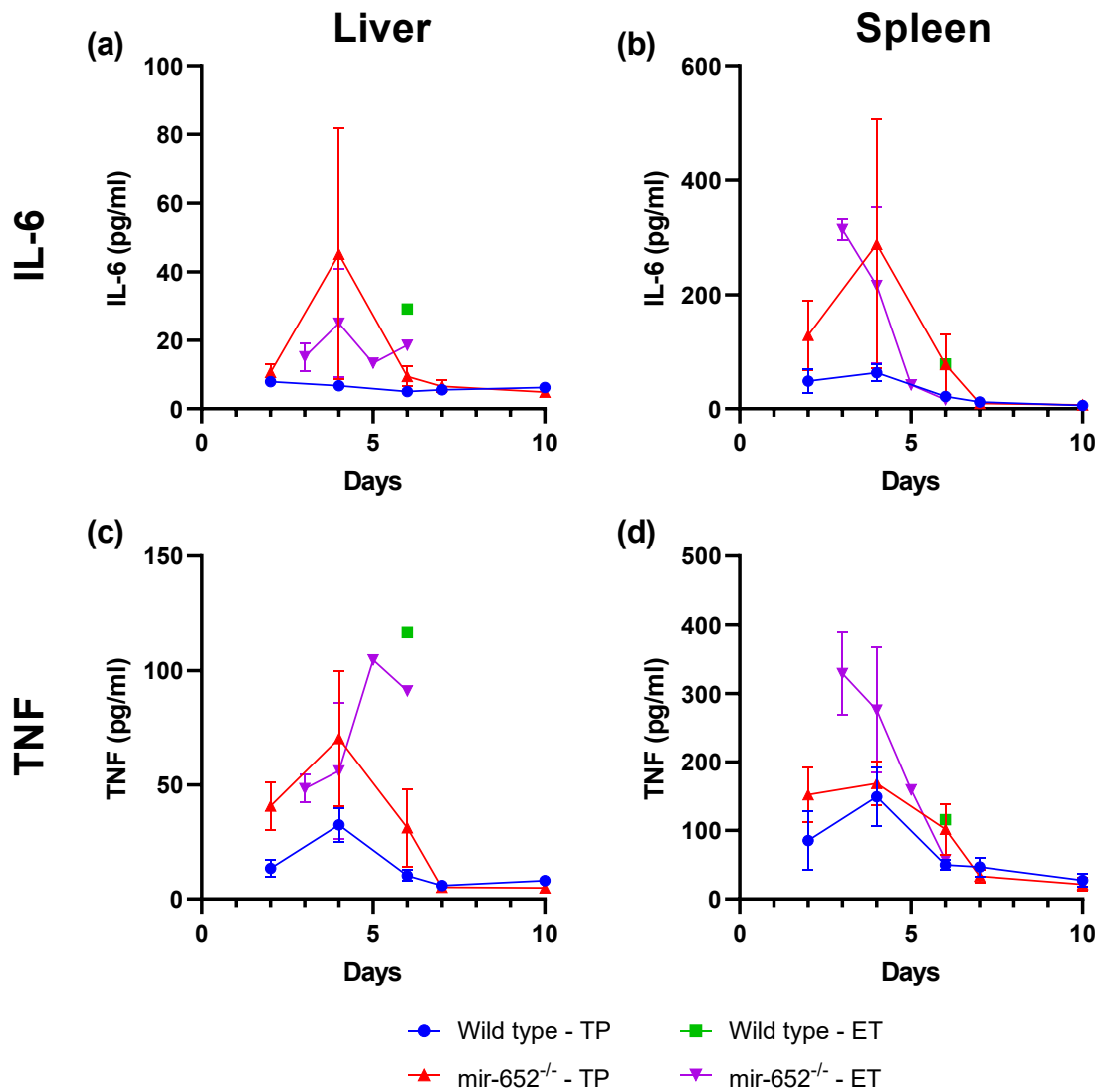
Figure 5.8. Cytokine expression is increased in miR-652$^{-/-}$ mice and moribund ET mice from both groups. Proinflammatory cytokine levels in *Listeria*-infected mouse tissues. Mice were infected as in Figure 5.6. Cytokine levels in tissue homogenates were quantified by CBA analysis. IL-6 expression in the (a) liver and (b) spleen, and TNF expression in the (c) liver and (d) spleen. Data are mean ± SEM from two replicate experiments (cohorts; n=34 wild type TP, n=26 miR-652$^{-/-}$ TP, n=1 wild type EP, n=9 miR-652$^{-/-}$ EP). Comparisons were made between wild type TP and miR-652$^{-/-}$ TP groups only, by 2-way ANOVA with multiple comparisons post-test, Šidák method corrected.
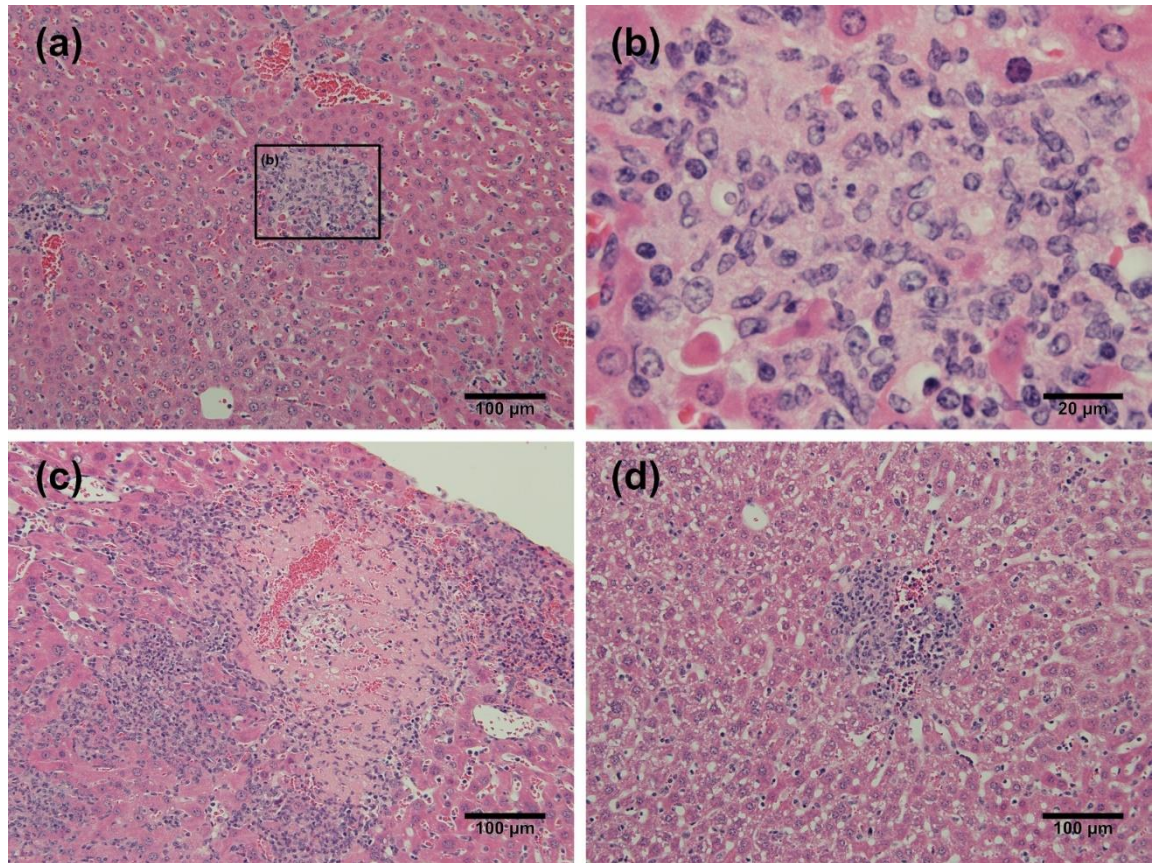
Figure 5.9. Wild type mice contain *L. monocytogenes* in compact liver lesions. Inflammatory lesions in liver tissue of *Listeria*-infected wild type mice. Mice were infected as in Figure 5.6. Formalin-fixed liver tissue sections were stained with haematoxylin and eosin, and imaged under bright field microscopy. At 4 days post-infection, (a) the liver contained frequent small contained lesions, (b) with a core of PMNs and macrophages. (c) The single moribund wild type mouse euthanised at day 6 presented large lesions with a necrotic core surrounded by a diffuse network of PMNs, macrophages, and lymphocytes. (d) By day 7, wild type mice had largely resolved liver inflammation. Lesions were predominantly dense collections of lymphocytes with some macrophages.
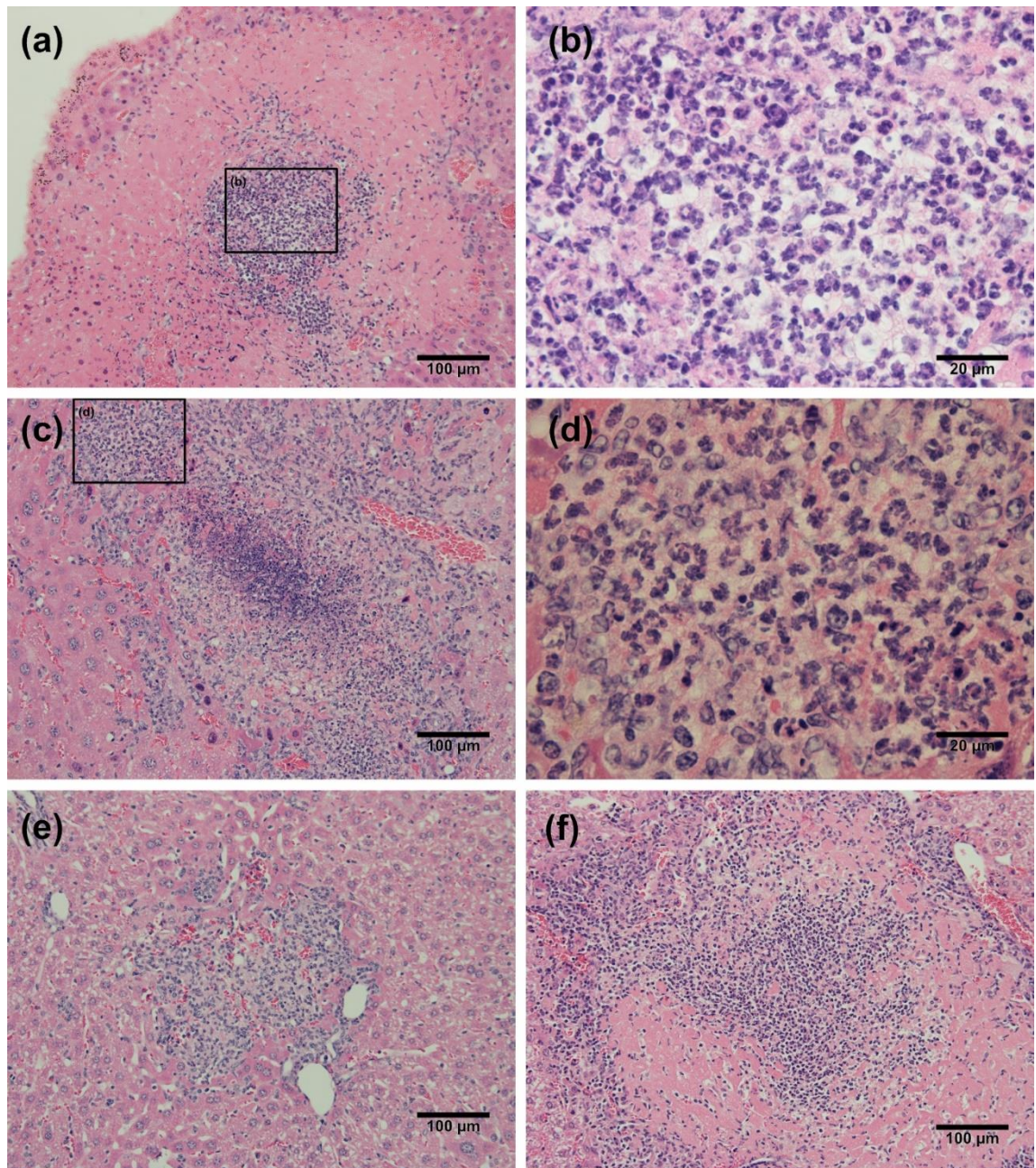
Figure 5.10. *L. monocytogenes* induces large necrotic liver lesions in miR-652$^{-/-}$ mice. Inflammatory lesions in liver tissue of *Listeria*-infected miR-652$^{-/-}$ mice. Mice were infected as in Figure 5.6. Formalin-fixed liver tissue sections were stained with haematoxylin and eosin, and imaged under bright field microscopy. (a) At 3 days post-infection, large lesions were very numerous, often surrounded by necrotic hepatocytes. (b) Lesions were dense with PMNs, and limited macrophages were obvious. Day 4 post-infection, (c) large disorganised lesions were frequent, with surrounding satellite lesions developing. (d) Lesions remained PMN-dominated, with T cell influx evident. (e) Resolution of inflammation had begun by day 7, and organised lesions were more common. (f) Necrotic lesions remained at day 10, with large scale lymphocyte recruitment.

From this data, it was clear that miR-652$^{-/-}$ mice showed increased inflammation following *L. monocytogenes* infection. To quantify the immune populations contributing to this inflammation, spleen leukocytes were analysed by flow cytometry. Only spleens from wild type TP and miR-652$^{-/-}$ TP mice were processed for flow cytometric analysis. There were no significant differences in major lymphocyte or myeloid cell populations between wild type and miR-652$^{-/-}$ mice at day 4 post-infection (Figure 5.11). The percentage of CD8$^+$ T cells was significantly lower in mir-652$^{-/-}$ mouse spleens at days 7 and 10 (Figure 5.11b). The proportion of CD4$^+$ T cells was notably, though not significantly, decreased in miR-652$^{-/-}$ mice at these time points (Figure 5.11a).

Whilst total CD4$^+$ T cell numbers were not different between mice at day 4 (Figure 5.11), the phenotypes of T cells found in the spleen differed. CD44^{hi} CD62L^{lo} effector CD4$^+$ cells were greatly increased in miR-652$^{-/-}$ mice (Figure 5.12a), with naïve CD4$^+$ cells correspondingly decreased (Figure 5.12c). A similar trend was observed in CD8$^+$ T cells, with mean CD8$^+$ effector cell numbers increased at day 4 (Figure 5.12d).

The markers CD69 and KLRG1 were used as indicators of T cell activation and terminal effector differentiation, respectively, to assess the anti-bacterial activity of spleen T cell populations. The percentage of both CD8$^+$ and CD4$^+$ T cells expressing the early activation marker CD69 peaked at day 4 and decreased significantly ($P < 0.001$) at days 7 and 10 (Figure 5.13b and d). KLRG1 expression was increased on wild type and miR-652$^{-/-}$ CD8$^+$ effector cells between days 4 and 7 (Figure 5.13c, $P < 0.0001$), indicating increased terminal differentiation of effector cells. Furthermore, KLRG1 expression was increased in wild type CD4$^+$ effector T cells at day 7 ($P < 0.001$). KLRG1 expression was increased at day 7 on miR-652$^{-/-}$ CD4$^+$ cells, reaching significance by day 10 (Figure 5.13a).

To determine the T cell cytokine expression phenotypes, splenic T cells were stimulated overnight with Heat-killed Listeria, and intracellular staining of cytokines IL-2, IFNγ, TNF and IL-17a was performed, as an indicator of T cell responses and activities. Cytokine expression by CD4$^+$ cells was not different between wild type and miR-652$^{-/-}$ cells (Figure 5.14a-d). The majority of cytokine expressing CD4$^+$ T cells were single positive for IFNγ, IL-2, or TNF (Figure 5.15a). The percentage of CD4$^+$ T cells expressing IFNγ decreased

with time (Figure 5.14a), with significant decreases in IFNγ ($P < 0.05$), IL-2 ($P < 0.001$), and IL-17a ($P < 0.001$). The percentage of wild type CD4$^+$ cells expressing TNF decreased from day 4 to 7 (P < 0.01). However, TNF expression in miR-652$^{-/-}$ CD4$^+$ T cells did not change with time, perhaps due to noticeably lower expression at day 4.

IL-2 expression by CD8$^+$ T cells was significantly increased in miR-652$^{-/-}$ mice (Figure 5.14f), and these cells were single-positive for IL-2 expression (Figure 5.15). However, all cytokine expression in CD8$^+$ T cells decreased by day 7 post-infection ($P < 0.001$, Figure 5.14e-h).

Figure 5.11 to Figure 5.15 display populations as a percentage of live cells, and these same population comparisons were also made with total cell numbers. The trends observed in total cell numbers and the resulting conclusions were reflected those seen in population percentages.

Overall, liver inflammation was increased in miR-652$^{-/-}$ mice early during the *L. monocytogenes* infection. That said, the makeup of spleen leukocyte populations was largely comparable between wild type TP and miR-652$^{-/-}$ TP mice. The difference in inflammation may not be related to leukocyte numbers, but rather in leukocyte activation and function during the infection.
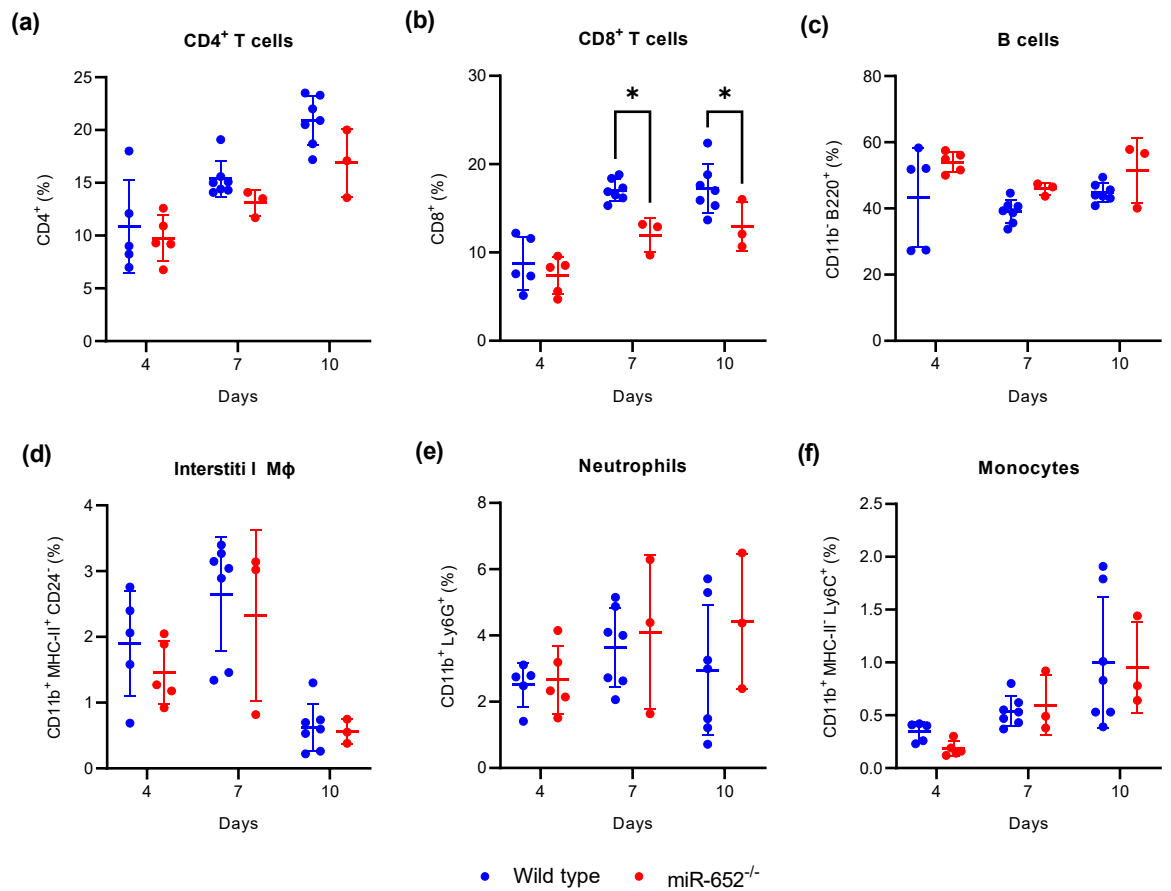
Figure 5.11. Spleen CD8+ T cell expansion was diminished in miR-652-/- mice after *L. monocytogenes* infection. Mice were infected as in Figure 5.6. Major spleen leukocyte populations were analysed by flow cytometry. Populations are expressed as a percentage of total CD45+ leukocytes. Data are mean ± SD of 3-7 individual animals. *$P < 0.05$, by 2-way ANOVA with multiple comparisons post-test, Šidák method corrected.
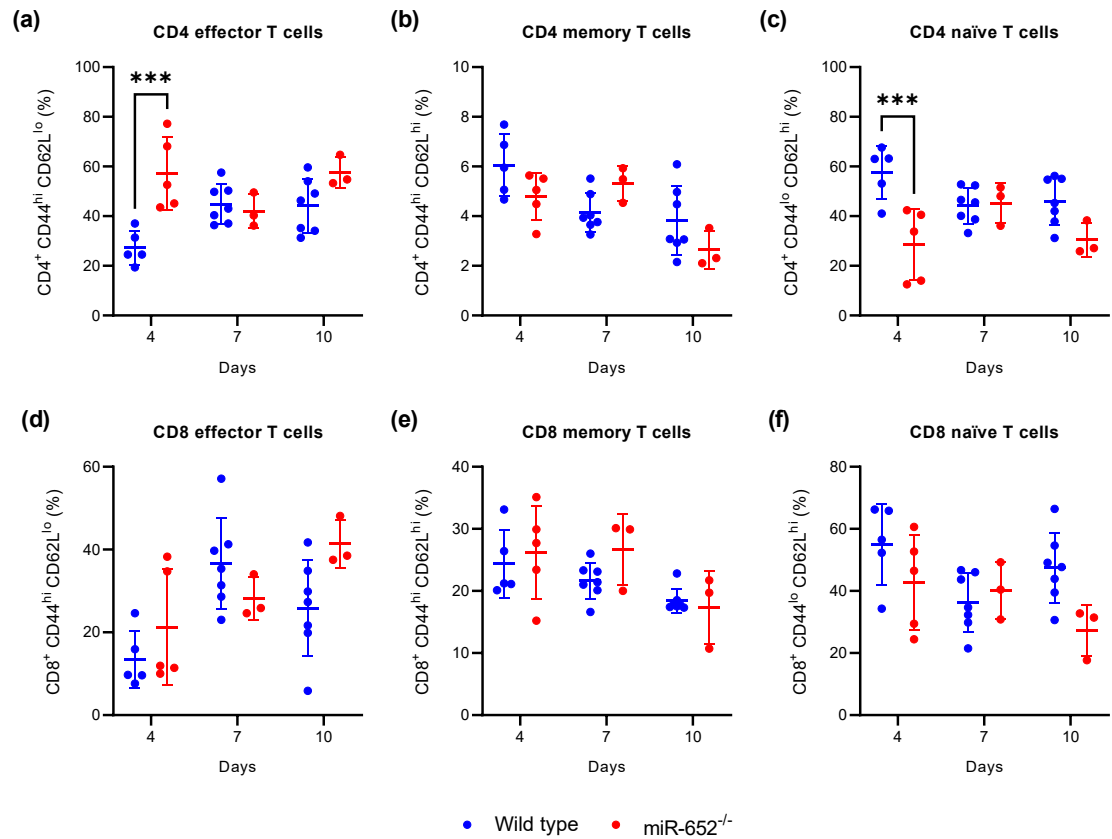
Figure 5.12. CD4$^+$ effector T cell populations are elevated in miR-652$^{-/-}$ mice early during *L. monocytogenes* infection. Mice were infected as in Figure 5.6. Spleen T cell subsets were analysed by flow cytometry. (a-c) CD4$^+$ and (d-f) CD8$^+$ T cell subset populations are expressed as a percentage of their parent CD4$^+$ of CD8$^+$ leukocytes. Data are mean ± SD of 3-7 individual animals. ***$P < 0.001$, by 2-way ANOVA with multiple comparisons post-test, Šidák method corrected.
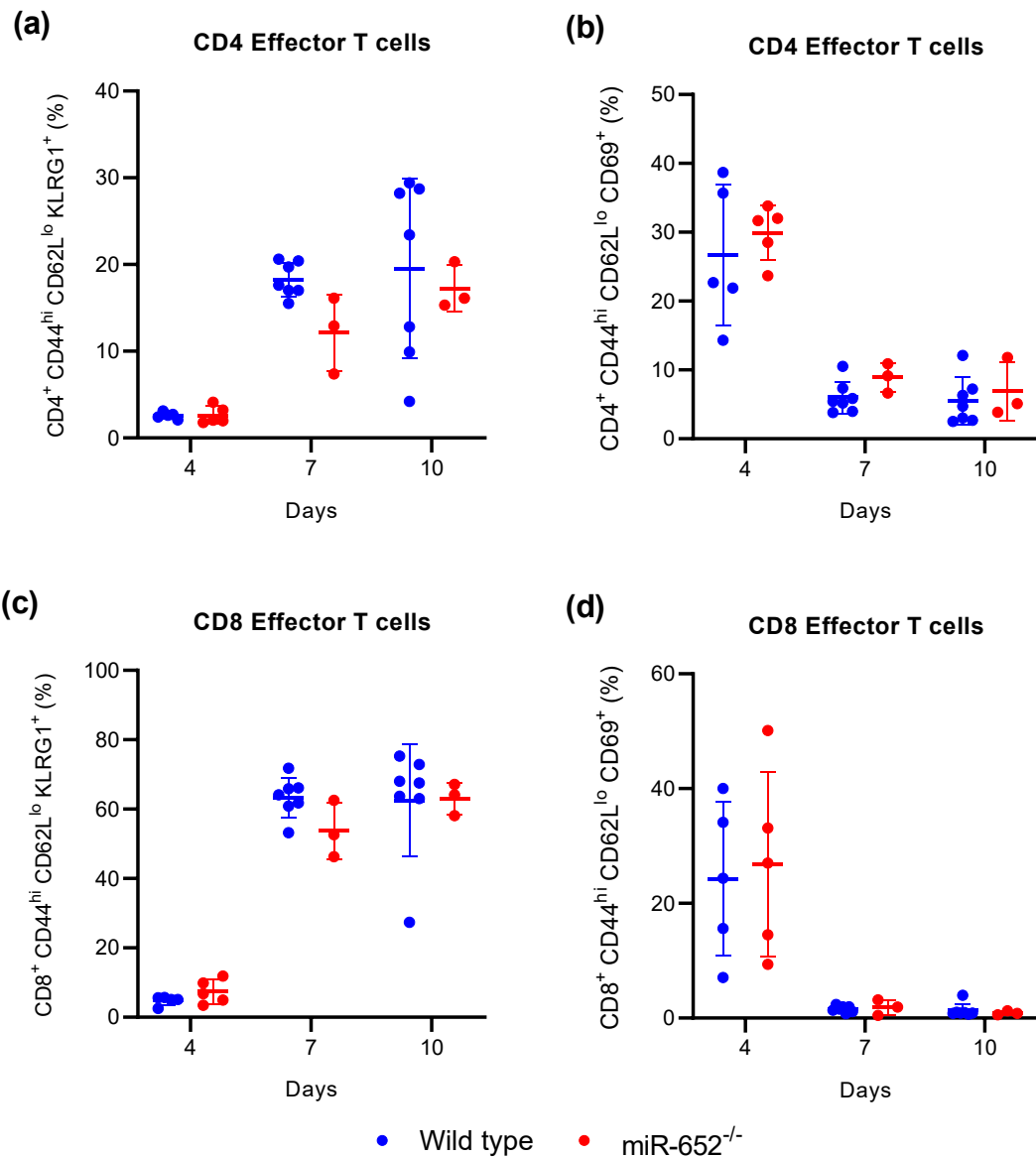
Figure 5.13. Activation marker expression is similar on wild type and miR-652^{-/-} effector T cells during *L. monocytogenes* infection. Activation and differentiation status of effector T cells in the spleen of *Listeria*-infected mice. Mice were infected as in Figure 5.6. Spleen T cell populations were analysed by flow cytometry for expression of (a,c) terminal differentiation marker KLRG1, and of (b,d) activation marker CD69. KLRG1^{+} and CD69^{+} cells are expressed as a percentage of parent effector T cell populations. Data are mean ± SD of 3-7 individual animals. Comparisons were made by 2-way ANOVA with multiple comparisons post-test, Šidák method corrected.
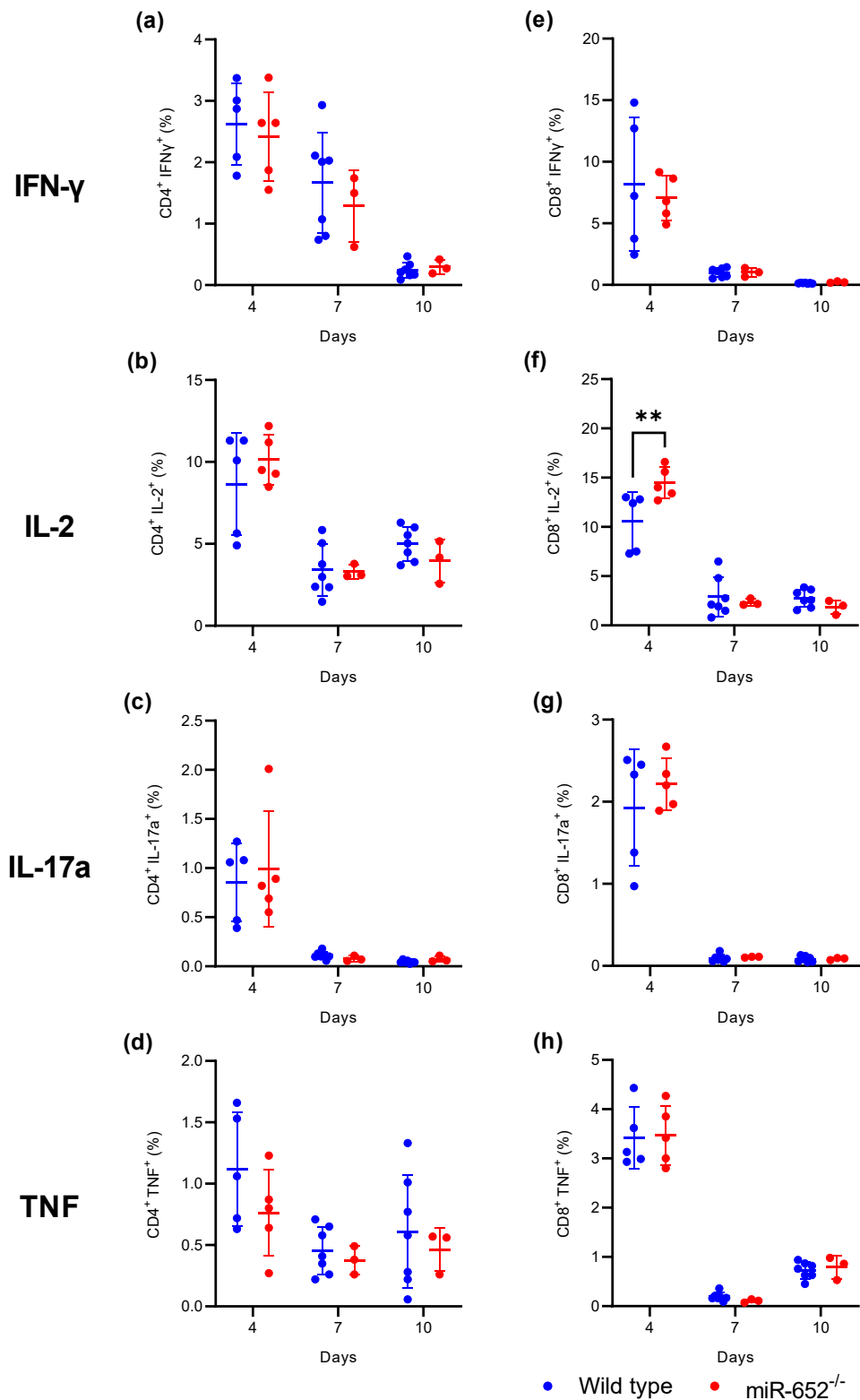
Figure 5.14. Cytokine-expressing T cell populations are similar in *L. monocytogenes*-infected wild type and miR-652$^{-/-}$ mice. Cytokine expression in (a-d) CD4$^+$ and (e-h) CD8$^+$ T cells. Mice were infected as in Figure 5.6. Spleen T cells were stained for intracellular cytokines and analysed by flow cytometry. Cytokine-positive populations are expressed as a percentage of parent CD4$^+$ of CD8$^+$ leukocytes. Data are mean ± SD of 3-7 individual animals. **$P < 0.01$, by 2-way ANOVA with multiple comparisons post-test, Šidák method corrected.
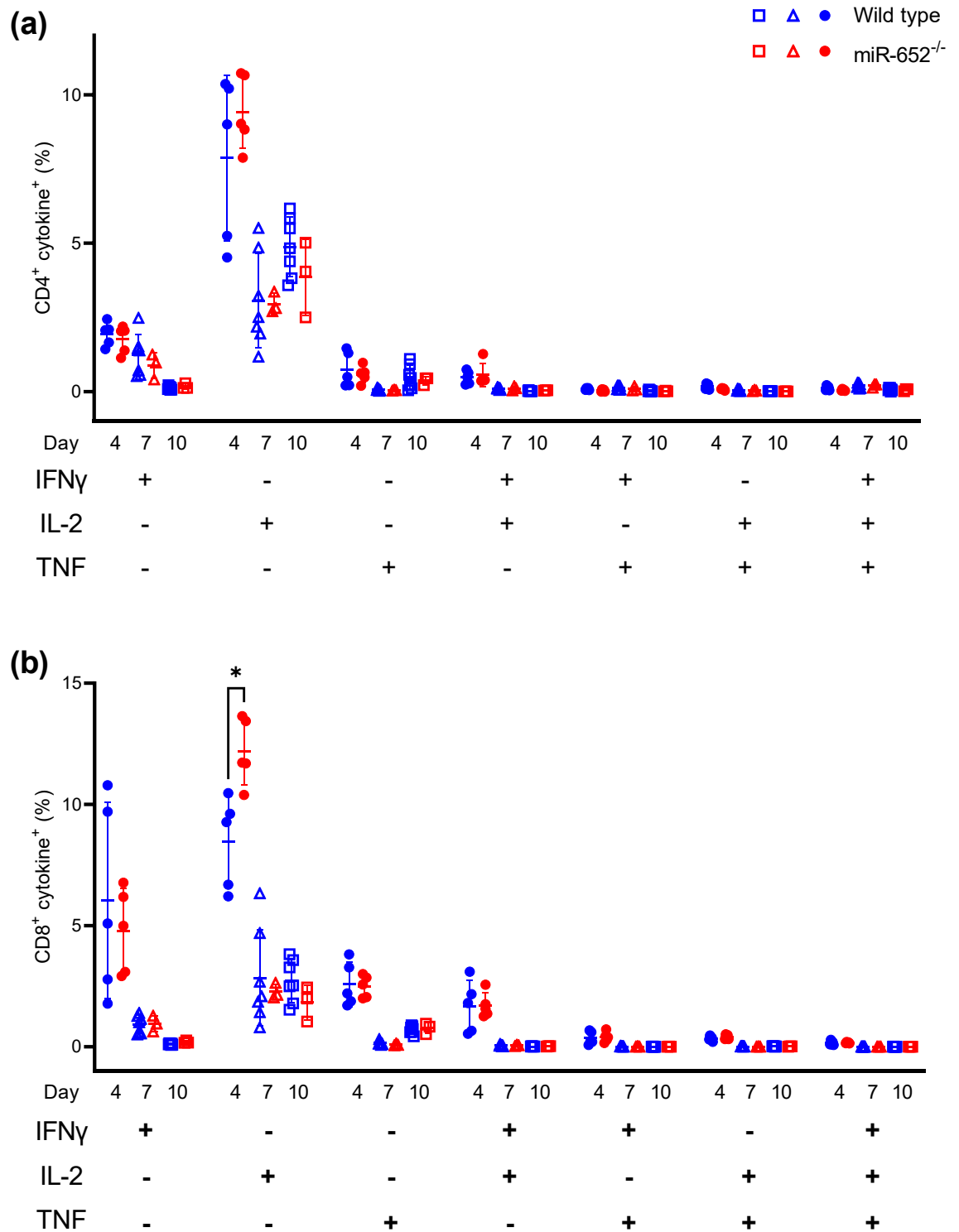
Figure 5.15. Single, double- and triple-positive cytokine expressing T cells are comparable between wild type and miR-652^{-/-} mice. (a) CD4⁺ and (b) CD8⁺ T cells in the spleen of *L. monocytogenes*-infected mice single, double, and triple-positive for cytokine expression. Mice were infected as in Figure 5.6. Spleen T cells were stained for intracellular cytokines and analysed by flow cytometry. Cytokine expression was compared between wild type and miR-652^{-/-} mice at each time point. *$P < 0.05$, by student's t test, Holm-Šidák method corrected.

5.3.3 miR-652$^{-/-}$ macrophages capably control *L. monocytogenes* bacterial load *in vitro*

The onset of increased mortality in miR-652$^{-/-}$ mice following *L. monocytogenes* infection occurred at day 2-4 post-infection, before the peak T cell response observed at day 7. This suggests that the innate, rather than the adaptive, immune response may be key in the differential survival of wild type and miR-652$^{-/-}$ mice. To assess the effect of miR-652 expression on macrophage defence against *Listeria*, mouse primary peritoneal macrophages were infected with *L. monocytogenes in vitro* at an MOI of 1. Adherent macrophages were infected with *L. monocytogenes* for one hour before being washed, and treated with gentamicin to kill extracellular bacteria.

The metabolic activity of infected cells was measured by resazurin fluorescence assay. Fluorescence data for 8 hours post-infection was normalised to fluorescence at 0 hours post-infection for each respective individual. Metabolic activity of neither wild type nor miR-652$^{-/-}$ macrophages was significantly affected by infection (Figure 5.16a). Macrophages were lysed to count intracellular CFU. The intracellular bacterial load of infected cells did not differ significantly between wild type and miR-652$^{-/-}$ macrophages up to 8 hours post-infection (Figure 5.16b).

Whilst both cell types were able to control *Listeria* growth over 8 hours *in vitro*, differential activity in proinflammatory pathways, including cytokine expression, could influence the immune response over an extended infection *in vivo*. To evaluate the impact of *Listeria* infection on cytokine secretion, IL-6 and TNF in cell culture supernatants was quantified by CBA. Cytokine secretion by uninfected cells was negligible in both wild type and miR-652$^{-/-}$ macrophages (Figure 5.17). IL-6 secretion by both wild type and miR-652$^{-/-}$ macrophages increased significantly between 4- and 8-hours post-infection (P = 0.003, Figure 5.17a), with similar levels of IL-6 expressed by both wild type and miR-652$^{-/-}$ macrophages at all time points. Similarly, TNF expression increased over time in both cell types (P = 0.002), again with no significant difference between infected wild type and miR-652$^{-/-}$ cells at any time (Figure 5.17b).
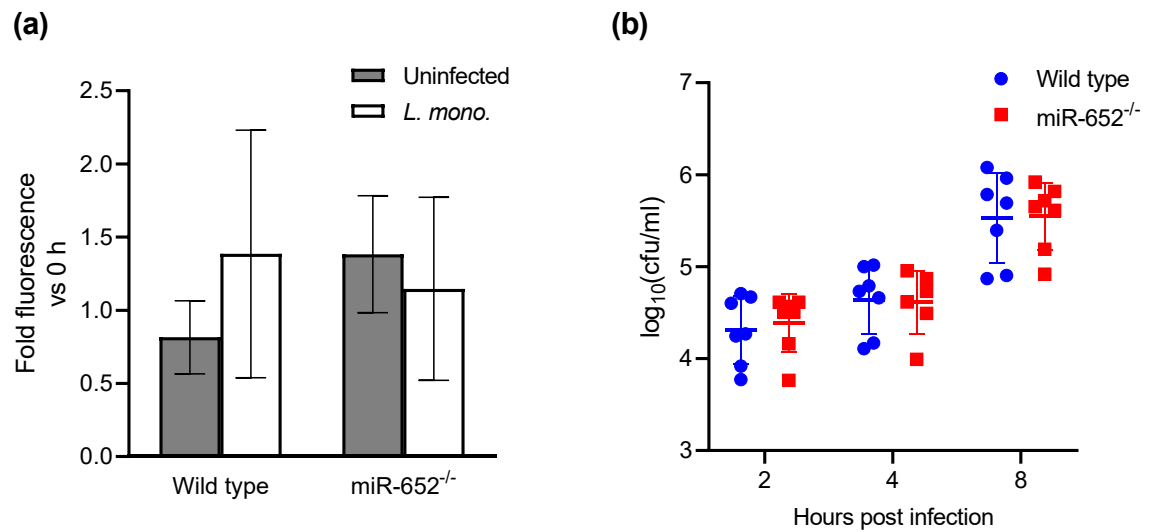
Figure 5.16. miR-652 expression does not affect mouse macrophage metabolic activity or control of *Listeria* infection. Wild type and miR-652$^{-/-}$ mouse peritoneal macrophages were infected *in vitro* with *L. monocytogenes* at a multiplicity of infection of 1. (a) A resazurin metabolic activity assay on uninfected and infected macrophages illustrates no impact of infection on fluorescence. (b) The *Listeria* bacterial load was controlled by wild type and miR-652$^{-/-}$ macrophages over 8 hours. Data are the mean ± SD of 7 biological replicates. Comparisons were made by 2-way ANOVA with multiple comparisons post-test, Šidák method corrected.
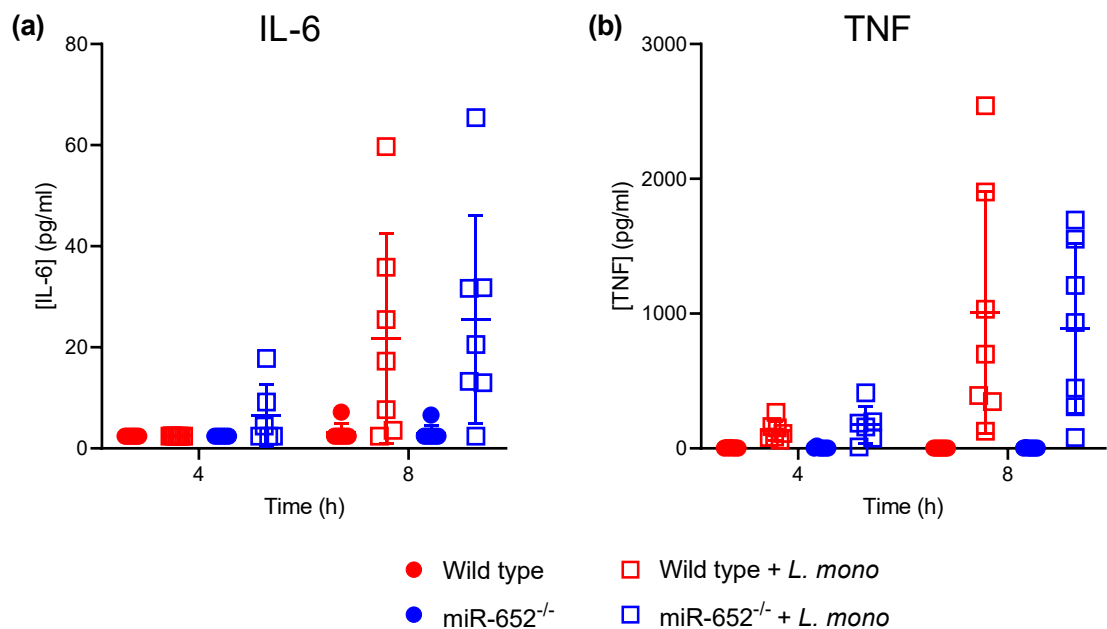
Figure 5.17. TNF expression is not suppressed in Listeria-infected miR-652$^{-/-}$ macrophages. Mouse peritoneal macrophages were infected as in Figure 5.16. (a) IL-6 and (b) TNF concentration in culture supernatant was quantified by CBA. Between 4 and 8 hours post-infection, IL-6 ($P = 0.003$) and TNF ($P = 0.002$) concentrations increased for both wild type and miR-652$^{-/-}$ cells. Data are mean ± SD of 7 biological replicates. Comparisons were made by 2-way ANOVA with multiple comparisons post-test, Šidák method corrected.

5.3.4 Proinflammatory pathways are downregulated in miR-652$^{-/-}$ macrophages

To develop a comprehensive inflammatory profile of the effect of *L. monocytogenes* infection on peritoneal macrophages, cells were lysed 8 hours post-infection for proteomic analysis. Protein samples were isolated from cell homogenates and trypsin-digested for analysis by LC/MS/MS. *Mus musculus* and *L. monocytogenes* proteins identified from MS/MS data were filtered to include only proteins identified with at least 5 unique peptides detected.

Of all proteins identified, 47% were detected in all groups; wild type uninfected and infected, and miR-652$^{-/-}$ uninfected and infected (Figure 5.18). There were 111 proteins undetected in uninfected miR-652$^{-/-}$ macrophages, and a further 248 proteins detected only in wild type macrophages. This was reflected in label-free quantitation comparisons performed using PEAKS software. Differentially expressed proteins were filtered down to those significantly changed between groups, with greater than 2-fold expression difference. When comparing uninfected macrophages, the vast majority of differentially expressed proteins are downregulated in miR-652$^{-/-}$ cells (Figure 5.19a). Furthermore, 90% of proteins dysregulated in infected macrophages were downregulated in miR-652$^{-/-}$ cells (Figure 5.19b).
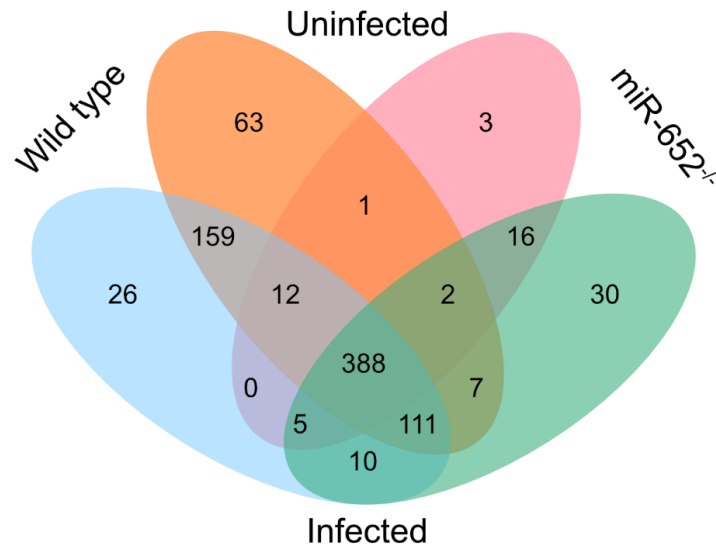
Figure 5.18. Protein expression patterns are altered by miR-652 knock-out. Proteins identified in wild type and miR-652$^{-/-}$ mouse peritoneal macrophage proteomes, uninfected and during *L. monocytogenes* infection. Macrophages were infected as in Figure 5.16. Cells were lysed and total cellular protein was purified. Cell proteomes were analysed by LC/MS/MS. Venn diagram analysis was restricted to proteins with at least 5 unique peptides detected.
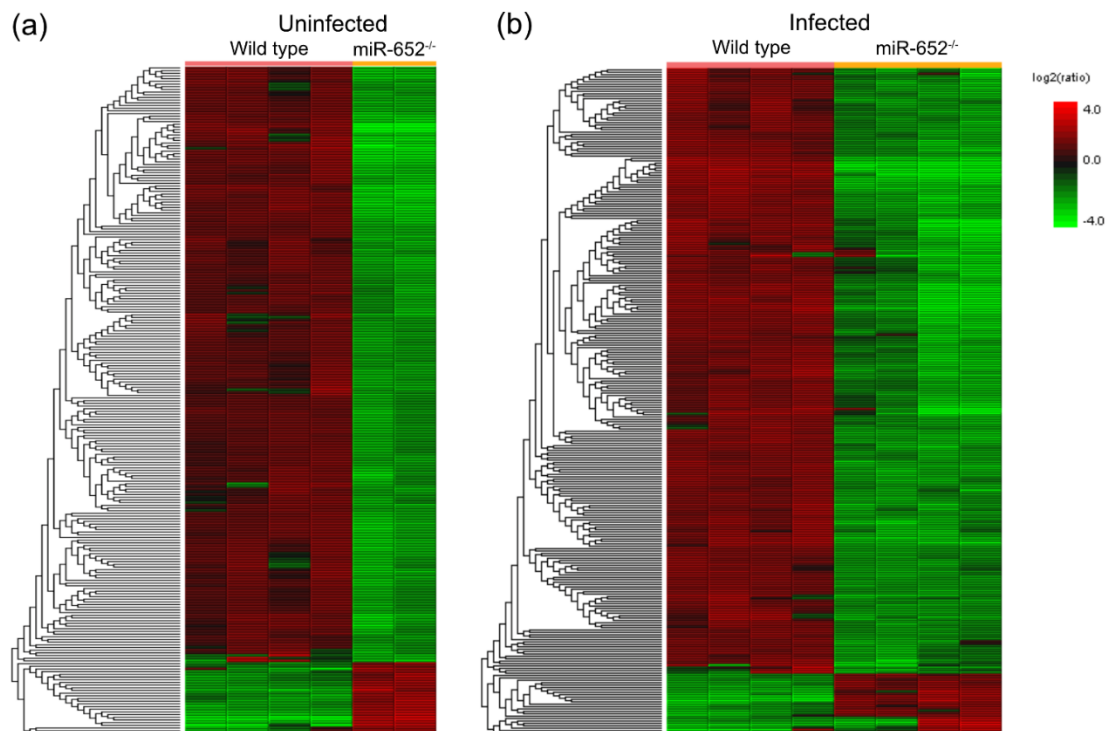
Figure 5.19. Essential cellular pathways downregulated in miR-652$^{-/-}$ macrophages. Relative protein expression in wild type and miR-652$^{-/-}$ peritoneal macrophages during *L. monocytogenes* infection. Macrophages were infected as in Figure 5.16. Cells were lysed and total cellular protein was purified. Cell proteomes were analysed by tandem LC/MS/MS. Protein expression was compared in uninfected and infected macrophages using Peaks Studio label-free quantitation methods. Proteomes filtered to include only differentially expressed proteins with at least 5 unique peptides detected.

To identify key pathways dysregulated in infected miR-652$^{-/-}$ macrophages, a protein network was generated using the STRING database (338). Input data consisted of all proteins significantly different between *L. monocytogenes*-infected wild type and miR-652$^{-/-}$ cells. The resulting network illustrates the high degree of interaction between dysregulated proteins, suggesting multiple key pathways may be regulated by miR-652 in macrophages (Figure 5.20). The STRING analysis included pathway analysis using KEGG (339). Proteins significantly increased or decreased in miR-652$^{-/-}$ cells were enriched for multiple pathways associated with defence against pathogens (Table 5.2). Interestingly, key members of the pentose phosphate pathway and the lysosome pathway were reduced in miR-652$^{-/-}$ cells (Figure 5.20). Both pathways are associated with macrophage defence against bacterial pathogens (274, 342). Furthermore, F-actin capping-protein subunit beta (CAPZB) was less abundant in miR-652$^{-/-}$ macrophages, whether uninfected or *L. monocytogenes*-infected (Figure 5.20). This protein has been identified *in silico* as a target of miR-652-3p in mice by the Target Scan v7.2 (99) and miRDB (343) databases.

To further investigate some of the key proteins identified by proteomic analysis, peritoneal macrophages were again infected with *L. monocytogenes*, and lysed 8 hours post-infection to collect mRNA. The expression of key dysregulated proteins was validated by qPCR. This included *Capzb*, and dysregulated members of the pentose phosphate pathway (*G6pdx*, *Gpi1*, *Pfkl*, *Pgd*, *Taldo1*, and *Tkt*) and lysosome pathway (*Ctsb*, *Ctsd*, and *Ctsz*). Interferon response genes *Isg15 and Ifnb1* were also assayed. Gene expression was not significantly different between infected wild type and miR-652$^{-/-}$ macrophages. However, with the exceptions of *Pfkl* and *Tkt*, there was a trend for higher mean expression in wild type cells compared to miR-652$^{-/-}$ cells (Figure 5.21). This correlates with proteomics data.

Type 1 interferon signalling is associated with *Listeria* infection, promoting cell-to-cell bacterial movement (344). Though IFN-β protein was not detected during proteomic analysis, *Ifnb1* mRNA was quantified by RT-qPCR. Interestingly, expression of *Ifnb1* was noticeably lower in miR-652$^{-/-}$ macrophages.
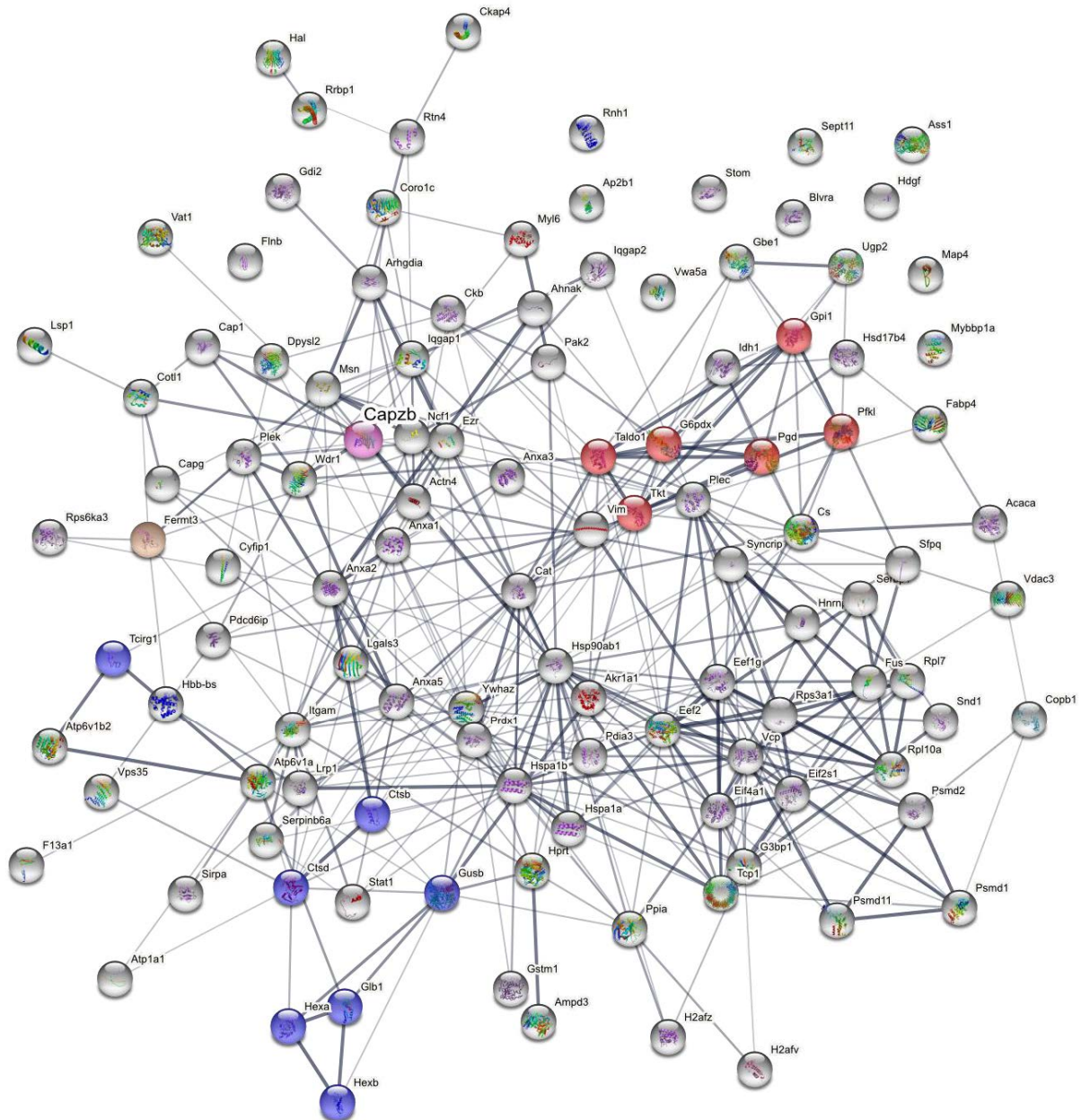
Figure 5.20. STRING network shows interacting pathways with known anti-bacterial activity were dysregulated in miR-652^{-/-} macrophages. Macrophages were infected as in Figure 5.16. Cells were lysed and total cellular protein was purified. Cell proteomes were analysed by tandem LC/MS/MS. Proteomes were filtered to include only differentially expressed proteins with at least 5 unique peptides detected. Network generated from STRING database for proteins differentially expressed between *Listeria*-infected wild type and miR-652^{-/-} peritoneal macrophages. Highlighted are the pentose phosphate pathway (blue) and lysosome (red) KEGG term members, and the *in silico* predicted miR-652-3p target Capzb (pink).

Table 5.2. KEGG pathways enriched in differentially expressed proteins from Listeria-infected peritoneal macrophages.

Rank	Term ID	Term description	Observed gene count	Term total gene count	Strength	False discovery rate
1	mmu01100	Metabolic pathways	28	1536	0.55	1.37E-06
2	mmu01200	Carbon metabolism	9	122	1.15	4.26E-06
3	mmu00030	Pentose phosphate pathway	6	33	1.55	5.10E-06
4	mmu01230	Biosynthesis of amino acids	6	77	1.18	3.00E-04
5	mmu04141	Protein processing in endoplasmic reticulum	8	168	0.96	3.00E-04
6	mmu04142	Lysosome	7	127	1.03	3.40E-04
7	mmu00531	Glycosaminoglycan degradation	4	21	1.57	3.70E-04
8	mmu04810	Regulation of actin cytoskeleton	8	212	0.86	7.70E-04
9	mmu05134	Legionellosis	5	60	1.21	7.90E-04
10	mmu04612	Antigen processing and presentation	5	74	1.12	1.80E-03
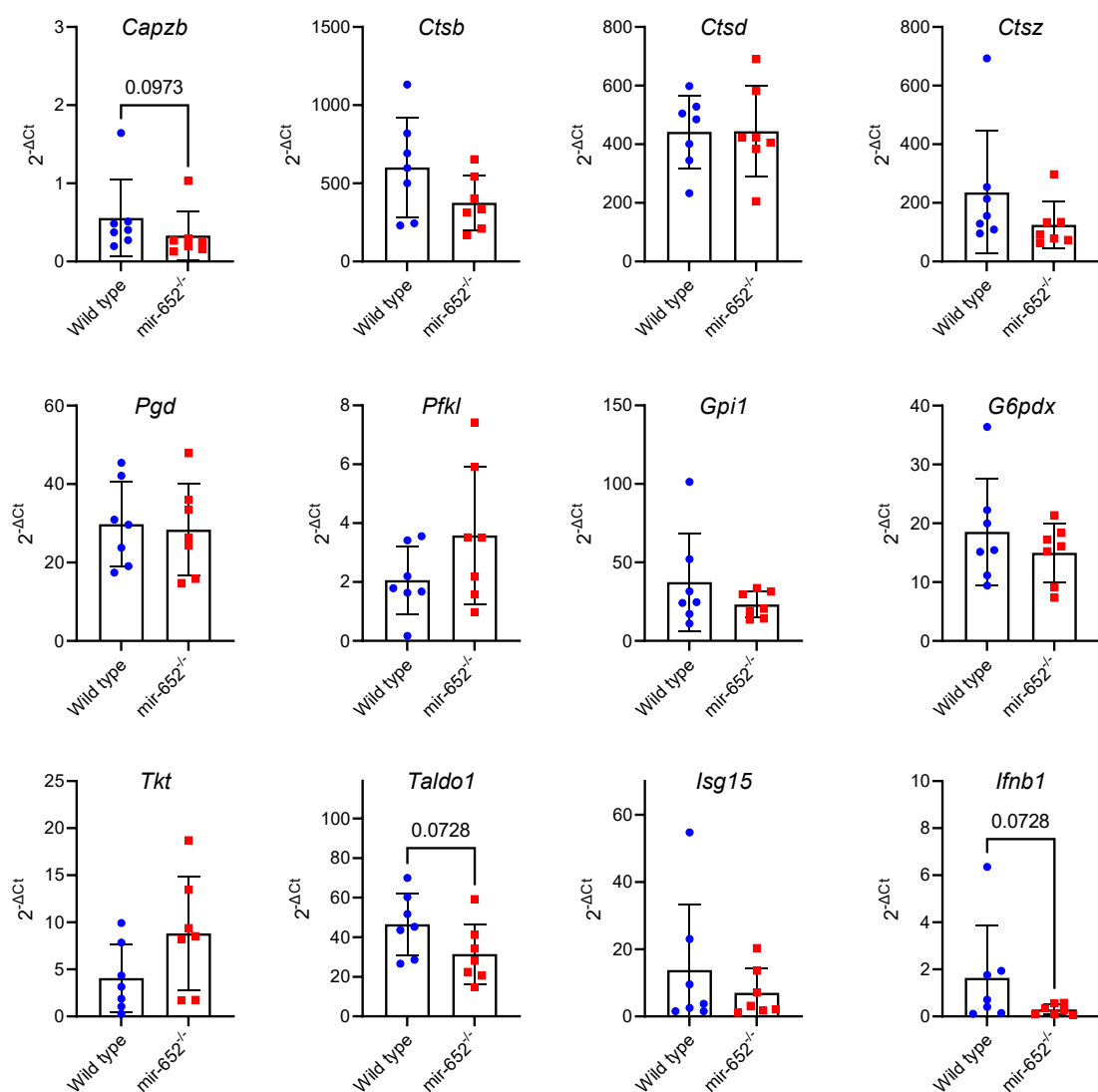
Figure 5.21. Gene expression trends infected macrophages correlated with differential protein expression. Macrophages were infected as in Figure 5.16. Cells were lysed with TRIsure reagent to isolate mRNA. A qPCR assay was run to assess transcription of dysregulated proteins highlighted in Figure 5.20. mRNA expression correlated with expression of translated proteins. *Ifnb1* mRNA expression was decreased in miR-652$^{-/-}$ cells, however, IFNβ protein was not detected in proteomics data. Data are the mean ± SD of 7 biological replicates. Wild type and miR-652$^{-/-}$ cells were compared by 2-way ANOVA with multiple comparisons post-test, Šidák method corrected.

5.3.5   miR-652 targeting of *Capzb* in mouse macrophages

Proteomic analysis of *L. monocytogenes*-infected macrophages identified CAPZB as significantly decreased in miR-652$^{-/-}$ cells, and RT-qPCR showed a trend for reduced *Capzb* expression in miR-652$^{-/-}$ macrophages. The *Capzb* mRNA transcript has a purported miR-652 target binding site in the 3'UTR. *Capzb* is important in cell motility and trafficking of cellular organelles (345, 346), but is also utilised for *L. monocytogenes*' intracellular movement (313). To confirm whether *Capzb* is a target of miR-652, *in vitro* transfection assays were performed using miRNA mimics.

IC-21 mouse peritoneal macrophages were transiently transfected with a miR-652 mimic or a negative control mimic. Expression levels of *Capzb* mRNA and CAPZB protein were analysed by RT-qPCR and western blot, respectively. Transfection with the miR-652 mimic significantly increased cellular concentration of mature miR-652-3p miRNA (Figure 5.22a), but did not have any effect on *Capzb* mRNA concentration (Figure 5.22b). Additionally, overexpression of miR-652 did not significantly alter the translation of CAPZB protein in miR-652 mimic-transfected cells (Figure 5.23).

To confirm whether miR-652 can bind the *Capzb* 3'UTR to inhibit protein translation, plasmid reporter constructs were generated on the pIS0 background. The plasmids encode for a firefly luciferase gene with either no 3'UTR (pIS0), the wild type *Capzb* 3'UTR (pIS0-Capzb-WT), or a control *Capzb* 3'UTR with a mutated binding site (pIS0-Capzb-mut). Each plasmid was co-transfected with a miR-652 mimic or a miR-146a mimic as a control. Luminescence decreased by more than 10% upon co-transfection of miR-652 with all three plasmids (Figure 5.24a). However, there was no significant difference in luminescence between pIS0-Capzb-WT- and pIS0-Capzb-mut-transfected wells, indicating miR-652 can inhibit luciferase translation, but irrespective of the *Capzb* 3'UTR predicted binding site. Similarly, miR-146a transfection decreased luciferase expression with all three pIS0 plasmids, but there was not luminescence difference between plasmids. Thus, whilst both miR-652 and miR-146a potentially bound and targeted luciferase mRNA, these data indicate that the predicted miR-652 binding site in the *Capzb* 3'UTR was not a valid miR-652 binding site.

(a)

(b)
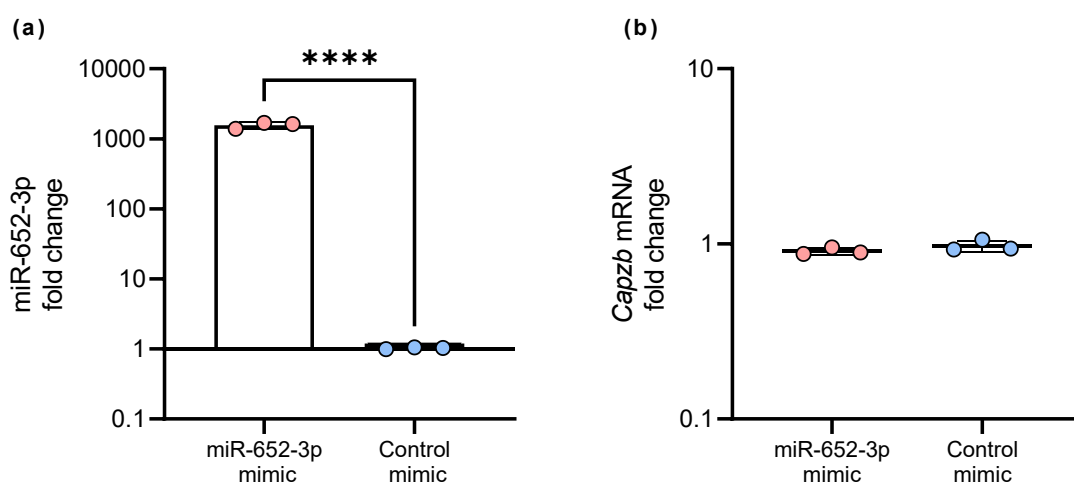
Figure 5.22. miR-652 overexpression did not impact *Capzb* transcription. The IC-21 peritoneal macrophage cell line was transiently transfected with miRNA mimics. After 24-hours, cells were lysed with TRIsure reagent to isolate miRNA and mRNA. A qPCR assay was run to assess the expression of (a) miR-652-3p and (b) *Capzb* in miR-652-3p mimic-transfected cells, versus in control mimic-transfected cells. Data are the mean ± SD of biological replicates. **** *P* < 0.0001, by student's t test.
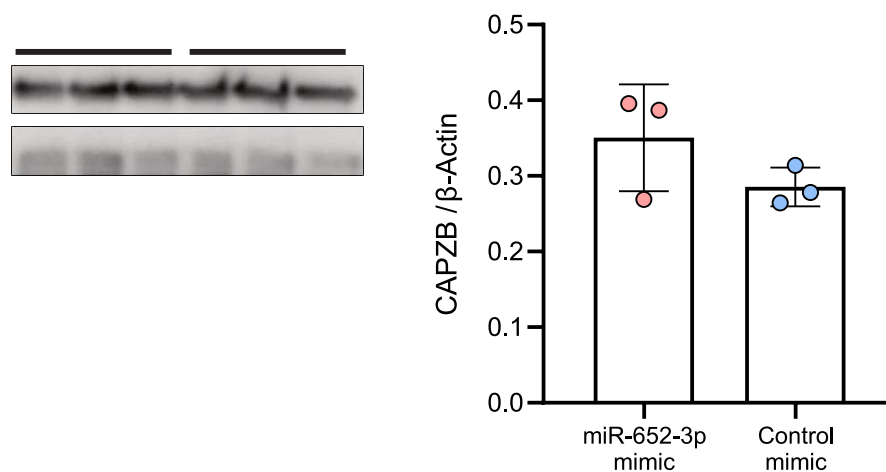
Figure 5.23. miR-652 overexpression did not cause decreased translation of CAPZB protein. IC-21 cells were transfected as in Figure 5.22. After 24-hours, cells were lysed with RIPA buffer to isolate cellular protein. (a) A western blot was run to assess expression of CAPZB protein. (b) CAPZB band density was calculated over the β-Actin reference protein band. Data are the mean ± SD of 3 replicates. Comparisons were made with student's t test.
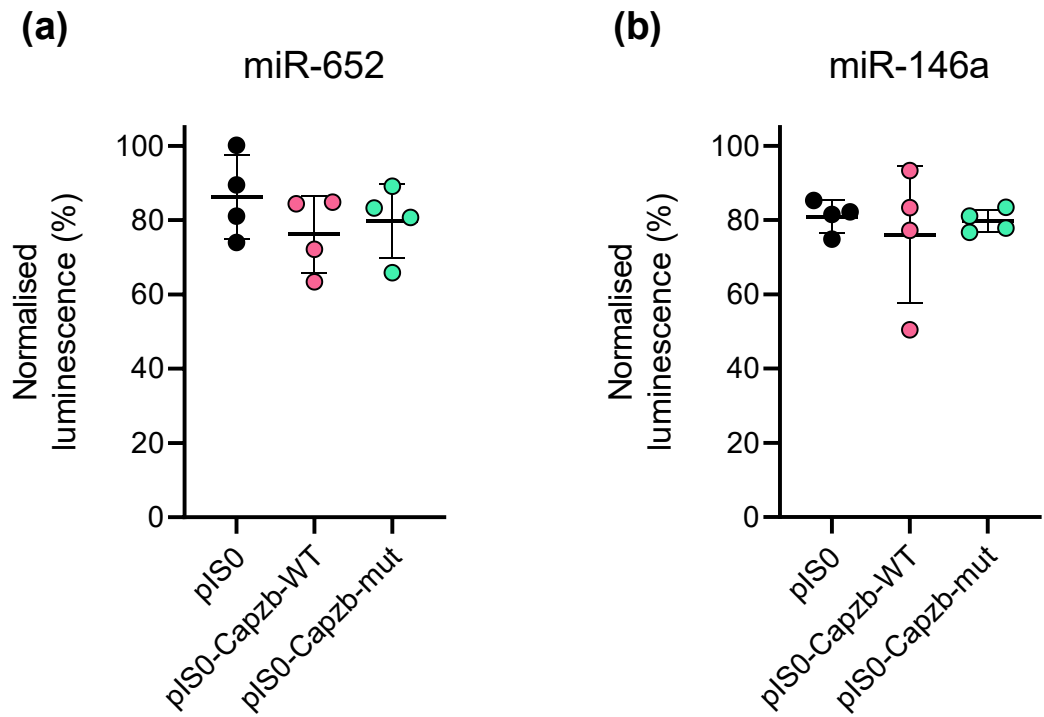
Figure 5.24. miR-652 does not target to predicted site in the *Capzb* 3'UTR. The HEK-293T embryonic kidney cell line was transiently co-transfected with pIS0 plasmids encoding firefly luciferase and either a (a) miR-652 or (b) miR-146a miRNA mimic. After 24 hours, cells were lysed and luciferase expression quantified by luminescence assay. Data are the mean ± SD of 3 replicates. Comparisons were made by one-way ANOVA, with multiple comparisons post-test, Šidák method corrected.

5.4. Discussion

Murine listeriosis is an important model for investigation of the cytotoxic T cell response to infection, and demonstrates key interactions between the innate and adaptive immune systems. This chapter has illustrated the importance of miRNA in immune regulation, in particular the impact of miR-652 for defence against this acute intracellular bacterial pathogen. miR-652$^{-/-}$ mice were extremely susceptible to *L. monocytogenes* infection. They lost significantly more weight than their wild type counterparts, and presented greatly increased mortality after low dose infection. The miR-652$^{-/-}$ mice more often failed to control bacterial growth in the liver and spleen. Inflammation and necrosis were much more prevalent in the liver of miR-652$^{-/-}$ mice, particularly at the early stages of infection. The increased mortality in knockout mice was apparent from days 3-4 post-infection, before the expansion of CD8$^+$ T cells typical from day 5 in *L. monocytogenes*-infected mice. This suggests that miR-652 deficiency has impaired the innate immune response. Numerous factors are known to be essential to innate anti-listerial defence, and each could contribute to susceptibility in miR-652$^{-/-}$ mice.

A coordinated cytokine response is requisite for the recruitment and activation of macrophages and neutrophils at the site of infection, involving type I IFNs, IFNγ, TNF, IL-12 and IL-6. Type I and type II interferon have contrasting influence on the survival of *Listeria*-infected mice. Type I IFN signalling through IFNAR1 is essential for anti-viral immunity and gives protection against several intracellular bacterial pathogens, but it is associated with susceptibility to *L. monocytogenes* infection (347-349). A recent study showed IFNAR1 activation promoted *L. monocytogenes* motility in the cytosol and increased intercellular spread of bacteria (344). IFNAR1$^{-/-}$ mice are resistant to IP and IV infection, containing bacteria in organised liver lesions (349, 350). However, the impact of type I IFNs appears to depend on the route of infection, as intragastrically-infected IFNAR$^{-/-}$ mice succumb to infection earlier than wild type mice (351). In the study described here, *Ifnb1* mRNA was lower in miR-652$^{-/-}$ macrophages infected *in vitro*. Macrophages are a major source of IFNβ after IP infection (347), and decreased expression may have implication for intercellular spread *in vivo*. That said, the diffuse,

necrotic lesions prevalent in miR-652^{-/-} mice demonstrate that *L. monocytogenes* was spreading effectively in the liver of these mice.

In contrast to type I IFNs, expression of type II IFNγ is essential for early defence against *L. monocytogenes* in the liver. IFNγ is expressed primarily by NK cells during the acute phase of infection (352), and is required to activate macrophages, inducing cytokine expression and bacterial killing (347, 353). IFNγ-deficient mice die within 5 days of IV *L. monocytogenes* infection (354). Although miR-652^{-/-} mice were prone to early mortality, mice which survived to day 7 were able to mount a normal T cell response. Spleen T cell expansion was comparable to wild type mice, and lymphocyte recruitment was evident in liver lesions at days 7 and 10 post-infection. Similarly, IFNγ^{-/-} mice infected with attenuated *L. monocytogenes* survive to generate a robust antigen-specific CD8^{+} T cell response (353). Intracellular IFNγ expression was not decreased in miR-652^{-/-} splenic CD4^{+} and CD8^{+} T cells. However, expression by liver NK cells was not evaluated; this would be a prudent addition to future experiments.

IL-6 and TNF were not differentially expressed by wild type and miR-652^{-/-} macrophages *in vitro*, but their expression was significantly increased in moribund mice. It is likely that this is due to the high bacterial load, and is not the driver of it. Mice deficient in IL-6 or the IL-6 receptor are susceptible to *L. monocytogenes* infection, with significantly increased mortality within 4 days of IV infection (355, 356). This mortality is rescuable with exogenous recombinant IL-6. The cellular targets of IL-6 during *L. monocytogenes* infection remain undetermined. IL-6 expression has impacts on macrophage and T cell responses, but does not appear essential for either (357). The activity of TNF in the anti-*Listeria* response is better characterised. TNF is expressed by macrophages and Kupffer cells and, in conjunction with IL-12, activates NK cells to express IFNγ (358). TNF^{-/-} mice are susceptible to low-dose *L. monocytogenes* infection when administered IV, as most mice succumb to infection within one week (359, 360). As described in chapter 4, miR-652^{-/-} BMDMs expressed significantly less TNF in the 24 hours after *in vitro M. tuberculosis* infection. Although miR-652^{-/-} macrophage TNF expression was not different after an 8-hour *in vitro L. monocytogenes* infection, a difference may have been more evident at a later time point. Furthermore, deficient TNF expression in the first

24-48 hours of an *in vivo* infection may have dramatic impact on the activation of liver macrophages in miR-652$^{-/-}$ mice.

Histological analysis of *Listeria*-infected livers showed miR-652$^{-/-}$ mice can recruit both neutrophils and macrophages to liver lesions, and yet cannot control the bacterial spread. Neutrophils and monocytes are both involved in the early stages of *L. monocytogenes* infection, recruited from the bone marrow to the site of infection (328). Neutrophils are adept at killing extracellular bacteria, through the release of cytotoxic granules and neutrophil extracellular traps (326), and also by direct phagocytosis (361). Early studies suggested that neutrophils were essential to the innate response towards *Listeria*, particularly in the liver (362). Neutrophil-depleted mice show decreased liver damage at early time points, but fail to control bacterial load, and succumb to mortality within 3-6 days (362-364). However, the necessity of neutrophils has come into question. These early depletion experiments were conducted with the anti-GR-1 antibody RC6-8C5, now known to target Ly6G on neutrophils, as well as Ly6C on circulating monocytes. Both would be depleted by systemic antibody administration, confounding results. More recent studies using Ly6G-specific antibody-based depletion have illustrated neutrophils, though still contributing to defence, are dispensable to the anti-*Listeria* response (326, 365). This is reflected in this chapter, as miR-652$^{-/-}$ mice succeeded to recruit neutrophils to the site of liver infection, and yet failed to control bacteria dissemination.

At the same time, the essential roles of macrophages and monocytes during the early response are becoming clearer. Peritoneal macrophages are the first macrophages to encounter *L. monocytogenes* following IP infection. They carry the bacteria to the mediastinal lymph node where it is thought to escape to the blood (366). Blood-borne bacilli are quickly phagocytised by CD169$^+$ macrophages in the spleen marginal zone (317, 367), and by Kupffer cells, the liver tissue resident macrophage population (324). Mice depleted of macrophages or circulating monocytes quickly perish after *Listeria* infection (324, 327, 367). The absence of the CD169$^+$ spleen macrophage population impairs antigen presentation to CD8$^+$ cells, and allows uncontrolled bacterial growth in the spleen (367). Importantly, macrophages kill 60% of engulfed *L. monocytogenes*

bacilli through phagosome acidification and lysosome fusion (308), and depletion of liver Kupffer cells leads to rampant invasion of hepatocytes and extensive bacterial growth (324). Infected Kupffer cells are the major source of early TNF and IL-6 expression (358), required to induce IFNγ release from NK cells, in turn activating bacterial killing by Kupffer cells and any recruited monocytes (317, 325). Several studies have shown monocyte recruit is essential to control *L. monocytogenes* in the liver, with CCL2 signalling important for chemoattraction (326, 327, 356, 368). Mice lacking CCR2+ monocytes quickly succumb to IV *L. monocytogenes* infection by day 4 (326). Prior to monocyte depletion, these mice produce regular inflammatory lesions in the liver; a neutrophil-rich core surrounded by macrophages, effectively containing *L. monocytogenes* within. Following monocyte depletion, neutrophils are still recruited to the liver lesions, but bacteria are no longer contained. In the current study, wild type liver lesions were predominantly small and dense, with organised neutrophils and macrophages. In contrast, miR-652$^{-/-}$ lesions were large, diffuse, and often surrounded by intense necrosis, suggesting bacteria were poorly contained. These lesions were present in both moribund mice, and mice which survived to day 10. This was reflected in the increased weight loss in all miR-652$^{-/-}$ mice. These data suggest that miR-652$^{-/-}$ deficiency could hinder early monocyte recruitment or macrophage activity, an idea investigated in the proteomic analysis of *Listeria*-infected peritoneal macrophages and discussed below.

Flow cytometry data did not indicate any failed recruitment of monocytes to the spleen in miR-652$^{-/-}$ mice. However, one limitation of the current study was, due to practical limitations, moribund mouse spleens were not processed for flow cytometry analysis. Furthermore, liver leukocyte populations were not quantified. Considering monocyte activity in the liver is crucial for bacterial containment, future analysis of liver populations during the infection would be judicious. Flow cytometry analysis did identify that CD8+ T cell populations were smaller at days 7 and 10 in miR-652$^{-/-}$ mice. Considering the vital participation of spleen macrophages in listerial antigen presentation to T cells (367), any impaired macrophage function in mice could have important impacts on the adaptive immune response. This has further implications for

miR-652 in the long-term defence against other intracellular pathogens, including *M. tuberculosis* (294, 295).

It became clear a more comprehensive picture of miR-652$^{-/-}$ macrophages would be required, to capture their basal phenotype and their immediate response to *L. monocytogenes* infection. This was undertaken by proteomic analysis of peritoneal macrophages infected *in vitro* with *L. monocytogenes*. Diverse pathways were dysregulated in miR-652$^{-/-}$ pathways, perhaps testament to the nature of miRNA, which are capable of regulating manifold pathways concurrently. Some pathways were chosen for further analysis based on their likely relevance to immunity to *Listeria* and other bacterial pathogens. Many other proteins and pathways must remain for future investigation.

Proteomic analysis highlighted dysregulated pathways central to macrophage antibacterial activities, and none are more intriguing than CAPZB and actin polymerisation. CAPZB protein was downregulated in miR-652$^{-/-}$ peritoneal macrophages, both before and after *L. monocytogenes* infection. CAPZB concentration is known to affect the rate of *L. monocytogenes* motility (369), suggesting altered CAPZB expression in miR-652$^{-/-}$ macrophages could potentially enhance intercellular spread of the bacteria. *In silico* predictions identified CAPZB as a target of miR-652, owing to the 7-consecutive base complementary sequence in the CAPZB 3'UTR (99, 343). However, this study determined *in vitro* overexpression of miR-652 had no impact on *Capzb* transcription or CAPZB translation. Whilst complementary binding of miRNA bases 2-8 is considered an indicator of likely binding and mRNA inhibition (8), recent studies have confirmed this is not essential. For example, human genes *ZEB1* (45), *CCND2* (73), and *ENPP1* (153) have all been validated as miR-652 target genes, and none of these genes show complete complementarity with bases 2-8 of miR-652, as shown in chapter 1. Differential CAPZB expression may still affect control of *Listeria* spread, but its regulation appears miR-652-independent, or at least not directly downstream of miR-652.

In addition to CAPZB, downregulation of proteins in the pentose phosphate and lysosome pathways could have important implications in macrophage activity. A total of 6 pentose phosphate pathway (PPP) and glycolysis proteins were downregulated in

infected miR-652$^{-/-}$ macrophages, including PGD and G6PDX in the PPP oxidative branch, and the glycolysis enzymes GPI1 and PFKL. Glycolysis is reported to be rapidly upregulated upon *L. monocytogenes* infection, to meet the high energy requirements for cell activation (274, 316). The PPP runs in parallel with glycolysis, facilitating nucleotide synthesis, but also importantly producing NADPH in the oxidative branch (370, 371). NADPH is a key substrate for macrophages generating reactive oxygen and nitrogen species, molecules key for immunoregulation and direct bactericidal action (257). *L. monocytogenes* infection induces swift glycolysis upregulation in mouse macrophages (372). Furthermore, *in vivo* inhibition of glycolysis by a glucose analogue impaired mouse control of *L. monocytogenes* (373). Similar to the present study, these glycolysis-inhibited mice present severe pathological inflammation in the spleen and liver, with a significantly decreased percentage of TNF$^+$ macrophages. In a comparable fashion, macrophage glycolysis is downregulated by addition of exogenous lactate, the terminal metabolite of aerobic glycolysis (374). The added lactate impaired the ability of macrophages to produce TNF and IL-1β in response to *M. tuberculosis* infection. The data presented in chapter 4 illustrate the decreased cytokine expression from miR-652$^{-/-}$ macrophages during *M. tuberculosis* infection. This is possibly due to macrophage metabolic reprogramming. Although macrophages and monocytes were successfully recruited to the liver and spleen of infected miR-652$^{-/-}$ mice, downregulation of glycolysis and the PPP could have hindered their antibacterial activities once there. Future studies should employ intracellular staining of spleen and liver myeloid cell populations to elucidate the inflammatory state of infected macrophages *in vivo*. Moreover, a metabolomic analysis of miR-652$^{-/-}$ macrophages is warranted. This would demonstrate the glycolytic flux in miR-652$^{-/-}$ macrophages, and could identify the mechanism regulating inflammatory activation of these cells.

Lysosome proteases Cathepsins B, D, and Z were also all decreased in miR-652$^{-/-}$ macrophages, and each has known associations to the antibacterial immune response. Cathepsin D has direct anti-listerial activity in the phagosome, cleaving the key virulence protein Listeriolysin O to prevent bacteria escaping the phagosome (375). Cathepsin D deficient macrophages fail to control *L. monocytogenes* growth *in vitro* (376). Decreased Cathepsin D expression may lead to enhanced phagosomal escape of

L. monocytogenes to the macrophage cytosol. Alternatively, a modest Cathepsin D decrease may facilitate the generation of spacious *Listeria*-containing phagosomes, termed SLAPs, a niche utilised by *Listeria* for intracellular replication (377). Cathepsin D has also been shown to cleave the MHC-II invariant chain in the endosome, to facilitate antigen loading for presentation to CD4$^+$ T cells (378). Additionally, cathepsins B and D cleave foreign peptides for loading into the mature MHC-II complex (378-380). Whilst CD4$^+$ help is not necessary in response to systemic *L. monocytogenes* infection (381), CD4$^+$ T cells are essential for defence against TB (217). If decreased miR-652 expression impairs MHC-II antigen presentation and T cell activation, this could have grave implications in chronic *M. tuberculosis* infection. That said, data in chapter 4 indicates miR-652$^{-/-}$ mice formed a robust CD4$^+$ T cell response to *M. tuberculosis*, and miR-652 deficiency may not impact lysosomal cathepsin activity or MHC-II presentation in that context. Future investigations could investigate whether these proteomic differences in miR-652$^{-/-}$ macrophages are pathogen-specific.

In addition to regulating MHC-II antigen presentation, diminished cathepsin activity in the endosome could impact detection of mycobacterial antigens by the endosomal toll like receptors (TLRs). The intracellular receptors TLR7 and TLR9 bind bacterial ssRNA and dsDNA, respectively, in the endosome and both receptors require cathepsin processing for proper activation (380, 382-384). Roles for TLR7 and TLR9 in *L. monocytogenes* infection remain unclear. On the other hand, TLR9 stimulation enhances MHC-II presentation of mycobacterial antigens (385), and induces IL-12 production in murine DCs (386). Another student in our laboratory has investigated TLR signalling in mouse wild type and miR-652$^{-/-}$ macrophages. Stimulation of macrophages with the TLR9 agonist ODN1585 induced significantly less IL-6, TNF, KC, and MIP-1α in miR-652$^{-/-}$ macrophages (Hansen, unpublished thesis), demonstrating TLR-dependent macrophage activation was inhibited by miR-652 deficiency. Clearly, lysosomal pathways are integral to antibacterial defence and miR-652 could very well be central to regulating these processes.

Finally, notably decreased in infected miR-652$^{-/-}$ cells was interferon-stimulated gene 15 (ISG15). A protein with ubiquitin-like structures and function, ISG15 is associated with

responses to both *M. tuberculosis* and *L. monocytogenes*. Soluble ISG15 can have cytokine-like functions, and conjugation of ISG15 to free lysine residues on target proteins can inhibit the polyubiquitination and proteasome degradation of said proteins (387). ISG15 is upregulated in *Listeria*-infected epithelial cells following cytosolic detection of bacterial DNA (377). It conjugates to endoplasmic reticulum and golgi proteins, enabling cytokine release. *M. bovis* BCG-infected PBMCs secrete ISG15, to induce IFNγ expression from NK cells and T cells (388). Similarly, *M. tuberculosis*-infected macrophages shed ISG15-containing microparticles, inducing cytokine expression from nearby uninfected macrophages (389), a potentially crucial process in a TB granuloma microenvironment. Human patients with congenital ISG15-deficiency are prone to mycobacterial infections (388), and a similar phenotype is apparent in ISG15 knockout mice (390). Whilst ISG15 was downregulated in infected miR-652$^{-/-}$ macrophages, the potential regulation of ISG15 by miR-652 requires further investigation. This was beyond the scope of the current study.

Although an exact mechanism for why miR-652$^{-/-}$ mice are so susceptible to *L. monocytogenes* infection remains hidden, the list of potentially contributing factors is extensive. Compromised cytokine expression is evident in *M. tuberculosis*-infected miR-652$^{-/-}$ macrophages, and similar decreases during the acute response to *Listeria* may terminally impair the immune response in the liver. The dynamics of cytokine release and cell migration between the liver, spleen, and bone marrow are fine-tuned. Disruption and dysregulation of these processes due to diminished miR-652 expression could spell disaster for defence against both acute and chronic intracellular bacterial pathogens. A priority for future investigations is to characterise the activities of macrophages, neutrophils, and NK cells in the liver of miR-652$^{-/-}$ mice during infection. These cell types and the relationships between them are integral to early anti-listerial response. Dysregulation of these relationships has implications for *L. monocytogenes* infection and beyond.

CHAPTER 6

General discussion

Chapter 6. General Discussion

The studies described in chapters 4 and 5 stem from an investigation of miRNA as biomarkers of TB disease (20). The data therein illustrate the diverse impacts miR-652 can have during bacterial infections. miR-652$^{-/-}$ mice tolerated a chronic *M. tuberculosis* infection, but were highly prone to an acute *L. monocytogenes* infection. miR-652 clearly plays an important role in infectious disease, the mechanisms of which are yet to be uncovered. Even so, considering the promise of miRNA therapeutics as host-directed therapies, and the complexity of TB as a host-pathogen interaction, there are excellent prospects for miRNA to tackle persistent complications and difficulties associated with TB treatment.

6.1. Tuberculosis and miR-652 as a prospective therapeutic
6.1.1 TB as a continuing problem

There are still around 1.5 million deaths attributable to TB each year (21), and 10% of these deaths are attributable to multidrug-resistant (MDR) *M. tuberculosis* (26). Depending on which drug resistances are present, antibiotic regimens have a duration of 6-20 months (221). The incidence of severe side effects during these treatments is very high, as are rates of non-compliance (23). The success of the 6-month bedaquiline-linezolid-pretomanid treatment as part of the NIX-trial is a welcome development for MDR TB patients (391). However, continued overuse and misuse of antibiotics worldwide suggests significant resistance to new drugs will arise.

A prominent concern associated with the length of MDR TB antibiotic treatment is the extensive inflammation which can develop in the lungs over the treatment period, and the long-term or permanent lung damage this can cause. Successfully treated TB patients have significantly increased all-cause mortality in the 16 years after treatment completion (225). Host-directed therapies have the capability to address lung hyperinflammation, and also the potential to assist MDR TB control, potentially accomplishing these aims without selecting for microbial resistances.

6.1.2   Targeting miR-652 as a host-directed therapy

There are 15 target genes validated for miR-652, including the most recently identified PRRX1 (392). These genes act in diverse cellular pathways, positioning miR-652 in a complex regulatory system. This is evidenced by the dramatic changes in the proteome of *L. monocytogenes*-infected miR-652$^{-/-}$ macrophages, and the effects of miR-652 deficiency may be just as stark in other cell types. Because the various miR-652 gene targets are validated in several cell types, either the upregulation or downregulation of miR-652 could be applied for beneficial effects, depending on the cellular or tissue context.

System administration of a naked miR-652 mimic did not cause any detectable organ toxicity in mice (79). There may be risks associated with repeat administration of a miR-652 mimic or inhibitor during a chronic TB infection. Chronic upregulation or downregulation of miR-652 is associated with oncogenesis (35, 46, 53, 98, 111, 112, 123). Furthermore, systemic knockout of miR-652 in our miR-652$^{-/-}$ mice made them extremely vulnerable to a common environmental pathogen in *L. monocytogenes*. These risks do not immediately devalue miR-652 as a therapeutic, and can be mitigated with careful patient monitoring. Alternatively, leukocyte-targeted miRNA delivery may be optimal in this situation to avoid adverse oncogenic effects, whether cell targeting to macrophages or T cells during TB; this will be discussed below.

M. tuberculosis is known to subvert host defences through several mechanisms. Inside an infected macrophage, phagocytised bacteria initiate phagosome perforation, prevent phagosome maturation, evade destruction by autophagy, inhibit inflammasome activation, inhibit apoptosis of the infected cell, and inhibit detection by cytosolic surveillance systems (393-395). The miR-652 validated targets ARRB1, ENPP1, HOXA9, KLF9, RORA, and ZEB1 each have relevance to these subversion methods, and the administration of miR-652 mimics or inhibitors to regulate their expression could reinforce host defences against *M. tuberculosis*, or curb host-inflammation during anti-microbial treatment.

6.1.3 Known miR-652 targets in TB therapy

6.1.3.1 ARRB1

β-arrestin1 (ARRB1) was originally characterised as a G protein-coupled receptor-binding protein facilitating receptor desensitisation post-activation. More recent research shows β-arrestin1 binds over 100 proteins, including important targets in inflammatory pathways (396). miR-652 regulates ARRB1 expression in CD4$^+$ T cells, and increased ARRB1 promotes Th17 differentiation (44). The immunoregulatory roles of ARRB1 can be proinflammatory or anti-inflammatory depending on cell type and setting. ARRB1 expression promotes cytokine expression in murine microglia, increasing IL-6, IL-1β, and TNF mRNA (397). Conversely, overexpression of ARRB1 in primary mouse Kupffer cells inhibits translation of the same cytokines after LPS stimulation (398). This is due to ARRB1 preventing poly-ubiquitination of TRAF6 downstream from TLR4, thus inhibiting activation of NF-κB (157). Other studies have determined ARRB1 interacts with the nuclear receptor and transcription factor PPAR-γ to inhibit inflammatory activity in mouse macrophages. ARRB1 binds PPAR-γ and prevents association with other transcription cofactors, preventing transcription of *Nos2, IL-6,* and *Tnf* mRNA (399). Similar to these studies, miR-652$^{-/-}$ macrophages expressed significantly less IL-6 and TNF compared to wild type macrophages. The absence of miR-652 in these cells would allow increased ARRB1 expression, potentially inhibiting both TRAF6 and PPAR-γ to suppress cytokine expression.

The opposing activity of ARRB1 in microglia and Kupffer cells is interesting. Both are resident phagocytes in tissues relevant to *M. tuberculosis* and *L. monocytogenes* infections. These pathogens each colonise the liver readily, and can cause bacterial meningitis (28, 317). Administration of a miR-652 mimic to these tissue-resident macrophages could effectively increase their inflammatory activity where and when it is required. The opposing tissue-dependent activities must be considered if miR-652 were to be dosed in TB patients with different disease presentations.

6.1.3.2 KLF9

Similar to ARRB1, regulation of the transcription factor Krüppel-like factor 9 (KLF9) by miR-652 could have both pro- and anti-mycobacterial results. miR-652 inhibits KLF9 translation, to promote proliferation and motility of osteosarcoma cell lines (132).

154

Overexpression of KLF9 promotes apoptosis of mouse RAW264.7 macrophages (400), and furthermore, KLF9 promotes apoptosis and autophagy in human synovial fibroblasts (401). Apoptosis of infected macrophages is thought to aid in *M. tuberculosis* killing, as bacteria are retained in apoptotic bodies and are destroyed by efferocytosis (402). Increased autophagy in infected macrophages may improve killing of intracellular and cytosolic *M. tuberculosis* (403). On the other hand, increased KLF9 expression in macrophages also limits their release of IL-6, IL-1β, and TNF (400). Likewise, KLF9 expression in colon cancer cells inhibits the IFNβ-dependent release of ISG15 (404), which, as discussed in chapter 5, is a proinflammatory mediator during *L. monocytogenes* and *M. tuberculosis* infections. Proteomics data demonstrated ISG15 was downregulated in *L. monocytogenes*-infected miR-652$^{-/-}$ macrophages, and RT-qPCR analysis suggested IFNβ expression is also decreased in these cells. Combined with the decreased cytokine expression by miR-652$^{-/-}$ macrophages during *M. tuberculosis* infection, these data indicate KLF9 may be eliciting an anti-inflammatory phenotype in the absence of miR-652.

On the other hand, the opposing immunoregulatory activities of KLF9 may act in tandem. Considering how essential a coordinated cytokine response is to controlling *M. tuberculosis* and to maintaining the granuloma structure, the increased benefit of macrophage autophagy and apoptosis may be offset by losses due to impaired cytokine release. The balance of these effects in tissue resident macrophages will need to be examined during development of a miR-652 therapeutic, accounting for all known gene targets and their opposing regulatory functions.

6.1.3.3   RORα

The retinoic acid receptor-related orphan receptor α (RORα) is negatively regulated by miR-652 in several cancers (46, 123). As a nuclear receptor and transcription factor, RORα has diverse functions in cell regulation and cancer prevention (124, 126), and several studies have linked RORα activation with anti-inflammatory activities. In primary smooth muscle cells, RORα promotes transcription of IκBα, the inhibitor of NF-κB activation (405). Overexpression of RORα leads to decreased IL-6 and IL-8 release, and decreased production of the enzyme COX-2, required for production of the

proinflammatory lipid mediator prostaglandin E2 (PGE2) (406). Conversely, RORα deletion in THP-1 cells and primary mouse macrophages increased basal and LPS-dependent release of IL-6, TNF, IL-18, and especially IL-1β (407, 408). By the same token, RORα stimulation in primary mouse Kuppfer cells promotes an M2 phenotype, whilst RORα deletion drives a switch to M1 (409). In chapter 5, glycolysis and pentose phosphate pathway enzymes were downregulated in miR-652$^{-/-}$ macrophages after *L. monocytogenes* infection. Downregulated glycolysis is one hallmark of M2 macrophages (410), and increased RORα expression in macrophages lacking miR-652 could induce this anti-inflammatory phenotype. Collectively these studies point to RORα as an excellent target gene for miRNA intervention in the macrophages of a TB granuloma. Targeting a miR-652 mimic to infected macrophages should decrease RORα expression to promote an inflammatory M1 phenotype. Additional direction of a miR-652 mimic towards CD8$^+$ T cells could also prove fruitful, as RORα deletion promotes IFNγ production and cytotoxic activity in these cells (407).

6.1.3.4   ZEB1

Zinc finger E-box-binding homeobox 1 (ZEB1) is a transcription factor with some oncogenic functions (94, 411), and was targeted by miR-652 in pancreatic cancer cells (45). Like RORα, ZEB1 expression promotes an M2 tumour-associated macrophage phenotype. Circulating monocytes upregulate ZEB1, which promotes high CCR2 expression, driving swift recruitment to tumours (412). However, these monocytes increase expression of the M2 marker CD206, as well as the anti-inflammatory cytokine IL-10. Another study expanded on this, showing that ZEB1 expression in recruited inflammatory macrophages inhibits expression of IL-6 and TNF, and promotes IL-10 (413). Hypothetically, macrophages with low miR-652 levels would increase ZEB1 expression to inhibit secretion these cytokines, reflecting precisely what occurred in miR-652$^{-/-}$ macrophages infected with *M. tuberculosis* in chapter 4. IL-6 and TNF expression was decreased in miR-652$^{-/-}$ macrophages after *M. tuberculosis* infection. In further support of this hypothesis, monocytes were readily recruited to the liver of *L. monocytogenes*-infected mice, suggesting ZEB1, and thus CCR2, may be upregulated in miR-652$^{-/-}$ circulating monocytes.

Interestingly, ZEB1 can also promote glycolysis in breast cancer cells under hypoxic conditions, directly initiating transcription of key glycolysis enzymes (414). Glycolytic activity is considered essential for inflammatory macrophage activity and for T cell expansion during infection. Inhibiting ZEB1 expression with a miR-652 mimic may increase cytokine expression in macrophages and monocytes, but hindering glycolysis could prevent a broader array of antibacterial mechanisms, due to impeded ATP generation. These competing promotive and inhibitive transcription factor roles of ZEB1 are entirely dependent on which co-transcription factors are also present in a given cell (415). Studies must be undertaken to ascertain which ZEB1 co-factors are expressed in macrophages under basal and infection conditions. This may determine the practicality of ZEB1 as a target gene for a therapeutic miR-652 mimic.

6.1.3.5 HOXA9

The transcription factor homeobox A9 (HOXA9) is the most well-validated miR-652 target gene, even though, as described in chapter 1, the identification of a miR-652 target sequence in the HOXA9 mRNA transcript is uncertain (416). miR-652 inhibition of HOXA9 promotes proliferation of melanoma and osteosarcoma cells (88, 417), and has similar proliferative action in placental trophoblasts (32). Studies have shown HOXA9 is either a positive or negative regulator of cell glycolysis, depending on the expression of certain co-factors. In squamous cell carcinoma cells, HOXA9 forms a heterodimer with co-factor CRIP2 to inhibit the transcription of HIF-1α (418). As a major glycolysis-promoting transcription factor, HIF-1α inhibition by HOXA9 decreased glycolytic switching and proliferation in these cancer cells. Converse to this situation, HOXA9 acts as a glycolysis promoter in haemopoietic stem cells, initiating transcription of HIF-1α (419). Here DNA binding required a heterodimer between HOXA9 and MEIS1. Thus, the role of HOXA9 as an immunometabolic regulator is not only dependent on its own expression, but also that of relevant co-factors. Chapter 5 proteomic data demonstrated glycolysis enzymes GPI1 and PFKL were downregulated in infected miR-652$^{-/-}$ macrophages, as were four enzymes of the pentose phosphate pathway. HIF-1α transcriptionally regulates PFKL directly (420), and is also an upstream regulator of GPI1 (421, 422). Furthermore, HIF-1α overexpression in mouse macrophages increases generation of pentose phosphate pathway metabolites (423), indicating HIF-1α also

promotes pentose phosphate pathway flux. Thus, increased HOXA9 expression in miR-652$^{-/-}$ cells could be responsible for downregulation of multiple metabolic pathways via HIF-1α inhibition. Modulating macrophage HOXA9 expression and controlling cell metabolism by means of a miR-652 mimic could be a useful mechanism to regulate the inflammatory activities of a cell. Particularly if said mimic were simultaneously targeting ZEB1 and RORα expression for compounded proinflammatory effect. However, the expression of HOXA9 in mature leukocytes is somewhat unclear. The Human Protein Atlas indicates HOXA9 transcripts are present in human monocytes and macrophages, though expression may potentially be relatively low (424). HOXA9 expression should be assessed in alveolar and granuloma-associated macrophages from TB patients, and potentially also in T cell populations, before considering HOXA9 as an intended gene target in these cell types.

6.1.3.6 ENPP1

Finally, ectonucleotide pyrophosphatase/phosphodiesterase family member 1 (ENPP1) is regulated by miR-652 in adipocytes to promote adipogenesis (153). Though, perhaps more relevant to *M. tuberculosis* infection is the role ENPP1 plays in the cytosolic detection of bacteria dsDNA and nucleotide pathogen-associated molecular patterns (PAMPs). Bacterial dsDNA in the cytosol is detected by the enzyme cGAS, which produces cyclic GMP-AMP (cGAMP) to stimulate the internal receptor STING and initiate a type I IFN response (393). *M. tuberculosis* secretes the cyclic nucleotide PAMP c-di-AMP, released into the cell cytosol through the perforated phagosome where it can also activate STING (425). Though largely a cell surface bound receptor, ENPP1 held on the endoplasmic reticulum can hydrolyse both cGMAP and c-di-AMP (426), minimising the detection of intracellular *M. tuberculosis* (393), *L. monocytogenes* (427), and likely other intracellular pathogens secreting nucleotide PAMPs. Targeted administration of a miR-652 mimic into infected macrophages could lower ENPP1 expression to prevent hydrolysis of *M. tuberculosis* c-di-AMP. Increasing detection of these PAMPs by STING could increase the type I IFN activity of infected macrophages, and may also increase destruction of intracellular bacteria by autophagy (428). miR-652$^{-/-}$ macrophages exhibited decreased IFNβ mRNA during *L. monocytogenes* infection, potentially due to decreased intracellular detection of the pathogen. Histology data in chapter 5

demonstrated that *L. monocytogenes* was spreading efficiently in the liver of miR-652$^{-/-}$ mice. Evasion of autophagy mechanisms in the cell cytosol is essential for intercellular spread of *Listeria* (314), a strategy potentially aided by increased ENPP1 expression in miR-652$^{-/-}$ mice. The *M. tuberculosis* enzyme CdnP possesses the same hydrolysis activity of ENPP1, cleaving c-di-AMP and cGAMP (425). Small molecule inhibitors for CdnP have already been identified (393), and co-loading of a therapeutic delivery vector with a miR-652 mimic and a small molecule CdnP inhibitor could prove to be a potent synergistic promoter for *M. tuberculosis* detection within infected macrophages of the TB granuloma.

In summary, a miR-652 mimic targeted to macrophages in active TB patients could act on multiple cell pathways to enhance defence against tuberculosis. The repression of transcription factors KLF9, ZEB1, and RORA by miR-652 has the potential to increase the proinflammatory phenotype of granuloma macrophages, including increased cytokine release. Modulation of HOXA9 has the potential to stimulate macrophage glycolysis, known to be associated with antibacterial activity, and regulation of ENPP1 could enhance detection of intracellular the intracellular pathogen. Conversely, upon resolution of the bacterial infection or during extended antibiotic treatment, a miR-652 inhibitor might be applied to quell the hyperinflammation often associated with chronic TB in the lung. The opportunities for miR-652 as a therapeutic entity are great indeed.

6.2. Metabolism and antimicrobial defence
6.2.1 Deconvolution of metabolism and leukocyte action

In chapter 5, proteomics results highlighted that miR-652 deficient macrophages have decreased expression of several enzymes involved in glycolysis and the pentose phosphate pathway. Because these two pathways are highly linked with the typical inflammatory M1 macrophage phenotype, these data suggest that broad failings in the miR-652$^{-/-}$ mouse immune response to *Listeria* could be a result of upstream influence on the macrophage metabolism. Immune cell metabolism can be regulated as part of immune function, to meet the changing needs of the cell. Rapidly dividing leukocytes, such as antigen-activated T cells, switch to glycolysis and produce lactate from pyruvate

(332), even though sufficient oxygen is available and the TCA cycle more efficiently produces ATP. Glycolysis and the parallel pentose phosphate pathway generate rapid energy in the form of ATP, and also synthesise materials required for proliferation and gene translation, including nucleotides and amino acids (271, 429). Interruption of these metabolic changes can strongly influence the host immune response, and unsurprisingly this is a strategy taken by many pathogens, including *L. monocytogenes* and *M. tuberculosis* (316, 372, 430, 431). The question then becomes, if pathogen-induced metabolic changes influence the immune response downstream, does it become more practical to attempt modulation of the host immune metabolism? In the case of *M. tuberculosis*, this is one thought now under serious investigation.

Considering that the miR-652$^{-/-}$ mice described here are a model of low circulating miR-652 in a sample of Chinese TB patients (20), the data in chapter 5 highlights how one regulatory miRNA could potentially change cell metabolism and ultimately determine patient outcomes. It remains to be seen if the proteomic differences observed in macrophage metabolic pathways are mirrored in other leukocyte populations, and what impact this could have *in vivo*. Naïve CD8$^+$ T cells rely primarily on fatty acid oxidation, before massively upregulating both glycolysis and oxidative phosphorylation within days of antigen stimulation (332). Terminal effector cells then switch to primary glycolysis for rapid proliferation and expansion, whilst effector memory precursor T cells move towards oxidative phosphorylation (OXPHOS) for long term cell maintenance. If these metabolic switches are obstructed by a pathogen, the development of adaptive immunity may be compromised. Furthermore, if host gene dysregulation modifies the basal capability of a cell for metabolic switching, the host may develop an extreme vulnerability to the invading pathogen. As *M. tuberculosis* is suspected to influence metabolism in several host cell types, these considerations are a pertinent concern for TB researchers.

6.2.2 Cell metabolism and tuberculosis

During active TB, the metabolism of macrophages is a key consideration, due to their status as the main intracellular niche for *M. tuberculosis*, and also their role as direct antimicrobial actors. Macrophage metabolism is broadly considered to align with the

M1-M2 phenotype axis. M1 macrophages activated with LPS quickly upregulate glycolysis, necessary for inflammasome activation and IL-1β secretion (316). Conversely, M2 macrophages rely on OXPHOS through the TCA cycle for sustained energy (410). Whilst *M. tuberculosis* antigens do stimulate TLR4, the receptor for LPS, the metabolism of *M. tuberculosis*-infected macrophages is not simply glycolytic. Early *in vitro* studies suggested macrophages stimulated with *M. tuberculosis* antigens upregulated glycolysis and increased expression of proinflammatory cytokines (270, 272). However, more recent investigations utilising metabolic flux assays suggest macrophages downregulate both OXPHOS and glycolysis after *M. tuberculosis* infection (430), or at least that the switching between glycolysis and OXPHOS is phasic and time-dependent (198, 432). This aligns with phenotype-focussed studies which highlight primary alveolar macrophages switching from an M1 to an M2 phenotype during chronic *M. tuberculosis* infection (188).

T cell release of IFNγ is essential for the control of *M. tuberculosis*. IFNγ-deficient mice are extremely vulnerable to *M. tuberculosis* infection (200), as are HIV-positive patients with low CD4$^+$ T cell counts (433). As detailed in chapter 5, splenic T cell IFNγ expression was similar between *L. monocytogenes*-infected wild type and miR-652$^{-/-}$ mice. However, this flow cytometry analysis was not performed on mice which met an ethical threshold for euthanasia. Liver IL-6 and TNF concentrations were much higher in these ET mice as they lost control of the bacterial load. Analysis of T cell cytokine expression in these vulnerable mice would help generate a more complete picture of how the miR-652$^{-/-}$ response to *Listeria* is failing, and whether this is IFNγ-dependent. IFNγ signalling is most important for macrophage function, where it stimulates release of proinflammatory cytokines and enhances bacterial killing by autophagy (217). Of particular note is the increased glycolytic metabolism induced by IFNγ stimulation. In fact, the major glycolysis regulator HIF-1α has been identified as a key mediator of IFNγ signalling in macrophages (247, 434-436). IFNγ upregulates glycolysis in *M. tuberculosis*-infected macrophages, necessary for increasing IL-1β, IL-12, and IL-6 expression, whilst decreasing IL-10 secretion (247). Epigenetic modifications to increase macrophage glycolysis induce similar increased IL-1β and decreased IL-10 expression (437), indicating the impact of IFNγ is not parallel to glycolysis, but rather through it. Treatment of human

macrophages with a small-molecule histone deacetylase inhibitor not only promoted glycolysis and cytokine release, but also augmented the antigen presenting capabilities of macrophages to induce greater IFNγ release from CD4$^+$ T cells (437). In this sense, driving macrophage glycolysis in macrophages assists not just the innate response, but also the adaptive immune system.

Whilst macrophage glycolysis favours proinflammatory activities, mycobacteria are able to decrease macrophage glycolysis for intracellular persistence. Infection of macrophages with live *M. tuberculosis* induces IFNβ signalling, via the intracellular receptor STING (438, 439). This type I IFN signalling leads to decreased glycolysis and ultimately mitochondrial damage in neighbouring cells. This illustrates how invasion of macrophages can have considerable bearing on the metabolism, and thus the function of the local tissue environment. Proteomic and RT-qPCR data showed IFNβ and glycolysis enzymes GPI1 and PFKL were all downregulated in miR-652$^{-/-}$ macrophages, indicating that any decrease in glycolytic flux may be IFNβ-independent in these cells. IFNβ-dependent glycolysis regulation is enormously interesting because stimulation of STING by *M. tuberculosis*-generated c-di-AMP also induces inflammasome activation and autophagy (393, 428). Thus, while STING activation may serve to regulate inflammation at a broader level, it can also aid mycobacterial control within the infected macrophage.

STING-independent induction of IFNβ can have a more anti-inflammatory activity in *M. tuberculosis*-infected macrophages. Virulent clinical *M. tuberculosis* isolates tend to induce greater release of IFNβ, whilst inducing less IL-1β (438). This effect was exacerbated in rifampicin-resistant strains. Rifampicin acts to inhibit bacterial RNA polymerase (440), and the single nucleotide polymorphisms (SNP) within the polymerase β subunit which grant rifampicin resistance also affect transcription of key mycobacterial lipid biosynthesis enzymes (438). This in turn adjusts the bacterial cell wall lipid composition, and transforms subsequent host-pathogen interactions. Rifampicin resistant *M. tuberculosis* strains induce additional IFNβ, decrease both IL-1β expression and glycolysis, and could also impair phagocytosis (438).

These virulent clinical strains of *M. tuberculosis* also shift macrophage metabolism and necrosis programming by controlling lipid uptake and storage. Macrophages infected

with *M. tuberculosis* increase lipid uptake and form internal lipid droplets (434, 441), eventually growing to foam cells. This was originally thought a *M. tuberculosis* survival strategy, guaranteeing the bacteria a carbon source (442). However, a recent study identified that, whilst *M. tuberculosis* does metabolise macrophage lipids, macrophage lipid droplets formation is IFNγ-dependent and works to prevent TB growth (434). The IFNγ-HIF-1α axis drives lipid droplet formation, to aid production of lipid mediators, including PGE2, from lipid droplets. As discussed above, dysregulated expression of glycolysis and pentose phosphate pathway enzymes suggests HIF-1α induction may be impaired in miR-652$^{-/-}$ cells. Should miR-652 deficiency prove to regulate HIF-1α expression, this would impact inflammatory pathways beyond glycolysis. PGE2 acts to prevent macrophage necrosis and is an essential proinflammatory mediator for *M. tuberculosis* control (432). However, the virulent *M. tuberculosis* strain HN878 is thought to induce more accumulation of lipids synthesised into arachidonic acid in lipid membranes, and away from PGE2 synthesis (432). HN878 induces increased glycolytic metabolism in infected macrophages, compared to more virulent rifampicin-resistant strains (438). From these studies it appears *M. tuberculosis* drug-resistance can coincide with broad macrophage metabolic dysregulation. As the prevalence of MDR TB continues to increase, host metabolism-directed therapies may prove to be extremely necessary and impactful.

Finally, macrophage metabolism can be also affected by anti-microbial drugs themselves. For example, the antibiotic Clofazimine acts to inhibits macrophage OXPHOS after *in vitro* infection with *M. tuberculosis* H37Rv (443). This may promote the antimicrobial M1 macrophage phenotype beneficial for clearance of live and dying bacteria, but after extended use, it may impair the generation of M2 healing macrophages required for post-infection resolution of inflammation. These drug-metabolism interactions should be considered when considering metabolic targets as host-directed therapeutics.

6.2.3   Metabolic targets as tuberculosis therapeutics

Host-directed therapies offer a valuable alternative to small molecule antimicrobial drugs, particularly with continuing rise of drug-resistant bacteria. The obvious influence

of cell metabolism on the immune response makes metabolic pathways an intriguing opportunity as therapy targets. Chapter 5 proteomics data indicates the metabolism of macrophages was impacted by miR-652 deficiency, and it remains unclear whether this effect is cell specific, or actually systemic in miR-652$^{-/-}$ mice clearly vulnerable to infection. As discussed, targeting transcription factors like ZEB1 and HOXA9 with a miR-652 mimic could increase glycolysis and inflammatory activation of macrophages for direct anti-mycobacterial defence. However, negative regulation of glycolysis could be equally as valuable as a means of limiting pathological inflammation in TB patients already receiving antibiotics. Small molecule inhibitors for glycolysis enzymes achieve *in vivo* attenuation of macrophage inflammation. 2-DG and Shikonin, which inhibit rate-limiting glycolysis enzymes hexokinase and pyruvate kinase muscle isozyme 2, respectively, both decrease glycolytic flux in macrophages, inhibiting inflammasome activation and IL-1β release (444, 445). In these studies, inhibition of glycolysis-dependent inflammation increased survival of LPS-stimulated and septic mice. Considering the low cytokine expression exhibited by miR-652$^{-/-}$ macrophages, an investigation of IL-6 and TNF expression after 2-DG or Shikonin treatment would help position these drugs as potential adjunct treatments in miR-652-low TB patients. However, the application of these molecules for human use needs further safety investigation. Shikonin has long been used as part of traditional Chinese medicine, however, some trials suggest it may induce nephrotoxicity with extended use (446).

Metformin, a drug commonly used to treat type 2 diabetes, has been identified to lower the risk of active TB and to increase TB patient response to antibiotics (447). Yet the biological mechanisms harnessed to achieve this outcome remain unknown. Recent studies have identified metabolic shifts in several leukocyte populations after treatment with metformin. Healthy patients receiving metformin showed increased lactate in whole blood, along with decreased OXPHOS-associated enzyme transcription (448). PBMCs isolated from these patients presented lower IL-1β, TNF, IFNγ, and IL10 after *in vitro* stimulation with *M. tuberculosis* lysate. Though in an apparent contradiction, these PBMCs demonstrated increased phagocytosis and better *M. tuberculosis* killing. Metformin-treated CD8$^+$ T cells exhibit increased OXPHOS and enhanced mitochondrial health (431, 449). This augments the contribution of T cells towards bacterial control, as

transfer of metformin-educated murine CD8$^+$ T cells imparts greater bacterial killing in recipient mice (449). Thus, metformin highlights the powerful impact of metabolism-targeting therapies for infectious disease, but also signals the potential for drug-drug interactions with any miRNA-based therapeutic also targeting leukocyte metabolism and demonstrates the need for further studies in this area.

Aside from glycolysis and OXPHOS, the dietary supplementation of omega-3 fatty acids has also been suggested as an adjunct treatment for TB (406). These polyunsaturated fatty acids serve as precursors for resolvins, anti-inflammatory lipid mediators acting in opposition to inflammatory mediators like PGE2 (450). The limited human trials conducted with omega-3 fatty acids and TB present inconclusive results, though preclinical animal studies suggest their anti-inflammatory activity can limit pathological inflammation during extended antibiotic treatment (406).

6.2.4   Host-microbe metabolic interactions – targets in the microbiome?

Dietary arginine supplementation was once seen as a promising adjunct therapy in active TB patients (451). Arginine is an essential substrate for inducible NO synthase (iNOS) in macrophages and other immune cells, and researchers hypothesised increased iNOS activity would aid bacterial clearance and allow inflammation resolution. However, several human trials offered mixed results, with reduced symptoms and increased weight gain only in a small number of patients (452-454). However, a recent animal study identified the benefit of dietary arginine may not be a result of host arginine utilisation, but rather the effect of arginine on the gut microbiome (455). In mice, arginine supplements aided control of pulmonary *M. abscessus,* and authors linked the benefit to two species of *Bifidobacterium* in the gut. Oral probiotic administration of these species gave the same benefit as arginine supplementation. The benefit of a probiotic may be limited in humans if given in conjunction with extended high-dose antibiotics. Unfortunately, this would likely be the case with most TB patients. The authors identified that the *Bifidobacterium* metabolite inosine may be the key mediator of arginine-dependent mycobacterial control. Clinical evaluation of inosine supplement as an adjunct therapy to TB antimicrobials would be highly valuable.

6.3. Developing miRNA molecules for infectious disease treatment

6.3.1 Feasibility of miRNA as therapeutic targets

Since the identification of miRNA in 2000, miRNA drugs have been touted as an up-and-coming field. And yet, more than 20 years later, no miRNA-based drugs have completed clinical trials for human use. miRNA regulatory networks are incredibly complex and the activities of most miRNA are yet to be uncovered. Chapters 4 and 5 describe the expansive effects of miR-652 deficiency on infected macrophages, influencing pathways from metabolism to antigen presentation, and likely beyond. This is only one cell context, and much more research is required to identify the effects in other cell lineages. So far 15 genes are known as miR-652 targets (392, 416), and new target genes will continue to be discovered. Existing *in silico* target prediction tools have known limitations (456), indicating the actual list of genes targets is beyond current expectations.

Experimental exploration of miRNA activities is complicated by regulation from redundant miRNA, all targeting the same gene transcript. For example, the miR-652 target HOXA9 is also regulated by miR-126-3p, miR-145-5p, and miR-210-3p (457, 458), and RORα by miR-33b-5p and miR-106a-5p (459, 460). As detailed in chapter 1, miR-126-3p and miR-145-5p are dysregulated with miR-652 in bladder and lung cancers (90, 91, 118). Furthermore, miR-106a-5p is dysregulated with miR-652 during endurance exercise and cardiac diseases (48, 63, 67, 461). These associations suggest the miRNAs are regulated together, and may have redundant gene silencing functions acting in parallel. There is the possibility that redundant regulatory miRNAs will diminish the efficacy of any miR-652 inhibitor *in vivo,* or alternatively may compound the effect of a miR-652 mimic. With such complexity and ambiguity associated with miRNA functions, it begs the question, will the administration of exogenous miRNA ever form a viable drug platform? Will such therapeutics ever actually be efficacious in a broad population?

The most common reason for RNA-based therapeutics to fail clinical trials is a lack of efficacy (462). In turn, poor efficacy can be a result of several factors, including the

unstable molecular structure of free miRNA, the very short half-life of miRNA in circulation, the high immunogenicity of exogenous RNA, and population genomic variability in miRNA and their target genes. Moreover, each of these factors can contribute to off-target miRNA binding and adverse events in patients.

6.3.1.1 Population variability

Depending on the conservation of target genes amongst various populations, genomic variability can affect miRNA binding affinity and ultimately drug efficacy. Genomic SNPs are demonstrated to prevent the binding of endogenous miRNA to target mRNA, and these SNPs can be strongly associated with oncogenesis (463-465). Thus, genes with a high incidence of intra- or inter-population SNPs may not be suitable targets for therapeutic miRNAs. The same considerations would be required for poorly conserved miRNA as targets for anti-miR oligonucleotides.

To estimate the impact of genomic SNPs on miR-652-dependent gene regulation, each of the validated miR-652 target genes discussed in chapter 1 were analysed for SNPs present in the identified miRNA binding region (Figure 1.4). SNPs in these regions were collected from the dbSNP database (accessed 14/7/2022) (466), and analysed for population frequency of each allele using the Ensembl database (release 107, human genome GRCh38.p13) (467). SNPs present in at least 0.1% of any population are listed in Table 6.1. All unlisted SNPs were present in <0.1% of all analysed populations.

The most prevalent SNP was rs73778612 in ENPP1, present in 4.2% of all subjects. However, this single change is outside the sequence binding the miR-652 seed region (base pairs 2-8 of the miRNA) and may not dramatically affect miR-652 binding. FOXK1 SNP rs200327172 was present in 2.6% of East Asian subjects, consisting of an insertion within the miR-652 seed binding sequence. However, the repetitive nature of the insertion means the seed region binding site would not change, only affecting complementary base pairs downstream of the miR-652 seed region, and thus are likely less consequential. Other SNPs listed in Table 6.1 are present in 0.1-1% of a specific population, and several could adversely affect miR-652 binding. These particular populations and variations should be assessed when considering these genes as *in vivo* targets of a miR-652-based therapeutics.

There is potential that genome wide SNPs could introduce new miRNA binding sites into previously unidentified target gene mRNA. This scenario could introduce off-target binding, with negative implications for efficacy and drug safety outcomes. The influence of genomic SNPs is difficult to gauge, especially considering *in silico* methods to predict miRNA binding already identify a wealth of false positives (456). Identification of key patient populations early in drug design would be a cost-effective strategy, as predominant SNP profiles can be introduced into the miRNA drug sequence. Screening individual patients for SNPs prior to treatment would likely be prohibitively expensive for low-income TB patient populations. To minimise the safety implications of SNP-dependent off-target effects, delivery vehicles should be engineered for direct targeting of recipient cell populations.

Table 6.1. Single nucleotide polymorphisms identified in the miR-652 binding sequence of target genes.

Gene	Accession	Ancestral/Variation	Allele prevalence (%)	Population	miR-652 seed region?
ENPP1	rs530876692	G/A/T	0.3	South Asian	No
	rs561164522	A/G	0.2	African	Yes
	rs73778612	G/A	4.2	All	No
			10.8	African	No
FOXK1	rs200327172	GGCG/GGCGGCG	0.5	All	Yes
			2.6	East Asian	Yes
ISL1	rs1231127610	G/A	0.2	Gambian	Yes
JAG1	rs554327524	C/T	0.1	East Asian	Yes
	rs778183555	CC/CCC	0.1	Latin American	Yes
KCNN3	rs534004979	C/A/T	0.3	East Asian	Yes
	rs566654745	T/C	0.2	East Asian	Yes
LLGL1	rs560887236	G/A	0.2	African	Yes

SNPs listed are those present in >0.1% of a given population. SNPs listed in dbSNP. Population genetics obtained from Ensembl database.

6.3.1.2   Off-target effects

Whilst targeting multiple related genes with a single miRNA makes for an efficient mechanism of action, it also breeds the opportunity for multiple off-target binding events with conceivably grave biological repercussions. Some miRNAs are well characterised and multiple target genes have already been validated. For other miRNAs, including miR-652, new targets are still being identified, and many of these targets were not predicted as targets by existing *in silico* methods (44, 45, 153, 416). Moreover, such *in silico* prediction tools presently have limitations in their applicability (456, 468). In depth study into a target miRNA is necessary for the development of a reliable and robust therapeutic, or specific design and engineering efforts must be taken to limit off-target effects.

Delivery vectors can be manufactured for delivery to specific cell types in a specific tissue location. As hypothesised in chapter 4, miR-652 may affect T cell differentiation through regulation of the cell polarity protein LLGL1 (35, 293), making T cells an interesting cell target in TB patients. Spleen CD8$^+$ T cells numbers were lower in miR-652$^{-/-}$ mice at 7 and 10 days after *L. monocytogenes* infection, and the formation of CD8$^+$ memory T cell populations was dysregulated in miR-652$^{-/-}$ 4 and 8 weeks after *M. tuberculosis* infection. As CD8$^+$ T cells are required for controlling chronic *M. tuberculosis* infection (295), specific delivery of miR-652 to T cells could ensure optimal mycobacterial control in latent patients during antibiotic treatment. T cells are not phagocytic and engage in little endocytosis, so ligand-receptor interaction-mediated is necessary for T cell targeting. Xie et al. successfully targeted activated T cells using polyethylenimine cationic polymer nanoparticles (NP) conjugated to the transferrin ligand, allowing specific siRNA delivery (469). The cationic polymer associated well with negative siRNA, allowing efficient NP loading, and endocytosis mediated through the transferrin receptor facilitated siRNA entry comparable to lipofectamine transfection *in vitro.* Similar success was achieved with an anti-CD4 antibody-conjugated lipid NP vector delivering siRNA to Th1 T cells (470).

Delivering miRNA to specific macrophages at the site of TB infection presents different challenges, when trying to avoid phagocytosis by unrelated tissue macrophages. An

ingenious solution may have been engineered by Zang et al. in their efforts to deliver a miR-155 mimic into M2 tumour-associated macrophages, and promote a switch to tumour clearing M1 macrophages (471). Their multi-layered calcium phosphonate NPs are PEGylated on the outer layer to prevent complement binding, and aggregate at the tumour due to the enhanced permeability and retention effect. The enhanced permeability and retention effect drives aggregation of NPs at tumour sites, hypothetically caused by increased local leaky vascularisation without sufficient adjacent lymph drainage (472). Zang et al. showed that within the acidic tumour microenvironment, their NPs' pH-sensitive outer lipids dissociate to uncover covalently bound PEG-mannose. Expression of the mannose receptor CD206 is high on the anti-inflammatory tumour-associated macrophages, and the now free mannose facilitates endocytosis and miRNA delivery (471). This same device could be applied to the TB granuloma with similar effect. Whilst the centre of the caseous granuloma is neutrally charged, the environment at the caseous cuff is acidic (473). In this scenario, miRNA-loaded particles would aggregate at the highly vascularised granuloma zone (474, 475), and extravasate towards the acidic caseous cuff microenvironment where mannose residues would be revealed in a pH-dependent manner. This would then allow uptake by granuloma macrophages exhibiting an M2 phenotype, delivering a miRNA package to propel phenotypic conversion. As observed in chapter 2, mycobacterial infection induced CD206 expression in alveolar and peritoneal macrophage cell lines. Moreover, CD206-expressing macrophages are common in human necrotic and non-necrotic TB granulomas (476). As discussed above, the already validated targets of miR-652 have marked relevance to macrophage function and TB disease, making miR-652 an excellent candidate for delivery in this system. The known oncogenic potential of miR-652 in specific tissue contexts emphasises the value in such targeted delivery systems, and the probable necessity for targeted delivery of miR-652. Alternatively, miR-652 gene targets associated with a specific disease could be targeted by different means, particularly in situations where oncogenesis is more likely.

6.4.   Limitations

The *in vitro* and *in vivo* infection studies described in chapter 4 have several limitations. miR-652$^{-/-}$ macrophages presented a clear phenotype of impaired cytokine expression, but the regulatory mechanisms controlling this in the absence of miR-652 were not elucidated. Differential activation of the AKT-mTOR pathway in these cells provides one avenue for investigation, but more detailed mechanistic investigation is necessary.

The ethical restrictions on survival studies, along with the practicality and expense of housing infected mice long-term prevented a survival analysis of *M. tuberculosis*-infected miR-652$^{-/-}$ mice. Functional analysis of leukocytes in chronically infection miR-652$^{-/-}$ mice was also not possible. Considering the importance of CD8$^+$ T cells in long term TB control and the potential regulation of CD8$^+$ T cell differentiation through LLGL1, analysis of infected mice over a longer timescale would be prudent. Analysis of other infections where CD8$^+$ T cells dominate, such as Influenza infection, would also be interesting to pursue.

Limitations were present in the analysis of *L. monocytogenes*-infected mice in chapter 5. Due to practical timing limitations, only the spleens of TP wild type and miR-652$^{-/-}$ mice were analysed by flow cytometry. Thus, the composition and activation status of spleen leukocyte populations were not analysed in the ET mice most susceptible to infection. Furthermore, liver tissue was not dissociated for flow cytometry analysis. Considering the dramatic differences seen in liver histology between wild type and miR-652$^{-/-}$ mice during *Listeria* infection, analysing leukocyte recruitment and activation in the liver would contribute greatly towards the picture of immune dysregulation in miR-652$^{-/-}$ mice.

Despite the wealth of information contained in the proteomic analysis in chapter 5, few of the identified proteins and pathways have been thoroughly investigated. As a result, the mechanisms by which key immune pathways are regulated remain elusive. This includes cathepsins in the lysosome pathway, and the enzymes of the glycolysis and pentose phosphate pathways. There is a valuable opportunity for the experimental analysis of these pathways in miR-652$^{-/-}$ mice during bacterial infection.

6.5.   Future Studies

As an initial priority, further research must characterise the activities of miR-652 in immune cell populations in-depth. This miRNA clearly has important functions in innate immunity, potentially in regulating the movement and function of macrophages, monocytes, neutrophils, or NK cells. The acute *Listeria* infection is a suitable model to dissect these effects, though the tissue context, especially when detailing the functions of tissue resident macrophages, must be carefully considered.

As discussed here, known targets of miR-652 could potentiate vulnerability to bacterial infection, and each of HOXA9, RORA, ZEB1, and KLF9 present as fantastic targets for investigation. As transcription factors these proteins have potential to manoeuvre broad pathways, with great influence over cell activities. The presence or absence of certain transcription cofactors has critical effect in determining the final activity of these proteins, and this should be investigated in the bacterial infection context.

Any influence miR-652 has on cell metabolism could have huge implications for both infectious and non-infectious disease. The application of metabolic flux assays would be useful to investigating miR-652$^{-/-}$ macrophage metabolism, with and without mycobacterial infection, to determine the associated regulatory mechanism.

The data in this thesis is decidedly valuable in elucidating the weighty impact of miR-652 on the immune system, and it has opened many exciting avenues for investigation.

6.6.   Conclusion

Mycobacterium tuberculosis continues to evolve with modern challenges, and anti-tuberculosis treatments must continue to evolve alongside. Host-directed miRNA therapies show the enormous potential needed to tackle MDR TB and the pathological inflammation of chronic TB. miR-652 has great prospect in this setting, though its activities in the innate immune cells must first be more fully elucidated. Chapter 2 described the phenotypic plasticity of tissue resident macrophages in response to mycobacterial infection. Chapter 4 demonstrated the proinflammatory roles miR-652

plays in this macrophage response. miR-652 deficiency led to decreased release of IL-6 *in vitro*, but did not impair bacterial control *in vivo*. Chapter 5 made it very clear miR-652 is an important regulator of the *in vivo* innate immune response to bacterial infection. miR-652$^{-/-}$ mice were very susceptible to acute *Listeria monocytogenes* infection, and proteomic results indicted dysregulation of key antimicrobial pathways in infected peritoneal macrophages. Overall, this thesis has depicted miR-652 as a prominent immune regulator, and discussed the exciting possibilities for a miR-652-based therapeutic in tuberculosis treatment.

Chapter 7. Bibliography

1. Hanna, J., G. S. Hossein, and J. Kocerha. 2019. The Potential for microRNA Therapeutics and Clinical Research. *Frontiers in Genetics* 10: 478.

2. Maute, R. L., R. Dalla-Favera, and K. Basso. 2014. RNAs with multiple personalities. *Wiley Interdisciplinary Reviews-RNA* 5: 1-13.

3. Lee, Y., M. Kim, J. J. Han, K. H. Yeom, S. Lee, S. H. Baek, and V. N. Kim. 2004. MicroRNA genes are transcribed by RNA polymerase II. *EMBO Journal* 23: 4051-4060.

4. Han, J. J., Y. Lee, K. H. Yeom, Y. K. Kim, H. Jin, and V. N. Kim. 2004. The Drosha-DGCR8 complex in primary microRNA processing. *Genes & Development* 18: 3016-3027.

5. Zeng, Y., and B. R. Cullen. 2004. Structural requirements for pre-microRNA binding and nuclear export by Exportin 5. *Nucleic Acids Research* 32: 4776-4785.

6. Ruby, J. G., C. H. Jan, and D. P. Bartel. 2007. Intronic microRNA precursors that bypass Drosha processing. *Nature* 448: 83-86.

7. Chendrimada, T. P., R. I. Gregory, E. Kumaraswamy, J. Norman, N. Cooch, K. Nishikura, and R. Shiekhattar. 2005. TRBP recruits the Dicer complex to Ago2 for microRNA processing and gene silencing. *Nature* 436: 740-744.

8. Mah, S. M., C. Buske, R. K. Humphries, and F. Kuchenbauer. 2010. miRNA*: A Passenger Stranded in RNA-Induced Silencing Complex? *Critical Reviews in Eukaryotic Gene Expression* 20: 141-148.

9. Park, J. H., and C. Shin. 2015. Slicer-independent mechanism drives small-RNA strand separation during human RISC assembly. *Nucleic Acids Research* 43: 9418-9433.

10. Bartel, D. P. 2009. MicroRNAs: Target Recognition and Regulatory Functions. *Cell* 136: 215-233.

11. Schwarz, D. S., G. Hutvagner, T. Du, Z. S. Xu, N. Aronin, and P. D. Zamore. 2003. Asymmetry in the Assembly of the RNAi Enzyme Complex. *Cell* 115: 199-208.

12. Orang, A. V., R. Safaralizadeh, and M. Kazemzadeh-Bavili. 2014. Mechanisms of miRNA-Mediated Gene Regulation from Common Downregulation to mRNA-Specific Upregulation. *International Journal of Genomics*: 970607.

13. Bonneau, E., B. Neveu, E. Kostantin, G. J. Tsongalis, and V. De Guire. 2019. How close are miRNAs from clinical practice? A perspective on the diagnostic and therapeutic market. *EJIFCC* 30: 114-127.

14. Lee, E. C., T. Valencia, C. Allerson, A. Schairer, A. Flaten, M. Yheskel, K. Kersjes, J. Li, S. Gatto, M. Takhar, S. Lockton, A. Pavlicek, M. Kim, T. Chu, R. Soriano, S. Davis, J. R. Androsavich, S. Sarwary, T. Owen, J. Kaplan, K. Liu, G. Jang, S. Neben, P. Bentley, T. Wright, and V. Patel. 2019. Discovery and preclinical evaluation of anti-miR-17 oligonucleotide RGLS4326 for the treatment of polycystic kidney disease. *Nat Commun* 10: 4148.

15. van Zandwijk, N., N. Pavlakis, S. C. Kao, A. Linton, M. J. Boyer, S. Clarke, Y. Huynh, A. Chrzanowska, M. J. Fulham, D. L. Bailey, W. A. Cooper, L. Kritharides, L. Ridley, S. T. Pattison, J. MacDiarmid, H. Brahmbhatt, and G. Reid. 2017. Safety and activity of microRNA-loaded minicells in patients with recurrent malignant pleural mesothelioma: a first-in-man, phase 1, open-label, dose-escalation study. *Lancet Oncology* 18: 1386-1396.

16. van der Ree, M. H., J. M. de Vree, F. Stelma, S. Willemse, M. van der Valk, S. Rietdijk, R. Molenkamp, J. Schinkel, A. van Nuenen, U. Beuers, S. Hadi, M. Harbers, E. van der Veer, K. Liu, J. Grundy, A. K. Patick, A. Pavlicek, J. Blem, M. Huang, P. Grint, S. Neben, N. W. Gibson, N. A. Kootstra, and H. W. Reesink. 2017. Safety, tolerability, and antiviral effect of RG-101 in patients with chronic hepatitis C: a phase 1B, double-blind, randomised controlled trial. *Lancet* 389: 709-717.

17. van der Ree, M. H., A. J. van der Meer, A. C. van Nuenen, J. de Bruijne, S. Ottosen, H. L. Janssen, N. A. Kootstra, and H. W. Reesink. 2016. Miravirsen dosing in chronic hepatitis C patients results in decreased microRNA-122 levels without affecting other microRNAs in plasma. *Alimentary Pharmacology & Therapeutics* 43: 102-113.

18. Gebert, L. F. R., M. Law, and I. J. MacRae. 2021. A structured RNA motif locks Argonaute2:miR-122 onto the 5' end of the HCV genome. *Nature Communications* 12: 6836.

19. Alam, T., and L. Lipovich. 2021. miRCOVID-19: Potential Targets of Human miRNAs in SARS-CoV-2 for RNA-Based Drug Discovery. *Noncoding RNA* 7: 18.

20. Barry, S. E., M. Ellis, Y. R. Yang, G. Y. Guan, X. L. Wang, W. J. Britton, and B. M. Saunders. 2018. Identification of a plasma microRNA profile in untreated pulmonary tuberculosis patients that is modulated by anti-mycobacterial therapy. *J. Infect.* 77: 341-348.

21. World Health Organisation. 2021. Global Tuberculosis Report 2021. World Health Organisation, Geneva.

22. World Health Organisation. 2019. World Health Statistics 2019. World Health Organisation, Geneva.

23. Fang, X. H., Y. L. Dan, J. Liu, L. Jun, Z. P. Zhang, X. H. Kan, D. C. Ma, and G. C. Wu. 2019. Factors influencing completion of treatment among pulmonary tuberculosis patients. *Patient Preference and Adherence* 13: 491-496.

24. Aia, P., M. Kal, E. Lavu, L. N. John, K. Johnson, C. Coulter, J. Ershova, O. Tosas, M. Zignol, S. Ahmadova, and T. Islam. 2016. The Burden of Drug-Resistant Tuberculosis in Papua New Guinea: Results of a Large Population-Based Survey. *PLoS One* 11: e0149806.

25. Bainomugisa, A., E. Lavu, S. Pandey, S. Majumdar, J. Banamu, C. Coulter, B. Marais, L. Coin, S. M. Graham, and P. du Cros. 2022. Evolution and spread of a highly drug resistant strain of Mycobacterium tuberculosis in Papua New Guinea. *BMC Infectious Diseases* 22: 437.

26. Murray, C. J. L., K. S. Ikuta, F. Sharara, L. Swetschinski, G. R. Aguilar, A. Gray, C. Han, C. Bisignano, P. Rao, E. Wool, S. C. Johnson, A. J. Browne, M. G. Chipeta, F. Fell, S. Hackett, G. Haines-Woodhouse, B. H. K. Hamadani, E. A. P. Kumaran, B. McManigal, R. Agarwal, S. Akech, S. Albertson, J. Amuasi, J. Andrews, A. Aravkin, E. Ashley, F. Bailey, S. Baker, B. Basnyat, A. Bekker, R. Bender, A. Bethou, J. Bielicki, S. Boonkasidecha, J. Bukosia, C. Carvalheiro, C. Castaneda-Orjuela, V. Chansamouth, S. Chaurasia, S. Chiurchiu, F. Chowdhury, A. J. Cook, B. Cooper, T.

R. Cressey, E. Criollo-Mora, M. Cunningham, S. Darboe, N. P. J. Day, M. De Luca, K. Dokova, A. Dramowski, S. J. Dunachie, T. Eckmanns, D. Eibach, A. Emami, N. Feasey, N. Fisher-Pearson, K. Forrest, D. Garrett, P. Gastmeier, A. Z. Giref, R. C. Greer, V. Gupta, S. Haller, A. Haselbeck, S. I. Hay, M. Holm, S. Hopkins, K. C. Iregbu, J. Jacobs, D. Jarovsky, F. Javanmardi, M. Khorana, N. Kissoon, E. Kobeissi, T. Kostyanev, F. Krapp, R. Krumkamp, A. Kumar, H. H. Kyu, C. Lim, D. Limmathurotsakul, M. J. Loftus, M. Lunn, J. Ma, N. Mturi, T. Munera-Huertas, P. Musicha, M. M. Mussi-Pinhata, T. Nakamura, R. Nanavati, S. Nangia, P. Newton, C. Ngoun, A. Novotney, D. Nwakanma, C. W. Obiero, A. Olivas-Martinez, P. Olliaro, E. Ooko, E. Ortiz-Brizuela, A. Y. Peleg, C. Perrone, N. Plakkal, A. Ponce-de-Leon, M. Raad, T. Ramdin, A. Riddell, T. Roberts, J. V. Robotham, A. Roca, K. E. Rudd, N. Russell, J. Schnall, J. A. G. Scott, M. Shivamallappa, J. Sifuentes-Osornio, N. Steenkeste, A. J. Stewardson, T. Stoeva, N. Tasak, A. Thaiprakong, G. Thwaites, C. Turner, P. Turner, H. R. van Doorn, S. Velaphi, A. Vongpradith, H. Vu, T. Walsh, S. Waner, T. Wangrangsimakul, T. Wozniak, P. Zheng, B. Sartorius, A. D. Lopez, A. Stergachis, C. Moore, C. Dolecek, M. Naghavi, and C. Antimicrobial Resistance. 2022. Global burden of bacterial antimicrobial resistance in 2019: a systematic analysis. *Lancet* 399: 629-655.

27. Gupte, A. N., M. Paradkar, S. Selvaraju, K. Thiruvengadam, V. B. Y. Shivakumar, K. Sekar, S. Marinaik, A. Momin, A. Gaikwad, P. Natrajan, M. Prithivi, G. Shivaramakrishnan, N. Pradhan, R. Kohli, S. Raskar, D. Jain, R. Velu, B. Karthavarayan, R. Lokhande, N. Suryavanshi, N. Gupte, L. Murali, S. Salvi, W. Checkley, J. Golub, R. Bollinger, V. Mave, C. Padmapriyadarasini, and A. Gupta. 2019. Assessment of lung function in successfully treated tuberculosis reveals high burden of ventilatory defects and COPD. *PLOS One* 14: e0217289.

28. Fox, G. J., V. N. Nguyen, N. S. Dinh, L. P. H. Nghiem, T. N. A. Le, T. A. Nguyen, B. H. Nguyen, H. D. Nguyen, N. B. Tran, T. L. Nguyen, T. N. Le, V. H. Nguyen, K. C. Nguyen, J. Ho, D. C. Pham, W. J. Britton, J. Bestrashniy, and G. B. Marks. 2019. Post-treatment Mortality Among Patients With Tuberculosis: A Prospective Cohort Study of 10 964 Patients in Vietnam. *Clinical Infectious Diseases* 68: 1359-1366.

29. Reinhart, B. J., F. J. Slack, M. Basson, A. E. Pasquinelli, J. C. Bettinger, A. E. Rougvie, H. R. Horvitz, and G. Ruvkun. 2000. The 21-nucleotide let-7 RNA regulates developmental timing in *Caenorhabditis elegans*. *Nature* 403: 901-906.

30. Ambros, V. 2004. The functions of animal microRNAs. *Nature* 431: 350-355.

31. Dai, R., and S. A. Ahmed. 2011. MicroRNA, a new paradigm for understanding immunoregulation, inflammation, and autoimmune diseases. *Transl. Res.* 157: 163-179.

32. Shi, Z. Y., B. Liu, Y. C. Li, F. F. Liu, X. H. Yuan, and Y. Q. Wang. 2019. MicroRNA-652-3p promotes the proliferation and invasion of the trophoblast HTR-8/SVneo cell line by targeting homeobox A9 to modulate the expression of ephrin receptor B4. *Clinical and Experimental Pharmacology and Physiology* 46: 587-596.

33. Wang, B., F. Lv, L. Zhao, K. Yang, Y. S. Gao, M. J. Du, and Y. J. Zhang. 2017. MicroRNA-652 inhibits proliferation and induces apoptosis of non-small cell lung cancer A549 cells. *Int. J. Clin. Exp. Pathol.* 10: 6719-6726.

34. Zhu, Q. L., D. M. Zhan, Y. K. Chong, L. Ding, and Y. G. Yang. 2019. MiR-652-3p promotes bladder cancer migration and invasion by targeting KCNN3. *European Review for Medical and Pharmacological Sciences* 23: 8806-8812.

35. Yang, W. H., C. C. Zhou, M. Luo, X. J. Shi, Y. Li, Z. M. Sun, F. Zhou, Z. L. Chen, and J. He. 2016. MiR-652-3p is upregulated in non-small cell lung cancer and promotes proliferation and metastasis by directly targeting Lgl1. *Oncotarget* 7: 16703-16715.

36. Cummins, J. M., Y. P. He, R. J. Leary, R. Pagliarini, L. A. Diaz, T. Sjoblom, O. Barad, Z. Bentwich, A. E. Szafranska, E. Labourier, C. K. Raymond, B. S. Roberts, H. Juhl, K. W. Kinzler, B. Vogelstein, and V. E. Velculescu. 2006. The colorectal microRNAome. *Proceedings of the National Academy of Sciences of the United States of America* 103: 3687-3692.

37. Gerhard, D. S., L. Wagner, E. A. Feingold, C. M. Shenmen, L. H. Grouse, G. Schuler, S. L. Klein, S. Old, R. Rasooly, P. Good, M. Guyer, A. M. Peck, J. G. Derge, D. Lipman, F. S. Collins, and M. G. C. P. Team. 2004. The Status, Quality, and

Expansion of the NIH Full-Length cDNA Project: The Mammalian Gene Collection (MGC). *Genome Research* 14: 2121-2127.

38.   de Rie, D., I. Abugessaisa, T. Alam, E. Arner, P. Arner, H. Ashoor, G. Astrom, M. Babina, N. Bertin, A. M. Burroughs, A. J. Carlisle, C. O. Daub, M. Detmar, R. Deviatiiarov, A. Fort, C. Gebhard, D. Goldowitz, S. Guhl, T. J. Ha, J. Harshbarger, A. Hasegawa, K. Hashimoto, M. Herlyn, P. Heutink, K. J. Hitchens, C. C. Hon, E. Huang, Y. Ishizu, C. Kai, T. Kasukawa, P. Klinken, T. Lassmann, C. H. Lecellier, W. Lee, M. Lizio, V. Makeev, A. Mathelier, Y. A. Medvedeva, N. Mejhert, C. J. Mungall, S. Noma, M. Ohshima, M. Okada-Hatakeyama, H. Persson, P. Rizzu, F. Roudnicky, P. Saetrom, H. Sato, J. Severin, J. W. Shin, R. K. Swoboda, H. Tarui, H. Toyoda, K. Vitting-Seerup, L. Winteringham, Y. Yamaguchi, K. Yasuzawa, M. Yoneda, N. Yumoto, S. Zabierowski, P. G. Zhang, C. A. Wells, K. M. Summers, H. Kawaji, A. Sandelin, M. Rehli, Y. Hayashizaki, P. Carninci, A. R. R. Forrest, M. J. L. de Hoon, and F. Consortium. 2017. An integrated expression atlas of miRNAs and their promoters in human and mouse. *Nature Biotechnology* 35: 872-878.

39.   Ramsingh, G., D. C. Koboldt, M. Trissal, K. B. Chiappinelli, T. Wylie, S. Koul, L. W. Chang, R. Nagarajan, T. A. Fehniger, P. Goodfellow, V. Magrini, R. K. Wilson, L. Ding, T. J. Ley, E. R. Mardis, and D. C. Link. 2010. Complete characterization of the microRNAome in a patient with acute myeloid leukemia. *Blood* 116: 5316-5326.

40.   Ji, F. J., Y. Y. Wu, Z. An, X. S. Liu, J. N. Jiang, F. F. Chen, and X. D. Fang. 2017. Expression of both poly r(C) binding protein 1 (PCBP1) and miRNA-3978 is suppressed in peritoneal gastric cancer metastasis. *Sci Rep* 7: 15488.

41.   Allantaz, F., D. T. Cheng, T. Bergauer, P. Ravindran, M. F. Rossier, M. Ebeling, L. Badi, B. Reis, H. Bitter, M. D'Asaro, A. Chiappe, S. Sridhar, G. D. Pacheco, M. E. Burczynski, D. Hochstrasser, J. Vonderscher, and T. Matthes. 2012. Expression Profiling of Human Immune Cell Subsets Identifies miRNA-mRNA Regulatory Relationships Correlated with Cell Type Specific Expression. *PLoS One* 7: e29979.

42.   Meng, Q. L., F. Liu, X. Y. Yang, X. M. Liu, X. Zhang, C. Zhang, and Z. D. Zhang. 2014. Identification of latent tuberculosis infection-related microRNAs in human U937

macrophages expressing *Mycobacterium tuberculosis* Hsp16.3. *BMC Microbiology* 14: 37.

43.   Roderburg, C., T. Mollnow, B. Bongaerts, N. Elfimova, D. V. Cardenas, K. Berger, H. Zimmermann, A. Koch, M. Vucur, M. Luedde, C. Hellerbrand, M. Odenthal, C. Trautwein, F. Tacke, and T. Luedde. 2012. Micro-RNA Profiling in Human Serum Reveals Compartment-Specific Roles of miR-571 and miR-652 in Liver Cirrhosis. *PLOS One* 7: e32999.

44.   Xuan, J., S. L. Guo, A. Huang, H. B. Xu, M. Shao, Y. Yang, and W. Wen. 2017. MiR-29a and miR-652 Attenuate Liver Fibrosis by Inhibiting the Differentiation of CD4+T Cells. *Cell Struct. Funct.* 42: 95-103.

45.   Deng, S. C., X. Li, Y. Niu, S. Zhu, Y. Jin, S. J. Deng, J. Y. Chen, Y. Liu, C. He, T. Yin, Z. Y. Yang, J. Tao, J. X. Xiong, H. S. Wu, C. Y. Wang, and G. Zhao. 2015. MiR-652 inhibits acidic microenvironment-induced epithelial-mesenchymal transition of pancreatic cancer cells by targeting ZEB1. *Oncotarget* 6: 39661-39675.

46.   Sun, X. M., S. Dongol, C. P. Qiu, Y. Xu, C. G. Sun, Z. W. Zhang, X. S. Yang, Q. Zhang, and B. H. Kong. 2018. miR-652 Promotes Tumor Proliferation and Metastasis by Targeting *RORA* in Endometrial Cancer. *Mol. Cancer Res.* 16: 1927-1939.

47.   Cheng, L., X. Sun, B. J. Scicluna, B. M. Coleman, and A. F. Hill. 2014. Characterization and deep sequencing analysis of exosomal and non-exosomal miRNA in human urine. *Kidney Int* 86: 433-444.

48.   Pergoli, L., L. Cantone, C. Favero, L. Angelici, S. Iodice, E. Pinatel, M. Hoxha, L. Dioni, M. Letizia, B. Albetti, L. Tarantini, F. Rota, P. A. Bertazzi, A. S. Tirelli, V. Dolo, A. Cattaneo, L. Vigna, C. Battaglia, M. Carugno, M. Bonzini, A. C. Pesatori, and V. Bollati. 2017. Extracellular vesicle-packaged miRNA release after short-term exposure to particulate matter is associated with increased coagulation. *Part. Fibre Toxicol.* 14: 13.

49.   Bruno, N., J. M. ter Maaten, E. S. Ovchinnikova, E. L. Vegter, M. A. E. Valente, P. van der Meer, R. A. de Boer, P. van der Harst, D. Schmitter, M. Metra, C. M. O'Connor, P. Ponikowski, J. R. Teerlink, G. Cotter, B. Davison, J. G. Cleland, M. M. Givertz, D. M. Bloomfield, H. C. Dittrich, Y. M. Pinto, D. J. van Veldhuisen, H. L. Hillege, E. Berezikov, and A. A. Voors. 2016. MicroRNAs relate to early worsening

of renal function in patients with acute heart failure. *International Journal of Cardiology* 203: 564-569.

50. Carreras-Badosa, G., A. Bonmati, F. J. Ortega, J. M. Mercader, M. Guindo-Martinez, D. Torrents, A. Prats-Puig, J. M. Martinez-Calcerrada, E. Platero-Gutierrez, F. De Zegher, L. Ibanez, J. M. Fernandez-Real, A. Lopez-Bermejo, and J. Bassols. 2015. Altered Circulating miRNA Expression Profile in Pregestational and Gestational Obesity. *Journal of Clinical Endocrinology & Metabolism* 100: E1446-E1456.

51. Fernandez-Costa, J. M., B. Llamusi, A. Bargiela, M. Zulaica, M. C. Alvarez-Abril, M. Perez-Alonso, A. L. de Munain, A. Lopez-Castel, and R. Artero. 2016. Six Serum miRNAs Fail to Validate as Myotonic Dystrophy Type 1 Biomarkers. *PLOS One* 11: 13.

52. Ji, D. B., M. Qiao, Y. F. Yao, M. Li, H. L. Chen, Q. Dong, J. Y. Jia, X. X. Cui, Z. W. Li, J. H. Xia, and J. Gu. 2018. Serum-based microRNA signature predicts relapse and therapeutic outcome of adjuvant chemotherapy in colorectal cancer patients. *Ebiomedicine* 35: 189-197.

53. Sahlberg, K. K., G. Bottai, B. Naume, B. Burwinkel, G. A. Calin, A. L. Borresen-Dale, and L. Santarpia. 2015. A Serum MicroRNA Signature Predicts Tumor Relapse and Survival in Triple-Negative Breast Cancer Patients. *Clinical Cancer Research* 21: 1207-1214.

54. Zhou, C. C., Z. L. Chen, J. S. Dong, J. G. Li, X. J. Shi, N. Sun, M. Luo, F. Zhou, F. W. Tan, and J. He. 2015. Combination of serum miRNAs with Cyfra21-1 for the diagnosis of non-small cell lung cancer. *Cancer Lett.* 367: 138-146.

55. Gaedcke, J., M. Grade, J. Camps, R. Sokilde, B. Kaczkowski, A. J. Schetter, M. J. Difilippantonio, C. C. Harris, B. M. Ghadimi, S. Moller, T. Beissbarth, T. Ried, and T. Litman. 2012. The Rectal Cancer microRNAome - microRNA Expression in Rectal Cancer and Matched Normal Mucosa. *Clinical Cancer Research* 18: 4919-4930.

56. Matsui, D., A. H. Zaidi, S. A. Martin, A. N. Omstead, J. E. Kosovec, L. Huleihel, L. T. Saldin, C. DiCarlo, J. F. Silverman, T. Hoppo, G. G. Finley, S. F. Badylak, R. J. Kelly, and B. A. Jobe. 2016. Primary tumor microRNA signature predicts recurrence and

survival in patients with locally advanced esophageal adenocarcinoma. *Oncotarget* 7: 81281-81291.

57. Vestergaard, A. L., C. H. Bang-Berthelsen, T. Floyel, J. L. Stahl, L. Christen, F. T. Sotudeh, P. D. Horskjaer, K. S. Frederiksen, F. G. Kofod, C. Bruun, L. A. Berchtold, J. Storling, R. Regazzi, S. Kaur, F. Pociot, and T. Mandrup-Poulsen. 2018. MicroRNAs and histone deacetylase inhibition-mediated protection against inflammatory β-cell damage. *PLOS One* 13: 22.

58. Zuo, M. L., A. P. Wang, G. L. Song, and Z. B. Yang. 2020. miR-652 protects rats from cerebral ischemia/reperfusion oxidative stress injury by directly targeting NOX2. *Biomedicine & Pharmacotherapy* 124: 109860.

59. Zurawek, M., A. Dzikiewicz-Krawczyk, K. Izykowska, I. Ziolkowska-Suchanek, B. Skowronska, M. Czainska, M. Podralska, P. Fichna, G. Przybylski, M. Fichna, and J. Nowak. 2018. miR-487a-3p upregulated in type 1 diabetes targets CTLA4 and FOXO3. *Diabetes Research and Clinical Practice* 142: 146-153.

60. Meijer, H. A., E. M. Smith, and M. Bushell. 2014. Regulation of miRNA strand selection: follow the leader? *Biochem. Soc. Trans.* 42: 1135-1140.

61. Mensah, G. A., G. A. Roth, and V. Fuster. 2019. The Global Burden of Cardiovascular Diseases and Risk Factors. *Journal of the American College of Cardiology* 74: 2529-2532.

62. Pilbrow, A. P., L. Cordeddu, V. A. Cameron, C. M. Frampton, R. W. Troughton, R. N. Doughty, G. A. Whalley, C. J. Ellis, T. G. Yandle, A. M. Richards, and R. S. Y. Foo. 2014. Circulating miR-323-3p and miR-652: Candidate markers for the presence and progression of acute coronary syndromes. *International Journal of Cardiology* 176: 375-385.

63. Ovchinnikova, E. S., D. Schmitter, E. L. Vegter, J. M. ter Maaten, M. A. E. Valente, L. C. Y. Liu, P. van der Harst, Y. M. Pinto, R. A. de Boer, S. Meyer, J. R. Teerlink, C. M. O'Connor, M. Metra, B. A. Davison, D. M. Bloomfield, G. Cotter, J. G. Cleland, A. Mebazaa, S. Laribi, M. M. Givertz, P. Ponikowski, P. van der Meer, D. J. van Veldhuisen, A. A. Voors, and E. Berezikov. 2016. Signature of circulating microRNAs in patients with acute heart failure. *European Journal of Heart Failure* 18: 414-423.

64. Vegter, E. L., E. S. Ovchinnikova, D. J. van Veldhuisen, T. Jaarsma, E. Berezikov, P. van der Meer, and A. A. Voors. 2017. Low circulating microRNA levels in heart failure patients are associated with atherosclerotic disease and cardiovascular-related rehospitalizations. *Clinical Research in Cardiology* 106: 598-609.

65. Vegter, E. L., E. S. Ovchinnikova, H. H. W. Sillje, L. M. G. Meems, A. van der Pol, A. R. van der Velde, E. Berezikov, A. A. Voors, R. A. de Boer, and P. van der Meer. 2017. Rodent heart failure models do not reflect the human circulating microRNA signature in heart failure. *PLOS One* 12: e0177242.

66. Liu, J. L., H. M. Zhang, X. Li, L. Wang, H. N. Yu, J. H. Huang, Q. J. Liu, C. Wang, and A. L. Jiang. 2020. Diagnostic and prognostic significance of aberrant miR-652-3p levels in patients with acute decompensated heart failure and acute kidney injury. *Journal of International Medical Research* 48: 1-12.

67. Wang, X., K. Sundquist, P. J. Svensson, H. Rastkhani, K. Palmer, A. A. Memon, J. Sundquist, and B. Zoller. 2019. Association of recurrent venous thromboembolism and circulating microRNAs. *Clinical Epigenetics* 11: 28.

68. Nordstrom, B. L., M. A. Evans, B. R. Murphy, E. A. Nutescu, J. R. Schein, and B. K. Bookhart. 2015. Risk of recurrent venous thromboembolism among deep vein thrombosis and pulmonary embolism patients treated with warfarin. *Current Medical Research and Opinion* 31: 439-447.

69. Wang, Y., C. X. Liu, W. Wei, and W. L. Chen. 2020. Predictive value of circulating coagulation related microRNAs expressions for major adverse cardiac and cerebral event risk in patients undergoing continuous ambulatory peritoneal dialysis: a cohort study. *Journal of Nephrology* 33: 157-165.

70. Benjamin, E. J., P. Muntner, A. Alonso, M. S. Bittencourt, C. W. Callaway, A. P. Carson, A. M. Chamberlain, A. R. Chang, S. Cheng, S. R. Das, F. N. Delling, L. Djousse, M. S. V. Elkind, J. F. Ferguson, M. Fornage, L. C. Jordan, S. S. Khan, B. M. Kissela, K. L. Knutson, T. W. Kwan, D. T. Lackland, T. T. Lewis, J. H. Lichtman, C. T. Longenecker, M. S. Loop, P. L. Lutsey, S. S. Martin, K. Matsushita, A. E. Moran, M. E. Mussolino, M. O'Flaherty, A. Pandey, A. M. Perak, W. D. Rosamond, G. A. Roth, U. K. A. Sampson, G. M. Satou, E. B. Schroeder, S. H. Shah, N. L. Spartano, A. Stokes, D. L. Tirschwell, C. W. Tsao, M. P. Turakhia, L. B. VanWagner, J. T. Wilkins,

S. S. Wong, S. S. Virani, E. Amer Heart Assoc Council, C. Prevention Stat, and S. Stroke Stat. 2019. Heart Disease and Stroke Statistics-2019 Update A Report From the American Heart Association. *Circulation* 139: E56-E528.

71.   Raggi, P., J. Genest, J. T. Giles, K. J. Rayner, G. Dwivedi, R. S. Beanlands, and M. Gupta. 2018. Role of inflammation in the pathogenesis of atherosclerosis and therapeutic interventions. *Atherosclerosis* 276: 98-108.

72.   Vromman, A., V. Ruvkun, E. Shvartz, G. Wojtkiewicz, G. S. Masson, Y. Tesmenitsky, E. Folco, H. Gram, M. Nahrendorf, F. K. Swirski, G. K. Sukhova, and P. Libby. 2019. Stage-dependent differential effects of interleukin-1 isoforms on experimental atherosclerosis. *European Heart Journal* 40: 2482-2491.

73.   Huang, R. Z., Z. C. Hu, Y. Cao, H. R. Li, H. Zhang, W. H. Su, Y. Xu, L. W. Liang, N. D. Melgiri, and L. H. Jiang. 2019. MiR-652-3p inhibition enhances endothelial repair and reduces atherosclerosis by promoting Cyclin D2 expression. *Ebiomedicine* 40: 685-694.

74.   Zhu, W. Q., M. Zhao, S. Mattapally, S. F. Chen, and J. Y. Zhang. 2018. CCND2 Overexpression Enhances the Regenerative Potency of Human Induced Pluripotent Stem Cell-Derived Cardiomyocytes: Remuscularization of Injured Ventricle. *Circulation Research* 122: 88-96.

75.   Liang, L. W., W. H. Su, L. Zhou, Y. Cao, X. L. Zhou, S. Q. Liu, Y. Zhao, X. X. Ding, Q. Wang, and H. Zhang. 2020. Statin downregulation of miR-652-3p protects dyslipidemia by promoting ISL1 expression endothelium. *Metabolism-Clinical and Experimental* 107: 154226.

76.   Li, H. G., S. Horke, and U. Forstermann. 2014. Vascular oxidative stress, nitric oxide and atherosclerosis. *Atherosclerosis* 237: 208-219.

77.   Huang, P. L., Z. H. Huang, H. Mashimo, K. D. Bloch, M. A. Moskowitz, J. A. Bevan, and M. C. Fishman. 1995. Hypertension in Mice Lacking the Gene For Endothelial Nitric-Oxide Synthase. *Nature* 377: 239-242.

78.   Kroll, J., and J. Waltenberger. 1998. VEGF-A induces expression of eNOS and iNOS in endothelial cells via VEGF receptor-2 (KDR). *Biochem. Biophys. Res. Commun.* 252: 743-746.

79. Bernardo, B. C., S. S. Nguyen, C. E. Winbanks, X. M. Gao, E. J. H. Boey, Y. K. Tham, H. Kiriazis, J. Y. Y. Ooi, E. R. Porrello, S. Igoor, C. J. Thomas, P. Gregorevic, R. C. Y. Lin, X. J. Du, and J. R. McMullen. 2014. Therapeutic silencing of miR-652 restores heart function and attenuates adverse remodeling in a setting of established pathological hypertrophy. *Faseb J.* 28: 5097-5110.

80. Amsen, D., C. Helbig, and R. A. Backer. 2015. Notch in T Cell Differentiation: All Things Considered. *Trends Immunol.* 36: 802-814.

81. Siebel, C., and U. Lendahl. 2017. Notch signaling in development, tissue homeostasis, and disease. *Physiological Reviews* 97: 1235-1294.

82. MacGrogan, D., J. Munch, and J. L. de la Pompa. 2018. Notch and interacting signalling pathways in cardiac development, disease, and regeneration. *Nature Reviews Cardiology* 15: 685-704.

83. Collesi, C., L. Zentilin, G. Sinagra, and M. Giacca. 2008. Notch1 signaling stimulates proliferation of immature cardiomyocytes. *Journal of Cell Biology* 183: 117-128.

84. Palaga, T., S. Ratanabunyong, T. Pattarakankul, N. Sangphech, W. Wongchana, Y. Hadae, and P. Kueanjinda. 2013. Notch signaling regulates expression of Mcl-1 and apoptosis in PPD-treated macrophages. *Cell. Mol. Immunol.* 10: 444-452.

85. Tondera, D., F. Czauderna, K. Paulick, R. Schwarzer, J. Kaufmann, and A. Santel. 2005. The mitochondrial protein MTP18 contributes to mitochondrial fission in mammalian cells. *Journal of Cell Science* 118: 3049-3059.

86. Beg, M. S., A. J. Brenner, J. Sachdev, M. Borad, Y. K. Kang, J. Stoudemire, S. Smith, A. G. Bader, S. Kim, and D. S. Hong. 2017. Phase I study of MRX34, a liposomal miR-34a mimic, administered twice weekly in patients with advanced solid tumors. *Investigational New Drugs* 35: 180-188.

87. Zhang, L., Y. Liao, and L. L. Tang. 2019. MicroRNA-34 family: a potential tumor suppressor and therapeutic candidate in cancer. *Journal of Experimental & Clinical Cancer Research* 38: 53.

88. Xia, Z. X., C. Y. Yang, X. X. Yang, S. D. Wu, Z. Z. Feng, L. Qu, X. H. Chen, L. Y. Liu, and Y. L. Ma. 2019. miR-652 Promotes Proliferation and Migration of Uveal Melanoma Cells by Targeting HOXA9. *Medical Science Monitor* 25: 8722-8732.

89. Zhen, C., J. S. Huang, and J. B. Lu. 2019. MicroRNA-652 inhibits the biological characteristics of esophageal squamous cell carcinoma by directly targeting fibroblast growth factor receptor 1. *Exp. Ther. Med.* 18: 4473-4480.

90. Andersen, M., M. Grauslund, J. Ravn, J. B. Sorensen, C. B. Andersen, and E. Santoni-Rugiu. 2014. Diagnostic Potential of miR-126, miR-143, miR-145, and miR-652 in Malignant Pleural Mesothelioma. *Journal of Molecular Diagnostics* 16: 418-430.

91. Gao, W., H. Shen, L. X. Liu, J. A. Xu, J. Xu, and Y. Q. Shu. 2011. MiR-21 overexpression in human primary squamous cell lung carcinoma is associated with poor patient prognosis. *Journal of Cancer Research and Clinical Oncology* 137: 557-566.

92. Barry, S. E., B. Chan, M. Ellis, Y. R. Yang, M. L. Plit, G. Y. Guan, X. L. Wang, W. J. Britton, and B. M. Saunders. 2015. Identification of miR-93 as a suitable miR for normalizing miRNA in plasma of tuberculosis patients. *J. Cell. Mol. Med.* 19: 1606-1613.

93. Cao, F., Y. Miao, K. D. Xu, and P. J. Liu. 2015. Lethal (2) Giant Larvae: An Indispensable Regulator of Cell Polarity and Cancer Development. *International Journal of Biological Sciences* 11: 380-389.

94. Krebs, A. M., J. Mitschke, M. L. Losada, O. Schmalhofer, M. Boerries, H. Busch, M. Boettcher, D. Mougiakakos, W. Reichardt, P. Bronsert, V. G. Brunton, C. Pilarsky, T. H. Winkler, S. Brabletz, M. P. Stemmler, and T. Brabletz. 2017. The EMT-activator Zeb1 is a key factor for cell plasticity and promotes metastasis in pancreatic cancer. *Nature Cell Biology* 19: 518-542.

95. Aigner, K., B. Dampier, L. Descovich, M. Mikula, A. Sultan, M. Schreiber, W. Mikulits, T. Brabletz, D. Strand, P. Obrist, W. Sommergruber, N. Schweifer, A. Wernitznig, H. Beug, R. Foisner, and A. Eger. 2007. The transcription factor ZEB1 (deltaEF1) promotes tumour cell dedifferentiation by repressing master regulators of epithelial polarity. *Oncogene* 26: 6979-6988.

96. Russ, A., J. M. V. Louderbough, D. Zarnescu, and J. A. Schroeder. 2012. Hugl1 and Hugl2 in Mammary Epithelial Cells: Polarity, Proliferation, and Differentiation. *PLOS One* 7: e47734.

97.   Stephens, R., K. Lim, M. Portela, M. Kvansakul, P. O. Humbert, and H. E. Richardson. 2018. The Scribble Cell Polarity Module in the Regulation of Cell Signaling in Tissue Development and Tumorigenesis. *Journal of Molecular Biology* 430: 3585-3612.

98.   Cuk, K., M. Zucknick, D. Madhavan, S. Schott, M. Golatta, J. Heil, F. Marme, A. Turchinovich, P. Sinn, C. Sohn, H. Junkermann, A. Schneeweiss, and B. Burwinkel. 2013. Plasma MicroRNA Panel for Minimally Invasive Detection of Breast Cancer. *PLOS One* 8: e76729.

99.   Agarwal, V., G. W. Bell, J. W. Nam, and D. P. Bartel. 2015. Predicting effective microRNA target sites in mammalian mRNAs. *eLife* 4: e05005.

100.   Mangolini, A., M. Ferracin, M. V. Zanzi, E. Saccenti, S. O. Ebnaof, V. V. Poma, J. M. Sanz, A. Passaro, M. Pedriali, A. Frassoldati, P. Querzoli, S. Sabbioni, P. Carcoforo, A. Hollingsworth, and M. Negrini. 2015. Diagnostic and prognostic microRNAs in the serum of breast cancer patients measured by droplet digital PCR. *Biomarker Research* 3: 12.

101.   McDermott, A. M., N. Miller, D. Wall, L. M. Martyn, G. Ball, K. J. Sweeney, and M. J. Kerin. 2014. Identification and Validation of Oncologic miRNA Biomarkers for Luminal A-like Breast Cancer. *PLOS One* 9: e87032.

102.   Madadi, S., H. Schwarzenbach, J. Lorenzen, and M. Soleimani. 2019. MicroRNA expression studies: challenge of selecting reliable reference controls for data normalization. *Cellular and Molecular Life Sciences* 76: 3497-3514.

103.   Xiang, M. Q., Y. Zeng, R. R. Yang, H. F. Xu, Z. Chen, J. Zhong, H. L. Xie, Y. H. Xu, and X. Zeng. 2014. U6 is not a suitable endogenous control for the quantification of circulating microRNAs. *Biochem. Biophys. Res. Commun.* 454: 210-214.

104.   Arnold, M., C. C. Abnet, R. E. Neale, J. Vignat, E. L. Giovannucci, K. A. McGlynn, and F. Bray. 2020. Global Burden of 5 Major Types Of Gastrointestinal Cancer. *Gastroenterology* 159: 335-349.

105.   Schlesinger-Raab, A., J. Werner, H. Friess, D. Holzel, and J. Engel. 2017. Age and Outcome in Gastrointestinal Cancers: A Population-Based Evaluation of Oesophageal, Gastric and Colorectal Cancer. *Visceral Medicine* 33: 245-253.

106. Zheng, Q., C. Y. Chen, H. Y. Guan, W. B. A. Kang, and C. J. Yu. 2017. Prognostic role of microRNAs in human gastrointestinal cancer: A systematic review and meta-analysis. *Oncotarget* 8: 46611-46623.

107. Zhao, B. S., S. G. Liu, T. Y. Wang, Y. H. Ji, B. Qi, Y. P. Tao, H. C. Li, and X. N. Wu. 2013. Screening of MicroRNA in Patients with Esophageal Cancer at Same Tumor Node Metastasis Stage with Different Prognoses. *Asian Pacific Journal of Cancer Prevention* 14: 139-143.

108. Dutt, A., A. H. Ramos, P. S. Hammerman, C. Mermel, J. Cho, T. Sharifnia, A. Chande, K. E. Tanaka, N. Stransky, H. Greulich, N. S. Gray, and M. Meyerson. 2011. Inhibitor-Sensitive *FGFR1* Amplification in Human Non-Small Cell Lung Cancer. *PLOS One* 6: e20351.

109. Sugiura, K., S. Ozawa, Y. Kitagawa, M. Ueda, and M. Kitajima. 2007. Co-expression of aFGF and FGFR-1 is predictive of a poor prognosis in patients with esophageal squamous cell carcinoma. *Oncol. Rep.* 17: 557-564.

110. Turner, N., A. Pearson, R. Sharpe, M. Lambros, F. Geyer, M. A. Lopez-Garcia, R. Natrajan, C. Marchio, E. Iorns, A. Mackay, C. Gillett, A. Grigoriadis, A. Tutt, J. S. Reis, and A. Ashworth. 2010. FGFR1 Amplification Drives Endocrine Therapy Resistance and Is a Therapeutic Target in Breast Cancer. *Cancer Research* 70: 2085-2094.

111. Liu, R., C. N. Zhang, Z. B. Hu, G. Li, C. Wang, C. H. Yang, D. Z. Huang, X. Chen, H. Y. Zhang, R. Zhuang, T. Deng, H. Liu, J. J. Yin, S. F. Wang, K. Zen, Y. Ba, and C. Y. Zhang. 2011. A five-microRNA signature identified from genome-wide serum microRNA expression profiling serves as a fingerprint for gastric cancer diagnosis. *European Journal of Cancer* 47: 784-791.

112. Shin, V. Y., E. K. O. Ng, V. W. Chan, A. Kwong, and K. M. Chu. 2015. A three-miRNA signature as promising non-invasive diagnostic marker for gastric cancer. *Molecular Cancer* 14: 202.

113. Hedayat, S., A. Lampis, G. Vlachogiannis, K. Khan, D. Cunningham, S. Marchetti, M. Fassan, R. Begum, M. Schirripa, F. Loupakis, and N. Valeri. 2019. Circulating miR-652-3p as a biomarker of drug resistance in metastatic colorectal cancer

patients. In *Conference on Molecular Analysis for Personalised Therapy (MAP)*, London.

114. Kanaan, Z., H. Roberts, M. R. Eichenberger, A. Billeter, G. Ocheretner, J. M. Pan, S. N. Rai, J. Jorden, A. Williford, and S. Galandiuk. 2013. A Plasma MicroRNA Panel for Detection of Colorectal Adenomas A Step Toward More Precise Screening for Colorectal Cancer. *Annals of Surgery* 258: 400-408.

115. Xu, M., Y. Kuang, M. Wang, X. Han, and Q. Yang. 2017. A microRNA expression signature as a predictor of survival for colon adenocarcinoma. *Neoplasma* 64: 56-64.

116. Wing-Lun, E., S. A. Eaton, S. S. J. Hur, A. Aiken, P. E. Young, M. E. Buckland, C. C. Y. Li, J. E. Cropley, and C. M. Suter. 2016. Nutrition has a pervasive impact on cardiac microRNA expression in isogenic mice. *Epigenetics* 11: 475-481.

117. Dluzen, D. F., N. N. Hooten, Y. Q. Zhang, Y. Kim, F. E. Glover, S. M. Tajuddin, K. D. Jacob, A. B. Zonderman, and M. K. Evans. 2016. Racial differences in microRNA and gene expression in hypertensive women. *Sci Rep* 6: 35815.

118. Urquidi, V., M. Netherton, E. Gomes-Giacoia, D. J. Serie, J. Eckel-Passow, C. J. Rosser, and S. Goodison. 2016. A microRNA biomarker panel for the non-invasive detection of bladder cancer. *Oncotarget* 7: 86290-86299.

119. Liu, X., L. W. Wei, B. B. Zhao, X. X. Cai, C. H. Dong, and F. Q. Yin. 2018. Low expression of KCNN3 may affect drug resistance in ovarian cancer. *Mol. Med. Rep.* 18: 1377-1386.

120. Potier, M., V. Joulin, S. Roger, P. Besson, M. L. Jourdan, J. Y. LeGuennec, P. Bougnoux, and C. Vandier. 2006. Identification of SK3 channel as a new mediator of breast cancer cell migration. *Molecular Cancer Therapeutics* 5: 2946-2953.

121. Steinestel, K., S. Eder, K. Ehinger, J. Schneider, F. Genze, E. Winkler, E. Wardelmann, A. J. Schrader, and J. Steinestel. 2016. The small conductance calcium-activated potassium channel 3 (SK3) is a molecular target for Edelfosine to reduce the invasive potential of urothelial carcinoma cells. *Tumor Biology* 37: 6275-6283.

122. Chantome, A., A. Girault, M. Potier, C. Collin, P. Vaudin, J. C. Pages, C. Vandier, and V. Joulin. 2009. KCa2.3 channel-dependent hyperpolarization increases melanoma cell motility. *Exp. Cell Res.* 315: 3620-3630.

123. Li, J. C., and X. M. Zou. 2019. MiR-652 serves as a prognostic biomarker in gastric cancer and promotes tumor proliferation, migration, and invasion via targeting RORA. *Cancer Biomarkers* 26: 323-331.

124. Kim, H., J. M. Lee, G. Lee, J. Bhin, S. K. Oh, K. Kim, K. E. Pyo, J. S. Lee, H. Y. Yim, K. I. Kim, D. Hwang, J. Chung, and S. H. Baek. 2011. DNA Damage-Induced RORα Is Crucial for p53 Stabilization and Increased Apoptosis. *Molecular Cell* 44: 797-810.

125. McAvoy, S., S. C. Ganapathiraju, A. L. Ducharme-Smith, J. R. Pritchett, F. Kosari, D. S. Perez, Y. Zhu, C. D. James, and D. I. Smith. 2007. Non-random inactivation of large common fragile site genes in different cancers. *Cytogenetic and Genome Research* 118: 260-269.

126. Wang, Y. J., L. A. Solt, D. J. Kojetin, and T. P. Burris. 2012. Regulation of p53 Stability and Apoptosis by a ROR Agonist. *PLOS One* 7: e34921.

127. Liu, Y., W. Ding, H. Ge, M. Ponnusamy, Q. Wang, X. D. Hao, W. Wu, Y. Zhang, W. P. Yu, X. Ao, and J. X. Wang. 2019. FOXK transcription factors: Regulation and critical role in cancer. *Cancer Lett.* 458: 1-12.

128. Faber, J., A. V. Krivtsov, M. C. Stubbs, R. Wright, T. N. Davis, M. van den Heuvel-Eibrink, C. M. Zwaan, A. L. Kung, and S. A. Armstrong. 2009. HOXA9 is required for survival in human *MLL*-rearranged acute leukemias. *Blood* 113: 2375-2385.

129. Hwang, J. A., B. B. Lee, Y. Kim, S. H. Hong, Y. H. Kim, J. Han, Y. M. Shim, C. Y. Yoon, Y. S. Lee, and D. H. Kim. 2015. HOXA9 inhibits migration of lung cancer cells and its hypermethylation is associated with recurrence in non-small cell lung cancer. *Molecular Carcinogenesis* 54: E72-E80.

130. Ramos-Mejia, V., O. Navarro-Montero, V. Ayllon, C. Bueno, T. Romero, P. J. Real, and P. Menendez. 2014. *HOXA9* promotes hematopoietic commitment of human embryonic stem cells. *Blood* 124: 3065-3075.

131. Lulla, R. R., F. F. Costa, J. M. Bischof, P. M. Chou, F. B. M. de, E. F. Vanin, and M. B. Soares. 2011. Identification of Differentially Expressed MicroRNAs in Osteosarcoma. *Sarcoma* 2011: 732690.

132. Jin, Y. P., L. Yang, and X. Li. 2020. MicroRNA-652 promotes cell proliferation and osteosarcoma invasion by directly targeting KLF9. *Exp. Ther. Med.* 20: 2953-2960.

133. Li, Y., Q. Sun, M. C. Jiang, S. Li, J. Y. Zhang, Z. Q. Xu, D. Y. Guo, T. N. Gu, B. Y. Wang, L. Xiao, T. H. Zhou, and W. Zhuo. 2019. KLF9 suppresses gastric cancer cell invasion and metastasis through transcriptional inhibition of MMP28. *Faseb J.* 33: 7915-7928.

134. Simmen, F. A., Y. Su, R. J. Xiao, Z. Y. Zeng, and R. C. M. Simmen. 2008. The Krüppel-like factor 9 (KLF9) network in HEC-1-A endometrial carcinoma cells suggests the carcinogenic potential of dys-regulated KLF9 expression. *Reproductive Biology and Endocrinology* 6: 41.

135. Gaudet, A. D., L. K. Fonken, L. R. Watkins, R. J. Nelson, and P. G. Popovich. 2018. MicroRNAs: Roles in Regulating Neuroinflammation. *Neuroscientist* 24: 221-245.

136. Im, H. I., and P. J. Kenny. 2012. MicroRNAs in neuronal function and dysfunction. *Trends in Neurosciences* 35: 325-334.

137. Issler, O., and A. Chen. 2015. Determining the role of microRNAs in psychiatric disorders. *Nature Reviews Neuroscience* 16: 201-212.

138. Santarelli, D. M., N. J. Beveridge, P. A. Tooney, and M. J. Cairns. 2011. Upregulation of Dicer and MicroRNA Expression in the Dorsolateral Prefrontal Cortex Brodmann Area 46 in Schizophrenia. *Biological Psychiatry* 69: 180-187.

139. Lewohl, J. M., Y. O. Nunez, P. R. Dodd, G. R. Tiwari, R. A. Harris, and R. D. Mayfield. 2011. Up-Regulation of MicroRNAs in Brain of Human Alcoholics. *Alcoholism-Clinical and Experimental Research* 35: 1928-1937.

140. Lai, C. Y., S. L. Yu, M. H. Hsieh, C. H. Chen, H. Y. Chen, C. C. Wen, Y. H. Huang, P. C. Hsiao, C. K. Hsiao, C. M. Liu, P. C. Yang, H. G. Hwu, and W. J. Chen. 2011. MicroRNA Expression Aberration as Potential Peripheral Blood Biomarkers for Schizophrenia. *PLOS One* 6: e21635.

141. Lai, C. Y., S. Y. Lee, E. Scarr, Y. H. Yu, Y. T. Lin, C. M. Liu, T. J. Hwang, M. H. Hsieh, C. C. Liu, Y. L. Chien, M. Udawela, A. S. Gibbons, I. P. Everall, H. G. Hwu, B. Dean, and W. J. Chen. 2016. Aberrant expression of microRNAs as biomarker for schizophrenia: from acute state to partial remission, and from peripheral blood to cortical tissue. *Transl. Psychiatr.* 6: 7.

142. Lee, M., H. Cho, S. H. Jung, S. H. Yim, S. M. Cho, J. W. Chun, S. H. Paik, Y. E. Park, D. H. Cheon, J. E. Lee, J. S. Choi, D. J. Kim, and Y. J. Chung. 2018. Circulating MicroRNA Expression Levels Associated With Internet Gaming Disorder. *Frontiers in Psychiatry* 9: 81.

143. Walker, R. M., J. Rybka, S. M. Anderson, H. S. Torrance, R. Boxall, J. E. Sussmann, D. J. Porteous, A. M. McIntosh, and K. L. Evans. 2015. Preliminary investigation of miRNA expression in individuals at high familial risk of bipolar disorder. *Journal of Psychiatric Research* 62: 48-55.

144. Schür, R. R., L. W. R. Draisma, J. P. Wijnen, M. P. Boks, M. Koevoets, M. Joels, D. W. Klomp, R. S. Kahn, and C. H. Vinkers. 2016. Brain GABA Levels Across Psychiatric Disorders: A Systematic Literature Review and Meta-Analysis of H-1-MRS Studies. *Human Brain Mapping* 37: 3337-3352.

145. Gladkevich, A., H. F. Kauffman, and J. Korf. 2004. Lymphocytes as a neural probe: potential for studying psychiatric disorders. *Progress in Neuro-Psychopharmacology & Biological Psychiatry* 28: 559-576.

146. Lindqvist, D., E. S. Epel, S. H. Mellon, B. W. Penninx, D. Revesz, J. E. Verhoeven, V. I. Reus, J. Lin, L. Mahan, C. M. Hough, R. Rosser, F. S. Bersani, E. H. Blackburn, and O. M. Wolkowitz. 2015. Psychiatric disorders and leukocyte telomere length: Underlying mechanisms linking mental illness with cellular aging. *Neuroscience and Biobehavioral Reviews* 55: 333-364.

147. Nuzziello, N., L. Vilardo, P. Pelucchi, A. Consiglio, S. Liuni, M. Trojano, and M. Liguori. 2018. Investigating the Role of MicroRNA and Transcription Factor Co-regulatory Networks in Multiple Sclerosis Pathogenesis. *Int. J. Mol. Sci.* 19: 3652.

148. Bach, T. L., W. T. Kerr, Y. F. Wang, E. M. Bauman, P. Kine, E. L. Whiteman, R. S. Morgan, E. K. Williamson, E. M. Ostap, J. K. Burkhardt, G. A. Koretzky, M. J. Birnbaum, and C. S. Abrams. 2007. PI3K regulates pleckstrin-2 in T-cell cytoskeletal reorganization. *Blood* 109: 1147-1155.

149. Wu, D. M., S. H. Deng, J. Zhou, R. Han, T. Liu, T. Zhang, J. Li, J. P. Chen, and Y. Xu. 2020. PLEK2 mediates metastasis and vascular invasion via the ubiquitin-dependent degradation of SHIP2 in non-small cell lung cancer. *International Journal of Cancer* 146: 2563-2575.

150. Grube, S., M. F. Gerchen, B. Adamcio, L. A. Pardo, S. Martin, D. Malzahn, S. Papiol, M. Begemann, K. Ribbe, H. Friedrichs, K. A. Radyushkin, M. Muller, F. Benseler, J. Riggert, P. Falkai, H. Bickeboller, K. A. Naue, N. Brose, W. Stuhmer, and H. Ehrenreich. 2011. A CAG repeat polymorphism of KCNN3 predicts SK3 channel function and cognitive performance in schizophrenia. *EMBO Molecular Medicine* 3: 309-319.

151. Smolin, B., R. Karry, S. Gal-Ben-Ari, and D. Ben-Shachar. 2012. Differential expression of genes encoding neuronal ion-channel subunits in major depression, bipolar disorder and schizophrenia: implications for pathophysiology. *International Journal of Neuropsychopharmacology* 15: 869-882.

152. Kimura, T., M. P. Takahashi, Y. Okuda, M. Kaido, H. Fujimura, T. Yanagihara, and S. Sakoda. 2000. The expression of ion channel mRNAs in skeletal muscles from patients with myotonic muscular dystrophy. *Neuroscience Letters* 295: 93-96.

153. Dahlman, I., Y. Belarbi, J. Laurencikiene, A. M. Pettersson, P. Arner, and A. Kulyte. 2017. Comprehensive functional screening of miRNAs involved in fat cell insulin sensitivity among women. *Am. J. Physiol.-Endocrinol. Metab.* 312: E482-E494.

154. Meyre, D., N. Bouatia-Naji, A. Tounian, C. Samson, C. Lecoeur, V. Vatin, M. Ghoussaini, C. Wachter, S. Hercberg, G. Charpentier, W. Patsch, F. Pattou, M. A. Charles, P. Tounian, K. Clement, B. Jouret, J. Weill, B. A. Maddux, I. D. Goldfine, A. Walley, P. Boutin, C. Dina, and P. Froguel. 2005. Variants of ENPP1 are associated with childhood and adult obesity and increase the risk of glucose intolerance and type 2 diabetes. *Nature Genetics* 37: 863-867.

155. Roberts, F., D. X. Zhu, C. Farquharson, and V. E. Macrae. 2019. ENPP1 in the Regulation of Mineralization and Beyond. *Trends in Biochemical Sciences* 44: 616-628.

156. Shi, Y. F., Y. Feng, J. H. Kang, C. Liu, Z. X. Li, D. S. Li, W. Cao, J. Qiu, Z. L. Guo, E. G. Bi, L. Zang, C. Z. Lu, J. Z. Zhang, and G. Pei. 2007. Critical regulation of CD4^{+} T cell survival and autoimmunity by β-arrestin 1. *Nature Immunology* 8: 817-824.

157. Wang, Y. Y., Y. W. Tang, L. Teng, Y. L. Wu, X. H. Zhao, and G. Pei. 2006. Association of β-arrestin and TRAF6 negatively regulates Toll-like receptor-interleukin 1 receptor signaling. *Nature Immunology* 7: 139-147.

158. Buchanan, F. G., D. L. Gorden, P. Matta, Q. Shi, L. M. Matrisian, and R. N. DuBois. 2006. Role of β-arrestin 1 in the metastatic progression of colorectal cancer. *Proceedings of the National Academy of Sciences of the United States of America* 103: 1492-1497.

159. Kapoor, N., Y. Narayana, S. A. Patil, and K. N. Balaji. 2010. Nitric Oxide Is Involved in *Mycobacterium bovis* Bacillus Calmette-Guerin-Activated Jagged1 and Notch1 Signaling. *J. Immunol.* 184: 3117-3126.

160. Yuan, X. Y., N. Berg, J. W. Lee, T. T. Le, V. Neudecker, N. Jing, and H. Eltzschig. 2018. MicroRNA miR-223 as Regulator of Innate Immunity. *J. Leukoc. Biol.* 104: 515-524.

161. Gao, Y. L., L. Lin, T. Li, J. R. Yang, and Y. B. Wei. 2017. The role of miRNA-223 in cancer: Function, diagnosis and therapy. *Gene* 616: 1-7.

162. Zhi, Y., J. H. Pan, W. H. Shen, P. He, J. Zheng, X. Z. Zhou, G. S. Lu, Z. W. Chen, and Z. S. Zhou. 2016. Ginkgolide B Inhibits Human Bladder Cancer Cell Migration and Invasion Through MicroRNA-223-3p. *Cell. Physiol. Biochem.* 39: 1787-1794.

163. Akao, Y., Y. Nakagawa, Y. Kitade, T. Kinoshita, and T. Naoe. 2007. Downregulation of microRNAs-143 and-145 in B-cell malignancies. *Cancer Science* 98: 1914-1920.

164. Clape, C., V. Fritz, C. Henriquet, F. Apparailly, P. L. Fernandez, F. Iborra, C. Avances, M. Villalba, S. Culine, and L. Fajas. 2009. miR-143 Interferes with ERK5 Signaling, and Abrogates Prostate Cancer Progression in Mice. *PLOS One* 4: e7542.

165. Boucher, J. M., S. M. Peterson, S. Urs, C. X. Zhang, and L. Liaw. 2011. The miR-143/145 Cluster Is a Novel Transcriptional Target of Jagged-1/Notch Signaling in Vascular Smooth Muscle Cells. *J. Biol. Chem.* 286: 28312-28321.

166. Shen, K. X., Z. Cao, R. Z. Zhu, L. You, and T. P. Zhang. 2019. The dual functional role of MicroRNA-18a (miR-18a) in cancer development. *Clinical and Translational Medicine* 8: 32.

167. Xu, X. X., S. Zhu, Z. W. Tao, and S. L. Ye. 2018. High circulating miR-18a, miR-20a, and miR-92a expression correlates with poor prognosis in patients with non-small cell lung cancer. *Cancer Medicine* 7: 21-31.

168. Jiang, Y., J. P. Zhou, J. S. Zhao, D. Q. Hou, H. Y. Zhang, L. Li, D. Zou, J. F. Hu, Y. Zhang, and Z. T. Jing. 2020. MiR-18a-downregulated RORA inhibits the proliferation and tumorigenesis of glioma using the TNF-α-mediated NF-κB signaling pathway. *Ebiomedicine* 52: 102651.

169. Chen, L., H. Xiao, Z. H. Wang, Y. Huang, Z. P. Liu, H. Ren, and H. Song. 2014. miR-29a suppresses growth and invasion of gastric cancer cells *in vitro* by targeting VEGF-A. *BMB Reports* 47: 39-44.

170. Sun, X. J., L. Wei, Q. Chen, and R. M. Terek. 2015. MicroRNA Regulates Vascular Endothelial Growth Factor Expression in Chondrosarcoma Cells. *Clinical Orthopaedics and Related Research* 473: 907-913.

171. Takahashi, Y., A. R. R. Forrest, E. Maeno, T. Hashimoto, C. O. Daub, and J. Yasuda. 2009. MiR-107 and MiR-185 Can Induce Cell Cycle Arrest in Human Non Small Cell Lung Cancer Cell Lines. *PLOS One* 4: e6677.

172. Chen, L., X. R. Chen, F. F. Chen, Y. Liu, P. Li, R. Zhang, K. Yan, Y. J. Yi, Z. M. Xu, and X. D. Jiang. 2013. MicroRNA-107 Inhibits U87 Glioma Stem Cells Growth and Invasion. *Cellular and Molecular Neurobiology* 33: 651-657.

173. Xue, X. C., A. T. Cao, X. C. Cao, S. X. Yao, E. D. Carlsen, L. Soong, C. G. Liu, X. P. Liu, Z. J. Liu, L. W. Duck, C. O. Elson, and Y. Z. Cong. 2014. Downregulation of microRNA-107 in intestinal CD11c^{+} myeloid cells in response to microbiota and proinflammatory cytokines increases IL-23p19 expression. *European Journal of Immunology* 44: 673-682.

174. Hennessy, E. J., F. J. Sheedy, D. Santamaria, M. Barbacid, and L. A. J. O'Neill. 2011. Toll-like Receptor-4 (TLR4) Down-regulates MicroRNA-107, Increasing Macrophage Adhesion via Cyclin-dependent Kinase 6. *J. Biol. Chem.* 286: 25531-25539.

175. Waterston, R. H., K. Lindblad-Toh, E. Birney, J. Rogers, J. F. Abril, P. Agarwal, R. Agarwala, R. Ainscough, M. Alexandersson, P. An, S. E. Antonarakis, J. Attwood, R. Baertsch, J. Bailey, K. Barlow, S. Beck, E. Berry, B. Birren, T. Bloom, P. Bork, M.

Botcherby, N. Bray, M. R. Brent, D. G. Brown, S. D. Brown, C. Bult, J. Burton, J. Butler, R. D. Campbell, P. Carninci, S. Cawley, F. Chiaromonte, A. T. Chinwalla, D. M. Church, M. Clamp, C. Clee, F. S. Collins, L. L. Cook, R. R. Copley, A. Coulson, O. Couronne, J. Cuff, V. Curwen, T. Cutts, M. Daly, R. David, J. Davies, K. D. Delehaunty, J. Deri, E. T. Dermitzakis, C. Dewey, N. J. Dickens, M. Diekhans, S. Dodge, I. Dubchak, D. M. Dunn, S. R. Eddy, L. Elnitski, R. D. Emes, P. Eswara, E. Eyras, A. Felsenfeld, G. A. Fewell, P. Flicek, K. Foley, W. N. Frankel, L. A. Fulton, R. S. Fulton, T. S. Furey, D. Gage, R. A. Gibbs, G. Glusman, S. Gnerre, N. Goldman, L. Goodstadt, D. Grafham, T. A. Graves, E. D. Green, S. Gregory, R. Guigo, M. Guyer, R. C. Hardison, D. Haussler, Y. Hayashizaki, L. W. Hillier, A. Hinrichs, W. Hlavina, T. Holzer, F. Hsu, A. Hua, T. Hubbard, A. Hunt, I. Jackson, D. B. Jaffe, L. S. Johnson, M. Jones, T. A. Jones, A. Joy, M. Kamal, E. K. Karlsson, D. Karolchik, A. Kasprzyk, J. Kawai, E. Keibler, C. Kells, W. J. Kent, A. Kirby, D. L. Kolbe, I. Korf, R. S. Kucherlapati, E. J. Kulbokas, D. Kulp, T. Landers, J. P. Leger, S. Leonard, I. Letunic, R. Levine, J. Li, M. Li, C. Lloyd, S. Lucas, B. Ma, D. R. Maglott, E. R. Mardis, L. Matthews, E. Mauceli, J. H. Mayer, M. McCarthy, W. R. McCombie, S. McLaren, K. McLay, J. D. McPherson, J. Meldrim, B. Meredith, J. P. Mesirov, W. Miller, T. L. Miner, E. Mongin, K. T. Montgomery, M. Morgan, R. Mott, J. C. Mullikin, D. M. Muzny, W. E. Nash, J. O. Nelson, M. N. Nhan, R. Nicol, Z. Ning, C. Nusbaum, M. J. O'Connor, Y. Okazaki, K. Oliver, E. O. Larty, L. Pachter, G. Parra, K. H. Pepin, J. Peterson, P. Pevzner, R. Plumb, C. S. Pohl, A. Poliakov, T. C. Ponce, C. P. Ponting, S. Potter, M. Quail, A. Reymond, B. A. Roe, K. M. Roskin, E. M. Rubin, A. G. Rust, R. Santos, V. Sapojnikov, B. Schultz, J. Schultz, M. S. Schwartz, S. Schwartz, C. Scott, S. Seaman, S. Searle, T. Sharpe, A. Sheridan, R. Shownkeen, S. Sims, J. B. Singer, G. Slater, A. Smit, D. R. Smith, B. Spencer, A. Stabenau, N. S. Strange-Thomann, C. Sugnet, M. Suyama, G. Tesler, J. Thompson, D. Torrents, E. Trevaskis, J. Tromp, C. Ucla, A. U. Vidal, J. P. Vinson, A. C. von Niederhausern, C. M. Wade, M. Wall, R. J. Weber, R. B. Weiss, M. C. Wendl, A. P. West, K. Wetterstrand, R. Wheeler, S. Whelan, J. Wierzbowski, D. Willey, S. Williams, R. K. Wilson, E. Winter, K. C. Worley, D. Wyman, S. Yang, S. P. Yang, E. M. Zdobnov, M.

C. Zody, E. S. Lander, and C. Mouse Genome Sequencing. 2002. Initial sequencing and comparative analysis of the mouse genome. *Nature* 420: 520-562.

176. Perlman, R. L. 2016. Mouse models of human disease: An evolutionary perspective. *Evolution Medicine and Public Health* 2016: 170-176.

177. Kozomara, A., M. Birgaoanu, and S. Griffiths-Jones. 2019. miRBase: from microRNA sequences to function. *Nucleic Acids Research* 47: D155-D162.

178. Lacey, D. C., A. Achuthan, A. J. Fleetwood, H. Dinh, J. Roiniotis, G. M. Scholz, M. W. Chang, S. K. Beckman, A. D. Cook, and J. A. Hamilton. 2012. Defining GM-CSF- and Macrophage-CSF Dependent Macrophage Responses by *In Vitro* Models. *J. Immunol.* 188: 5752-5765.

179. Shapouri-Moghaddam, A., S. Mohammadian, H. Vazini, M. Taghadosi, S. A. Esmaeili, F. Mardani, B. Seifi, A. Mohammadi, J. T. Afshari, and A. Sahebkar. 2018. Macrophage plasticity, polarization, and function in health and disease. *Journal of Cellular Physiology* 233: 6425-6440.

180. Mantovani, A., S. K. Biswas, M. R. Galdiero, A. Sica, and M. Locati. 2013. Macrophage plasticity and polarization in tissue repair and remodelling. *J. Pathol.* 229: 176-185.

181. Arora, S., K. Dev, B. Agarwal, P. Das, and M. A. Syed. 2018. Macrophages: Their role, activation and polarization in pulmonary diseases. *Immunobiology* 223: 383-396.

182. Gosselin, D., V. M. Link, C. E. Romanoski, G. J. Fonseca, D. Z. Eichenfield, N. J. Spann, J. D. Stender, H. B. Chun, H. Garner, F. Geissmann, and C. K. Glass. 2014. Environment Drives Selection and Function of Enhancers Controlling Tissue-Specific Macrophage Identities. *Cell* 159: 1327-1340.

183. Lavin, Y., D. Winter, R. Blecher-Gonen, E. David, H. Keren-Shaul, M. Merad, S. Jung, and I. Amit. 2014. Tissue-Resident Macrophage Enhancer Landscapes Are Shaped by the Local Microenvironment. *Cell* 159: 1312-1326.

184. Okabe, Y., and R. Medzhitov. 2014. Tissue-Specific Signals Control Reversible Program of Localization and Functional Polarization of Macrophages. *Cell* 157: 832-844.

185. Bellon, T., V. Martinez, B. Lucendo, G. del Peso, M. J. Castro, L. S. Aroeira, A. Rodriguez-Sanz, M. Ossorio, R. Sanchez-Villanueva, R. Selgas, and M. A. Bajo. 2011. Alternative activation of macrophages in human peritoneum: implications for peritoneal fibrosis. *Nephrology Dialysis Transplantation* 26: 2995-3005.

186. Mitsi, E., R. Kamng'ona, J. Rylance, C. Solorzano, J. Jesus Reine, H. C. Mwandumba, D. M. Ferreira, and K. C. Jambo. 2018. Human alveolar macrophages predominately express combined classical M1 and M2 surface markers in steady state. *Respiratory Research* 19: 66.

187. Bazzan, E., G. Turato, M. Tine, C. M. Radu, E. Balestro, C. Rigobello, D. Biondini, M. Schiavon, F. Lunardi, S. Baraldo, F. Rea, P. Simioni, F. Calabrese, M. Saetta, and M. G. Cosio. 2017. Dual polarization of human alveolar macrophages progressively increases with smoking and COPD severity. *Respiratory Research* 18: 40.

188. Redente, E. F., D. M. Higgins, L. D. Dwyer-Nield, I. M. Orme, M. Gonzalez-Juarrero, and A. M. Malkinson. 2010. Differential polarization of alveolar macrophages and bone marrow-derived monocytes following chemically and pathogen-induced chronic lung inflammation. *J. Leukoc. Biol.* 88: 159-168.

189. Orecchioni, M., Y. Ghosheh, A. B. Pramod, and K. Ley. 2019. Macrophage Polarization: Different Gene Signatures in M1(LPS+) vs. Classically and M2(LPS-) vs. Alternatively Activated Macrophages. *Front. Immunol.* 10: 1084.

190. Fleetwood, A. J., T. Lawrence, J. A. Hamilton, and A. D. Cook. 2007. Granulocyte-Macrophage Colony-Stimulating Factor (CSF) and Macrophage CSF-Dependent Macrophage Phenotypes Display Differences in Cytokine Profiles and Transcription Factor Activities: Implications for CSF Blockade in Inflammation. *J. Immunol.* 178: 5245-5252.

191. Witmer-Pack, M. D., D. A. Hughes, G. Schuler, L. Lawson, A. McWilliam, K. Inaba, R. M. Steinman, and S. Gordon. 1993. Identification of macrophages and dendritic cells in the osteopetrotic (op/op) mouse. *Journal of Cell Science* 104: 1021-1029.

192. Chamberlain, L. M., D. Holt-Casper, M. Gonzalez-Juarrero, and D. W. Grainger. 2015. Extended culture of macrophages from different sources and maturation

results in a common M2 phenotype. *J. Biomed. Mater. Res. Part A* 103: 2864-2874.

193. Mauel, J., and V. Defendi. 1971. Infection and transformation of mouse peritoneal macrophages by simian virus 40. *Journal of Experimental Medicine* 134: 335-350.

194. Palleroni, A. V., L. Varesio, R. B. Wright, and M. J. Brunda. 1991. Tumoricidal alveolar macrophage and tumor infiltrating macrophage cell lines. *International Journal of Cancer* 49: 296-302.

195. Oliveira, P. M., B. N. Matos, P. A. T. Pereira, T. Gratieri, L. H. Faccioli, M. S. S. Cunha, and G. M. Gelfuso. 2017. Microparticles prepared with 50-190 kDa chitosan as promising non-toxic carriers for pulmonary delivery of isoniazid. *Carbohydrate Polymers* 174: 421-431.

196. Bai, X. Y., R. E. Oberley-Deegan, A. Bai, A. R. Ovrutsky, W. H. Kinney, M. Weaver, G. Zhang, J. R. Honda, and E. D. Chan. 2016. Curcumin enhances human macrophage control of *Mycobacterium tuberculosis* infection. *Respirology* 21: 951-957.

197. Woo, M., C. Wood, D. Kwon, K. H. P. Park, G. Fejer, and V. Delorme. 2018. *Mycobacterium tuberculosis* Infection and Innate Responses in a New Model of Lung Alveolar Macrophages. *Front. Immunol.* 9: 438.

198. Huang, L., E. V. Nazarova, S. M. Tan, Y. C. Liu, and D. G. Russell. 2018. Growth of *Mycobacterium tuberculosis in vivo* segregates with host macrophage metabolism and ontogeny. *Journal of Experimental Medicine* 215: 1135-1152.

199. Guirado, E., M. V. S. Rajaram, A. Chawla, J. Daigle, K. M. D. La Perle, E. Arnett, J. Turner, and L. S. Schlesinger. 2018. Deletion of PPARγ in lung macrophages provides an immunoprotective response against *M. tuberculosis* infection in mice. *Tuberculosis* 111: 170-177.

200. O'Garra, A., P. S. Redford, F. W. McNab, C. I. Bloom, R. J. Wilkinson, and M. P. R. Berry. 2013. The Immune Response in Tuberculosis. In *Annual Review of Immunology, Vol 31*. D. R. Littman, and W. M. Yokoyama, eds. Annual Reviews, Palo Alto. 475-527.

201. Saukkonen, J. J., B. Bazydlo, M. Thomas, R. M. Strieter, J. Keane, and H. Kornfeld. 2002. β-chemokines Are Induced by *Mycobacterium tuberculosis* and Inhibit Its Growth. *Infection and Immunity* 70: 1684-1693.

202. Ansari, A. W., A. Kamaruizaman, and R. E. Schmidt. 2013. Multifaceted impact of host C-C chemokine CCL2 in the immuno-pathogenesis of HIV-1/*M. tuberculosis* co-infection. *Front. Immunol.* 4: 312.

203. Cambier, C. J., S. M. O'Leary, M. P. O'Sullivan, J. Keane, and L. Ramakrishnan. 2017. Phenolic Glycolipid Facilitates Mycobacterial Escape from Microbicidal Tissue-Resident Macrophages. *Immunity* 47: 552-565.

204. East, L., and C. M. Isacke. 2002. The mannose receptor family. *Biochimica Et Biophysica Acta-General Subjects* 1572: 364-386.

205. Killick, K. E., C. N. Cheallaigh, C. O'Farrelly, K. Hokamp, D. E. MacHugh, and J. Harris. 2013. Receptor-mediated recognition of mycobacterial pathogens. *Cell Microbiol.* 15: 1484-1495.

206. Chen, C. Y., A. Gault, L. J. Shen, and N. Nabavi. 1994. Molecular cloning and expression of early T cell costimulatory molecule-1 and its characterization as B7-2 molecule. *J. Immunol.* 152: 4929-4936.

207. Edwards, J. P., X. Zhang, K. A. Frauwirth, and D. M. Mosser. 2006. Biochemical and functional characterization of three activated macrophage populations. *J. Leukoc. Biol.* 80: 1298-1307.

208. Yekta, S., I. H. Shih, and D. P. Bartel. 2004. MicroRNA-directed cleavage of HOXB8 mRNA. *Science* 304: 594-596.

209. Schindelin, J., I. Arganda-Carreras, E. Frise, V. Kaynig, M. Longair, T. Pietzsch, S. Preibisch, C. Rueden, S. Saalfeld, B. Schmid, J. Y. Tinevez, D. J. White, V. Hartenstein, K. Eliceiri, P. Tomancak, and A. Cardona. 2012. Fiji - an Open-Source platform for biological-image analysis. *Nature Methods* 9: 676-682.

210. Tanaka, A., J. To, B. O'Brien, S. Donnelly, and M. Lund. 2017. Selection of reliable reference genes for the normalisation of gene expression levels following time course LPS stimulation of murine bone marrow derived macrophages. *BMC Immunology* 18.

211. Cohen, S. B., B. H. Gern, J. L. Delahaye, K. N. Adams, C. R. Plumlee, J. K. Winkler, D. R. Sherman, M. Y. Gerner, and K. B. Urdahl. 2018. Alveolar Macrophages Provide an Early *Mycobacterium tuberculosis* Niche and Initiate Dissemination. *Cell Host & Microbe* 24: 439-446.

212. Awuh, J. A., and T. H. Flo. 2017. Molecular basis of mycobacterial survival in macrophages. *Cellular and Molecular Life Sciences* 74: 1625-1648.

213. Stanley, S. A., A. K. Barczak, M. R. Silvis, S. S. Luo, K. Sogi, M. Vokes, M. A. Bray, A. E. Carpenter, C. B. Moore, N. Siddiqi, E. J. Rubin, and D. T. Hung. 2014. Identification of Host-Targeted Small Molecules That Restrict Intracellular *Mycobacterium tuberculosis* Growth. *PLoS Pathog.* 10: e1003946.

214. Harding, J. S., A. Rayasam, H. A. Schreiber, Z. Fabry, and M. Sandor. 2015. Mycobacterium-Infected Dendritic Cells Disseminate Granulomatous Inflammation. *Sci Rep* 5: 15248.

215. Humphreys, I. R., G. R. Stewart, D. J. Turner, J. Patel, D. Karamanou, R. J. Snelgrove, and D. B. Young. 2006. A role for dendritic cells in the dissemination of mycobacterial infection. *Microbes and Infection* 8: 1339-1346.

216. Ramakrishnan, L. 2012. Revisiting the role of the granuloma in tuberculosis. *Nature Reviews Immunology* 12: 352-366.

217. Cooper, A. M. 2009. Cell-Mediated Immune Responses in Tuberculosis. *Annu. Rev. Immunol.* 27: 393-422.

218. Getahun, H., A. Matteelli, R. E. Chaisson, and M. Raviglione. 2015. Latent *Mycobacterium tuberculosis* Infection. *New England Journal of Medicine* 372: 2127-2135.

219. Houben, R., and P. J. Dodd. 2016. The Global Burden of Latent Tuberculosis Infection: A Re-estimation Using Mathematical Modelling. *PLOS Medicine* 13: e1002152.

220. Acar, M., M. Sutcu, N. Salman, and A. Sourer. 2017. The Risk of Tuberculosis and TNF-alpha Inhibitors. *Journal of Pediatric Infection* 11: E71-E75.

221. Mirzayev, F., K. Viney, N. N. Linh, L. Gonzalez-Angulo, M. Gegia, E. Jaramillo, M. Zignol, and T. Kasaeva. 2021. World Health Organization recommendations on

the treatment of drug-resistant tuberculosis, 2020 update. *European Respiratory Journal* 57: 2003300.

222. Dookie, N., S. Rambaran, N. Padayatchi, S. Mahomed, and K. Naidoo. 2018. Evolution of drug resistance in *Mycobacterium tuberculosis*: a review on the molecular determinants of resistance and implications for personalized care. *Journal of Antimicrobial Chemotherapy* 73: 1138-1151.

223. Culqui, D. R., C. V. Munayco, C. G. Grijalva, J. A. Cayla, O. Horna-Campos, K. A. Ch, and L. A. Suarez. 2012. Factors Associated With the Non-Completion of Conventional Anti-Tuberculosis Treatment in Peru. *Archivos De Bronconeumologia* 48: 150-155.

224. Johansson, E., N. H. Long, V. K. Diwan, and A. Winkvist. 1999. Attitudes to compliance with tuberculosis treatment among women and men in Vietnam. *International Journal of Tuberculosis and Lung Disease* 3: 862-868.

225. Miller, T. L., F. A. Wilson, J. W. Pang, S. Beavers, S. Hoger, S. Sharnprapai, M. Pagaoa, D. J. Katz, and S. E. Weis. 2015. Mortality Hazard and Survival After Tuberculosis Treatment. *American Journal of Public Health* 105: 930-937.

226. Ravimohan, S., H. Kornfeld, D. Weissman, and G. P. Bisson. 2018. Tuberculosis and lung damage: from epidemiology to pathophysiology. *European Respiratory Review* 27: 170077.

227. World Health Organisation. 2021. WHO consolidated guidelines on tuberculosis. Module 3: Diagnosis - Rapid diagnostics for tuberculosis detection 2021 update. World Health Organisation, Geneva.

228. Elbrolosy, A. M., R. H. El Helbawy, O. M. Mansour, and R. A. Latif. 2021. Diagnostic utility of GeneXpert MTB/RIF assay versus conventional methods for diagnosis of pulmonary and extra-pulmonary tuberculosis. *BMC Microbiology* 21: 144.

229. Chang, K., W. P. Lu, J. J. Wang, K. J. Zhang, S. R. Jia, F. Li, S. L. Deng, and M. Chen. 2012. Rapid and effective diagnosis of tuberculosis and rifampicin resistance with Xpert MTB/RIF assay: A meta-analysis. *J. Infect.* 64: 580-588.

230. Vaezipour, N., N. Fritschi, N. Brasier, S. Belard, J. Dominguez, M. Tebruegge, D. Portevin, and N. Ritz. 2022. Towards Accurate Point-of-Care Tests for Tuberculosis in Children. *Pathogens* 11: 327.

231. Pedersen, J. L., N. J. Bokil, and B. M. Saunders. 2019. Developing new TB biomarkers, are miRNA the answer? *Tuberculosis* 118: 101860.

232. Sabir, N., T. Hussain, S. Z. A. Shah, A. Peramo, D. M. Zhao, and X. M. Zhou. 2018. miRNAs in Tuberculosis: New Avenues for Diagnosis and Host-Directed Therapy. *Front. Microbiol.* 9: 602.

233. Misharin, A. V., L. Morales-Nebreda, G. M. Mutlu, G. R. S. Budinger, and H. Perlman. 2013. Flow Cytometric Analysis of Macrophages and Dendritic Cell Subsets in the Mouse Lung. *Am. J. Respir. Cell Mol. Biol.* 49: 503-510.

234. Cooper, A. M. 2015. Mouse Model of Tuberculosis. *Cold Spring Harbor Perspectives in Medicine* 5: a018556.

235. Vergadi, E., E. Ieronymaki, K. Lyroni, K. Vaporidi, and C. Tsatsanis. 2017. Akt Signaling Pathway in Macrophage Activation and M1/M2 Polarization. *J. Immunol.* 198: 1006-1014.

236. Bansal, K., Y. Narayana, S. A. Patil, and K. N. Balaji. 2009. *M. bovis* BCG induced expression of COX-2 involves nitric oxide-dependent and -independent signaling pathways. *J. Leukoc. Biol.* 85: 804-816.

237. Cooper, A. M., K. D. Mayer-Barber, and A. Sher. 2011. Role of innate cytokines in mycobacterial infection. *Mucosal Immunology* 4: 252-260.

238. Sawant, K. V., R. L. Xu, R. Cox, H. Hawkins, E. Sbrana, D. Kolli, R. P. Garofalo, and K. Rajarathnam. 2015. Chemokine CXCL1-Mediated Neutrophil Trafficking in the Lung: Role of CXCR2 Activation. *Journal of Innate Immunity* 7: 647-658.

239. Li, B., L. L. Jones, and T. L. Geiger. 2018. IL-6 Promotes T Cell Proliferation and Expansion under Inflammatory Conditions in Association with Low-Level RORγt Expression. *J. Immunol.* 201: 2934-2946.

240. Busatto, C., J. S. Vianna, L. V. da Silva, I. B. Ramis, and P. E. A. da Silva. 2019. *Mycobacterium avium*: an overview. *Tuberculosis* 114: 127-134.

241. Prevots, D. R., and T. K. Marras. 2015. Epidemiology of Human Pulmonary Infection with Nontuberculous Mycobacteria: A Review. *Clinics in Chest Medicine* 36: 13-34.

242. Domingo-Gonzalez, R., O. Prince, A. Cooper, and S. A. Khader. 2016. Cytokines and Chemokines in *Mycobacterium tuberculosis* Infection. *Microbiology Spectrum* 4.

243. Algood, H. M., P. L. Lin, and J. L. Flynn. 2005. Tumor Necrosis Factor and Chemokine Interactions in the Formation and Maintenance of Granulomas in Tuberculosis. *Clin. Infect. Dis.* 41 Suppl 3: S189-193.

244. Roach, D. R., A. G. D. Bean, C. Demangel, M. P. France, H. Briscoe, and W. J. Britton. 2002. TNF Regulates Chemokine Induction Essential for Cell Recruitment, Granuloma Formation, and Clearance of Mycobacterial Infection. *J. Immunol.* 168: 4620-4627.

245. Saunders, B. M., S. Tran, S. Ruuls, J. D. Sedgwick, H. Briscoe, and W. J. Britton. 2005. Transmembrane TNF Is Sufficient to Initiate Cell Migration and Granuloma Formation and Provide Acute, but Not Long-Term, Control of *Mycobacterium tuberculosis* Infection. *J. Immunol.* 174: 4852-4859.

246. Allie, N., S. I. Grivennikov, R. Keeton, N. J. Hsu, M. L. Bourigault, N. Court, C. Fremond, V. Yeremeev, Y. Shebzukhov, B. Ryffel, S. A. Nedospasov, V. F. J. Quesniaux, and M. Jacobs. 2013. Prominent role for T cell-derived Tumour Necrosis Factor for sustained control of *Mycobacterium tuberculosis* infection. *Sci Rep* 3: 1809.

247. Braverman, J., K. M. Sogi, D. Benjamin, D. K. Nomura, and S. A. Stanley. 2016. HIF-1α Is an Essential Mediator of IFN-γ-Dependent Immunity to *Mycobacterium tuberculosis*. *J. Immunol.* 197: 1287-1297.

248. Bean, A. G., D. R. Roach, H. Briscoe, M. P. France, H. Korner, J. D. Sedgwick, and W. J. Britton. 1999. Structural Deficiencies in Granuloma Formation in TNF Gene-Targeted Mice Underlie the Heightened Susceptibility to Aerosol *Mycobacterium tuberculosis* Infection, Which Is Not Compensated for by Lymphotoxin. *J. Immunol.* 162: 3504-3511.

249. Saunders, B. M., H. Briscoe, and W. J. Britton. 2004. T cell-derived tumour necrosis factor is essential, but not sufficient, for protection against *Mycobacterium tuberculosis* infection. *Clinical and Experimental Immunology* 137: 279-287.

250. Saunders, B. M., A. A. Frank, I. M. Orme, and A. M. Cooper. 2000. Interleukin-6 Induces Early Gamma Interferon Production in the Infected Lung but Is Not Required for Generation of Specific Immunity to *Mycobacterium tuberculosis* Infection. *Infection and Immunity* 68: 3322-3326.

251. Ladel, C. H., C. Blum, A. Dreher, K. Reifenberg, M. Kopf, and S. H. E. Kaufmann. 1997. Lethal tuberculosis in interleukin-6-deficient mutant mice. *Infection and Immunity* 65: 4843-4849.

252. Nolan, A., R. Condos, M. L. Huie, R. Dawson, K. Dheda, E. Bateman, W. N. Rom, and M. D. Weiden. 2013. Elevated IP-10 and IL-6 from bronchoalveolar lavage cells are biomarkers of non-cavitary tuberculosis. *International Journal of Tuberculosis and Lung Disease* 17: 922-927.

253. Jin, L. L., S. Batra, D. N. Douda, N. Palaniyar, and S. Jeyaseelan. 2014. CXCL1 Contributes to Host Defense in Polymicrobial Sepsis via Modulating T Cell and Neutrophil Functions. *J. Immunol.* 193: 3549-3558.

254. Monin, L., and S. A. Khader. 2014. Chemokines in tuberculosis: The good, the bad and the ugly. *Semin. Immunol.* 26: 552-558.

255. Kumar, N. P., K. Moideen, A. Nancy, V. Viswanathan, B. S. Shruthi, S. Sivakumar, M. Natarajan, H. Kornfeld, and S. Babu. 2019. Plasma chemokines are biomarkers of disease severity, higher bacterial burden and delayed sputum culture conversion in pulmonary tuberculosis. *Sci Rep* 9: 18217.

256. Kumar, N. P., K. Moideen, A. Nancy, V. Viswanathan, K. Thiruvengadam, D. Nair, V. V. Banurekha, S. Sivakumar, S. Hissar, H. Kornfeld, and S. Babu. 2021. Plasma Chemokines Are Baseline Predictors of Unfavorable Treatment Outcomes in Pulmonary Tuberculosis. *Clinical Infectious Diseases* 73: E3419-E3427.

257. Covarrubias, A. J., H. I. Aksoylar, and T. Horng. 2015. Control of macrophage metabolism and activation by mTOR and Akt signaling. *Semin. Immunol.* 27: 286-296.

258. Singh, P., and S. Subbian. 2018. Harnessing the mTOR Pathway for Tuberculosis Treatment. *Front. Microbiol.* 9: 70.

259. Sarbassov, D. D., D. A. Guertin, S. M. Ali, and D. M. Sabatini. 2005. Phosphorylation and Regulation of Akt/PKB by the Rictor-mTOR Complex. *Science* 307: 1098-1101.

260. Arranz, A., C. Doxaki, E. Vergadi, Y. M. de la Torre, K. Vaporidi, E. D. Lagoudaki, E. Ieronymaki, A. Androulidaki, M. Venihaki, A. N. Margioris, E. N. Stathopoulos, P. N. Tsichlis, and C. Tsatsanis. 2012. Akt1 and Akt2 protein kinases differentially contribute to macrophage polarization. *Proceedings of the National Academy of Sciences of the United States of America* 109: 9517-9522.

261. Linton, M. F., J. J. Moslehi, and V. R. Babaev. 2019. Akt Signaling in Macrophage Polarization, Survival, and Atherosclerosis. *Int. J. Mol. Sci.* 20: 2703.

262. Reyes-Gordillo, K., R. Shah, J. Arellanes-Robledo, Y. Cheng, J. Ibrahim, and P. L. Tuma. 2019. Akt1 and Akt2 Isoforms Play Distinct Roles in Regulating the Development of Inflammation and Fibrosis Associated with Alcoholic Liver Disease. *Cells* 8: 1337.

263. Mahon, R. N., O. J. Sande, R. E. Rojas, A. D. Levine, C. V. Harding, and W. H. Boom. 2012. *Mycobacterium tuberculosis* ManLAM inhibits T-cell-receptor signaling by interference with ZAP-70, Lck and LAT phosphorylation. *Cellular Immunology* 275: 98-105.

264. Karim, A. F., O. J. Sande, S. E. Tomechko, X. D. Ding, M. Li, S. Maxwell, R. M. Ewing, C. V. Harding, R. E. Rojas, M. R. Chance, and W. H. Boom. 2017. Proteomics and Network Analyses Reveal Inhibition of Akt-mTOR Signaling in CD4^{+} T Cells by *Mycobacterium tuberculosis* Mannose-Capped Lipoarabinomannan. *Proteomics* 17: 1700233.

265. Zhang, X. X., T. Y. Huang, Y. Wu, W. G. Peng, H. B. Xie, M. C. Pan, H. B. Zhou, B. Z. Cai, and Y. E. Wa. 2017. Inhibition of the PI3K-Akt-mTOR signaling pathway in T lymphocytes in patients with active tuberculosis. *International Journal of Infectious Diseases* 59: 110-117.

266. Sha, S. S., Y. Shi, Y. W. Tang, L. Q. Jia, X. Y. Han, Y. X. Liu, X. Li, and Y. F. Ma. 2021. *Mycobacterium tuberculosis* Rv1987 protein induces M2 polarization of

macrophages through activating the PI3K/Akt1/mTOR signaling pathway. *Immunol. Cell Biol.* 99: 570-585.

267. Xu, F., Y. H. Kang, H. Zhang, Z. H. Piao, H. P. Yin, R. Diao, J. Y. Xia, and L. Y. Shi. 2013. Akt1-Mediated Regulation of Macrophage Polarization in a Murine Model of *Staphylococcus aureus* Pulmonary Infection. *Journal of Infectious Diseases* 208: 528-538.

268. Li, H., S. H. Lu, Y. Chen, L. Z. Zheng, L. Y. Chen, H. J. Ding, J. Z. Ding, D. Lou, F. F. Liu, and B. Zheng. 2019. AKT2 phosphorylation of hexokinase 2 at T473 promotes tumorigenesis and metastasis in colon cancer cells via NF-κB, HIF1α, MMP2, and MMP9 upregulation. *Cell. Signal.* 58: 99-110.

269. Ding, L., S. Biswas, R. E. Morton, J. D. Smith, N. Hay, T. V. Byzova, M. Febbraio, and E. A. Podrez. 2012. Akt3 Deficiency in Macrophages Promotes Foam Cell Formation and Atherosclerosis in Mice. *Cell Metabolism* 15: 861-872.

270. Lachmandas, E., M. Beigier-Bompadre, S. C. Cheng, V. Kumar, A. van Laarhoven, X. H. Wang, A. Ammerdorffer, L. Boutens, D. de Jong, T. D. Kanneganti, M. S. Gresnigt, T. H. M. Ottenhoff, L. A. B. Joosten, R. Stienstra, C. Wijmenga, S. H. E. Kaufmann, R. van Crevel, and M. G. Netea. 2016. Rewiring cellular metabolism via the AKT/mTOR pathway contributes to host defence against *Mycobacterium tuberculosis* in human and murine cells. *European Journal of Immunology* 46: 2574-2586.

271. Sheedy, F. J., and M. Divangahi. 2021. Targeting immunometabolism in host defence against *Mycobacterium tuberculosis*. *Immunology* 162: 145-159.

272. Gleeson, L. E., F. J. Sheedy, E. M. Palsson-McDermott, D. Triglia, S. M. O'Leary, M. P. O'Sullivan, L. A. J. O'Neill, and J. Keane. 2016. Cutting Edge: *Mycobacterium tuberculosis* Induces Aerobic Glycolysis in Human Alveolar Macrophages That Is Required for Control of Intracellular Bacillary Replication. *J. Immunol.* 196: 2444-2449.

273. Huang, C., X. J. Liu, QunZhou, J. Xie, T. T. Ma, X. M. Meng, and J. Li. 2016. MiR-146a modulates macrophage polarization by inhibiting Notch1 pathway in RAW264.7 macrophages. *International Immunopharmacology* 32: 46-54.

274. Galvan-Pena, S., and L. A. J. O'Neill. 2014. Metabolic reprograming in macrophage polarization. *Front. Immunol.* 5: 420.

275. Backer, R. A., C. Helbig, R. Gentek, A. Kent, B. J. Laidlaw, C. X. Dominguez, Y. S. de Souza, S. E. van Trierum, R. van Beek, G. F. Rimmelzwaan, A. ten Brinke, A. M. Willemsen, A. H. C. van Kampen, S. M. Kaech, J. M. Blander, K. van Gisbergen, and D. Amsen. 2014. A central role for Notch in effector CD8^{+} T cell differentiation. *Nature Immunology* 15: 1143-1151.

276. De Sousa, D. M., F. Duval, J. F. Daudelin, S. Boulet, and N. Labrecque. 2019. The Notch signaling pathway controls CD8^{+} T cell differentiation independently of the classical effector HES1. *PLOS One* 14: e0215012.

277. Li, Q. F., H. Zhang, L. Yu, C. Wu, X. H. Luo, H. Sun, and J. B. Ding. 2018. Down-regulation of Notch signaling pathway reverses the Th1/Th2 imbalance in tuberculosis patients. *International Immunopharmacology* 54: 24-32.

278. Mathieu, M., F. Duval, J. F. Daudelin, and N. Labrecque. 2015. The Notch Signaling Pathway Controls Short-Lived Effector CD8^{+} T Cell Differentiation but Is Dispensable for Memory Generation. *J. Immunol.* 194: 5654-5662.

279. He, W. G., J. X. Sun, Q. W. Zhang, Y. H. Li, Y. Fu, Y. J. Zheng, and X. Jiang. 2020. Andrographolide exerts anti-inflammatory effects in *Mycobacterium tuberculosis*-infected macrophages by regulating the Notch1/Akt/NF-κB axis. *J. Leukoc. Biol.* 108: 1747-1764.

280. Wen, J. J., C. X. Chen, M. Q. Luo, X. C. Liu, J. D. Guo, T. T. Wei, X. Y. Gu, S. N. Gu, Y. S. Ning, and Y. Li. 2021. Notch Signaling Ligand Jagged1 Enhances Macrophage-Mediated Response to *Helicobacter pylori*. *Front. Microbiol.* 12: 692832.

281. Wongchana, W., P. Kongkavitoon, P. Tangtanatakul, C. Sittplangkoon, P. Butta, S. Chawalitpong, T. Pattarakankul, B. A. Osborne, and T. Palaga. 2018. Notch signaling regulates the responses of lipopolysaccharide-stimulated macrophages in the presence of immune complexes. *PLOS One* 13: e0198609.

282. Zheng, R. J., H. P. Liu, Y. L. Zhou, D. P. Yan, J. X. Chen, D. P. Ma, Y. H. Feng, L. H. Qin, F. Liu, X. C. Huang, J. Wang, and B. X. Ge. 2018. Notch4 Negatively Regulates the Inflammatory Response to *Mycobacterium tuberculosis* Infection by Inhibiting TAK1 Activation. *Journal of Infectious Diseases* 218: 312-323.

283. Narayana, Y., and K. N. Balaji. 2008. NOTCH1 Up-regulation and Signaling Involved in *Mycobacterium bovis* BCG-induced SOCS3 Expression in Macrophages. *J. Biol. Chem.* 283: 12501-12511.

284. Bai, X. Z., J. L. Zhang, M. Y. Cao, S. C. Han, Y. Liu, K. J. Wang, F. Han, X. Q. Li, Y. H. Jia, X. J. Wang, J. H. Shi, and D. H. Hu. 2018. MicroRNA-146a protects against LPS-induced organ damage by inhibiting Notch1 in macrophage. *International Immunopharmacology* 63: 220-226.

285. Foldi, J., A. Y. Chung, H. X. Xu, J. Zhu, H. H. Outtz, J. Kitajewski, Y. M. Li, X. Y. Hu, and L. B. Ivashkiv. 2010. Autoamplification of Notch Signaling in Macrophages by TLR-Induced and RBP-J-Dependent Induction of Jagged1. *J. Immunol.* 185: 5023-5031.

286. Wongchana, W., and T. Palaga. 2012. Direct regulation of interleukin-6 expression by Notch signaling in macrophages. *Cell. Mol. Immunol.* 9: 155-162.

287. Pagie, S., N. Gerard, and B. Charreau. 2018. Notch signaling triggered via the ligand DLL4 impedes M2 macrophage differentiation and promotes their apoptosis. *Cell Communication and Signaling* 16: 4.

288. Apt, A., and I. Kramnik. 2009. Man and mouse TB: Contradictions and solutions. *Tuberculosis* 89: 195-198.

289. Rhoades, E. R., A. A. Frank, and I. M. Orme. 1997. Progression of chronic pulmonary tuberculosis in mice aerogenically infected with virulent *Mycobacterium tuberculosis*. *Tubercle and Lung Disease* 78: 57-66.

290. Yang, H. J., D. C. Wang, X. Wen, D. M. Weiner, and L. E. Via. 2021. One Size Fits All? Not in In Vivo Modeling of Tuberculosis Chemotherapeutics. *Front. Cell. Infect. Microbiol.* 11: 613149.

291. Plumlee, C. R., F. J. Duffy, B. H. Gern, J. L. Delahaye, S. B. Cohen, C. R. Stoltzfus, T. R. Rustad, S. G. Hansen, M. K. Axthelm, L. J. Picker, J. D. Aitchison, D. R. Sherman, V. V. Ganusov, M. Y. Gerner, D. E. Zak, and K. B. Urdahl. 2021. Ultra-low Dose Aerosol Infection of Mice with *Mycobacterium tuberculosis* More Closely Models Human Tuberculosis. *Cell Host & Microbe* 29: 68-82.

292. Chang, J. T., V. R. Palanivel, I. Kinjyo, F. Schambach, A. M. Intlekofer, A. Banerjee, S. A. Longworth, K. E. Vinup, P. Mrass, J. Oliaro, N. Killeen, J. S. Orange, S. M.

Russell, W. Weninger, and S. L. Reiner. 2007. Asymmetric T Lymphocyte Division in the Initiation of Adaptive Immune Responses. *Science* 315: 1687-1691.

293. Ramsbottom, K. M., F. Sacirbegovic, E. D. Hawkins, A. Kallies, G. T. Belz, V. Van Ham, N. M. Haynes, M. J. Durrant, P. O. Humbert, S. M. Russell, and J. Oliaro. 2016. Lethal giant larvae-1 deficiency enhances the CD8+ effector T-cell response to antigen challenge *in vivo*. *Immunol. Cell Biol.* 94: 306-311.

294. Chen, C. Y., D. Huang, R. C. Wang, L. Shen, G. C. Zeng, S. Y. Yao, Y. Shen, L. Halliday, J. Fortman, M. McAllister, J. Estep, R. Hunt, D. Vasconcelos, G. Du, S. A. Porcelli, M. H. Larsen, W. R. Jacobs, B. F. Haynes, N. L. Letvin, and Z. W. Chen. 2009. A Critical Role for CD8 T Cells in a Nonhuman Primate Model of Tuberculosis. *PLoS Pathog.* 5: e1000392.

295. van Pinxteren, L. A. H., J. P. Cassidy, B. H. C. Smedegaard, E. M. Agger, and P. Andersen. 2000. Control of latent *Mycobacterium tuberculosis* infection is dependent on CD8 T cells. *European Journal of Immunology* 30: 3689-3698.

296. Mogues, T., M. E. Goodrich, L. Ryan, R. LaCourse, and R. J. North. 2001. The Relative Importance of T Cell Subsets in Immunity and Immunopathology of Airborne *Mycobacterium tuberculosis* Infection in Mice. *Journal of Experimental Medicine* 193: 271-280.

297. Metz, P. J., J. Arsenio, B. Kakaradov, S. H. Kim, K. A. Remedios, K. Oakley, K. Akimoto, S. Ohno, G. W. Yeo, and J. T. Chang. 2015. Regulation of Asymmetric Division and CD8+ T Lymphocyte Fate Specification by Protein Kinase Cζ and Protein Kinase C λ/ι. *J. Immunol.* 194: 2249-2259.

298. Metz, P. J., J. Lopez, S. H. Kim, K. Akimoto, S. Ohno, and J. T. Chang. 2016. Regulation of Asymmetric Division by Atypical Protein Kinase C Influences Early Specification of CD8+T Lymphocyte Fates. *Sci Rep* 6: 19182.

299. Stenger, S., D. A. Hanson, R. Teitelbaum, P. Dewan, K. R. Niazi, C. J. Froelich, T. Ganz, S. Thoma-Uszynski, A. Melian, C. Bogdan, S. A. Porcelli, B. R. Bloom, A. M. Krensky, and R. L. Modlin. 1998. An Antimicrobial Activity of Cytolytic T Cells Mediated by Granulysin. *Science* 282: 121-125.

300. Rozot, V., S. Vigano, J. Mazza-Stalder, E. Idrizi, C. L. Day, M. Perreau, C. Lazor-Blanchet, E. Petruccioli, W. Hanekom, D. Goletti, P. A. Bart, L. Nicod, G. Pantaleo,

and A. Harari. 2013. *Mycobacterium tuberculosis*-specific CD8$^+$ T cells are functionally and phenotypically different between latent infection and active disease. *European Journal of Immunology* 43: 1568-1577.

301. Hao, L., J. L. Ma, C. W. Shi, X. S. Lin, Y. D. Zhang, B. N. Jo-Lewis, Q. Lei, N. Ullah, Z. J. Yao, and X. L. Fan. 2020. Enhanced tuberculosis clearance through the combination treatment with recombinant adenovirus-mediated granulysin delivery. *Theranostics* 10: 10046-10056.

302. Bai, F. F., R. M. McCormack, S. Hower, G. V. Plano, M. G. Lichtenheld, and G. P. Munson. 2018. Perforin-2 Breaches the Envelope of Phagocytosed Bacteria Allowing Antimicrobial Effectors Access to Intracellular Targets. *J. Immunol.* 201: 2710-2720.

303. Kägi, D., B. Ledermann, K. Bürki, H. Hengartner, and R. M. Zinkernagel. 1994. CD8$^+$ T cell-mediated protection against an intracellular bacterium by perforin-dependent cytotoxicity. *European Journal of Immunology* 24: 3068-3072.

304. Lecuit, M. 2020. *Listeria monocytogenes*, a model in infection biology. *Cell Microbiol.* 22: e13186.

305. Orndorff, P. E., T. S. Hamrick, I. W. Smoak, and E. A. Havell. 2006. Host and bacterial factors in listeriosis pathogenesis. *Veterinary Microbiology* 114: 1-15.

306. Bonazzi, M., M. Lecuit, and P. Cossart. 2009. *Listeria monocytogenes* internalin and E-cadherin: from structure to pathogenesis. *Cell Microbiol.* 11: 693-702.

307. Shen, Y., K. Naujokas, M. Park, and K. Ireton. 2000. InlB-Dependent Internalization of *Listeria* Is Mediated by the Met Receptor Tyrosine Kinase. *Cell* 103: 501-510.

308. De Chastellier, C., and P. Berche. 1994. Fate of *Listeria monocytogenes* in Murine Macrophages: Evidence for Simultaneous Killing and Survival of Intracellular Bacteria. *Infection and Immunity* 62: 543-553.

309. Camejo, A., F. Carvalho, O. Reis, E. Leitao, S. Sousa, and D. Cabanes. 2011. The arsenal of virulence factors deployed by *Listeria monocytogenes* to promote its cell infection cycle. *Virulence* 2: 379-394.

310. Camilli, A., L. G. Tilney, and D. A. Portnoy. 1993. Dual roles of plcA in *Listeria monocytogenes* pathogenesis. *Molecular Microbiology* 8: 143-157.

311. Petrišič, N., M. Kozorog, S. Aden, M. Podobnik, and G. Anderluh. 2021. The molecular mechanisms of listeriolysin O-induced lipid membrane damage. *Biochimica Et Biophysica Acta-Biomembranes* 1863: 183604.

312. Jasnin, M., S. Asano, E. Gouin, R. Hegerl, J. M. Plitzko, E. Villa, P. Cossart, and W. Baumeister. 2013. Three-dimensional architecture of actin filaments in *Listeria monocytogenes* comet tails. *Proceedings of the National Academy of Sciences of the United States of America* 110: 20521-20526.

313. Lambrechts, A., K. Gevaert, P. Cossart, J. Vandekerckhove, and M. Van Troys. 2008. *Listeria* comet tails: the actin-based motility machinery at work. *Trends in Cell Biology* 18: 220-227.

314. Mitchell, G., L. Ge, Q. Y. Huang, C. Chen, S. Kianian, M. F. Roberts, R. Schekman, and D. A. Portnoy. 2015. Avoidance of Autophagy Mediated by PlcA or ActA Is Required for *Listeria monocytogenes* Growth in Macrophages. *Infection and Immunity* 83: 2175-2184.

315. Yoshikawa, Y., M. Ogawa, T. Hain, M. Yoshida, M. Fukumatsu, M. Kim, H. Mimuro, I. Nakagawa, T. Yanagawa, T. Ishii, A. Kakizuka, E. Sztul, T. Chakraborty, and C. Sasakawa. 2009. *Listeria monocytogenes* ActA-mediated escape from autophagic recognition. *Nature Cell Biology* 11: 1233-U1175.

316. Rosenberg, G., S. Riquelme, A. Prince, and R. Avraham. 2022. Immunometabolic crosstalk during bacterial infection. *Nature Microbiology* 7: 497-507.

317. Qiu, Z. J., C. Khairallah, and B. S. Sheridan. 2018. *Listeria monocytogenes*: A Model Pathogen Continues to Refine Our Knowledge of the CD8 T Cell Response. *Pathogens* 7: 55.

318. Jones, G. S., K. M. Bussell, T. Myers-Morales, A. M. Fieldhouse, E. N. B. Ghanem, and S. E. F. D'Orazio. 2015. Intracellular *Listeria monocytogenes* Comprises a Minimal but Vital Fraction of the Intestinal Burden following Foodborne Infection. *Infection and Immunity* 83: 3146-3156.

319. Pron, B., C. Boumaila, F. Jaubert, P. Berche, G. Milon, F. Geissmann, and J. L. Gaillard. 2001. Dendritic cells are early cellular targets of *Listeria monocytogenes* after intestinal delivery and are involved in bacterial spread in the host. *Cell Microbiol.* 3: 331-340.

320. Sierro, F., M. Evrard, S. Rizzetto, M. Melino, A. J. Mitchell, M. Florido, L. Beattie, S. B. Walters, S. S. Tay, B. Lu, L. E. Holz, B. Roediger, Y. C. Wong, A. Warren, W. Ritchie, C. McGuffog, W. Weninger, D. G. Le Couteur, F. Ginhoux, W. J. Britton, W. R. Heath, B. M. Saunders, G. W. McCaughan, F. Luciani, K. P. A. MacDonald, L. G. Ng, D. G. Bowen, and P. Bertolino. 2017. A Liver Capsular Network of Monocyte-Derived Macrophages Restricts Hepatic Dissemination of Intraperitoneal Bacteria by Neutrophil Recruitment. *Immunity* 47: 374-388.

321. Lecuit, M., S. Dramsi, C. Gottardi, M. Fedor-Chaiken, B. Gumbiner, and P. Cossart. 1999. A single amino acid in E-cadherin responsible for host specificity towards the human pathogen *Listeria monocytogenes*. *EMBO Journal* 18: 3956-3963.

322. Beattie, L., A. Sawtell, J. Mann, T. C. M. Frame, B. Teal, F. D. Rivera, N. Brown, K. Walwyn-Brown, J. W. J. Moore, S. MacDonald, E. K. Lim, J. E. Dalton, C. R. Engwerda, K. P. MacDonald, and P. M. Kaye. 2016. Bone marrow-derived and resident liver macrophages display unique transcriptomic signatures but similar biological functions. *Journal of Hepatology* 65: 758-768.

323. Drevets, D. A., M. J. Dillon, J. S. Schawang, N. van Rooijen, J. Ehrchen, C. Sunderkotter, and P. J. M. Leenen. 2004. The Ly-6C^{high} Monocyte Subpopulation Transports *Listeria monocytogenes* into the Brain during Systemic Infection of Mice. *J. Immunol.* 172: 4418-4424.

324. Ebe, Y., G. Hasegawa, H. Takatsuka, H. Umezu, M. Mitsuyama, M. Arakawa, N. Mukaida, and M. Naito. 1999. The role of Kupffer cells and regulation of neutrophil migration into the liver by macrophage inflammatory protein-2 in primary listeriosis in mice. *Pathology International* 49: 519-532.

325. Stavru, F., C. Archambaud, and P. Cossart. 2011. Cell biology and immunology of *Listeria monocytogenes* infections: novel insights. *Immunological Reviews* 240: 160-184.

326. Shi, C., T. M. Hohl, I. Leiner, M. J. Equinda, X. Z. Fan, and E. G. Pamer. 2011. Ly6G^{+} Neutrophils Are Dispensable for Defense against Systemic *Listeria monocytogenes* Infection. *J. Immunol.* 187: 5293-5298.

327. Wang, G., H. J. Zhao, B. Q. Zheng, D. X. Li, Y. Yuan, Q. J. Han, Z. G. Tian, and J. Zhang. 2019. TLR2 Promotes Monocyte/Macrophage Recruitment Into the Liver

and Microabscess Formation to Limit the Spread of *Listeria monocytogenes*. *Front. Immunol.* 10: 1388.

328. Witter, A. R., B. M. Okunnu, and R. E. Berg. 2016. The Essential Role of Neutrophils during Infection with the Intracellular Bacterial Pathogen *Listeria monocytogenes*. *J. Immunol.* 197: 1557-1565.

329. Drevets, D. A., and M. S. Bronze. 2008. *Listeria monocytogenes*: epidemiology, human disease, and mechanisms of brain invasion. *FEMS Immunology and Medical Microbiology* 53: 151-165.

330. Hasegawa, T., T. Tanaka, and Y. Yoshikai. 1992. The appearance and role of γδ T cells in the peritoneal cavity and liver during primary infection with *Listeria monocytogenes* in rats. *International Immunology* 4: 1129-1136.

331. Hiromatsu, K., Y. Yoshikai, G. Matsuzaki, S. Ohga, K. Muramori, K. Matsumoto, J. A. Bluestone, and K. Nomoto. 1992. A Protective Role of δ/γ T Cells in Primary Infection with *Listeria monocytogenes* in Mice. *Journal of Experimental Medicine* 175: 49-56.

332. Levine, L. S., K. J. Hiam-Galvez, D. M. Marquez, I. Tenvooren, M. Z. Madden, D. C. Contreras, D. O. Dahunsi, J. M. Irish, O. O. Oluwole, J. C. Rathmell, and M. H. Spitzer. 2021. Single-cell analysis by mass cytometry reveals metabolic states of early-activated CD8^{+} T cells during the primary immune response. *Immunity* 54: 829-844.

333. Porter, B. B., and J. T. Harty. 2006. The Onset of CD8^{+}-T-Cell Contraction Is Influenced by the Peak of *Listeria monocytogenes* Infection and Antigen Display. *Infection and Immunity* 74: 1528-1536.

334. Obar, J. J., E. R. Jellison, B. S. Sheridan, D. A. Blair, Q. M. Pham, J. M. Zickovich, and L. Lefrançois. 2011. Pathogen-Induced Inflammatory Environment Controls Effector and Memory CD8^{+} T Cell Differentiation. *J. Immunol.* 187: 4967-4978.

335. Mandel, T. E., and C. Cheers. 1980. Resistance and Susceptibility of Mice to Bacterial Infection: Histopathology of Listeriosis in Resistant and Susceptible Strains. *Infection and Immunity* 30: 851-861.

336. Sheridan, B. S., Q. M. Pham, Y. T. Lee, L. S. Cauley, L. Puddington, and L. Lefrançois. 2014. Oral Infection Drives a Distinct Population of Intestinal Resident Memory CD8^{+} T Cells with Enhanced Protective Function. *Immunity* 40: 747-757.

337. Hughes, C. S., S. Moggridge, T. Muller, P. H. Sorensen, G. B. Morin, and J. Krijgsveld. 2019. Single-pot, solid-phase-enhanced sample preparation for proteomics experiments. *Nature Protocols* 14: 68-85.

338. Szklarczyk, D., A. L. Gable, K. C. Nastou, D. Lyon, R. Kirsch, S. Pyysalo, N. T. Doncheva, M. Legeay, T. Fang, P. Bork, L. J. Jensen, and C. von Mering. 2021. The STRING database in 2021: customizable protein-protein networks, and functional characterization of user-uploaded gene/measurement sets. *Nucleic Acids Research* 49: D605-D612.

339. Kanehisa, M., Y. Sato, and M. Kawashima. 2022. KEGG mapping tools for uncovering hidden features in biological data. *Protein Science* 31: 47-53.

340. Longo, P. A., J. M. Kavran, M. S. Kim, and D. J. Leahy. 2013. Transient mammalian cell transfection with polyethylenimine (PEI). *Methods Enzymol* 529: 227-240.

341. Ramesh, G., and W. B. Reeves. 2002. TNF-α mediates chemokine and cytokine expression and renal injury in cisplatin nephrotoxicity. *Journal of Clinical Investigation* 110: 835-842.

342. Fu, Q. H., J. B. Yuan, L. T. Wang, H. Y. Ran, F. Li, F. Liu, J. Y. Zhang, W. H. Liu, W. Huang, Y. Huang, and X. F. Xia. 2020. Proteomic analysis of murine macrophages mitochondria and lysosomes reveal Cathepsin D as a potential broad-spectrum antimicrobial protein. *Journal of Proteomics* 223: 103821.

343. Chen, Y., and X. Wang. 2020. miRDB: an online database for prediction of functional microRNA targets. *Nucleic Acids Research* 48: D127-D131.

344. Osborne, S. E., B. Sit, A. Shaker, E. Currie, J. M. J. Tan, J. van Rijn, D. E. Higgins, and J. H. Brumell. 2017. Type I interferon promotes cell-to-cell spread of *Listeria monocytogenes*. *Cell Microbiol.* 19: e12660.

345. Carlier, M. F., J. Pernier, P. Montaville, S. Shekhar, S. Kuhn, and G. Cytoskeleton Dynamics Motility. 2015. Control of polarized assembly of actin filaments in cell motility. *Cellular and Molecular Life Sciences* 72: 3051-3067.

346. Mukaihara, K., Y. Suehara, S. Kohsaka, D. Kubota, M. Toda-Ishii, K. Akaike, T. Fujimura, E. Kobayashi, T. Yao, M. Ladanyi, K. Kaneko, and T. Saito. 2016. Expression of F-actin-capping protein subunit beta, CAPZB, is associated with cell growth and motility in epithelioid sarcoma. *BMC Cancer* 16: 206.

347. Dussurget, O., H. Bierne, and P. Cossart. 2014. The bacterial pathogen *Listeria monocytogenes* and the interferon family: type I, type II and type III interferons. *Front. Cell. Infect. Microbiol.* 4: 50.

348. McNab, F., K. Mayer-Barber, A. Sher, A. Wack, and A. O'Garra. 2015. Type I interferons in infectious disease. *Nature Reviews Immunology* 15: 87-103.

349. O'Connell, R. M., S. K. Saha, S. A. Vaidya, K. W. Bruhn, G. A. Miranda, B. Zarnegar, A. K. Perry, B. O. Nguyen, T. E. Lane, T. Taniguchi, J. F. Miller, and G. H. Cheng. 2004. Type I Interferon Production Enhances Susceptibility to *Listeria monocytogenes* Infection. *Journal of Experimental Medicine* 200: 437-445.

350. Carrero, J. A., B. Calderon, and E. R. Unanue. 2004. Type I Interferon Sensitizes Lymphocytes to Apoptosis and Reduces Resistance to *Listeria* Infection. *Journal of Experimental Medicine* 200: 535-540.

351. Kernbauer, E., V. Maier, I. Rauch, M. Muller, and T. Decker. 2013. Route of Infection Determines the Impact of Type I Interferons on Innate Immunity to *Listeria monocytogenes*. *PLOS One* 8: e65007.

352. Thale, C., and A. F. Kiderlen. 2005. Sources of interferon-gamma (IFN-γ) in early immune response to *Listeria monocytogenes*. *Immunobiology* 210: 673-683.

353. Harty, J. T., and M. J. Bevan. 1995. Specific Immunity to *Listeria monocytogenes* in the Absence of IFNγ. *Immunity* 3: 109-117.

354. Huang, S., W. Hendriks, A. Althage, S. Hemmi, H. Bluethmann, R. Kamijo, J. Vilcek, R. M. Zinkernagel, and M. Aguet. 1993. Immune Response in Mice that Lack the Interferon-γ Receptor. *Science* 259: 1742-1745.

355. Dalrymple, S. A., L. A. Lucian, R. Slattery, T. McNeil, D. M. Aud, S. Fuchino, F. Lee, and R. Murray. 1995. Interleukin-6-Deficient Mice Are Highly Susceptible to *Listeria monocytogenes* Infection: Correlation with Inefficient Neutrophilia. *Infection and Immunity* 63: 2262-2268.

356. Hoge, J., I. Yan, N. Janner, V. Schumacher, A. Chalaris, O. M. Steinmetz, D. R. Engel, J. Scheller, S. Rose-John, and H. W. Mittrucker. 2013. IL-6 Controls the Innate Immune Response against *Listeria monocytogenes* via Classical IL-6 Signaling. *J. Immunol.* 190: 703-711.

357. Lucke, K., I. Yan, S. Krohn, A. Volmari, S. Klinge, J. Schmid, V. Schumacher, O. M. Steinmetz, S. Rose-John, and H. W. Mittrucker. 2018. Control of *Listeria monocytogenes* infection requires classical IL-6 signaling in myeloid cells. *PLOS One* 13: e0203395.

358. Unanue, E. R. 1996. Macrophages, NK cells and neutrophils in the cytokine loop of *Listeria* resistance. *Research in Immunology* 147: 499-505.

359. Pfeffer, K., T. Matsuyama, T. M. Kundig, A. Wakeham, K. Kishihara, A. Shahinian, K. Wiegmann, P. S. Ohashi, M. Kronke, and T. W. Mak. 1993. Mice Deficient for the 55 kd Tumor Necrosis Factor Receptor Are Resistant to Endotoxic Shock, yet Succumb to *L. monocytogenes* Infection. *Cell* 73: 457-467.

360. Rothe, J., W. Lesslauer, H. Lotscher, Y. Lang, P. Koebel, F. Kontgen, A. Althage, R. Zinkernagel, M. Steinmetz, and H. Bluethmann. 1993. Mice lacking the tumour necrosis factor receptor 1 are resistant to IMF-mediated toxicity but highly susceptible to infection by *Listeria monocytogenes*. *Nature* 364: 798-802.

361. Liu, M. Y., K. Q. Chen, T. Yoshimura, Y. Liu, W. H. Gong, A. M. Wang, J. L. Gao, P. M. Murphy, and J. M. Wang. 2012. Formylpeptide receptors are critical for rapid neutrophil mobilization in host defense against *Listeria monocytogenes*. *Sci Rep* 2: 786.

362. Conlan, J. W., and R. J. North. 1994. Neutrophils Are Essential for Early Anti-*Listeria* Defense in the Liver, but Not in the Spleen or Peritoneal Cavity, as Revealed by a Granulocyte-depleting Monoclonal Antibody. *Journal of Experimental Medicine* 179: 259-268.

363. Conlan, J. W. 1997. Neutrophils and tumour necrosis factor-α are important for controlling early gastrointestinal stages of experimental murine listeriosis. *Journal of Medical Microbiology* 46: 239-250.

364. Rogers, H. W., and E. R. Unanue. 1993. Neutrophils Are Involved in Acute, Nonspecific Resistance to *Listeria monocytogenes* in Mice. *Infection and Immunity* 61: 5090-5096.

365. Carr, K. D., A. N. Sieve, M. Indramohan, T. J. Break, S. Lee, and R. E. Berg. 2011. Specific depletion reveals a novel role for neutrophil-mediated protection in the liver during *Listeria monocytogenes* infection. *European Journal of Immunology* 41: 2666-2676.

366. Marco, A. J., M. Domingo, J. Ruberte, A. Carretero, V. Briones, and L. Dominguez. 1992. Lymphatic drainage of *Listeria monocytogenes* and Indian ink inoculated in the peritoneal cavity of the mouse. *Laboratory Animals* 26: 200-205.

367. Perez, O. A., S. T. Yeung, P. Vera-Licona, P. A. Romagnoli, T. Samji, B. B. Ural, L. Maher, M. Tanaka, and K. M. Khanna. 2017. CD169+ macrophages orchestrate innate immune responses by regulating bacterial localization in the spleen. *Science Immunology* 2.

368. Lieschke, G. J., D. Grail, G. Hodgson, D. Metcalf, E. Stanley, C. Cheers, K. J. Fowler, S. Basu, Y. F. Zhan, and A. R. Dunn. 1994. Mice Lacking Granulocyte Colony-Stimulating Factor Have Chronic Neutropenia, Granulocyte and Macrophage Progenitor Cell Deficiency, and Impaired Neutrophil Mobilization. *Blood* 84: 1737-1746.

369. Loisel, T. P., R. Boujemaa, D. Pantaloni, and M. F. Carlier. 1999. Reconstitution of actin-based motility of *Listeria* and *Shigella* using pure proteins. *Nature* 401: 613-616.

370. Tang, C. Y., and C. Mauro. 2017. Similarities in the Metabolic Reprogramming of Immune System and Endothelium. *Front. Immunol.* 8: 837.

371. Tang, C. Y., and C. Mauro. 2017. Similarities in the Metabolic Reprogramming of Immune System and Endothelium. *Front. Immunol.* 8.

372. Gillmaier, N., A. Gotz, A. Schulz, W. Eisenreich, and W. Goebel. 2012. Metabolic Responses of Primary and Transformed Cells to Intracellular *Listeria monocytogenes*. *PLOS One* 7: e52378.

373. Yu, Q., Y. F. Wang, L. Dong, Y. He, R. C. Liu, Q. L. Yang, Y. J. Cao, Y. X. Wang, A. N. Jia, Y. J. Bi, and G. W. Liu. 2020. Regulations of Glycolytic Activities on

Macrophages Functions in Tumor and Infectious Inflammation. *Front. Cell. Infect. Microbiol.* 10: 287.

374. Ó Maoldomhnaigh, C., D. J. Cox, J. J. Phelan, M. Mitermite, D. M. Murphy, G. Leisching, L. Thong, S. M. O'Leary, K. M. Gogan, K. McQuaid, A. M. Coleman, S. V. Gordon, S. A. Basdeo, and J. Keane. 2021. Lactate Alters Metabolism in Human Macrophages and Improves Their Ability to Kill *Mycobacterium tuberculosis*. *Front. Immunol.* 12: 663695.

375. Carrasco-Marin, E., F. Madrazo-Toca, J. R. de los Toyos, E. Cacho-Alonso, R. Tobes, E. Pareja, A. Paradela, J. P. Albar, W. Chen, M. T. Gomez-Lopez, and C. Alvarez-Dominguez. 2009. The innate immunity role of cathepsin-D is linked to Trp-491 and Trp-492 residues of listeriolysin O. *Molecular Microbiology* 72: 668-682.

376. del Cerro-Vadillo, E., F. Madrazo-Toca, E. Carrasco-Marin, L. Fernandez-Prieto, C. Beck, F. Leyva-Cobian, P. Saftig, and C. Alvarez-Dominguez. 2006. Cutting Edge: A Novel Nonoxidative Phagosomal Mechanism Exerted by Cathepsin-D Controls *Listeria monocytogenes* Intracellular Growth. *J. Immunol.* 176: 1321-1325.

377. Radoshevich, L., and P. Cossart. 2018. *Listeria monocytogenes*: towards a complete picture of its physiology and pathogenesis. *Nature Reviews Microbiology* 16: 32-46.

378. Zhang, T., Y. Maekawa, J. Hanba, T. Dainichi, B. F. Nashed, H. Hisaeda, T. Sakai, T. Asao, K. Himeno, R. A. Good, and N. Katunuma. 2000. Lysosomal cathepsin B plays an important role in antigen processing, while cathepsin D is involved in degradation of the invariant chain in ovalbumin-immunized mice. *Immunology* 100: 13-20.

379. Mizuochi, T., S. T. Yee, M. Kasai, T. Kakiuchi, D. Muno, and E. Kominami. 1994. Both cathepsin B and cathepsin D are necessary for processing of ovaibumin as well as for degradation of class II MHC invariant chain. *Immunology Letters* 43: 189-193.

380. Szulc-Dabrowska, L., M. Bossowska-Nowicka, J. Struzik, and F. N. Toka. 2020. Cathepsins in Bacteria-Macrophage Interaction: Defenders or Victims of Circumstance? *Front. Cell. Infect. Microbiol.* 10: 601072.

381. Shedlock, D. J., J. K. Whitmire, J. Tan, A. S. MacDonald, R. Ahmed, and H. Shen. 2003. Role of CD4 T cell help and costimulation in CD8 T cell responses during *Listeria monocytogenes* infection. *J. Immunol.* 170: 2053-2063.

382. Garcia-Cattaneo, A., F. X. Gobert, M. Muller, F. Toscano, M. Flores, A. Lescure, E. Del Nery, and P. Benaroch. 2012. Cleavage of Toll-like receptor 3 by cathepsins B and H is essential for signaling. *Proceedings of the National Academy of Sciences of the United States of America* 109: 9053-9058.

383. Matsumoto, F., S. I. Saitoh, R. Fukui, T. Kobayashi, N. Tammura, K. Konnio, Y. Kusumoto, S. Akashi-Takamura, and K. Miyake. 2008. Cathepsins are required for toll-like receptor 9 responses. *Biochem. Biophys. Res. Commun.* 367: 693-699.

384. Petes, C., N. Odoardi, and K. Gee. 2017. The Toll for Trafficking: Toll-Like Receptor 7 Delivery to the Endosome. *Front. Immunol.* 8: 1075.

385. Bakhru, P., N. Sirisaengtaksin, E. Soudani, S. Mukherjee, A. Khan, and C. Jagannath. 2014. BCG vaccine mediated reduction in the MHC-II expression of macrophages and dendritic cells is reversed by activation of Toll-like receptors 7 and 9. *Cellular Immunology* 287: 53-61.

386. Bafica, A., C. A. Scanga, C. G. Feng, C. Leifer, A. Cheever, and A. Sher. 2005. TLR9 regulates Th1 responses and cooperates with TLR2 in mediating optimal resistance to *Mycobacterium tuberculosis*. *Journal of Experimental Medicine* 202: 1715-1724.

387. Mirzalieva, O., M. Juncker, J. Schwartzenburg, and S. Desai. 2022. ISG15 and ISGylation in Human Diseases. *Cells* 11: 538.

388. Bogunovic, D., M. Byun, L. A. Durfee, A. Abhyankar, O. Sanal, D. Mansouri, S. Salem, I. Radovanovic, A. V. Grant, P. Adimi, N. Mansouri, S. Okada, V. L. Bryant, X. F. Kong, A. Kreins, M. M. Velez, B. Boisson, S. Khalilzadeh, U. Ozcelik, I. A. Darazam, J. W. Schoggins, C. M. Rice, S. Al-Muhsen, M. Behr, G. Vogt, A. Puel, J. Bustamante, P. Gros, J. M. Huibregtse, L. Abel, S. Boisson-Dupuis, and J. L. Casanova. 2012. Mycobacterial Disease and Impaired IFN-γ Immunity in Humans with Inherited ISG15 Deficiency. *Science* 337: 1684-1688.

389. Hare, N. J., B. Chan, E. Chan, K. L. Kaufman, W. J. Britton, and B. M. Saunders. 2015. Microparticles released from *Mycobacterium tuberculosis*-infected human

macrophages contain increased levels of the type I interferon inducible proteins including ISG15. *Proteomics* 15: 3020-3029.

390. Kimmey, J. M., J. A. Campbell, L. A. Weiss, K. J. Monte, D. J. Lenschow, and C. L. Stallings. 2017. The impact of ISGylation during *Mycobacterium tuberculosis* infection in mice. *Microbes and Infection* 19: 249-258.

391. Conradie, F., A. H. Diacon, N. Ngubane, P. Howell, D. Everitt, A. M. Crook, C. M. Mendel, E. Egizi, J. Moreira, J. Timm, T. D. McHugh, G. H. Wills, A. Bateson, R. Hunt, C. Van Niekerk, M. C. Li, M. Olugbosi, M. Spigelman, and T. B. T. T. Nix. 2020. Treatment of Highly Drug-Resistant Pulmonary Tuberculosis. *New England Journal of Medicine* 382: 893-902.

392. Lee, Y. J., C. W. Kang, J. H. Oh, J. Kim, J. P. Park, J. H. Moon, E. H. Kim, S. Lee, S. H. Kim, C. R. Ku, and E. J. Lee. 2022. Downregulation of miR-216a-5p and miR-652-3p is associated with growth and invasion by targeting JAK2 and PRRX1 in GH-producing pituitary tumours. *Journal of Molecular Endocrinology* 68: 51-62.

393. Dey, R. J., B. Dey, Y. Zheng, L. S. Cheung, J. Zhou, D. Sayre, P. Kumar, H. D. Guo, G. Lamichhane, H. Sintim, and W. R. Bishai. 2017. Inhibition of innate immune cytosolic surveillance by an *M. tuberculosis* phosphodiesterase. *Nature Chemical Biology* 13: 210-217.

394. Lienard, J., E. Nobs, V. Lovins, E. Movert, C. Valfridsson, and F. Carlsson. 2020. The *Mycobacterium marinum* ESX-1 system mediates phagosomal permeabilization and type I interferon production via separable mechanisms. *Proceedings of the National Academy of Sciences of the United States of America* 117: 1160-1166.

395. Upadhyay, S., E. Mittal, and J. A. Philips. 2018. Tuberculosis and the art of macrophage manipulation. *Pathogens and Disease* 76: fty037.

396. Freedman, N. J., and S. K. Shenoy. 2018. Regulation of inflammation by β-arrestins: Not just receptor tales. *Cell. Signal.* 41: 41-45.

397. Fang, Y. Q., Q. L. Jiang, S. S. Li, H. Zhu, R. Xu, N. S. Song, X. Ding, J. Q. Liu, M. M. Chen, M. M. Song, J. H. Ding, M. Lu, G. Y. Wu, and G. Hu. 2021. Opposing functions of β-arrestin 1 and 2 in Parkinson's disease via microglia inflammation and Nprl3. *Cell Death Differ.* 28: 1822-1836.

398. Lei, Y. M., S. Z. Wan, H. L. Liu, H. X. Zhou, L. J. Chen, Y. D. Yang, and B. Wu. 2021. ARRB1 suppresses the activation of hepatic macrophages via modulating endoplasmic reticulum stress in lipopolysaccharide-induced acute liver injury. *Cell Death Discovery* 7: 223.

399. Zhuang, L. N., W. X. Hu, S. M. Xin, J. Zhao, and G. Pei. 2011. β-Arrestin-1 Protein Represses Adipogenesis and Inflammatory Responses through Its Interaction with Peroxisome Proliferator-activated Receptor-γ (PPARγ). *J. Biol. Chem.* 286: 28403-28413.

400. Ai, F. L., G. H. Zhao, W. Lv, B. Liu, and J. Lin. 2020. Dexamethasone induces aberrant macrophage immune function and apoptosis. *Oncol. Rep.* 43: 427-436.

401. Chen, M., M. H. Li, N. Zhang, W. W. Sun, H. Wang, and W. Wei. 2021. Mechanism of miR-218-5p in autophagy, apoptosis and oxidative stress in rheumatoid arthritis synovial fibroblasts is mediated by KLF9 and JAK/STAT3 pathways. *Journal of Investigative Medicine* 69: 824-832.

402. Martin, C. J., M. G. Booty, T. R. Rosebrock, C. Nunes-Alves, D. M. Desjardins, I. Keren, S. M. Fortune, H. G. Remold, and S. M. Behar. 2012. Efferocytosis Is an Innate Antibacterial Mechanism. *Cell Host Microbe* 12: 289-300.

403. Moraco, A. H., and H. Kornfeld. 2014. Cell death and autophagy in tuberculosis. *Semin. Immunol.* 26: 497-511.

404. Brown, A. R., R. C. M. Simmen, V. R. Raj, T. T. Van, S. L. MacLeod, and F. A. Simmen. 2015. Krüppel-like factor 9 (KLF9) prevents colorectal cancer through inhibition of interferon-related signaling. *Carcinogenesis* 36: 946-955.

405. Delerive, P., D. Monte, G. Dubois, F. Trottein, J. Fruchart-Najib, J. Mariani, J. C. Fruchart, and B. Staels. 2001. The orphan nuclear receptor RORα is a negative regulator of the inflammatory response. *EMBO Reports* 2: 42-48.

406. Nienaber, A., F. E. A. Hayford, E. Variava, N. Martinson, and L. Malan. 2021. The Manipulation of the Lipid Mediator Metabolism as Adjunct Host-Directed Therapy in Tuberculosis. *Front. Immunol.* 12: 623941.

407. Dzhagalov, I., V. Giguere, and Y. W. He. 2004. Lymphocyte Development and Function in the Absence of Retinoic Acid-Related Orphan Receptor α. *J. Immunol.* 173: 2952-2959.

408. Moharrami, N. N., E. B. Tande, L. Ryan, T. Espevik, and V. Boyartchuk. 2018. RORα controls inflammatory state of human macrophages. *PLOS One* 13: e0207374.

409. Han, Y. H., H. J. Kim, H. Na, M. W. Nam, J. Y. Kim, J. S. Kim, S. H. Koo, and M. O. Lee. 2017. RORα Induces KLF4-Mediated M2 Polarization in the Liver Macrophages that Protect against Nonalcoholic Steatohepatitis. *Cell Reports* 20: 124-135.

410. Russell, D. G., L. Huang, and B. C. VanderVen. 2019. Immunometabolism at the interface between macrophages and pathogens. *Nature Reviews Immunology* 19: 291-304.

411. Spaderna, S., O. Schmalhofer, M. Wahlbuhl, A. Dimmler, K. Bauer, A. Sultan, F. Hlubek, A. Jung, D. Strand, A. Eger, T. Kirchner, J. Behrens, and T. Brabletz. 2008. The Transcriptional Repressor ZEB1 Promotes Metastasis and Loss of Cell Polarity in Cancer. *Cancer Research* 68: 537-544.

412. Cortes, M., L. Sanchez-Moral, O. de Barrios, M. J. Fernandez-Acenero, M. C. Martinez-Campanario, A. Esteve-Codina, D. S. Darling, B. Gyorffy, T. Lawrence, D. C. Dean, and A. Postigo. 2017. Tumor-associated macrophages (TAMs) depend on ZEB1 for their cancer-promoting roles. *EMBO Journal* 36: 3336-3355.

413. Siles, L., C. Ninfali, M. Cortes, D. S. Darling, and A. Postigo. 2019. ZEB1 protects skeletal muscle from damage and is required for its regeneration. *Nature Communications* 10: 1364.

414. Jiang, H. M., H. M. Wei, H. Wang, Z. Y. Wang, J. J. Li, Y. Ou, X. C. Xiao, W. H. Wang, A. T. Chang, W. Sun, L. Zhao, and S. Yang. 2022. Zeb1-induced metabolic reprogramming of glycolysis is essential for macrophage polarization in breast cancer. *Cell Death & Disease* 13: 206.

415. Li, H., J. Zou, X. H. Yu, X. Ou, and C. K. Tang. 2021. Zinc finger E-box binding homeobox 1 and atherosclerosis: New insights and therapeutic potential. *Journal of Cellular Physiology* 236: 4216-4230.

416. Stevens, M. T., and B. M. Saunders. 2021. Targets and regulation of microRNA-652-3p in homoeostasis and disease. *Journal of Molecular Medicine* 99: 755-769.

417. Yang, C., Y. Chen, W. H. Xiong, and K. Xu. 2022. miR-652 Inhibits the Proliferation, Migration, and Invasion of Osteosarcoma Cells by Targeting HOXA9 and Regulating the PI3K/Akt Signaling Pathway. *Journal of Oncology* 2022: 4809312.

418. Zhou, L., Y. H. Wang, M. J. Zhou, Y. Zhang, P. F. Wang, X. X. Li, J. Yang, H. M. Wang, and Z. H. Ding. 2018. HOXA9 inhibits HIF-1α-mediated glycolysis through interacting with CRIP2 to repress cutaneous squamous cell carcinoma development. *Nature Communications* 9: 1480.

419. Kocabas, F., L. Xie, J. J. Xie, Z. Yu, R. J. DeBerardinis, W. Kimura, S. Thet, A. F. Elshamy, H. Abouellail, S. Muralidhar, X. Y. Liu, C. Q. Chen, H. A. Sadek, C. C. Zhang, and J. K. Zheng. 2015. Hypoxic metabolism in human hematopoietic stem cells. *Cell and Bioscience* 5: 39.

420. Semenza, G. L., P. H. Roth, H. M. Fang, and G. L. Wang. 1994. Transcriptional Regulation of Genes Encoding Glycolytic Enzymes by Hypoxia-inducible Factor 1. *J. Biol. Chem.* 269: 23757-23763.

421. Greijer, A. E., P. van der Groep, D. Kemming, A. Shvarts, G. L. Semenza, G. A. Meijer, M. A. van de Wiel, J. A. M. Belien, P. J. van Diest, and E. van der Wall. 2005. Up-regulation of gene expression by hypoxia is mediated predominantly by hypoxia-inducible factor 1 (HIF-1). *Journal of Pathology* 206: 291-304.

422. Lu, Y., S. S. Yu, M. Zong, S. S. Fan, T. B. Lu, R. H. Gong, L. S. Sun, and L. Y. Fan. 2017. Glucose-6-Phosphate Isomerase (G6PI) Mediates Hypoxia-Induced Angiogenesis in Rheumatoid Arthritis. *Sci Rep* 7: 40274.

423. Wang, T., H. Y. Liu, G. Lian, S. Y. Zhang, X. Wang, and C. T. Jiang. 2017. HIF1α-Induced Glycolysis Metabolism Is Essential to the Activation of Inflammatory Macrophages. *Mediators of Inflammation* 2017: 9029327.

424. Uhlen, M., L. Fagerberg, B. M. Hallstrom, C. Lindskog, P. Oksvold, A. Mardinoglu, A. Sivertsson, C. Kampf, E. Sjostedt, A. Asplund, I. Olsson, K. Edlund, E. Lundberg, S. Navani, C. A. Szigyarto, J. Odeberg, D. Djureinovic, J. O. Takanen, S. Hober, T. Alm, P. H. Edqvist, H. Berling, H. Tegel, J. Mulder, J. Rockberg, P. Nilsson, J. M. Schwenk, M. Hamsten, K. von Feilitzen, M. Forsberg, L. Persson, F. Johansson, M. Zwahlen, G. von Heijne, J. Nielsen, and F. Ponten. 2015. Tissue-based map of the human proteome. *Science* 347: 1260419.

425. Yang, J., Y. L. Bai, Y. Zhang, V. D. Gabrielle, L. Jin, and G. C. Bai. 2014. Deletion of the cyclic di-AMP phosphodiesterase gene (cnpB) in *Mycobacterium tuberculosis* leads to reduced virulence in a mouse model of infection. *Molecular Microbiology* 93: 65-79.

426. Onyedibe, K. I., M. D. Wang, and H. O. Sintim. 2019. ENPP1, an Old Enzyme with New Functions, and Small Molecule Inhibitors-A STING in the Tale of ENPP1. *Molecules* 24: 4192.

427. Woodward, J. J., A. T. Iavarone, and D. A. Portnoy. 2010. c-di-AMP Secreted by Intracellular *Listeria monocytogenes* Activates a Host Type I Interferon Response. *Science* 328: 1703-1705.

428. Watson, R. O., S. L. Bell, D. A. MacDuff, J. M. Kimmey, E. J. Diner, J. Olivas, R. E. Vance, C. L. Stallings, H. W. Virgin, and J. S. Cox. 2015. The Cytosolic Sensor cGAS Detects *Mycobacterium tuberculosis* DNA to Induce Type I Interferons and Activate Autophagy. *Cell Host & Microbe* 17: 811-819.

429. Vander Heiden, M. G., L. C. Cantley, and C. B. Thompson. 2009. Understanding the Warburg Effect: The Metabolic Requirements of Cell Proliferation. *Science* 324: 1029-1033.

430. Cumming, B. M., K. W. Addicott, J. H. Adamson, and A. J. Steyn. 2018. *Mycobacterium tuberculosis* induces decelerated bioenergetic metabolism in human macrophages. *eLife* 7: e39169.

431. Russell, S. L., D. A. Lamprecht, T. Mandizvo, T. T. Jones, V. Naidoo, K. W. Addicott, C. Moodley, B. Ngcobo, D. K. Crossman, G. Wells, and A. J. C. Steyn. 2019. Compromised Metabolic Reprogramming Is an Early Indicator of CD8^{+} T Cell Dysfunction during Chronic *Mycobacterium tuberculosis* Infection. *Cell Reports* 29: 3564-3579.

432. Shi, L. B., Q. K. Jiang, Y. Bushkin, S. Subbian, and S. Tyagi. 2019. Biphasic Dynamics of Macrophage Immunometabolism during *Mycobacterium tuberculosis* Infection. *mBio* 10: e02550-02518.

433. Pawlowski, A., M. Jansson, M. Skold, M. E. Rottenberg, and G. Kallenius. 2012. Tuberculosis and HIV Co-Infection. *PLoS Pathog.* 8: e1002464.

434. Knight, M., J. Braverman, K. Asfaha, K. Gronert, and S. Stanley. 2018. Lipid droplet formation in *Mycobacterium tuberculosis* infected macrophages requires IFN-γ/HIF-1α signaling and supports host defense. *PLoS Pathog.* 14: e1006874.

435. Osada-Oka, M., N. Goda, H. Saiga, M. Yamamoto, K. Takeda, Y. Ozeki, T. Yamaguchi, T. Soga, Y. Tateishi, K. Miura, D. Okuzaki, K. Kobayashi, and S. Matsumoto. 2019. Metabolic adaptation to glycolysis is a basic defense mechanism of macrophages for *Mycobacterium tuberculosis* infection. *International Immunology* 31: 781-793.

436. Resende, M., C. M. Ferreira, A. M. Barbosa, M. S. Cardoso, J. Sousa, M. Saraiva, A. G. Castro, R. Appelberg, and E. Torrado. 2020. Myeloid HIF-1α regulates pulmonary inflammation during experimental *Mycobacterium tuberculosis* infection. *Immunology* 159: 121-129.

437. Cox, D. J., A. M. Coleman, K. M. Gogan, J. J. Phelan, C. Ó Maoldomhnaigh, P. J. Dunne, S. A. Basdeo, and J. Keane. 2020. Inhibiting Histone Deacetylases in Human Macrophages Promotes Glycolysis, IL-1β, and T Helper Cell Responses to *Mycobacterium tuberculosis*. *Front. Immunol.* 11: 1609.

438. Howard, N. C., N. D. Marin, M. Ahmed, B. A. Rosa, J. Martin, M. Bambouskova, A. Sergushichev, E. Loginicheva, N. Kurepina, J. Rangel-Moreno, L. Chen, B. N. Kreiswirth, R. S. Klein, J. M. Balada-Llasat, J. B. Torrelles, G. K. Amarasinghe, M. Mitreva, M. N. Artyomov, F. F. Hsu, B. Mathema, and S. A. Khader. 2018. *Mycobacterium tuberculosis* carrying a rifampicin drug resistance mutation reprograms macrophage metabolism through cell wall lipid changes. *Nature Microbiology* 3: 1099-1108.

439. Olson, G. S., T. A. Murray, A. N. Jahn, D. Mai, A. H. Diercks, E. S. Gold, and A. Aderem. 2021. Type I interferon decreases macrophage energy metabolism during mycobacterial infection. *Cell Reports* 35: 109195.

440. Kwan, B. W., J. A. Valenta, M. J. Benedik, and T. K. Wood. 2013. Arrested Protein Synthesis Increases Persister-Like Cell Formation. *Antimicrobial Agents and Chemotherapy* 57: 1468-1473.

441. Russell, D. G., P. J. Cardona, M. J. Kim, S. Allain, and F. Altare. 2009. Foamy macrophages and the progression of the human TB granuloma. *Nature Immunology* 10: 943-948.

442. Singh, V., S. Jamwal, R. Jain, P. Verma, R. Gokhale, and K. V. S. Rao. 2012. *Mycobacterium tuberculosis*-Driven Targeted Recalibration of Macrophage Lipid Homeostasis Promotes the Foamy Phenotype. *Cell Host & Microbe* 12: 669-681.

443. Cahill, C., D. J. Cox, F. O'Connell, S. A. Basdeo, K. M. Gogan, C. Ó Maoldomhnaigh, J. O'Sullivan, J. Keane, and J. J. Phelan. 2021. The Effect of Tuberculosis Antimicrobials on the Immunometabolic Profiles of Primary Human Macrophages Stimulated with *Mycobacterium tuberculosis*. *Int. J. Mol. Sci.* 22: 12189.

444. Yang, L. C., M. Xie, M. H. Yang, Y. Yu, S. Zhu, W. Hou, R. Kang, M. T. Lotze, T. R. Billiar, H. C. Wang, L. Z. Cao, and D. L. Tang. 2014. PKM2 regulates the Warburg effect and promotes HMGB1 release in sepsis. *Nature Communications* 5: 4436.

445. Zhong, W. J., H. H. Yang, X. X. Guan, J. B. Xiong, C. C. Sun, C. Y. Zhang, X. Q. Luo, Y. F. Zhang, J. Zhang, J. X. Duan, Y. Zhou, and C. X. Guan. 2019. Inhibition of glycolysis alleviates lipopolysaccharide-induced acute lung injury in a mouse model. *Journal of Cellular Physiology* 234: 4641-4654.

446. Sun, Q., T. Gong, M. L. Liu, S. Ren, H. Yang, S. Zeng, H. Zhao, L. Chen, T. Q. Ming, X. L. Meng, and H. B. Xu. 2022. Shikonin, a naphthalene ingredient: Therapeutic actions, pharmacokinetics, toxicology, clinical trials and pharmaceutical researches. *Phytomedicine* 94: 153805.

447. Singhal, A., L. Jie, P. Kumar, G. S. Hong, M. K. S. Leow, B. Paleja, L. Tsenova, N. Kurepina, J. M. Chen, F. Zolezzi, B. Kreiswirth, M. Poidinger, C. Chee, G. Kaplan, Y. T. Wang, and G. De Libero. 2014. Metformin as adjunct antituberculosis therapy. *Science Translational Medicine* 6: 263ra159.

448. Lachmandas, E., C. Eckold, J. Bohme, V. Koeken, M. B. Marzuki, B. Blok, R. J. W. Arts, J. M. Chen, K. W. W. Teng, J. Ratter, E. J. Smolders, C. van den Heuvel, R. Stienstra, H. M. Dockrell, E. Newell, M. G. Netea, A. Singhal, J. M. Cliff, and R. van Crevel. 2019. Metformin Alters Human Host Responses to *Mycobacterium tuberculosis* in Healthy Subjects. *Journal of Infectious Diseases* 220: 139-150.

449.   Bohme, J., N. Martinez, S. M. Li, A. Lee, M. Marzuki, A. M. Tizazu, D. Ackart, J. H. Frenkel, A. Todd, E. Lachmandas, J. Lum, F. Shihui, T. P. Ng, B. Lee, A. Larbi, M. G. Netea, R. Basaraba, R. van Crevel, E. Newell, H. Kornfeld, and A. Singhal. 2020. Metformin enhances anti-mycobacterial responses by educating CD8+ T-cell immunometabolic circuits. *Nature Communications* 11: 5225.

450.   Ruiz, A., C. Sarabia, M. Torres, and E. Juarez. 2019. Resolvin D1 (RvD1) and maresin 1 (Mar1) contribute to human macrophage control of *M. tuberculosis* infection while resolving inflammation. *International Immunopharmacology* 74: 105694.

451.   Crowther, R. R., and J. E. Qualls. 2021. Metabolic Regulation of Immune Responses to *Mycobacterium tuberculosis*: A Spotlight on L-Arginine and L-Tryptophan Metabolism. *Front. Immunol.* 11: 628432.

452.   Ralph, A. P., G. Waramori, G. J. Pontororing, E. Kenangalem, A. Wiguna, E. Tjitra, Sandjaja, D. B. Lolong, T. W. Yeo, M. D. Chatfield, R. K. Soemanto, I. Bastian, R. Lumb, G. P. Maguire, J. Eisman, R. N. Price, P. S. Morris, P. M. Kelly, and N. M. Anstey. 2013. L-arginine and Vitamin D Adjunctive Therapies in Pulmonary Tuberculosis: A Randomised, Double-Blind, Placebo-Controlled Trial. *PLOS One* 8: e70032.

453.   Schon, T., D. Elias, F. Moges, E. Melese, T. Tessema, O. Stendahl, S. Britton, and T. Sundqvist. 2003. Arginine as an adjuvant to chemotherapy improves clinical outcome in active tuberculosis. *European Respiratory Journal* 21: 483-488.

454.   Schon, T., J. Idh, A. Westman, D. Elias, E. Abate, E. Diro, F. Moges, A. Kassu, B. Ayele, T. Forslund, A. Getachew, S. Britton, O. Stendahl, and T. Sundqvist. 2011. Effects of a food supplement rich in arginine in patients with smear positive pulmonary tuberculosis - A randomised trial. *Tuberculosis* 91: 370-377.

455.   Kim, Y. J., J. Y. Lee, J. J. Lee, S. M. Jeon, P. Silwal, I. S. Kim, H. J. Kim, C. R. Park, C. Chung, J. E. Han, J. W. Choi, E. J. Tak, J. H. Yoo, S. W. Jeong, D. Y. Kim, W. Ketphan, S. Y. Kim, B. W. Jhun, J. Whang, J. M. Kim, H. Eoh, J. W. Bae, and E. K. Jo. 2022. Arginine-mediated gut microbiome remodeling promotes host pulmonary immune defense against nontuberculous mycobacterial infection. *Gut Microbes* 14: e2073132.

456. Fridrich, A., Y. Hazan, and Y. Moran. 2019. Too Many False Targets for MicroRNAs: Challenges and Pitfalls in Prediction of miRNA Targets and Their Gene Ontology in Model and Non-model Organisms. *Bioessays* 41: 1800169.

457. Shen, W. F., Y. L. Hu, L. Uttarwar, E. Passegue, and C. Largman. 2008. MicroRNA-126 Regulates HOXA9 by Binding to the Homeobox. *Mol. Cell. Biol.* 28: 4609-4619.

458. Huang, X., L. H. Ding, K. L. Bennewith, R. T. Tong, S. M. Welford, K. K. Ang, M. Story, Q. T. Le, and A. J. Giaccia. 2009. Hypoxia-Inducible mir-210 Regulates Normoxic Gene Expression Involved in Tumor Initiation. *Molecular Cell* 35: 856-867.

459. Kästle, M., S. Bartel, K. Geillinger-Kästle, M. Irmler, J. Beckers, B. Ryffel, O. Eickelberg, and S. Krauss-Etschmann. 2017. microRNA cluster 106a~363 is involved in T helper 17 cell differentiation. *Immunology* 152: 402-413.

460. Ramírez, C. M., L. Goedeke, N. Rotllan, J. H. Yoon, D. Cirera-Salinas, J. A. Mattison, Y. Suárez, R. de Cabo, M. Gorospe, and C. Fernández-Hernando. 2013. MicroRNA 33 Regulates Glucose Metabolism. *Mol. Cell. Biol.* 33: 2891-2902.

461. Nielsen, S., T. Akerstrom, A. Rinnov, C. Yfanti, C. Scheele, B. K. Pedersen, and M. J. Laye. 2014. The miRNA Plasma Signature in Response to Acute Aerobic Exercise and Endurance Training. *PLOS One* 9: e87308.

462. Winkle, M., S. M. El-Daly, M. Fabbri, and G. A. Calin. 2021. Noncoding RNA therapeutics - challenges and potential solutions. *Nature Reviews Drug Discovery* 20: 629-651.

463. Christensen, B. C., B. J. Moyer, M. Avissar, L. G. Ouellet, S. L. Plaza, M. D. McClean, C. J. Marsit, and K. T. Kelsey. 2009. A let-7 microRNA-binding site polymorphism in the KRAS 3' UTR is associated with reduced survival in oral cancers. *Carcinogenesis* 30: 1003-1007.

464. Nicoloso, M. S., H. Sun, R. Spizzo, H. Kim, P. Wickramasinghe, M. Shimizu, S. E. Wojcik, J. Ferdin, T. Kunej, L. C. Xiao, S. Manoukian, G. Secreto, F. Ravagnani, X. M. Wang, P. Radice, C. M. Croce, R. V. Davuluri, and G. A. Calin. 2010. Single-Nucleotide Polymorphisms Inside MicroRNA Target Sites Influence Tumor Susceptibility. *Cancer Research* 70: 2789-2798.

465. Dzikiewicz-Krawczyk, A., A. Macieja, E. Maly, D. Januszkiewicz-Lewandowska, M. Mosor, M. Fichna, E. Strauss, and J. Nowak. 2014. Polymorphisms in microRNA target sites modulate risk of lymphoblastic and myeloid leukemias and affect microRNA binding. *Journal of Hematology & Oncology* 7: 43.

466. Sherry, S. T., M. H. Ward, M. Kholodov, J. Baker, L. Phan, E. M. Smigielski, and K. Sirotkin. 2001. dbSNP: the NCBI database of genetic variation. *Nucleic Acids Research* 29: 308-311.

467. Cunningham, F., J. E. Allen, J. Allen, J. Alvarez-Jarreta, M. R. Amode, I. M. Armean, O. Austine-Orimoloye, A. G. Azov, I. Barnes, R. Bennett, A. Berry, J. Bhai, A. Bignell, K. Billis, S. Boddu, L. Brooks, M. Charkhchi, C. Cummins, L. D. Fioretto, C. Davidson, K. Dodiya, S. Donaldson, B. El Houdaigui, T. El Naboulsi, R. Fatima, C. G. Giron, T. Genez, J. G. Martinez, C. Guijarro-Clarke, A. Gymer, M. Hardy, Z. Hollis, T. Hourlier, T. Hunt, T. Juettemann, V. Kaikala, M. Kay, I. Lavidas, T. Le, D. Lemos, J. C. Marugan, S. Mohanan, A. Mushtaq, M. Naven, D. N. Ogeh, A. Parker, A. Parton, M. Perry, I. Pilizota, I. Prosovetskaia, M. P. Sakthivel, A. I. A. Salam, B. M. Schmitt, H. Schuilenburg, D. Sheppard, J. G. Perez-Silva, W. Stark, E. Steed, K. Sutinen, R. Sukumaran, D. Sumathipala, M. M. Suner, M. Szpak, A. Thormann, F. F. Tricomi, D. Urbina-Gomez, A. Veidenberg, T. A. Walsh, B. Walts, N. Willhoft, A. Winterbottom, E. Wass, M. Chakiachvili, B. Flint, A. Frankish, S. Giorgetti, L. Haggerty, S. E. Hunt, G. R. Iisley, J. E. Loveland, F. J. Martin, B. Moore, J. M. Mudge, M. Muffato, E. Perry, M. Ruffier, J. Tate, D. Thybert, S. J. Trevanion, S. Dyer, P. W. Harrison, K. L. Howe, A. D. Yates, D. R. Zerbino, and P. Flicek. 2022. Ensembl 2022. *Nucleic Acids Research* 50: D988-D995.

468. Pinzon, N., B. Li, L. Martinez, A. Sergeeva, J. Presumey, F. Apparailly, and H. Seitz. 2017. microRNA target prediction programs predict many false positives. *Genome Research* 27: 234-245.

469. Xie, Y. R., N. H. Kim, V. Nadithe, D. Schalk, A. Thakur, A. Kilic, L. G. Lum, D. J. P. Bassett, and O. M. Merkel. 2016. Targeted delivery of siRNA to activated T cells via transferrin-polyethylenimine (Tf-PEI) as a potential therapy of asthma. *Journal of Controlled Release* 229: 120-129.

470. Ramishetti, S., R. Kedmi, M. Goldsmith, F. Leonard, A. G. Sprague, B. Godin, M. Gozin, P. R. Cullis, D. M. Dykxhoorn, and D. Peer. 2015. Systemic Gene Silencing in Primary T Lymphocytes Using Targeted Lipid Nanoparticles. *ACS Nano* 9: 6706-6716.

471. Zang, X. L., X. X. Zhang, X. L. Zhao, H. Y. Hu, M. X. Qiao, Y. H. Deng, and D. W. Chen. 2019. Targeted Delivery of miRNA 155 to Tumor Associated Macrophages for Tumor Immunotherapy. *Molecular Pharmaceutics* 16: 1714-1722.

472. Matsumura, Y., and H. Maeda. 1986. A New Concept for Macromolecular Therapeutics in Cancer Chemotherapy: Mechanism of Tumoritropic Accumulation of Proteins and the Antitumor Agent Smancs. *Cancer Research* 46: 6387-6392.

473. Lavin, R. C., and S. M. Tan. 2022. Spatial relationships of intra-lesion heterogeneity in *Mycobacterium tuberculosis* microenvironment, replication status, and drug efficacy. *PLoS Pathog.* 18: e1010459.

474. Fenaroli, F., U. Repnik, Y. T. Xu, K. Johann, S. Van Herck, P. Dey, F. M. Skjeldal, D. M. Frei, S. Bagherifam, A. Kocere, R. Haag, B. G. De Geest, M. Barz, D. G. Russell, and G. Griffiths. 2018. Enhanced Permeability and Retention-like Extravasation of Nanoparticles from the Vasculature into Tuberculosis Granulomas in Zebrafish and Mouse Models. *ACS Nano* 12: 8646-8661.

475. Liao, Y. H., B. Li, Z. Zhao, Y. Fu, Q. Q. Tan, X. Y. Li, W. Wang, J. L. Yin, H. Shan, B. Z. Tang, and X. Huang. 2020. Targeted Theranostics for Tuberculosis: A Rifampicin-Loaded Aggregation-Induced Emission Carrier for Granulomas Tracking and Anti-Infection. *ACS Nano* 14: 8046-8058.

476. Huang, Z. K., Q. Luo, Y. Guo, J. Chen, G. L. Xiong, Y. P. Peng, J. Q. Ye, and J. M. Li. 2015. *Mycobacterium tuberculosis*-Induced Polarization of Human Macrophage Orchestrates the Formation and Development of Tuberculous Granulomas *In Vitro*. *PLOS One* 10: e0129744.

Appendix 1

Published paper for Chapter 1 "Targets and regulation of microRNA-652-3p

in homoeostasis and disease"

JMolMed

REVIEW

Targets and regulation of microRNA-652-3p in homoeostasis and disease

Maxwell T. Stevens[1] · Bernadette M. Saunders[1,2]

Abstract

microRNA are small non-coding RNA molecules which inhibit gene expression by binding mRNA, preventing its translation. As important regulators of gene expression, there is increasing interest in microRNAs as potential diagnostic biomarkers and therapeutic targets. Studies investigating the role of one of the miRNA—miR-652-3p—detail diverse roles for this miRNA in normal cell homoeostasis and disease states, including cancers, cardiovascular disease, mental health, and central nervous system diseases. Here, we review recent literature surrounding miR-652-3p, discussing its known target genes and their relevance to disease progression. These studies demonstrate that miR-652-3p targets *LLGL1* and *ZEB1* to modulate cell polarity mechanisms, with impacts on cancer metastasis and asymmetric cell division. Inhibition of the NOTCH ligand *JAG1* by miR-652-3p can have diverse effects on angiogenesis and immune cell regulation. Investigation of miR-652-3p and other dysregulated miRNAs identified a number of pathways potentially regulated by miR-652-3p. This review demonstrates that miR-652-3p has great promise as a diagnostic or therapeutic target due to its activity across multiple cellular systems.

Keywords miR-652 · Cancer · Cardiovascular disease · Notch signalling · Mental health

✉ Bernadette M. Saunders
bernadette.saunders@uts.edu.au

1 School of Life Sciences, Faculty of Science, University of
   Technology Sydney, Sydney, NSW, Australia

2 Centenary Institute, The University of Sydney, Sydney, NSW,
   Australia

🖄 Springer

Appendix 2

Supporting data for Chapter 1 "Targets and regulation of microRNA-652-3p

in homoeostasis and disease"

Targets and regulation of microRNA-652-3p in homeostasis and disease

Maxwell T. Stevens[a], Bernadette M. Saunders[a,b#]

Cellular and Molecular Life Sciences

[a]School of Life Sciences, Faculty of Science, University of Technology Sydney, Sydney, NSW, Australia

[b]Centenary Institute, The University of Sydney, Sydney, NSW, Australia

[#]Address correspondence to Bernadette M. Saunders, bernadette.saunders@uts.edu.au

Online Resource 1 miRNAs dysregulated with miR-652-3p

* Frequency column describes how many times each miRNA is dysregulated with miR-652-3p

Author	Year	Journal	Species	Disease/indication/cells	Compartment	miR-652-3p change	Assoc. miR	Assoc. miR change	Frequency	Accession
Allantz et al.	2012	PLOS One	Human	Immune cell subsets	Circulating leukocytes	Up	hsa-miR-143-3p	Up	6	MIMAT0000435
Allantz et al.	2012	PLOS One	Human	Immune cell subsets	Circulating leukocytes	Up	hsa-miR-223-3p	Up	7	MIMAT0000280
Andersen et al.	2014	Journal of Molecular Diagnostics	Human	Malignant pleural mesothelioma	Tumour biopsy	Down	hsa-miR-126-3p	Down	4	MIMAT0000445
Andersen et al.	2014	Journal of Molecular Diagnostics	Human	Malignant pleural mesothelioma	Tumour biopsy	Down	hsa-miR-143-3p	Down	6	MIMAT0000435
Andersen et al.	2014	Journal of Molecular Diagnostics	Human	Malignant pleural mesothelioma	Tumour biopsy	Down	hsa-miR-145-5p	Down	3	MIMAT0000437
Barry et al.	2018	Journal of Infection	Human	Tuberculosis	Plasma	Down	hsa-miR-133a-3p	Up	1	MIMAT0000427
Barry et al.	2018	Journal of Infection	Human	Tuberculosis	Plasma	Down	hsa-miR-146a-5p	Up	5	MIMAT0000449
Barry et al.	2018	Journal of Infection	Human	Tuberculosis	Plasma	Down	hsa-miR-21-5p	Up	6	MIMAT0000076
Barry et al.	2018	Journal of Infection	Human	Tuberculosis	Plasma	Down	hsa-miR-221-3p	Up	4	MIMAT0000278
Barry et al.	2018	Journal of Infection	Human	Tuberculosis	Plasma	Down	hsa-miR-223-3p	Up	7	MIMAT0000280
Barry et al.	2018	Journal of Infection	Human	Tuberculosis	Plasma	Down	hsa-miR-26a-5p	Up	4	MIMAT0000082
Barry et al.	2018	Journal of Infection	Human	Tuberculosis	Plasma	Down	hsa-miR-28-5p	Up	1	MIMAT0000085
Barry et al.	2018	Journal of Infection	Human	Tuberculosis	Plasma	Down	hsa-miR-29a-3p	Up	6	MIMAT0000086
Barry et al.	2018	Journal of Infection	Human	Tuberculosis	Plasma	Down	hsa-miR-99b-5p	Up	4	MIMAT0000689
Bruno et al.	2016	International Journal of Cardiology	Human	Heart failure	Plasma	Down	hsa-let-7i-5p	Up	2	MIMAT0000415
Bruno et al.	2016	International Journal of Cardiology	Human	Heart failure	Plasma	Down	hsa-miR-199a-3p	Up	5	MIMAT0000232
Bruno et al.	2016	International Journal of Cardiology	Human	Heart failure	Plasma	Down	hsa-miR-27a-3p	Down	5	MIMAT0000084
Bruno et al.	2016	International Journal of Cardiology	Human	Heart failure	Plasma	Down	hsa-miR-423-5p	Up	5	MIMAT0004748
Carreras-Badosa et al.	2015	Journal of Clinical Endocrinology & Metabolism	Human	Gestational obesity	Plasma	Down	hsa-miR-122-5p	Down	1	MIMAT0000421
Carreras-Badosa et al.	2015	Journal of Clinical Endocrinology & Metabolism	Human	Gestational obesity	Plasma	Down	hsa-miR-324-3p	Down	2	MIMAT0000762
Carreras-Badosa et al.	2015	Journal of Clinical Endocrinology & Metabolism	Human	Gestational obesity	Plasma	Down	hsa-miR-375-3p	Down	2	MIMAT0000728
Carreras-Badosa et al.	2015	Journal of Clinical Endocrinology & Metabolism	Human	Gestational obesity	Plasma	Down	hsa-miR-625-5p	Up	1	MIMAT0003294
Cuk et al.	2013	PLOS One	Human	Breast cancer	Plasma	Up	hsa-miR-127-3p	Down	1	MIMAT0000446
Cuk et al.	2013	PLOS One	Human	Breast cancer	Plasma	Up	hsa-miR-148b-3p	Down	3	MIMAT0000759
Cuk et al.	2013	PLOS One	Human	Breast cancer	Plasma	Up	hsa-miR-376a-3p	Down	2	MIMAT0000729
Cuk et al.	2013	PLOS One	Human	Breast cancer	Plasma	Up	hsa-miR-376c-3p	Down	2	MIMAT0000720
Cuk et al.	2013	PLOS One	Human	Breast cancer	Plasma	Up	hsa-miR-409-3p	Down	1	MIMAT0001639
Dahlman et al.	2017	American Journal of Physiology-Endocrinology and Metabolism	Human	Obesity	White adipose tissue	Down	hsa-miR-143-3p	Up	6	MIMAT0000435
Fernandez-Costa et al.	2016	PLOS One	Human	Myotonic dystrophy type 1	Serum	Up	hsa-miR-103a-3p	Up	4	MIMAT0000101
Fernandez-Costa et al.	2016	PLOS One	Human	Myotonic dystrophy type 1	Serum	Up	hsa-miR-107	Up	4	MIMAT0000104
Fernandez-Costa et al.	2016	PLOS One	Human	Myotonic dystrophy type 1	Serum	Up	hsa-miR-21-5p	Down	6	MIMAT0000076
Fernandez-Costa et al.	2016	PLOS One	Human	Myotonic dystrophy type 1	Serum	Up	hsa-miR-29a-3p	Down	6	MIMAT0000086
Fernandez-Costa et al.	2016	PLOS One	Human	Myotonic dystrophy type 1	Serum	Up	hsa-miR-30c-5p	Up	2	MIMAT0000244
Gao et al.	2011	Journal of Cancer Research and Clinical Oncology	Human	Non-small cell lung cancer	Tumour tissue	Down	hsa-miR-100-5p	Down	1	MIMAT0000098
Gao et al.	2011	Journal of Cancer Research and Clinical Oncology	Human	Non-small cell lung cancer	Tumour tissue	Down	hsa-miR-101-3p	Down	3	MIMAT0000099
Gao et al.	2011	Journal of Cancer Research and Clinical Oncology	Human	Non-small cell lung cancer	Tumour tissue	Down	hsa-miR-125b-5p	Down	1	MIMAT0000423
Gao et al.	2011	Journal of Cancer Research and Clinical Oncology	Human	Non-small cell lung cancer	Tumour tissue	Down	hsa-miR-126-3p	Down	4	MIMAT0000445
Gao et al.	2011	Journal of Cancer Research and Clinical Oncology	Human	Non-small cell lung cancer	Tumour tissue	Down	hsa-miR-126-3p	Down	4	MIMAT0000445
Gao et al.	2011	Journal of Cancer Research and Clinical Oncology	Human	Non-small cell lung cancer	Tumour tissue	Down	hsa-miR-130a-3p	Down	1	MIMAT0000425
Gao et al.	2011	Journal of Cancer Research and Clinical Oncology	Human	Non-small cell lung cancer	Tumour tissue	Down	hsa-miR-143-3p	Down	6	MIMAT0000435
Gao et al.	2011	Journal of Cancer Research and Clinical Oncology	Human	Non-small cell lung cancer	Tumour tissue	Down	hsa-miR-145-5p	Down	3	MIMAT0000437
Gao et al.	2011	Journal of Cancer Research and Clinical Oncology	Human	Non-small cell lung cancer	Tumour tissue	Down	hsa-miR-181a-5p	Down	6	MIMAT0000256
Gao et al.	2011	Journal of Cancer Research and Clinical Oncology	Human	Non-small cell lung cancer	Tumour tissue	Down	hsa-miR-18a-5p	Up	6	MIMAT0000072
Gao et al.	2011	Journal of Cancer Research and Clinical Oncology	Human	Non-small cell lung cancer	Tumour tissue	Down	hsa-miR-21-5p	Up	6	MIMAT0000076
Gao et al.	2011	Journal of Cancer Research and Clinical Oncology	Human	Non-small cell lung cancer	Tumour tissue	Down	hsa-miR-22-3p	Up	3	MIMAT0000077
Gao et al.	2011	Journal of Cancer Research and Clinical Oncology	Human	Non-small cell lung cancer	Tumour tissue	Down	hsa-miR-26a-5p	Down	4	MIMAT0000082
Gao et al.	2011	Journal of Cancer Research and Clinical Oncology	Human	Non-small cell lung cancer	Tumour tissue	Down	hsa-miR-26b-5p	Down	5	MIMAT0000083

Gao et al.	2011	Journal of Cancer Research and Clinical Oncology	Human	Non-small cell lung cancer	Tumour tissue	Down	hsa-miR-29a-3p	Down	6	MIMAT0000086
Gao et al.	2011	Journal of Cancer Research and Clinical Oncology	Human	Non-small cell lung cancer	Tumour tissue	Down	hsa-miR-29c-3p	Down	3	MIMAT0000681
Gao et al.	2011	Journal of Cancer Research and Clinical Oncology	Human	Non-small cell lung cancer	Tumour tissue	Down	hsa-miR-30a-5p	Down	2	MIMAT0000087
Gao et al.	2011	Journal of Cancer Research and Clinical Oncology	Human	Non-small cell lung cancer	Tumour tissue	Down	hsa-miR-30b-5p	Down	3	MIMAT0000420
Gao et al.	2011	Journal of Cancer Research and Clinical Oncology	Human	Non-small cell lung cancer	Tumour tissue	Down	hsa-miR-30d-5p	Down	2	MIMAT0000245
Gao et al.	2011	Journal of Cancer Research and Clinical Oncology	Human	Non-small cell lung cancer	Tumour tissue	Down	hsa-miR-30e-5p	Down	3	MIMAT0000692
Gao et al.	2011	Journal of Cancer Research and Clinical Oncology	Human	Non-small cell lung cancer	Tumour tissue	Down	hsa-miR-31-5p	Up	2	MIMAT0000089
Gao et al.	2011	Journal of Cancer Research and Clinical Oncology	Human	Non-small cell lung cancer	Tumour tissue	Down	hsa-miR-320a-3p	Down	3	MIMAT0000510
Gao et al.	2011	Journal of Cancer Research and Clinical Oncology	Human	Non-small cell lung cancer	Tumour tissue	Down	hsa-miR-34a-5p	Up	4	MIMAT0000255
Gao et al.	2011	Journal of Cancer Research and Clinical Oncology	Human	Non-small cell lung cancer	Tumour tissue	Down	hsa-miR-412-3p	Up	1	MIMAT0002170
Gao et al.	2011	Journal of Cancer Research and Clinical Oncology	Human	Non-small cell lung cancer	Tumour tissue	Down	hsa-miR-451a	Down	2	MIMAT0001631
Gao et al.	2011	Journal of Cancer Research and Clinical Oncology	Human	Non-small cell lung cancer	Tumour tissue	Down	hsa-miR-504-5p	Up	1	MIMAT0002875
Gao et al.	2011	Journal of Cancer Research and Clinical Oncology	Human	Non-small cell lung cancer	Tumour tissue	Down	hsa-miR-99a-5p	Down	1	MIMAT0000097
He et al.	2018	Journal of Cellular Biochemistry	Rat	Neuron differentiation	Neural stem cells	Up	rno-miR-155-5p	Up	1	MIMAT0030409
He et al.	2018	Journal of Cellular Biochemistry	Rat	Neuron differentiation	Neural stem cells	Up	rno-miR-210-3p	Up	1	MIMAT0000881
He et al.	2018	Journal of Cellular Biochemistry	Rat	Neuron differentiation	Neural stem cells	Up	rno-miR-29a-5p	Up	1	MIMAT0004718
He et al.	2018	Journal of Cellular Biochemistry	Rat	Neuron differentiation	Neural stem cells	Up	rno-miR-674-5p	Up	1	MIMAT0005329
Ji et al.	2018	Ebiomedicine	Human	Colorectal cancer	Serum	Down	hsa-miR-328-3p	Down	3	MIMAT0000752
Ji et al.	2018	Ebiomedicine	Human	Colorectal cancer	Serum	Down	hsa-miR-342-3p	Down	1	MIMAT0000753
Ji et al.	2018	Ebiomedicine	Human	Colorectal cancer	Serum	Down	hsa-miR-501-3p	Down	1	MIMAT0004774
Kanaan et al.	2013	Annals of Surgery	Human	Colorectal adenoma	Plasma	Up	hsa-miR-142-3p	Up	3	MIMAT0000434
Kanaan et al.	2013	Annals of Surgery	Human	Colorectal adenoma	Plasma	Up	hsa-miR-155-5p	Up	1	MIMAT0000646
Kanaan et al.	2013	Annals of Surgery	Human	Colorectal adenoma	Plasma	Up	hsa-miR-15b-5p	Up	5	MIMAT0000417
Kanaan et al.	2013	Annals of Surgery	Human	Colorectal adenoma	Plasma	Up	hsa-miR-17-5p	Up	2	MIMAT0000070
Kanaan et al.	2013	Annals of Surgery	Human	Colorectal adenoma	Plasma	Up	hsa-miR-193a-5p	Up	1	MIMAT0004614
Kanaan et al.	2013	Annals of Surgery	Human	Colorectal adenoma	Plasma	Up	hsa-miR-195-5p	Up	1	MIMAT0000461
Kanaan et al.	2013	Annals of Surgery	Human	Colorectal adenoma	Plasma	Up	hsa-miR-21-5p	Up	6	MIMAT0000076
Kanaan et al.	2013	Annals of Surgery	Human	Colorectal adenoma	Plasma	Up	hsa-miR-29a-3p	Up	6	MIMAT0000086
Kanaan et al.	2013	Annals of Surgery	Human	Colorectal adenoma	Plasma	Up	hsa-miR-29c-3p	Up	3	MIMAT0000681
Kanaan et al.	2013	Annals of Surgery	Human	Colorectal adenoma	Plasma	Up	hsa-miR-331-3p	Up	3	MIMAT0000760
Kanaan et al.	2013	Annals of Surgery	Human	Colorectal adenoma	Plasma	Up	hsa-miR-339-3p	Up	2	MIMAT0004702
Kanaan et al.	2013	Annals of Surgery	Human	Colorectal adenoma	Plasma	Up	hsa-miR-423-5p	Up	5	MIMAT0004748
Kanaan et al.	2013	Annals of Surgery	Human	Colorectal adenoma	Plasma	Up	hsa-miR-532-3p	Up	2	MIMAT0004780
Kanaan et al.	2013	Annals of Surgery	Human	Colorectal adenoma	Plasma	Up	hsa-miR-532-5p	Up	3	MIMAT0002888
Lai et al.	2011	PLOS One	Human	Schizophrenia	Periferal blood mononuclear cells	Up	hsa-miR-34a-5p	Up	4	MIMAT0000255
Lai et al.	2011	PLOS One	Human	Schizophrenia	Periferal blood mononuclear cells	Up	hsa-miR-432-5p	Down	1	MIMAT0002814
Lai et al.	2011	PLOS One	Human	Schizophrenia	Periferal blood mononuclear cells	Up	hsa-miR-449a	Up	2	MIMAT0001541
Lai et al.	2011	PLOS One	Human	Schizophrenia	Periferal blood mononuclear cells	Up	hsa-miR-548d-3p	Up	1	MIMAT0003323
Lai et al.	2011	PLOS One	Human	Schizophrenia	Periferal blood mononuclear cells	Up	hsa-miR-564	Up	1	MIMAT0003228
Lai et al.	2011	PLOS One	Human	Schizophrenia	Periferal blood mononuclear cells	Up	hsa-miR-572	Up	1	MIMAT0003237
Lai et al.	2016	Translational Psychiatry	Human	Schizophrenia	Periferal blood mononuclear cells	None	hsa-miR-34a-5p	Up	4	MIMAT0000255
Lai et al.	2016	Translational Psychiatry	Human	Schizophrenia	Periferal blood mononuclear cells	None	hsa-miR-449a	Up	2	MIMAT0001541
Lee et al.	2018	Frontiers in Psychiatry	Human	Internet gaming disorder	Plasma	Down	hsa-miR-200c-3p	Down	3	MIMAT0000617
Lee et al.	2018	Frontiers in Psychiatry	Human	Internet gaming disorder	Plasma	Down	hsa-miR-26b-5p	Down	5	MIMAT0000083
Lewohl et al.	2011	Alcoholism-Clinical and Experimental Research	Human	Alcoholism	Brain tissue	Up	hsa-let-7f-5p	Up	2	MIMAT0000067
Lewohl et al.	2011	Alcoholism-Clinical and Experimental Research	Human	Alcoholism	Brain tissue	Up	hsa-let-7g-5p	Up	1	MIMAT0000414
Lewohl et al.	2011	Alcoholism-Clinical and Experimental Research	Human	Alcoholism	Brain tissue	Up	hsa-miR-101-3p	Up	3	MIMAT0000099
Lewohl et al.	2011	Alcoholism-Clinical and Experimental Research	Human	Alcoholism	Brain tissue	Up	hsa-miR-135b-5p	Up	2	MIMAT0000758
Lewohl et al.	2011	Alcoholism-Clinical and Experimental Research	Human	Alcoholism	Brain tissue	Up	hsa-miR-1-3p	Up	2	MIMAT0000416
Lewohl et al.	2011	Alcoholism-Clinical and Experimental Research	Human	Alcoholism	Brain tissue	Up	hsa-miR-140-5p	Up	3	MIMAT0000431
Lewohl et al.	2011	Alcoholism-Clinical and Experimental Research	Human	Alcoholism	Brain tissue	Up	hsa-miR-144-3p	Up	1	MIMAT0000436
Lewohl et al.	2011	Alcoholism-Clinical and Experimental Research	Human	Alcoholism	Brain tissue	Up	hsa-miR-146a-5p	Up	5	MIMAT0000449
Lewohl et al.	2011	Alcoholism-Clinical and Experimental Research	Human	Alcoholism	Brain tissue	Up	hsa-miR-152-3p	Up	1	MIMAT0000438
Lewohl et al.	2011	Alcoholism-Clinical and Experimental Research	Human	Alcoholism	Brain tissue	Up	hsa-miR-153-3p	Up	1	MIMAT0000439
Lewohl et al.	2011	Alcoholism-Clinical and Experimental Research	Human	Alcoholism	Brain tissue	Up	hsa-miR-15b-5p	Up	5	MIMAT0000417
Lewohl et al.	2011	Alcoholism-Clinical and Experimental Research	Human	Alcoholism	Brain tissue	Up	hsa-miR-18a-5p	Up	6	MIMAT0000072
Lewohl et al.	2011	Alcoholism-Clinical and Experimental Research	Human	Alcoholism	Brain tissue	Up	hsa-miR-194-5p	Up	2	MIMAT0000460
Lewohl et al.	2011	Alcoholism-Clinical and Experimental Research	Human	Alcoholism	Brain tissue	Up	hsa-miR-196a-5p	Up	1	MIMAT0000226
Lewohl et al.	2011	Alcoholism-Clinical and Experimental Research	Human	Alcoholism	Brain tissue	Up	hsa-miR-196b-5p	Up	2	MIMAT0001080
Lewohl et al.	2011	Alcoholism-Clinical and Experimental Research	Human	Alcoholism	Brain tissue	Up	hsa-miR-203a-3p	Up	1	MIMAT0000264
Lewohl et al.	2011	Alcoholism-Clinical and Experimental Research	Human	Alcoholism	Brain tissue	Up	hsa-miR-301a-3p	Up	2	MIMAT0000688
Lewohl et al.	2011	Alcoholism-Clinical and Experimental Research	Human	Alcoholism	Brain tissue	Up	hsa-miR-339-5p	Up	2	MIMAT0000764

Author	Year	Journal	Species	Disease	Tissue	Reg	miRNA	Reg2	N	MIMAT
Lewohl et al.	2011	Alcoholism-Clinical and Experimental Research	Human	Alcoholism	Brain tissue	Up	hsa-miR-34c-5p	Up	1	MIMAT0000686
Lewohl et al.	2011	Alcoholism-Clinical and Experimental Research	Human	Alcoholism	Brain tissue	Up	hsa-miR-369-3p	Up	1	MIMAT0000721
Lewohl et al.	2011	Alcoholism-Clinical and Experimental Research	Human	Alcoholism	Brain tissue	Up	hsa-miR-374b-5p	Up	2	MIMAT0004955
Lewohl et al.	2011	Alcoholism-Clinical and Experimental Research	Human	Alcoholism	Brain tissue	Up	hsa-miR-376c-3p	Up	2	MIMAT0000720
Lewohl et al.	2011	Alcoholism-Clinical and Experimental Research	Human	Alcoholism	Brain tissue	Up	hsa-miR-380-3p	Up	1	MIMAT0000735
Lewohl et al.	2011	Alcoholism-Clinical and Experimental Research	Human	Alcoholism	Brain tissue	Up	hsa-miR-423-5p	Up	5	MIMAT0004748
Lewohl et al.	2011	Alcoholism-Clinical and Experimental Research	Human	Alcoholism	Brain tissue	Up	hsa-miR-454-3p	Up	1	MIMAT0003885
Lewohl et al.	2011	Alcoholism-Clinical and Experimental Research	Human	Alcoholism	Brain tissue	Up	hsa-miR-515-3p	Up	1	MIMAT0002827
Lewohl et al.	2011	Alcoholism-Clinical and Experimental Research	Human	Alcoholism	Brain tissue	Up	hsa-miR-519b-3p	Up	1	MIMAT0002837
Lewohl et al.	2011	Alcoholism-Clinical and Experimental Research	Human	Alcoholism	Brain tissue	Up	hsa-miR-553	Up	1	MIMAT0003216
Lewohl et al.	2011	Alcoholism-Clinical and Experimental Research	Human	Alcoholism	Brain tissue	Up	hsa-miR-580-3p	Up	1	MIMAT0003245
Lewohl et al.	2011	Alcoholism-Clinical and Experimental Research	Human	Alcoholism	Brain tissue	Up	hsa-miR-586	Up	1	MIMAT0003252
Lewohl et al.	2011	Alcoholism-Clinical and Experimental Research	Human	Alcoholism	Brain tissue	Up	hsa-miR-665	Up	1	MIMAT0004952
Lewohl et al.	2011	Alcoholism-Clinical and Experimental Research	Human	Alcoholism	Brain tissue	Up	hsa-miR-7-5p	Up	2	MIMAT0000252
Lewohl et al.	2011	Alcoholism-Clinical and Experimental Research	Human	Alcoholism	Brain tissue	Up	hsa-miR-802	Up	1	MIMAT0004185
Lewohl et al.	2011	Alcoholism-Clinical and Experimental Research	Human	Alcoholism	Brain tissue	Up	hsa-miR-92a-3p	Up	2	MIMAT0000092
Liguori et al.	2018	Human Molecular Genetics	Human	Multiple Sclerosis	Whole blood	Up	hsa-let-7a-5p	Up	3	MIMAT0000062
Liguori et al.	2018	Human Molecular Genetics	Human	Multiple Sclerosis	Whole blood	Up	hsa-let-7b-5p	Up	1	MIMAT0000063
Liguori et al.	2018	Human Molecular Genetics	Human	Multiple Sclerosis	Whole blood	Up	hsa-miR-125a-5p	Up	3	MIMAT0000443
Liguori et al.	2018	Human Molecular Genetics	Human	Multiple Sclerosis	Whole blood	Up	hsa-miR-148b-3p	Down	3	MIMAT0000759
Liguori et al.	2018	Human Molecular Genetics	Human	Multiple Sclerosis	Whole blood	Up	hsa-miR-181a-5p	Up	6	MIMAT0000256
Liguori et al.	2018	Human Molecular Genetics	Human	Multiple Sclerosis	Whole blood	Up	hsa-miR-182-5p	Up	2	MIMAT0000259
Liguori et al.	2018	Human Molecular Genetics	Human	Multiple Sclerosis	Whole blood	Up	hsa-miR-185-5p	Up	4	MIMAT0000455
Liguori et al.	2018	Human Molecular Genetics	Human	Multiple Sclerosis	Whole blood	Up	hsa-miR-221-3p	Up	4	MIMAT0000278
Liguori et al.	2018	Human Molecular Genetics	Human	Multiple Sclerosis	Whole blood	Up	hsa-miR-25-3p	Up	3	MIMAT0000081
Liguori et al.	2018	Human Molecular Genetics	Human	Multiple Sclerosis	Whole blood	Up	hsa-miR-320a-3p	Up	3	MIMAT0000510
Liguori et al.	2018	Human Molecular Genetics	Human	Multiple Sclerosis	Whole blood	Up	hsa-miR-942-5p	Up	2	MIMAT0004985
Liguori et al.	2018	Human Molecular Genetics	Human	Multiple Sclerosis	Whole blood	Up	hsa-miR-99b-5p	Up	4	MIMAT0000689
Liu et al.	2011	European Journal of Cancer	Human	Gastric cancer	Serum	Up	hsa-miR-1-3p	Up	2	MIMAT0000416
Liu et al.	2011	European Journal of Cancer	Human	Gastric cancer	Serum	Up	hsa-miR-20a-5p	Up	3	MIMAT0000075
Liu et al.	2011	European Journal of Cancer	Human	Gastric cancer	Serum	Up	hsa-miR-27a-3p	Up	5	MIMAT0000084
Liu et al.	2011	European Journal of Cancer	Human	Gastric cancer	Serum	Up	hsa-miR-34a-5p	Up	4	MIMAT0000255
Liu et al.	2011	European Journal of Cancer	Human	Gastric cancer	Serum	Up	hsa-miR-423-5p	Up	5	MIMAT0004748
Lulla et al.	2011	Sarcoma	Human	Osteosarcoma	Tumour tissue	Up	hsa-miR-135b-5p	Up	2	MIMAT0000758
Lulla et al.	2011	Sarcoma	Human	Osteosarcoma	Tumour tissue	Up	hsa-miR-150-5p	Up	2	MIMAT0000451
Lulla et al.	2011	Sarcoma	Human	Osteosarcoma	Tumour tissue	Up	hsa-miR-542-5p	Up	1	MIMAT0003340
Mangolini et al.	2015	Biomarker Research	Human	Breast cancer	Serum	Down	hsa-miR-148b-3p	Down	3	MIMAT0000759
McDermott et al.	2014	PLOS One	Human	Breast cancer	Blood	Down	hsa-miR-181a-5p	Down	6	MIMAT0000256
McDermott et al.	2014	PLOS One	Human	Breast cancer	Blood	Down	hsa-miR-223-3p	Down	7	MIMAT0000280
McDermott et al.	2014	PLOS One	Human	Breast cancer	Blood	Down	hsa-miR-29a-3p	Down	6	MIMAT0000086
Meng et al.	2014	BMC Microbiology	Human	Macrophages	Macrophage cell line	Down	hsa-let-7a-5p	Down	3	MIMAT0000062
Meng et al.	2014	BMC Microbiology	Human	Macrophages	Macrophage cell line	Down	hsa-let-7d-3p	Up	2	MIMAT0004484
Meng et al.	2014	BMC Microbiology	Human	Macrophages	Macrophage cell line	Down	hsa-let-7d-5p	Down	1	MIMAT0000065
Meng et al.	2014	BMC Microbiology	Human	Macrophages	Macrophage cell line	Down	hsa-let-7f-5p	Down	2	MIMAT0000067
Meng et al.	2014	BMC Microbiology	Human	Macrophages	Macrophage cell line	Down	hsa-miR-106b-5p	Down	2	MIMAT0000680
Meng et al.	2014	BMC Microbiology	Human	Macrophages	Macrophage cell line	Down	hsa-miR-107	Down	4	MIMAT0000104
Meng et al.	2014	BMC Microbiology	Human	Macrophages	Macrophage cell line	Down	hsa-miR-1184	Up	1	MIMAT0005829
Meng et al.	2014	BMC Microbiology	Human	Macrophages	Macrophage cell line	Down	hsa-miR-1236-3p	Up	1	MIMAT0005591
Meng et al.	2014	BMC Microbiology	Human	Macrophages	Macrophage cell line	Down	hsa-miR-1255b-2-3p	Up	1	MIMAT0022725
Meng et al.	2014	BMC Microbiology	Human	Macrophages	Macrophage cell line	Down	hsa-miR-125b-2-3p	Up	1	MIMAT0004603
Meng et al.	2014	BMC Microbiology	Human	Macrophages	Macrophage cell line	Down	hsa-miR-1260a	Down	1	MIMAT0005911
Meng et al.	2014	BMC Microbiology	Human	Macrophages	Macrophage cell line	Down	hsa-miR-1260b	Down	1	MIMAT0015041
Meng et al.	2014	BMC Microbiology	Human	Macrophages	Macrophage cell line	Down	hsa-miR-1275	Down	1	MIMAT0005929
Meng et al.	2014	BMC Microbiology	Human	Macrophages	Macrophage cell line	Down	hsa-miR-130b-3p	Up	2	MIMAT0000691
Meng et al.	2014	BMC Microbiology	Human	Macrophages	Macrophage cell line	Down	hsa-miR-133b	Up	1	MIMAT0000770
Meng et al.	2014	BMC Microbiology	Human	Macrophages	Macrophage cell line	Down	hsa-miR-138-2-3p	Down	1	MIMAT0004596
Meng et al.	2014	BMC Microbiology	Human	Macrophages	Macrophage cell line	Down	hsa-miR-142-3p	Down	3	MIMAT0000434
Meng et al.	2014	BMC Microbiology	Human	Macrophages	Macrophage cell line	Down	hsa-miR-142-5p	Down	2	MIMAT0000433
Meng et al.	2014	BMC Microbiology	Human	Macrophages	Macrophage cell line	Down	hsa-miR-146a-5p	Down	5	MIMAT0000449
Meng et al.	2014	BMC Microbiology	Human	Macrophages	Macrophage cell line	Down	hsa-miR-147b-3p	Up	1	MIMAT0004928
Meng et al.	2014	BMC Microbiology	Human	Macrophages	Macrophage cell line	Down	hsa-miR-148a-3p	Down	1	MIMAT0000243
Meng et al.	2014	BMC Microbiology	Human	Macrophages	Macrophage cell line	Down	hsa-miR-150-5p	Up	2	MIMAT0000451

Meng et al.	2014	BMC Microbiology	Human	Macrophages	Macrophage cell line	Down	hsa-miR-1587	Down	1	MIMAT0019077
Meng et al.	2014	BMC Microbiology	Human	Macrophages	Macrophage cell line	Down	hsa-miR-15a-5p	Down	1	MIMAT0000068
Meng et al.	2014	BMC Microbiology	Human	Macrophages	Macrophage cell line	Down	hsa-miR-15b-5p	Down	5	MIMAT0000417
Meng et al.	2014	BMC Microbiology	Human	Macrophages	Macrophage cell line	Down	hsa-miR-16-5p	Down	1	MIMAT0000069
Meng et al.	2014	BMC Microbiology	Human	Macrophages	Macrophage cell line	Down	hsa-miR-181a-5p	Down	6	MIMAT0000256
Meng et al.	2014	BMC Microbiology	Human	Macrophages	Macrophage cell line	Down	hsa-miR-185-5p	Down	4	MIMAT0000455
Meng et al.	2014	BMC Microbiology	Human	Macrophages	Macrophage cell line	Down	hsa-miR-18b-3p	Up	1	MIMAT0004751
Meng et al.	2014	BMC Microbiology	Human	Macrophages	Macrophage cell line	Down	hsa-miR-196b-3p	Down	1	MIMAT0009201
Meng et al.	2014	BMC Microbiology	Human	Macrophages	Macrophage cell line	Down	hsa-miR-1973	Down	1	MIMAT0009448
Meng et al.	2014	BMC Microbiology	Human	Macrophages	Macrophage cell line	Down	hsa-miR-197-3p	Down	3	MIMAT0000227
Meng et al.	2014	BMC Microbiology	Human	Macrophages	Macrophage cell line	Down	hsa-miR-19a-3p	Down	2	MIMAT0000073
Meng et al.	2014	BMC Microbiology	Human	Macrophages	Macrophage cell line	Down	hsa-miR-200b-3p	Up	1	MIMAT0000318
Meng et al.	2014	BMC Microbiology	Human	Macrophages	Macrophage cell line	Down	hsa-miR-20b-3p	Down	1	MIMAT0004752
Meng et al.	2014	BMC Microbiology	Human	Macrophages	Macrophage cell line	Down	hsa-miR-20b-5p	Down	2	MIMAT0001413
Meng et al.	2014	BMC Microbiology	Human	Macrophages	Macrophage cell line	Down	hsa-miR-2113	Up	1	MIMAT0009206
Meng et al.	2014	BMC Microbiology	Human	Macrophages	Macrophage cell line	Down	hsa-miR-2115-3p	Down	1	MIMAT0011159
Meng et al.	2014	BMC Microbiology	Human	Macrophages	Macrophage cell line	Down	hsa-miR-21-5p	Down	6	MIMAT0000076
Meng et al.	2014	BMC Microbiology	Human	Macrophages	Macrophage cell line	Down	hsa-miR-221-5p	Up	1	MIMAT0004568
Meng et al.	2014	BMC Microbiology	Human	Macrophages	Macrophage cell line	Down	hsa-miR-223-3p	Down	7	MIMAT0000280
Meng et al.	2014	BMC Microbiology	Human	Macrophages	Macrophage cell line	Down	hsa-miR-22-3p	Down	3	MIMAT0000077
Meng et al.	2014	BMC Microbiology	Human	Macrophages	Macrophage cell line	Down	hsa-miR-224-3p	Up	1	MIMAT0009198
Meng et al.	2014	BMC Microbiology	Human	Macrophages	Macrophage cell line	Down	hsa-miR-2355-3p	Up	1	MIMAT0017950
Meng et al.	2014	BMC Microbiology	Human	Macrophages	Macrophage cell line	Down	hsa-miR-23b-3p	Down	2	MIMAT0000418
Meng et al.	2014	BMC Microbiology	Human	Macrophages	Macrophage cell line	Down	hsa-miR-23c	Up	1	MIMAT0018000
Meng et al.	2014	BMC Microbiology	Human	Macrophages	Macrophage cell line	Down	hsa-miR-24-3p	Down	1	MIMAT0000080
Meng et al.	2014	BMC Microbiology	Human	Macrophages	Macrophage cell line	Down	hsa-miR-25-3p	Down	3	MIMAT0000081
Meng et al.	2014	BMC Microbiology	Human	Macrophages	Macrophage cell line	Down	hsa-miR-26a-5p	Down	4	MIMAT0000082
Meng et al.	2014	BMC Microbiology	Human	Macrophages	Macrophage cell line	Down	hsa-miR-27a-3p	Down	5	MIMAT0000084
Meng et al.	2014	BMC Microbiology	Human	Macrophages	Macrophage cell line	Down	hsa-miR-27b-3p	Down	3	MIMAT0000419
Meng et al.	2014	BMC Microbiology	Human	Macrophages	Macrophage cell line	Down	hsa-miR-296-5p	Up	1	MIMAT0000690
Meng et al.	2014	BMC Microbiology	Human	Macrophages	Macrophage cell line	Down	hsa-miR-299-3p	Down	1	MIMAT0000687
Meng et al.	2014	BMC Microbiology	Human	Macrophages	Macrophage cell line	Down	hsa-miR-29c-3p	Down	3	MIMAT0000681
Meng et al.	2014	BMC Microbiology	Human	Macrophages	Macrophage cell line	Down	hsa-miR-301a-3p	Down	2	MIMAT0000688
Meng et al.	2014	BMC Microbiology	Human	Macrophages	Macrophage cell line	Down	hsa-miR-30a-5p	Down	2	MIMAT0000087
Meng et al.	2014	BMC Microbiology	Human	Macrophages	Macrophage cell line	Down	hsa-miR-30b-5p	Down	3	MIMAT0000420
Meng et al.	2014	BMC Microbiology	Human	Macrophages	Macrophage cell line	Down	hsa-miR-30e-3p	Up	1	MIMAT0000693
Meng et al.	2014	BMC Microbiology	Human	Macrophages	Macrophage cell line	Down	hsa-miR-30e-5p	Down	3	MIMAT0000692
Meng et al.	2014	BMC Microbiology	Human	Macrophages	Macrophage cell line	Down	hsa-miR-3156-3p	Up	1	MIMAT0019209
Meng et al.	2014	BMC Microbiology	Human	Macrophages	Macrophage cell line	Down	hsa-miR-3175	Down	1	MIMAT0015052
Meng et al.	2014	BMC Microbiology	Human	Macrophages	Macrophage cell line	Down	hsa-miR-3182	Down	1	MIMAT0015062
Meng et al.	2014	BMC Microbiology	Human	Macrophages	Macrophage cell line	Down	hsa-miR-3191-5p	Up	1	MIMAT0022732
Meng et al.	2014	BMC Microbiology	Human	Macrophages	Macrophage cell line	Down	hsa-miR-323a-3p	Up	2	MIMAT0000755
Meng et al.	2014	BMC Microbiology	Human	Macrophages	Macrophage cell line	Down	hsa-miR-331-3p	Down	3	MIMAT0000760
Meng et al.	2014	BMC Microbiology	Human	Macrophages	Macrophage cell line	Down	hsa-miR-339-5p	Down	2	MIMAT0000764
Meng et al.	2014	BMC Microbiology	Human	Macrophages	Macrophage cell line	Down	hsa-miR-33b-5p	Up	1	MIMAT0003301
Meng et al.	2014	BMC Microbiology	Human	Macrophages	Macrophage cell line	Down	hsa-miR-361-5p	Up	2	MIMAT0000703
Meng et al.	2014	BMC Microbiology	Human	Macrophages	Macrophage cell line	Down	hsa-miR-3646	Down	1	MIMAT0018065
Meng et al.	2014	BMC Microbiology	Human	Macrophages	Macrophage cell line	Down	hsa-miR-3651	Down	1	MIMAT0018071
Meng et al.	2014	BMC Microbiology	Human	Macrophages	Macrophage cell line	Down	hsa-miR-3654	Down	1	MIMAT0018074
Meng et al.	2014	BMC Microbiology	Human	Macrophages	Macrophage cell line	Down	hsa-miR-365a-3p	Down	1	MIMAT0000710
Meng et al.	2014	BMC Microbiology	Human	Macrophages	Macrophage cell line	Down	hsa-miR-3680-5p	Up	1	MIMAT0018106
Meng et al.	2014	BMC Microbiology	Human	Macrophages	Macrophage cell line	Down	hsa-miR-3685	Up	1	MIMAT0018113
Meng et al.	2014	BMC Microbiology	Human	Macrophages	Macrophage cell line	Down	hsa-miR-374a-5p	Down	1	MIMAT0000727
Meng et al.	2014	BMC Microbiology	Human	Macrophages	Macrophage cell line	Down	hsa-miR-374b-3p	Up	1	MIMAT0004956
Meng et al.	2014	BMC Microbiology	Human	Macrophages	Macrophage cell line	Down	hsa-miR-374b-5p	Down	2	MIMAT0004955
Meng et al.	2014	BMC Microbiology	Human	Macrophages	Macrophage cell line	Down	hsa-miR-374c-3p	Up	1	MIMAT0022735
Meng et al.	2014	BMC Microbiology	Human	Macrophages	Macrophage cell line	Down	hsa-miR-375-3p	Down	2	MIMAT0000728
Meng et al.	2014	BMC Microbiology	Human	Macrophages	Macrophage cell line	Down	hsa-miR-377-5p	Up	1	MIMAT0004689
Meng et al.	2014	BMC Microbiology	Human	Macrophages	Macrophage cell line	Down	hsa-miR-378c	Down	1	MIMAT0016847
Meng et al.	2014	BMC Microbiology	Human	Macrophages	Macrophage cell line	Down	hsa-miR-3938	Up	1	MIMAT0018353
Meng et al.	2014	BMC Microbiology	Human	Macrophages	Macrophage cell line	Down	hsa-miR-3941	Up	1	MIMAT0018357
Meng et al.	2014	BMC Microbiology	Human	Macrophages	Macrophage cell line	Down	hsa-miR-424-5p	Down	1	MIMAT0001341

Meng et al.	2014	BMC Microbiology	Human	Macrophages	Macrophage cell line	Down	hsa-miR-4268	Up	1	MIMAT0016896
Meng et al.	2014	BMC Microbiology	Human	Macrophages	Macrophage cell line	Down	hsa-miR-4278	Up	1	MIMAT0016910
Meng et al.	2014	BMC Microbiology	Human	Macrophages	Macrophage cell line	Down	hsa-miR-4279	Down	1	MIMAT0016909
Meng et al.	2014	BMC Microbiology	Human	Macrophages	Macrophage cell line	Down	hsa-miR-4286	Down	1	MIMAT0016916
Meng et al.	2014	BMC Microbiology	Human	Macrophages	Macrophage cell line	Down	hsa-miR-4324	Up	1	MIMAT0016876
Meng et al.	2014	BMC Microbiology	Human	Macrophages	Macrophage cell line	Down	hsa-miR-4429	Down	1	MIMAT0018944
Meng et al.	2014	BMC Microbiology	Human	Macrophages	Macrophage cell line	Down	hsa-miR-4431	Up	1	MIMAT0018947
Meng et al.	2014	BMC Microbiology	Human	Macrophages	Macrophage cell line	Down	hsa-miR-4436b-5p	Up	1	MIMAT0019940
Meng et al.	2014	BMC Microbiology	Human	Macrophages	Macrophage cell line	Down	hsa-miR-4445-5p	Down	1	MIMAT0018963
Meng et al.	2014	BMC Microbiology	Human	Macrophages	Macrophage cell line	Down	hsa-miR-4450	Down	1	MIMAT0018971
Meng et al.	2014	BMC Microbiology	Human	Macrophages	Macrophage cell line	Down	hsa-miR-4454	Down	1	MIMAT0018976
Meng et al.	2014	BMC Microbiology	Human	Macrophages	Macrophage cell line	Down	hsa-miR-4467	Down	1	MIMAT0018994
Meng et al.	2014	BMC Microbiology	Human	Macrophages	Macrophage cell line	Down	hsa-miR-4500	Down	1	MIMAT0019036
Meng et al.	2014	BMC Microbiology	Human	Macrophages	Macrophage cell line	Down	hsa-miR-4511	Up	1	MIMAT0019048
Meng et al.	2014	BMC Microbiology	Human	Macrophages	Macrophage cell line	Down	hsa-miR-451a	Up	2	MIMAT0001631
Meng et al.	2014	BMC Microbiology	Human	Macrophages	Macrophage cell line	Down	hsa-miR-451b	Down	1	MIMAT0019840
Meng et al.	2014	BMC Microbiology	Human	Macrophages	Macrophage cell line	Down	hsa-miR-4540	Up	1	MIMAT0019083
Meng et al.	2014	BMC Microbiology	Human	Macrophages	Macrophage cell line	Down	hsa-miR-4633-5p	Down	1	MIMAT0019689
Meng et al.	2014	BMC Microbiology	Human	Macrophages	Macrophage cell line	Down	hsa-miR-4636	Down	1	MIMAT0019693
Meng et al.	2014	BMC Microbiology	Human	Macrophages	Macrophage cell line	Down	hsa-miR-4644	Down	1	MIMAT0019704
Meng et al.	2014	BMC Microbiology	Human	Macrophages	Macrophage cell line	Down	hsa-miR-4653-3p	Down	1	MIMAT0019719
Meng et al.	2014	BMC Microbiology	Human	Macrophages	Macrophage cell line	Down	hsa-miR-4664-3p	Up	1	MIMAT0019738
Meng et al.	2014	BMC Microbiology	Human	Macrophages	Macrophage cell line	Down	hsa-miR-4668-5p	Down	1	MIMAT0019745
Meng et al.	2014	BMC Microbiology	Human	Macrophages	Macrophage cell line	Down	hsa-miR-4678	Up	1	MIMAT0019762
Meng et al.	2014	BMC Microbiology	Human	Macrophages	Macrophage cell line	Down	hsa-miR-4685-3p	Up	1	MIMAT0019772
Meng et al.	2014	BMC Microbiology	Human	Macrophages	Macrophage cell line	Down	hsa-miR-4695-3p	Down	1	MIMAT0019789
Meng et al.	2014	BMC Microbiology	Human	Macrophages	Macrophage cell line	Down	hsa-miR-4728-3p	Up	1	MIMAT0019850
Meng et al.	2014	BMC Microbiology	Human	Macrophages	Macrophage cell line	Down	hsa-miR-4787-5p	Down	1	MIMAT0019956
Meng et al.	2014	BMC Microbiology	Human	Macrophages	Macrophage cell line	Down	hsa-miR-4804-3p	Up	1	MIMAT0019985
Meng et al.	2014	BMC Microbiology	Human	Macrophages	Macrophage cell line	Down	hsa-miR-483-3p	Down	1	MIMAT0002173
Meng et al.	2014	BMC Microbiology	Human	Macrophages	Macrophage cell line	Down	hsa-miR-485-3p	Up	1	MIMAT0002176
Meng et al.	2014	BMC Microbiology	Human	Macrophages	Macrophage cell line	Down	hsa-miR-486-5p	Up	1	MIMAT0002177
Meng et al.	2014	BMC Microbiology	Human	Macrophages	Macrophage cell line	Down	hsa-miR-493-5p	Down	1	MIMAT0002813
Meng et al.	2014	BMC Microbiology	Human	Macrophages	Macrophage cell line	Down	hsa-miR-498-5p	Up	1	MIMAT0002824
Meng et al.	2014	BMC Microbiology	Human	Macrophages	Macrophage cell line	Down	hsa-miR-5000-3p	Down	1	MIMAT0021020
Meng et al.	2014	BMC Microbiology	Human	Macrophages	Macrophage cell line	Down	hsa-miR-5002-3p	Up	1	MIMAT0021024
Meng et al.	2014	BMC Microbiology	Human	Macrophages	Macrophage cell line	Down	hsa-miR-5089-5p	Down	1	MIMAT0021081
Meng et al.	2014	BMC Microbiology	Human	Macrophages	Macrophage cell line	Down	hsa-miR-532-5p	Down	3	MIMAT0002888
Meng et al.	2014	BMC Microbiology	Human	Macrophages	Macrophage cell line	Down	hsa-miR-548ao-3p	Up	1	MIMAT0021030
Meng et al.	2014	BMC Microbiology	Human	Macrophages	Macrophage cell line	Down	hsa-miR-548as-3p	Up	1	MIMAT0022268
Meng et al.	2014	BMC Microbiology	Human	Macrophages	Macrophage cell line	Down	hsa-miR-550a-3p	Up	1	MIMAT0003257
Meng et al.	2014	BMC Microbiology	Human	Macrophages	Macrophage cell line	Down	hsa-miR-550b-3p	Up	1	MIMAT0018445
Meng et al.	2014	BMC Microbiology	Human	Macrophages	Macrophage cell line	Down	hsa-miR-551a	Up	1	MIMAT0003214
Meng et al.	2014	BMC Microbiology	Human	Macrophages	Macrophage cell line	Down	hsa-miR-5581-3p	Down	1	MIMAT0022276
Meng et al.	2014	BMC Microbiology	Human	Macrophages	Macrophage cell line	Down	hsa-miR-5684	Down	1	MIMAT0022473
Meng et al.	2014	BMC Microbiology	Human	Macrophages	Macrophage cell line	Down	hsa-miR-5689	Up	1	MIMAT0022481
Meng et al.	2014	BMC Microbiology	Human	Macrophages	Macrophage cell line	Down	hsa-miR-5690	Up	1	MIMAT0022482
Meng et al.	2014	BMC Microbiology	Human	Macrophages	Macrophage cell line	Down	hsa-miR-615-3p	Up	1	MIMAT0003283
Meng et al.	2014	BMC Microbiology	Human	Macrophages	Macrophage cell line	Down	hsa-miR-657	Up	1	MIMAT0003335
Meng et al.	2014	BMC Microbiology	Human	Macrophages	Macrophage cell line	Down	hsa-miR-660-5p	Down	2	MIMAT0003338
Meng et al.	2014	BMC Microbiology	Human	Macrophages	Macrophage cell line	Down	hsa-miR-664b-5p	Down	1	MIMAT0022271
Meng et al.	2014	BMC Microbiology	Human	Macrophages	Macrophage cell line	Down	hsa-miR-675-3p	Up	1	MIMAT0006790
Meng et al.	2014	BMC Microbiology	Human	Macrophages	Macrophage cell line	Down	hsa-miR-7-2-3p	Up	1	MIMAT0004554
Meng et al.	2014	BMC Microbiology	Human	Macrophages	Macrophage cell line	Down	hsa-miR-7-5p	Down	2	MIMAT0000252
Meng et al.	2014	BMC Microbiology	Human	Macrophages	Macrophage cell line	Down	hsa-miR-92b-3p	Down	1	MIMAT0003218
Meng et al.	2014	BMC Microbiology	Human	Macrophages	Macrophage cell line	Down	hsa-miR-93-3p	Down	1	MIMAT0004509
Meng et al.	2014	BMC Microbiology	Human	Macrophages	Macrophage cell line	Down	hsa-miR-935	Up	1	MIMAT0004978
Meng et al.	2014	BMC Microbiology	Human	Macrophages	Macrophage cell line	Down	hsa-miR-93-5p	Down	2	MIMAT0000093
Meng et al.	2014	BMC Microbiology	Human	Macrophages	Macrophage cell line	Down	hsa-miR-937-3p	Down	1	MIMAT0004980
Nielsen et al.	2014	PLOS One	Human	Endurance exercise	Plasma	Down	hsa-let-7i-5p	Down	2	MIMAT0000415
Nielsen et al.	2014	PLOS One	Human	Endurance exercise	Plasma	Down	hsa-miR-106a-5p	Down	4	MIMAT0000103
Nielsen et al.	2014	PLOS One	Human	Endurance exercise	Plasma	Down	hsa-miR-146a-5p	Down	5	MIMAT0000449

Nielsen et al.	2014	PLOS One	Human	Endurance exercise	Plasma	Down	hsa-miR-151a-3p	Down	2	MIMAT0000757
Nielsen et al.	2014	PLOS One	Human	Endurance exercise	Plasma	Down	hsa-miR-151a-5p	Down	1	MIMAT0004697
Nielsen et al.	2014	PLOS One	Human	Endurance exercise	Plasma	Down	hsa-miR-221-3p	Down	4	MIMAT0000278
Nielsen et al.	2014	PLOS One	Human	Endurance exercise	Plasma	Down	hsa-miR-30b-5p	Down	3	MIMAT0000420
Nuzziello et al.	2018	International Journal of Molecular Sciences	Human	Multiple Sclerosis	Whole blood	Up	hsa-miR-125a-5p	Up	3	MIMAT0000443
Nuzziello et al.	2018	International Journal of Molecular Sciences	Human	Multiple Sclerosis	Whole blood	Up	hsa-miR-185-5p	Up	4	MIMAT0000455
Nuzziello et al.	2018	International Journal of Molecular Sciences	Human	Multiple Sclerosis	Whole blood	Up	hsa-miR-25-3p	Up	3	MIMAT0000081
Nuzziello et al.	2018	International Journal of Molecular Sciences	Human	Multiple Sclerosis	Whole blood	Up	hsa-miR-320a-3p	Up	3	MIMAT0000510
Nuzziello et al.	2018	International Journal of Molecular Sciences	Human	Multiple Sclerosis	Whole blood	Up	hsa-miR-942-5p	Up	2	MIMAT0004985
Ovchinnikova	2016	European Journal of Heart Failure	Human	Heart failure	Plasma	Down	hsa-miR-106a-5p	Down	4	MIMAT0000103
Ovchinnikova et al.	2016	European Journal of Heart Failure	Human	Heart failure	Plasma	Down	hsa-miR-18a-5p	Down	6	MIMAT0000072
Ovchinnikova et al.	2016	European Journal of Heart Failure	Human	Heart failure	Plasma	Down	hsa-miR-199a-3p	Down	5	MIMAT0000232
Ovchinnikova et al.	2016	European Journal of Heart Failure	Human	Heart failure	Plasma	Down	hsa-miR-26b-5p	Down	5	MIMAT0000083
Ovchinnikova et al.	2016	European Journal of Heart Failure	Human	Heart failure	Plasma	Down	hsa-miR-27a-3p	Down	5	MIMAT0000084
Ovchinnikova et al.	2016	European Journal of Heart Failure	Human	Heart failure	Plasma	Down	hsa-miR-30e-5p	Down	3	MIMAT0000692
Pergoli et al.	2017	Particle and Fibre Toxicology	Human	Cardiovascular disease	Extracellular vescicles	Down	hsa-let-7c-5p	Down	1	MIMAT0000064
Pergoli et al.	2017	Particle and Fibre Toxicology	Human	Cardiovascular disease	Extracellular vescicles	Down	hsa-miR-106a-5p	Down	4	MIMAT0000103
Pergoli et al.	2017	Particle and Fibre Toxicology	Human	Cardiovascular disease	Extracellular vescicles	Down	hsa-miR-143-3p	Down	6	MIMAT0000435
Pergoli et al.	2017	Particle and Fibre Toxicology	Human	Cardiovascular disease	Extracellular vescicles	Down	hsa-miR-185-5p	Down	4	MIMAT0000455
Pergoli et al.	2017	Particle and Fibre Toxicology	Human	Cardiovascular disease	Extracellular vescicles	Down	hsa-miR-218-5p	Down	1	MIMAT0000275
Pergoli et al.	2017	Particle and Fibre Toxicology	Human	Cardiovascular disease	Extracellular vescicles	Down	hsa-miR-331-3p	Down	3	MIMAT0000760
Pergoli et al.	2017	Particle and Fibre Toxicology	Human	Cardiovascular disease	Extracellular vescicles	Down	hsa-miR-642a-5p	Down	1	MIMAT0003312
Pergoli et al.	2017	Particle and Fibre Toxicology	Human	Cardiovascular disease	Extracellular vescicles	Down	hsa-miR-99b-5p	Down	4	MIMAT0000689
Pilbrow et al.	2014	International Journal of Cardiology	Human	Acute coronary syndrome	Plasma	Up	hsa-miR-27b-3p	Up	3	MIMAT0000419
Pilbrow et al.	2014	International Journal of Cardiology	Human	Acute coronary syndrome	Plasma	Up	hsa-miR-323a-3p	Up	2	MIMAT0000755
Roderburg et al.	2012	PLOS One	Human	Liver cirrhosis	Serum	Down	hsa-miR-513a-3p	Up	1	MIMAT0004777
Roderburg et al.	2012	PLOS One	Human	Liver cirrhosis	Serum	Down	hsa-miR-571	Up	1	MIMAT0003236
Sahlberg et al.	2015	Clinical Cancer Research	Human	Breast cancer	Serum	Up	hsa-miR-101-3p	Down	3	MIMAT0000099
Sahlberg et al.	2015	Clinical Cancer Research	Human	Breast cancer	Serum	Up	hsa-miR-103a-3p	Up	4	MIMAT0000101
Sahlberg et al.	2015	Clinical Cancer Research	Human	Breast cancer	Serum	Up	hsa-miR-107	Up	4	MIMAT0000104
Sahlberg et al.	2015	Clinical Cancer Research	Human	Breast cancer	Serum	Up	hsa-miR-18b-5p	Up	1	MIMAT0001412
Sahlberg et al.	2015	Clinical Cancer Research	Human	Breast cancer	Serum	Up	hsa-miR-20a-5p	Up	3	MIMAT0000075
Sahlberg et al.	2015	Clinical Cancer Research	Human	Breast cancer	Serum	Up	hsa-miR-223-3p	Up	7	MIMAT0000280
Sahlberg et al.	2015	Clinical Cancer Research	Human	Breast cancer	Serum	Up	hsa-miR-30d-5p	Up	2	MIMAT0000245
Sahlberg et al.	2015	Clinical Cancer Research	Human	Breast cancer	Serum	Up	hsa-miR-32-5p	Down	2	MIMAT0000090
Santarelli et al.	2011	Biological Psychiatry	Human	Schizophrenia	Brain tissue	Up	hsa-miR-107	Up	4	MIMAT0000104
Santarelli et al.	2011	Biological Psychiatry	Human	Schizophrenia	Brain tissue	Up	hsa-miR-134-5p	Up	1	MIMAT0000447
Santarelli et al.	2011	Biological Psychiatry	Human	Schizophrenia	Brain tissue	Up	hsa-miR-17-5p	Up	2	MIMAT0000070
Santarelli et al.	2011	Biological Psychiatry	Human	Schizophrenia	Brain tissue	Up	hsa-miR-328-3p	Up	3	MIMAT0000752
Santarelli et al.	2011	Biological Psychiatry	Human	Schizophrenia	Brain tissue	Up	hsa-miR-382-5p	Up	1	MIMAT0000737
Shin et al.	2015	Molecular Cancer	Human	Gastric cancer	Plasma	Up	hsa-miR-140-5p	Up	3	MIMAT0000431
Shin et al.	2015	Molecular Cancer	Human	Gastric cancer	Plasma	Up	hsa-miR-18a-5p	Up	6	MIMAT0000072
Shin et al.	2015	Molecular Cancer	Human	Gastric cancer	Plasma	Up	hsa-miR-199a-3p	Up	5	MIMAT0000232
Shin et al.	2015	Molecular Cancer	Human	Gastric cancer	Plasma	Up	hsa-miR-627-5p	Up	1	MIMAT0003296
Shin et al.	2015	Molecular Cancer	Human	Gastric cancer	Plasma	Up	hsa-miR-629-3p	Up	1	MIMAT0003298
Urquidi et al.	2016	Oncotarget	Human	Bladder cancer	Urothelial portion in urine	Up	hsa-miR-106b-5p	Up	2	MIMAT0000680
Urquidi et al.	2016	Oncotarget	Human	Bladder cancer	Urothelial portion in urine	Up	hsa-miR-126-3p	Up	4	MIMAT0000445
Urquidi et al.	2016	Oncotarget	Human	Bladder cancer	Urothelial portion in urine	Up	hsa-miR-1305	Down	1	MIMAT0005893
Urquidi et al.	2016	Oncotarget	Human	Bladder cancer	Urothelial portion in urine	Up	hsa-miR-140-3p	Up	1	MIMAT0004597
Urquidi et al.	2016	Oncotarget	Human	Bladder cancer	Urothelial portion in urine	Up	hsa-miR-140-5p	Up	3	MIMAT0000431
Urquidi et al.	2016	Oncotarget	Human	Bladder cancer	Urothelial portion in urine	Up	hsa-miR-142-3p	Up	3	MIMAT0000434
Urquidi et al.	2016	Oncotarget	Human	Bladder cancer	Urothelial portion in urine	Up	hsa-miR-142-5p	Up	2	MIMAT0000433
Urquidi et al.	2016	Oncotarget	Human	Bladder cancer	Urothelial portion in urine	Up	hsa-miR-143-3p	Up	6	MIMAT0000435
Urquidi et al.	2016	Oncotarget	Human	Bladder cancer	Urothelial portion in urine	Up	hsa-miR-145-5p	Up	3	MIMAT0000437
Urquidi et al.	2016	Oncotarget	Human	Bladder cancer	Urothelial portion in urine	Up	hsa-miR-146a-5p	Up	5	MIMAT0000449
Urquidi et al.	2016	Oncotarget	Human	Bladder cancer	Urothelial portion in urine	Up	hsa-miR-146b-5p	Up	3	MIMAT0002809
Urquidi et al.	2016	Oncotarget	Human	Bladder cancer	Urothelial portion in urine	Up	hsa-miR-151a-3p	Up	2	MIMAT0000757
Urquidi et al.	2016	Oncotarget	Human	Bladder cancer	Urothelial portion in urine	Up	hsa-miR-181a-5p	Up	6	MIMAT0000256
Urquidi et al.	2016	Oncotarget	Human	Bladder cancer	Urothelial portion in urine	Up	hsa-miR-182-5p	Up	2	MIMAT0000259
Urquidi et al.	2016	Oncotarget	Human	Bladder cancer	Urothelial portion in urine	Up	hsa-miR-18a-5p	Up	6	MIMAT0000072
Urquidi et al.	2016	Oncotarget	Human	Bladder cancer	Urothelial portion in urine	Up	hsa-miR-191-5p	Up	1	MIMAT0000440
Urquidi et al.	2016	Oncotarget	Human	Bladder cancer	Urothelial portion in urine	Up	hsa-miR-199a-3p	Up	5	MIMAT0000232

Author	Year	Journal	Species	Disease	Sample	Dir	miRNA	Dir	N	MIMAT
Urquidi et al.	2016	Oncotarget	Human	Bladder cancer	Urothelial portion in urine	Up	hsa-miR-19a-3p	Up	2	MIMAT0000073
Urquidi et al.	2016	Oncotarget	Human	Bladder cancer	Urothelial portion in urine	Up	hsa-miR-19b-3p	Up	1	MIMAT0000074
Urquidi et al.	2016	Oncotarget	Human	Bladder cancer	Urothelial portion in urine	Up	hsa-miR-200a-3p	Up	1	MIMAT0000682
Urquidi et al.	2016	Oncotarget	Human	Bladder cancer	Urothelial portion in urine	Up	hsa-miR-200c-3p	Up	3	MIMAT0000617
Urquidi et al.	2016	Oncotarget	Human	Bladder cancer	Urothelial portion in urine	Up	hsa-miR-20a-5p	Up	3	MIMAT0000075
Urquidi et al.	2016	Oncotarget	Human	Bladder cancer	Urothelial portion in urine	Up	hsa-miR-20b-5p	Up	2	MIMAT0001413
Urquidi et al.	2016	Oncotarget	Human	Bladder cancer	Urothelial portion in urine	Up	hsa-miR-221-3p	Up	4	MIMAT0000278
Urquidi et al.	2016	Oncotarget	Human	Bladder cancer	Urothelial portion in urine	Up	hsa-miR-222-3p	Up	2	MIMAT0000279
Urquidi et al.	2016	Oncotarget	Human	Bladder cancer	Urothelial portion in urine	Up	hsa-miR-223-3p	Up	7	MIMAT0000280
Urquidi et al.	2016	Oncotarget	Human	Bladder cancer	Urothelial portion in urine	Up	hsa-miR-224-5p	Up	1	MIMAT0000281
Urquidi et al.	2016	Oncotarget	Human	Bladder cancer	Urothelial portion in urine	Up	hsa-miR-26a-5p	Up	4	MIMAT0000082
Urquidi et al.	2016	Oncotarget	Human	Bladder cancer	Urothelial portion in urine	Up	hsa-miR-26b-5p	Up	5	MIMAT0000083
Urquidi et al.	2016	Oncotarget	Human	Bladder cancer	Urothelial portion in urine	Up	hsa-miR-324-3p	Up	2	MIMAT0000762
Urquidi et al.	2016	Oncotarget	Human	Bladder cancer	Urothelial portion in urine	Up	hsa-miR-339-3p	Up	2	MIMAT0004702
Urquidi et al.	2016	Oncotarget	Human	Bladder cancer	Urothelial portion in urine	Up	hsa-miR-429	Up	1	MIMAT0001536
Urquidi et al.	2016	Oncotarget	Human	Bladder cancer	Urothelial portion in urine	Up	hsa-miR-491-5p	Up	1	MIMAT0002807
Urquidi et al.	2016	Oncotarget	Human	Bladder cancer	Urothelial portion in urine	Up	hsa-miR-573	Up	1	MIMAT0003238
Urquidi et al.	2016	Oncotarget	Human	Bladder cancer	Urothelial portion in urine	Up	hsa-miR-93-5p	Up	2	MIMAT0000093
Urquidi et al.	2016	Oncotarget	Human	Bladder cancer	Urothelial portion in urine	Up	hsa-miR-96-5p	Up	1	MIMAT0000095
Urquidi et al.	2016	Oncotarget	Human	Bladder cancer	Urothelial portion in urine	Up	hsa-miR-99b-5p	Up	4	MIMAT0000689
Vegter et al.	2017	Clinical Research in Cardiology	Human	Heart failure	Plasma	Down	hsa-miR-18a-5p	Down	6	MIMAT0000072
Vegter et al.	2017	Clinical Research in Cardiology	Human	Heart failure	Plasma	Down	hsa-miR-199a-3p	Down	5	MIMAT0000232
Vegter et al.	2017	Clinical Research in Cardiology	Human	Heart failure	Plasma	Down	hsa-miR-223-3p	Down	7	MIMAT0000280
Vegter et al.	2017	Clinical Research in Cardiology	Human	Heart failure	Plasma	Down	hsa-miR-27a-3p	Down	5	MIMAT0000084
Walker et al.	2015	Journal of Psychiatric Research	Human	Bipolar disorder	Whole blood	Up	hsa-miR-132-3p	Up	1	MIMAT0000426
Walker et al.	2015	Journal of Psychiatric Research	Human	Bipolar disorder	Whole blood	Up	hsa-miR-15b-5p	Up	5	MIMAT0000417
Wang et al.	2019	Clinical Epigenetics	Human	Venous thromboembolism	Plasma	Down	hsa-miR-103a-3p	Down	4	MIMAT0000101
Wang et al.	2019	Clinical Epigenetics	Human	Venous thromboembolism	Plasma	Down	hsa-miR-106a-5p	Down	4	MIMAT0000103
Wang et al.	2019	Clinical Epigenetics	Human	Venous thromboembolism	Plasma	Down	hsa-miR-146b-5p	Up	3	MIMAT0002809
Wang et al.	2019	Clinical Epigenetics	Human	Venous thromboembolism	Plasma	Down	hsa-miR-15b-5p	Up	5	MIMAT0000417
Wang et al.	2019	Clinical Epigenetics	Human	Venous thromboembolism	Plasma	Down	hsa-miR-197-3p	Down	3	MIMAT0000227
Wang et al.	2019	Clinical Epigenetics	Human	Venous thromboembolism	Plasma	Down	hsa-miR-21-5p	Up	6	MIMAT0000076
Wang et al.	2019	Clinical Epigenetics	Human	Venous thromboembolism	Plasma	Down	hsa-miR-222-3p	Up	2	MIMAT0000279
Wang et al.	2019	Clinical Epigenetics	Human	Venous thromboembolism	Plasma	Down	hsa-miR-22-3p	Up	3	MIMAT0000077
Wang et al.	2019	Clinical Epigenetics	Human	Venous thromboembolism	Plasma	Down	hsa-miR-26b-5p	Up	5	MIMAT0000083
Wang et al.	2019	Clinical Epigenetics	Human	Venous thromboembolism	Plasma	Down	hsa-miR-27b-3p	Down	3	MIMAT0000419
Wang et al.	2019	Clinical Epigenetics	Human	Venous thromboembolism	Plasma	Down	hsa-miR-30c-5p	Up	2	MIMAT0000244
Wang et al.	2019	Clinical Epigenetics	Human	Venous thromboembolism	Plasma	Down	hsa-miR-361-5p	Down	2	MIMAT0000703
Wang et al.	2019	Clinical Epigenetics	Human	Venous thromboembolism	Plasma	Down	hsa-miR-532-5p	Up	3	MIMAT0002888
Wang et al.	2020	Journal of Nephrology	Human	End-stage kidney failure	Plasma	Down	hsa-miR-126-5p	Down	1	MIMAT0000444
Wang et al.	2020	Journal of Nephrology	Human	End-stage kidney failure	Plasma	Down	hsa-miR-423-5p	Up	5	MIMAT0004748
Wang et al.	2020	Journal of Nephrology	Human	End-stage kidney failure	Plasma	Down	hsa-miR-92a-3p	Down	2	MIMAT0000092
Xu et al.	2017	Neoplasma	Human	Colorectal cancer	Tumour tissue	Down	hsa-let-7a-5p	Down	3	MIMAT0000062
Xu et al.	2017	Neoplasma	Human	Colorectal cancer	Tumour tissue	Down	hsa-miR-181a-5p	Down	6	MIMAT0000256
Xu et al.	2017	Neoplasma	Human	Colorectal cancer	Tumour tissue	Down	hsa-miR-197-3p	Down	3	MIMAT0000227
Xu et al.	2017	Neoplasma	Human	Colorectal cancer	Tumour tissue	Down	hsa-miR-32-5p	Up	2	MIMAT0000090
Xu et al.	2017	Neoplasma	Human	Colorectal cancer	Tumour tissue	Down	hsa-miR-328-3p	Down	3	MIMAT0000752
Xu et al.	2017	Neoplasma	Human	Colorectal cancer	Tumour tissue	Down	hsa-miR-505-3p	Down	1	MIMAT0002876
Zhang et al.	2014	Journal of Diabetes Research	Rat	Diabetes	Blood	Down	rno-let-7b-5p	Up	1	MIMAT0000775
Zhang et al.	2014	Journal of Diabetes Research	Rat	Diabetes	Blood	Down	rno-let-7e-5p	Up	1	MIMAT0000777
Zhang et al.	2014	Journal of Diabetes Research	Rat	Diabetes	Blood	Down	rno-miR-10b-5p	Up	1	MIMAT0000783
Zhang et al.	2014	Journal of Diabetes Research	Rat	Diabetes	Blood	Down	rno-miR-134-5p	Down	1	MIMAT0000840
Zhang et al.	2014	Journal of Diabetes Research	Rat	Diabetes	Blood	Down	rno-miR-142-5p	Up	1	MIMAT0000847
Zhang et al.	2014	Journal of Diabetes Research	Rat	Diabetes	Blood	Down	rno-miR-188-5p	Up	1	MIMAT0005301
Zhang et al.	2014	Journal of Diabetes Research	Rat	Diabetes	Blood	Down	rno-miR-200a-3p	Up	1	MIMAT0000874
Zhang et al.	2014	Journal of Diabetes Research	Rat	Diabetes	Blood	Down	rno-miR-208a-3p	Up	1	MIMAT0000880
Zhang et al.	2014	Journal of Diabetes Research	Rat	Diabetes	Blood	Down	rno-miR-296-5p	Up	1	MIMAT0000898
Zhang et al.	2014	Journal of Diabetes Research	Rat	Diabetes	Blood	Down	rno-miR-301b-3p	Down	1	MIMAT0005304
Zhang et al.	2014	Journal of Diabetes Research	Rat	Diabetes	Blood	Down	rno-miR-30d-5p	Up	1	MIMAT0000807
Zhang et al.	2014	Journal of Diabetes Research	Rat	Diabetes	Blood	Down	rno-miR-336-5p	Up	1	MIMAT0000576
Zhang et al.	2014	Journal of Diabetes Research	Rat	Diabetes	Blood	Down	rno-miR-375-3p	Up	1	MIMAT0005307
Zhang et al.	2014	Journal of Diabetes Research	Rat	Diabetes	Blood	Down	rno-miR-448-3p	Up	1	MIMAT0001534

Zhang et al.	2014	Journal of Diabetes Research	Rat	Diabetes	Blood	Down	rno-miR-500-3p	Up	1	MIMAT0005321
Zhang et al.	2014	Journal of Diabetes Research	Rat	Diabetes	Blood	Down	rno-miR-501-5p	Up	1	MIMAT0003116
Zhang et al.	2014	Journal of Diabetes Research	Rat	Diabetes	Blood	Down	rno-miR-540-3p	Up	1	MIMAT0003174
Zhang et al.	2014	Journal of Diabetes Research	Rat	Diabetes	Blood	Down	rno-miR-874-3p	Up	1	MIMAT0005284
Zhang et al.	2014	Journal of Diabetes Research	Rat	Diabetes	Blood	Down	rno-miR-879-5p	Up	1	MIMAT0005287
Zhang et al.	2014	Journal of Diabetes Research	Rat	Diabetes	Blood	Down	rno-miR-880-3p	Up	1	MIMAT0005288
Zhao et al.	2013	Asian Pacific Journal of Cancer Prevention	Human	Oesophageal cancer	Tumour tissue	Up	hsa-let-7e-5p	Down	1	MIMAT0000066
Zhao et al.	2013	Asian Pacific Journal of Cancer Prevention	Human	Oesophageal cancer	Tumour tissue	Up	hsa-miR-103a-3p	Down	4	MIMAT0000101
Zhao et al.	2013	Asian Pacific Journal of Cancer Prevention	Human	Oesophageal cancer	Tumour tissue	Up	hsa-miR-125a-5p	Up	3	MIMAT0000443
Zhao et al.	2013	Asian Pacific Journal of Cancer Prevention	Human	Oesophageal cancer	Tumour tissue	Up	hsa-miR-130b-3p	Down	2	MIMAT0000691
Zhao et al.	2013	Asian Pacific Journal of Cancer Prevention	Human	Oesophageal cancer	Tumour tissue	Up	hsa-miR-146b-5p	Up	3	MIMAT0002809
Zhao et al.	2013	Asian Pacific Journal of Cancer Prevention	Human	Oesophageal cancer	Tumour tissue	Up	hsa-miR-186-5p	Up	1	MIMAT0000456
Zhao et al.	2013	Asian Pacific Journal of Cancer Prevention	Human	Oesophageal cancer	Tumour tissue	Up	hsa-miR-196b-5p	Up	2	MIMAT0001080
Zhao et al.	2013	Asian Pacific Journal of Cancer Prevention	Human	Oesophageal cancer	Tumour tissue	Up	hsa-miR-200c-3p	Up	3	MIMAT0000617
Zhao et al.	2013	Asian Pacific Journal of Cancer Prevention	Human	Oesophageal cancer	Tumour tissue	Up	hsa-miR-205-5p	Up	1	MIMAT0000266
Zhao et al.	2013	Asian Pacific Journal of Cancer Prevention	Human	Oesophageal cancer	Tumour tissue	Up	hsa-miR-23b-3p	Up	2	MIMAT0000418
Zhao et al.	2013	Asian Pacific Journal of Cancer Prevention	Human	Oesophageal cancer	Tumour tissue	Up	hsa-miR-29a-3p	Up	6	MIMAT0000086
Zhao et al.	2013	Asian Pacific Journal of Cancer Prevention	Human	Oesophageal cancer	Tumour tissue	Up	hsa-miR-31-5p	Up	2	MIMAT0000089
Zhao et al.	2013	Asian Pacific Journal of Cancer Prevention	Human	Oesophageal cancer	Tumour tissue	Up	hsa-miR-376a-3p	Up	2	MIMAT0000729
Zhao et al.	2013	Asian Pacific Journal of Cancer Prevention	Human	Oesophageal cancer	Tumour tissue	Up	hsa-miR-410-3p	Up	1	MIMAT0002171
Zhao et al.	2013	Asian Pacific Journal of Cancer Prevention	Human	Oesophageal cancer	Tumour tissue	Up	hsa-miR-532-3p	Up	2	MIMAT0004780
Zhao et al.	2013	Asian Pacific Journal of Cancer Prevention	Human	Oesophageal cancer	Tumour tissue	Up	hsa-miR-598-3p	Up	1	MIMAT0003266
Zhou et al.	2015	Cancer Letters	Human	Non-small cell lung cancer	Serum	Up	hsa-miR-194-5p	Up	2	MIMAT0000460
Zhou et al.	2015	Cancer Letters	Human	Non-small cell lung cancer	Serum	Up	hsa-miR-660-5p	Up	2	MIMAT0003338
Zurawek et al.	2018	Diabetes Research and Clinical Practice	Human	Diabetes	PBMCs	Up	hsa-let-7d-3p	Down	2	MIMAT0004484
Zurawek et al.	2018	Diabetes Research and Clinical Practice	Human	Diabetes	PBMCs	Up	hsa-miR-1247-3p	Down	1	MIMAT0022721
Zurawek et al.	2018	Diabetes Research and Clinical Practice	Human	Diabetes	PBMCs	Up	hsa-miR-3180	Down	1	MIMAT0018178
Zurawek et al.	2018	Diabetes Research and Clinical Practice	Human	Diabetes	PBMCs	Up	hsa-miR-3180-3p	Down	1	MIMAT0015058
Zurawek et al.	2018	Diabetes Research and Clinical Practice	Human	Diabetes	PBMCs	Up	hsa-miR-3652	Down	1	MIMAT0018072
Zurawek et al.	2018	Diabetes Research and Clinical Practice	Human	Diabetes	PBMCs	Up	hsa-miR-4750-5p	Down	1	MIMAT0019887
Zurawek et al.	2018	Diabetes Research and Clinical Practice	Human	Diabetes	PBMCs	Up	hsa-miR-487a-3p	Up	1	MIMAT0002178
Zurawek et al.	2018	Diabetes Research and Clinical Practice	Human	Diabetes	PBMCs	Up	hsa-miR-885-3p	Down	1	MIMAT0004948

Targets and regulation of microRNA-652-3p in homeostasis and disease

Maxwell T. Stevens[a], Bernadette M. Saunders[a,b#]

Cellular and Molecular Life Sciences

[a]School of Life Sciences, Faculty of Science, University of Technology Sydney, Sydney, NSW, Australia

[b]Centenary Institute, The University of Sydney, Sydney, NSW, Australia

[#]Address correspondence to Bernadette M. Saunders, bernadette.saunders@uts.edu.au

Online Resource 2 Identified disease biomarker signatures utilising miR-652-3p

Author	Year	Journal	Species	Indication/disease	miRNA location	Change
Andersen et al.	2014	Journal of Molecular Diagnostics	Human	Malignant pleural mesothelioma	Tumour biopsy	Downregulated
Barry et al.	2018	Journal of Infection	Human	Tuberculosis	Plasma	Downregulated
Carreras-Badosa et al.	2015	Journal of Clinical Endocrinology & Metabolism	Human	Gestational obesity	Plasma	Downregulated
Cuk et al.	2013	PLOS One	Human	Breast cancer	Plasma	Upregulated
Ji et al.	2018	Ebiomedicine	Human	Colorectal cancer	Serum	No difference
Kanaan et al.	2013	Annals of Surgery	Human	Colorectal adenoma (pre-cancer)	Plasma	Upregulated
Lai et al.	2011	PLOS One	Human	Schizophrenia	PBMCs	Upregulated
Lai et al.	2016	Translational Psychiatry	Human	Schizophrenia	PBMCs and brain tissue	None
Lee et al.	2018	Frontiers in Psychiatry	Human	Internet gaming disorder	Plasma	Downregulated
McDermott et al.	2014	PLOS One	Human	Breast cancer	Blood and tissue	Downregulated
Ovchinnikova et al.	2016	European Journal of Heart Failure	Human	Heart failure	Plasma	Downregulated
Roderburg et al.	2012	PLOS One	Human	Liver cirrhosis	Serum, circulating leukocytes	Downregulated
Sahlberg et al.	2015	Clinical Cancer Research	Human	Breast cancer	Serum	Upregulated
Shin et al.	2015	Molecular Cancer	Human	Gastric cancer	Plasma	Upregulated
Urquidi et al.	2016	Oncotarget	Human	Bladder cancer	Urothelial portion in urine	Upregulated
Xu et al.	2017	Neoplasma	Human	Colorectal cancer	Tumour tissue	Upregulated
Zhou et al.	2015	Cancer Letters	Human	NSCLC (non-small cell lung cancer)	Serum	Upregulated

Targets and regulation of microRNA-652-3p in homeostasis and disease

Maxwell T. Stevens[a], Bernadette M. Saunders[a,b#]
Cellular and Molecular Life Sciences

[a]School of Life Sciences, Faculty of Science, University of Technology Sydney, Sydney, NSW, Australia
[b]Centenary Institute, The University of Sydney, Sydney, NSW, Australia
[#]Address correspondence to Bernadette M. Saunders, bernadette.saunders@uts.edu.au

Online Resource 3 Sequences used for inter-species alignment analysis of validated miR-652-3p target genes

Species	Gene	Accession number	
Mus musculus	Rora	NM_013646.2	
Homo sapiens	RORA	NM_134261.3	
Mus musculus	Arrb1	NM_177231.2	
Homo sapiens	ARRB1	NM_004041.5	
Mus musculus	Mtp18	NM_026443.4	
Homo sapiens	MTP18	NM_016498.5	
Mus musculus	Enpp1	NM_001308327.1	
Homo sapiens	ENPP1	NM_006208.3	
Homo sapiens	LLGL1	NM_004140.4	
Mus musculus	Llgl1	NM_001159405.2	
Homo sapiens	ZEB1	NM_001128128.3	
Mus musculus	Zeb1	NM_011546.3	
Homo sapiens	JAG1	NM_000214.3	
Mus musculus	Jag1	NM_013822.5	
Homo sapiens	HOXA9	NG_029923.1	
Mus musculus	Hoxa9	AC113985.11	Reverse
Mus musculus	Foxk1	NM_199068.2	
Homo sapiens	FOXK1	NM_001037165.2	
Homo sapiens	FGFR1	NM_023110.3	
Mus musculus	Fgfr1	NM_010206.3	
Homo sapiens	KCNN3	NM_002249.6	
Mus musculus	Kcnn3	NM_080466.2	
Homo sapiens	CCND2	NM_001759.4	
Mus musculus	Ccnd2	NM_009829.3	
Homo sapiens	ISL1	NM_002202.3	
Mus musculus	Isl1	NM_021459.4	
Homo sapiens	KLF9	NM_001206.4	
Mus musculus	Klf9	NM_010638.5	

Appendix 3

Published paper for Chapter 2 "Macrophages of different tissue origin exhibit distinct inflammatory responses to mycobacterial infection"

SHORT COMMUNICATION

Macrophages of different tissue origin exhibit distinct inflammatory responses to mycobacterial infection

Maxwell T Stevens[1] (iD), Beatrice D Nagaria[2], Warwick J Britton[2,3,4] (iD) & Bernadette M Saunders[1,2] (iD)

1 School of Life Sciences, Faculty of Science, University of Technology Sydney, Sydney, NSW, Australia
2 Centenary Institute, The University of Sydney, Sydney, NSW, Australia
3 Central Clinical School, Faculty of Medicine and Health, The University of Sydney, Sydney, NSW, Australia
4 Department of Clinical Immunology, Royal Prince Alfred Hospital, Camperdown, NSW, Australia

Abstract

Macrophages display marked plasticity with functions in both inflammation and tissue repair. Evidence demonstrates that this spectrum of macrophage phenotypes is influenced by their local microenvironment and tissue origin. However, *in vitro* macrophage experiments often do not or cannot readily use macrophages from the most relevant tissue of origin. This study investigated if the origin of two C57BL/6 mouse macrophage cell lines of alveolar (AMJ2-C11) and peritoneal (IC-21) origin may influence their response to mycobacterial infection. Both cell lines equally controlled the growth of *Mycobacterium bovis* BCG and *Mycobacterium tuberculosis*, although the expression of all proinflammatory cytokines and chemokines measured (TNF, IL-6, MCP-1, MIP-1α, MIP-1β, and RANTES) was significantly higher in AMJ2-C11 cells than in IC-21 cells. During *M. tuberculosis* infection, IL-6, MCP-1, and RANTES expression increased 5-fold, and MIP-1β expression increased 30-fold. Additionally, AMJ2-C11 cells exhibited significantly higher inducible nitric oxide synthase activity than IC-21 cells, indicative of a more polarized M1 response. The expression of multiple surface markers was also assessed by flow cytometry. CD80 and CD86 were significantly upregulated in AMJ2-C11 cells and downregulated in IC-21 cells during *M. tuberculosis* infection. The results support the notion that the origin of tissue-resident macrophages influences their phenotype and antimicrobial response and demonstrate hereto unrecognized potential for these cell lines in *in vitro* studies.

INTRODUCTION

Macrophages are often the first leukocytes to interact with invading pathogens and form an integral part of the innate and adaptive immune systems. Macrophage activity is influenced by environmental stimuli and the macrophage phenotype is often lineated into two categories. M1 macrophages are produced *in vitro* by stimulation with pathogen-associated molecules such as lipopolysaccharide, with or without GM-CSF or IFN-γ, and express proinflammatory cytokines including IL-1β, IL-6, IL-12, and TNF.[1,2] By contrast, Th2-related or anti-inflammatory cytokines such as IL-4, IL-13, IL-10, and

TGF-β stimulate M2 macrophages, expressing arginase 1 (ARG1) and the anti-inflammatory cytokine IL-10.[3] Macrophage plasticity allows switching between the M1 and M2 phenotypes as stimuli change.[4] Recent studies have demonstrated that a binary M1-M2 phenotype classification does not apply universally to many tissue-resident macrophage subtypes, and that the macrophage phenotype is strongly influenced by the tissue of origin.[5]

Local tissue microenvironments and disease states generate gene expression profiles unique to tissue-resident macrophage subtypes, modulating the gene enhancer landscape of transplanted macrophages to produce a spectrum of M1-M2 phenotypes.[6] Retinoic acid produced

in the mouse peritoneal cavity induces expression of the peritoneal macrophage-specific transcription factor GATA6, which in turn induces TGF-β and ARG1 production, both M2 markers.[7] GATA6 is downregulated when peritoneal macrophages are transplanted to the lung.[6] Peritoneal macrophages express typical M2 macrophage markers, including CD206 and TGF-β.[5,8] In comparison, alveolar macrophages commonly express both M2 marker CD206 as well as M1 marker CD86 in steady state.[9] The percentage of alveolar macrophages expressing CD206 and M1-activation associated enzyme, inducible nitrogen oxide synthase (iNOS), is increased in smokers and chronic obstructive pulmonary disease patients.[10] Acute *Mycobacterium tuberculosis* infection drives mouse alveolar macrophages toward an iNOS$^+$ M1 phenotype, before switching to an ARG1$^+$ M2 phenotype as chronic infection persists.[11]

Many *in vitro* studies utilize immortalized phagocyte cell lines, such as human THP-1 or murine RAW 264.7 cells, or commonly differentiate macrophages from circulating human monocytes or mouse bone marrow progenitors. The polarity of mouse bone marrow-derived macrophages (BMDM) depends heavily on the cytokines used in their differentiation.[12] BMDMs differentiated with GM-CSF and M-CSF are phenotypically M1 and M2, respectively, the former expressing TNF and IL-6, whilst the latter secrete IL-10 and CCL2.[13] Studies in M-CSF deficient mice identified that M-CSF was essential for the *in vivo* development of peritoneal macrophages, but not alveolar macrophages.[14] Secreted cytokine levels may vary markedly between macrophage cell lines and change during extended culture.[15] Variability in the steady state phenotype of model cells may influence the cell's response to *M. tuberculosis* infection.

Here we examine the response to mycobacterial infection by two immortalized C57BL/6 mouse macrophage cell lines of peritoneal and alveolar origin. We compare the ability of each cell line to control bacterial growth, demonstrating distinct proinflammatory cytokine expression patterns and differing iNOS activity in macrophage cell lines of different tissue origin. We demonstrate a more M1 phenotypic profile in the AMJ2-C11 cells compared with the IC-21 cells, and this also influences the surface receptor expression patterns associated with mycobacterial infection.

RESULTS

Macrophages from distinct origins retain control of mycobacterial growth

In order to assess the effect of tissue origin on the ability of macrophages to control mycobacteria, bacterial growth in AMJ2-C11 and IC-21 cultures were measured over time. Bacterial loads in *Mycobacterium bovis* Bacillus Calmette-Guérin (BCG)-infected macrophages remained stable up to 24 h post-infection (hpi), with both cell lines showing mycobacterial killing by 48 h ($P < 0.05$, Figure 1a). Macrophages infected with *M. tuberculosis* exhibited a stable bacterial load over the 48 h infection, and there was no significant difference in the capacity to control bacterial growth between the two cell lines (Figure 1b).

iNOS activity is influenced by macrophage tissue origin

The proinflammatory iNOS activity of the macrophage cell lines was compared through quantification of nitrite, a downstream product of NO. AMJ2-C11 macrophages exhibited more iNOS activity than IC-21 macrophages (Figure 1c). BCG infection of AMJ2-C11 cells induced significantly more nitrate than BCG infection of IC-21 cells. AMJ2-C11 cells produced similar nitrite levels during BCG and *M. tuberculosis* infection. No nitrite production by IC-21 cells was detected following *M. tuberculosis* infection.

Increased proinflammatory cytokines expression in alveolar macrophages

The inflammatory response of these macrophages during mycobacterial infection were investigated by measuring the cell lines' proinflammatory cytokine expression during BCG and *M. tuberculosis* infection. Infection with the less virulent BCG induced more cytokine and chemokine expression in both cell lines compared with infection with the more virulent *M. tuberculosis*. In particular, the production of the chemokines IL-6, TNF, MCP-1, and MIP-1β was increased considerably during BCG infection (Figure 2).

Bacillus Calmette-Guérin infection induced a similar cytokine response from both cell lines (Figure 2a), although the production of the chemokines MIP-1α and MIP-1β was increased in IC-21 cells at 6 and 24 hpi, respectively, whilst RANTES production in AMJ2-C11 cells was almost 9-fold higher at 24 hpi (Figure 2a). Late IL-6 and MCP-1 expression was significantly higher at 48 hpi in AMJ2-C11 cells. A significant decrease in bacterial load at 24–48 hpi (Figure 1a) coincided with increases in cytokine expression, particularly MIP-1β, MCP-1, and IL-6.

However, *M. tuberculosis* infection induced differential responses between the cell lines. AMJ2-C11 cells expressed over 5-fold more IL-6, MCP-1, and RANTES, and more than 30-fold more MIP-1β at 48 hpi compared with IC-21 cells (Figure 2b).
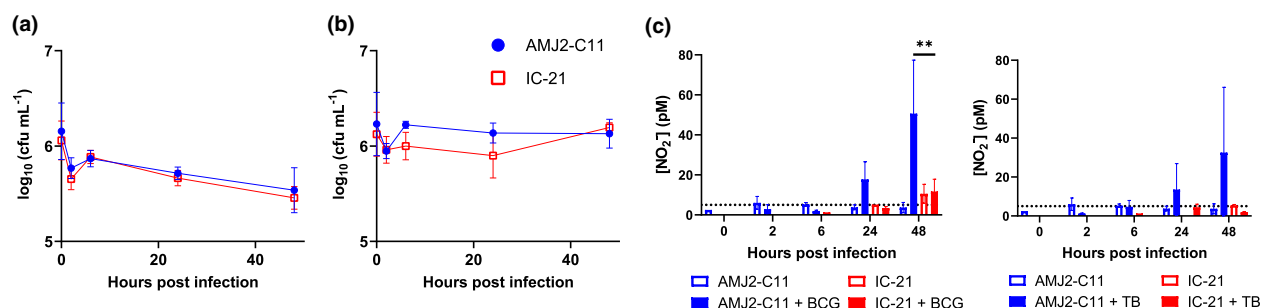
Figure 1. Bacterial growth in alveolar AMJ2-C11 and peritoneal IC-21 macrophage cultures infected with **(a)** BCG and **(b)** *Mycobacterium tuberculosis*. Data are the mean ± s.e.m. of nine replicates, from three repeat experiments. **(c)** Supernatant nitrite concentration of AMJ2-C11 and IC-21 macrophage cultures during BCG and *M. tuberculosis* infection. Data are the mean ± s.d. of nine replicate wells, from three repeat experiments. Dotted lines represent the assay's lower limit of quantitation. **P < 0.01, by the Student's *t*-test, Holm-Šidák method corrected.
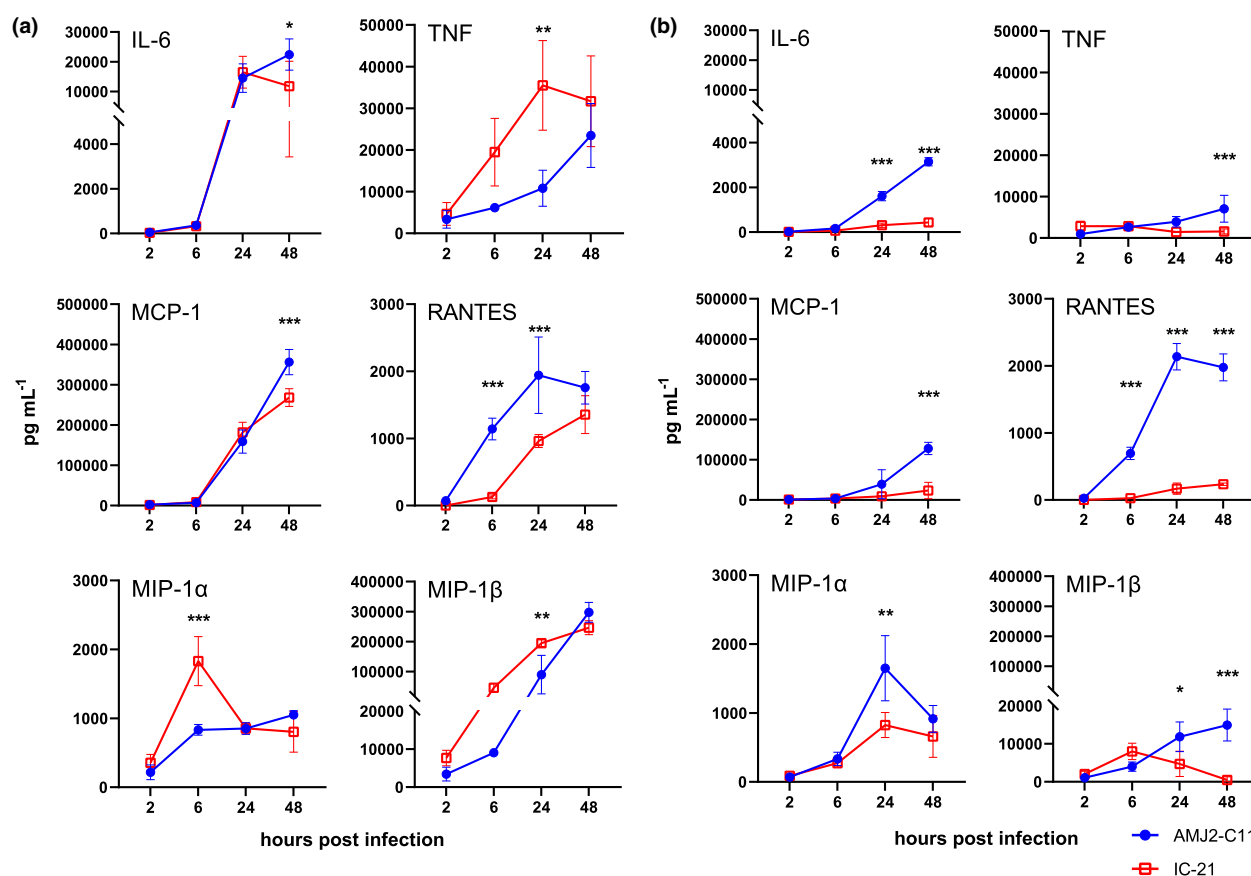
Figure 2. Increased cytokine expression by AMJ2-C11 alveolar macrophages compared with IC-21 peritoneal macrophages following infection with **(a)** BCG or **(b)** *M. tuberculosis*, relative to uninfected cells. Data are the mean ± s.d. of triplicate wells, representative of three repeat experiments. Repeat experiment data are shown in Supplementary figures 3 and 4. Asterisks represent significant difference between AMJ2-C11 and IC-21 expression by 2-way ANOVA with multiple comparisons post-test, Šidák method corrected. *P < 0.05, **P < 0.01, ***P < 0.001.

Surface phenotype of alveolar macrophages indicates stronger proinflammatory response to mycobacterial infection

Cell surface marker expression is an indicator of macrophage subtype and inflammatory state. We quantitated the expression of 12 cell-surface proteins on AMJ2-C11 and IC-21 cells by flow cytometry, comparing the median fluorescence intensity (MFI) between cell lines, uninfected and after infection with BCG and *M. tuberculosis*. A resazurin fluorescence assay confirmed no decrease in mitochondrial activity following

mycobacterial infection, indicating that the cells remain viable at 24 hpi (Supplementary figure 1).

The expression of most markers was greater in uninfected IC-21 cells compared with uninfected AMJ2-C11 cells (Figure 3a). Only Ly6C expression was skewed towards AMJ2-C11 cells, and this difference was exaggerated upon mycobacterial infection. Expression of the M1 marker CD86 was higher in IC-21 peritoneal macrophages prior to infection, though AMJ2-C11 alveolar macrophages showed significantly higher expression after infection. Furthermore, uninfected IC-21 cells expressed more of the M2 marker CD206, as well as CD11b, CD24, and Siglec-F. Expression of these markers was not significantly different between the cell lines during BCG infection, and was similar during *M. tuberculosis* infection. Expression of MHC-II was equivalent on the uninfected cell lines; however, this rose significantly on AMJ2-C11 cells following BCG infection. Expression of the M1 marker CD80, as well as CD11c, Ly6G, and immunoglobulin receptor, CD64, was greater on IC-21 cells under all conditions.

Infection with BCG and *M. tuberculosis* induced comparable responses in AMJ2-C11 macrophages, with increased expression of all tested markers (Figure 3). This activation was also reflected in the strong iNOS (Figure 1c) and cytokine response (Figure 2) from AMJ2-C11 cells to both bacterial species. In contrast, IC-21 cells downregulated Ly-6C upon BCG infection, and downregulated multiple inflammatory markers upon *M. tuberculosis* infection, including CD80 and CD86 (Figure 3). Moreover, downregulation of CD64 and CD11b by *M. tuberculosis* infected IC-21 cells could indicate a shift towards an anti-inflammatory phenotype.

The comparable marker upregulation seen in AMJ2-C11 and IC-21 cells following BCG infection reflects the similar cytokine responses by both cell lines (Figure 2a). In contrast, the downregulation of inflammatory surface markers by IC-21 cells upon *M. tuberculosis* infection coincides with lower cytokine expression (Figure 2b) and undetectable iNOS activity (Figure 1c).

DISCUSSION

Mice are the most commonly used animal model of mycobacterial infection, with C57BL/6 the most common genetic background used. In this study, we compared two C57BL/6 mouse macrophage cell lines of differing tissue origin, in response to *in vitro* mycobacterial infection. Whilst both the AMJ2-C11 alveolar macrophages and IC-21 peritoneal macrophages controlled the growth of BCG and *M. tuberculosis* to the same extent, AMJ2-C11 cells exhibited significantly greater proinflammatory cytokine expression and iNOS activity in response to the bacterial species. Additionally, AMJ2-C11 cells presented a more inflammatory surface phenotype during *M. tuberculosis* infection. The response to infection may be influenced by the tissue origin of the two cell lines.

When using primary macrophages or macrophage-derived cell lines for *in vitro* models of infection, it is important to consider both the site of *in vivo* infection and the origin of the macrophage cells. The IC-21 line was prepared from mouse peritoneal macrophages virally transduced *in vitro*.[16] In contrast, the AMJ2-C11 line was virally immortalized from characterized primary mouse alveolar macrophages[17] and readily expressed proinflammatory cytokines when activated.[18]
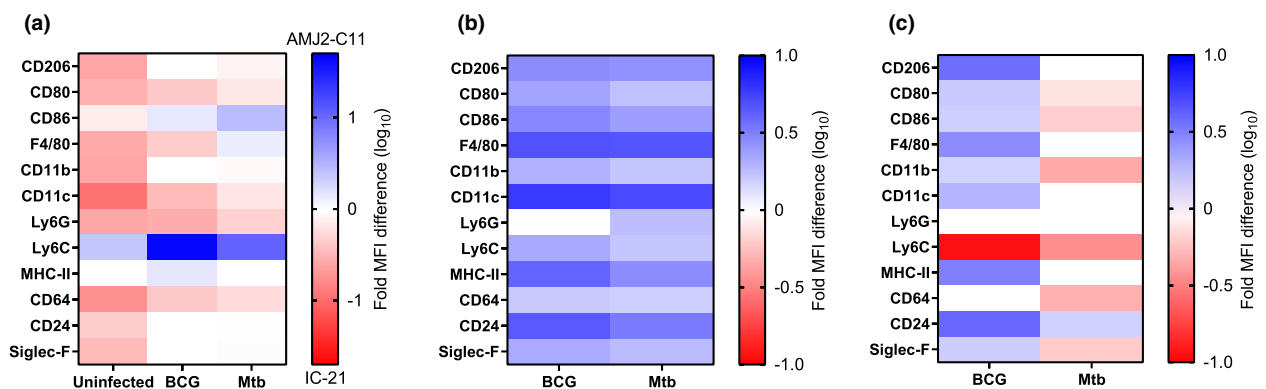

Figure 3. Expression of surface markers on AMJ2-C11 alveolar macrophages and IC-21 peritoneal macrophages during BCG and *Mycobacterium tuberculosis* infection, as determined by flow cytometry. **(a)** Fold MFI difference for surface markers expressed on AMJ2-C11 and IC-21 cells, uninfected, and 24 h after BCG and *M. tuberculosis* infection. Fold difference is a ratio of AMJ2-C11 MFI to IC-21 MFI. **(b)** Fold change in surface marker expression of AMJ2-C11 cells following 24 h mycobacterial infection, compared with uninfected cells. **(c)** Fold change in surface marker expression of IC-21 cells following 24-h mycobacterial infection, compared to uninfected cells. Data are the mean of triplicate wells. All colored rectangles represent $P < 0.05$, the Student's *t*-test, Holm-Šidák method corrected.

Development of a cell-based model of *M. tuberculosis* infection should take into account the basal alveolar macrophage phenotype and cellular changes associated with chronic disease.[10,11] Here we illustrated the polarity and anti-microbial response of the alveolar and peritoneal macrophage cell lines, AMJ2-C11 and IC-21, during acute mycobacterial infection.

During acute *M. tuberculosis* infection *in vitro*, the control of bacterial replication does not appear to be influenced by macrophage origin. THP-1 monocytic cells controlled *M. tuberculosis* load as efficiently as primary human alveolar macrophages over 4 days,[19] and MPI cells, a recently derived murine alveolar macrophage line, exhibited a similar infection pattern to THP-1, RAW 264.7, and BMDM cells.[20] Likewise, this study shows both AMJ2-C11 and IC-21 cells demonstrated comparable control of BCG and *M. tuberculosis* growth during a 48 h infection. However, this may not replicate *in vivo* infection completely, as following intranasal infection in mice, alveolar macrophages were more permissive to intracellular *M. tuberculosis* replication than pulmonary interstitial macrophages.[21] *Ex vivo* lung and peritoneal macrophages comparably controlled *M. tuberculosis* H37Rv bacterial load up to 3 days, before bacterial growth accelerated in lung macrophages.[22] Extended *M. tuberculosis* infection of AMJ2-C11 cells may present similar results.

Cytokine secretion is central to macrophage antimicrobial and anti-inflammatory functions,[2] and pro-inflammatory M1 macrophages release cytokines, including TNF and IL-6, that are critical for anti-mycobacterial protection.[23] We observed significantly greater IL-6 expression from AMJ2-C11 cells, indicative of the M1-primed polarity seen in alveolar macrophages.[9] The alveolar cell line MPI also displays an M1 dominant phenotype, expressing high levels of TNF and IL-6 compared with BMDMs, when infected with *M. tuberculosis*.[20] Like AMJ2-C11 cells, human alveolar macrophages are known to express chemokines associated with an M1 phenotype, including MIP-1α, MIP-1β, and RANTES, following *M. tuberculosis* infection.[24] Although peritoneal macrophage-derived cell lines can also express these chemokines,[15] our results indicate infection-induced chemokine upregulation is delayed (Figure 2).

Alveolar macrophage-expressed MCP-1 recruits circulating monocytes during *M. tuberculosis* infection, aiding in bacterial dissemination.[25,26] In the current study avirulent BCG induced higher MCP-1 expression on AMJ2-C11 cells than virulent *M. tuberculosis* H37Rv. Similarly, primary human alveolar macrophages expressed more MCP-1 when infected with avirulent *M. tuberculosis* H37Ra, compared with H37Rv.[24] We observed IC-21 cells expressed comparable MCP-1 to AMJ2-C11 cells during

BCG infection, but significantly less during *M. tuberculosis* infection. In turn, IC-21 cells expressed more MCP-1 than BMDMs differentiated with M-CSF-containing L929 supernatant.[15] Tissue-resident macrophages are difficult to obtain in large numbers from small laboratory animals and mouse bone marrow is commonly used as a source of macrophages *in vitro* due to the quantity of cells generated. Although BMDMs may be a more practical for many laboratories than primary tissue-resident macrophages, basal phenotypic differences such as chemokine expression should be considered when planning experimentation.

A number of surface protein markers are regularly used to characterize macrophage polarity, including CD206, CD80, and CD86.[2] The M2 marker CD206 is the mannose receptor, involved in post-infection remediation of inflammation, binding bacterial glycoproteins and heavily glycosylated anti-bacterial proteins such as myeloperoxidase.[27] CD206 also facilitates mycobacterial colonization of macrophages.[28] CD80 and CD86 are inflammatory co-receptors required for antigen presentation and T-cell activation.[29] Pro-inflammatory M1 macrophages are known to express high levels of CD80 and CD86,[2] whereas only a subset of M2 macrophages express CD86.[30] We found that CD206, CD80, and CD86 levels were all higher for uninfected IC-21 compared with AMJ2-C11. However, whilst IC-21 upregulation of CD206 was notably higher during BCG infection, AMJ2-C11 cells showed significantly more upregulation of CD80 and CD86 during BCG and TB infection. Studies have shown that during acute *M. tuberculosis* infection, alveolar macrophages present an inflammatory phenotype, with high CD86 expression and strong iNOS activity,[11] similar to what was shown here with AMJ2-C11 alveolar macrophages. Yet, as the granuloma structures typical of chronic tuberculosis develop, macrophages decrease iNOS activity and upregulate the anti-inflammatory cytokine IL-10.[11] The subdued cytokine expression and weak iNOS activity of IC-21 cells during *M. tuberculosis* infection suggests these cells may not be an appropriate model of acute macrophage infection in the lung.

Our findings demonstrate that macrophage cell lines of different tissue-origin display marked differences in their response to infection, and this should be considered when utilizing cell lines in *in vitro* assays. Mycobacterial infection induced significantly increased cytokine expression and iNOS activity in AMJ2-C11 cells, highlighting the M1/M2 phenotype of their alveolar macrophage origin. In contrast, IC-21 cells, whilst still controlling mycobacterial infection over the time frame of this experiment, displayed a more M2 phenotype, with lower cytokine expression and

downregulation of proinflammatory markers. Our work supports the idea that acute *M. tuberculosis* infection models should consider using M1-like macrophages, particularly when using polarity-dependent readouts, such as cytokine expression and surface markers. The development of more alveolar macrophage-representative cell models, such as the MPI cell line,[20] may also aid future tuberculosis research.

METHODS

Cell culture

Murine AMJ2-C11 cells of C57BL/6 origin (ATCC, Manassas, VA, USA) were maintained in DMEM (Thermo Fisher Scientific, Waltham, MA, USA) supplemented with 25 mM HEPES, 100 U mL^{-1} penicillin, 100 μg mL^{-1} streptomycin, and 10% fetal bovine serum. Murine IC-21 cells of C57BL/6 origin (ATCC) were maintained in RPMI 1640 medium (Thermo Fisher Scientific) supplemented with 25 mM HEPES, 100 U mL^{-1} penicillin, 100 μg mL^{-1} streptomycin, and 10% fetal bovine serum.

Bacterial cultures

Mycobacterium bovis Bacillus Calmette-Guérin (BCG) Pasteur and *M. tuberculosis* H37Rv were grown in Middlebrook 7H9 broth (BD Biosciences, Franklin Lakes, NJ, USA) supplemented with 5 g L^{-1} bovine serum albumin (BSA), 2 g L^{-1} glucose, 4 mg L^{-1} catalase, 0.2% glycerol, and 0.05% Tween 20. The cell concentration was routinely determined by OD at 600 nm. CFU was determined by plating serial dilutions on Middlebrook 7H11 agar (BD Biosciences) supplemented with 5 g L^{-1} BSA, 2 g L^{-1} glucose, 4 mg L^{-1} catalase, 500 mg L^{-1} oleic acid, and 0.5% glycerol, and incubating for 3 weeks at 37°C.

Macrophage infections with mycobacteria

The AMJ2-C11 and IC-21 cells were stimulated with 100 U mL^{-1} IFN-γ (R&D Systems, Minneapolis, MN, USA) and infected with BCG or *M. tuberculosis* at a multiplicity of infection of 5 or 1, respectively. The cells were washed after 4–6 h to remove extracellular bacteria. At time points from 0 to 48 h post-infection, the supernatant was removed for cytokine and nitrite quantification. The cells were lysed with 0.1% Triton X-100 solution for CFU determination. The lysates were plated on 7H11 agar and incubated at 37°C for 21 days to determine the CFU.

Cytometric bead array

The concentrations of IL-6, TNF, MCP-1, MIP-1α, MIP-1β, and RANTES in supernatants were determined by cytometric bead array (BD Biosciences) according to the manufacturer's

protocol. Data were analyzed using FCAP Array software (BD Biosciences).

Nitrite assay

Nitrite concentrations of supernatant samples were determined using Griess reagent, consisting of 3.85 mM N-(naphthyl) ethylenediamine dihydrochloride (Sigma-Aldrich, St Louis, MO, USA), 58 mM sulphanilamide (Sigma-Aldrich), and 0.4 M phosphoric acid (Sigma-Aldrich) in water. Nitrite standards were prepared using sodium nitrite (Sigma-Aldrich). Griess reagent was added to supernatant samples at a ratio of 1:1, and the immediate color change was quantified by measuring absorbance at 550 nm using a FLUOstar plate reader (BMG Labtech, Ortenberg, Germany).

Flow cytometry

AMJ2-C11 and IC-21 cells were assessed by flow cytometry before infection and 24 h after infection with BCG or *M. tuberculosis*. The cells were incubated with Fc Block (BD Biosciences) for 30 min and then stained with fluorochrome-labeled antibodies (see Supplementary table 1 for a list of antibodies, clones, fluorochromes, and manufacturers) for 30 min at room temperature in the dark. Stained samples were fixed with 10% neutral buffered formalin (Fronine, Riverstone, NSW, Australia). Data acquisition was performed on a BD Fortessa X20 using the BD FACS Diva software (BD Biosciences). Compensation and data analysis were performed in FlowJo v10 software (BD Biosciences). Cells were gated using forward scatter and side scatter to remove debris and dead cells (see Supplementary figure 2 for an example dot-plot). The expression of surface markers is presented as fold MFI difference. This is calculated as a ratio of individual surface marker expression on infected cells (BCG or *M. tuberculosis*) compared with uninfected cells, or on AMJ2-C11 cells compared with IC-21 cells, both infected (BCG and *M. tuberculosis*) and uninfected.

Cell viability

Macrophage viability was confirmed using a resazurin assay for mitochondrial activity. Macrophages were incubated with 5.5 mM resazurin (Sigma Aldrich) for 3 h at 37°C. Conversion of resazurin to resorufin was evaluated by measuring fluorescence using a FLUOstar plate reader, excitation at 550 nm, emission at 590 nm.

Statistical analysis

GraphPad Prism (GraphPad Software, San Diego, CA, USA) was used for statistical analyses. The CFU and cytokine concentration over time were compared by two-way analysis of variance with multiple comparisons post-test, corrected using the Šidák method. The nitrate concentration and flow cytometry MFI were compared using the Student's *t*-test, corrected for multiple comparisons using the Holm-Šidák method.

ACKNOWLEDGMENTS

AUTHOR CONTRIBUTIONS

Maxwell Stevens: Conceptualization; Data curation; Formal analysis; Investigation; Methodology; Visualization; Writing-original draft; Writing-review & editing. **Beatrice Nagaria:** Conceptualization. **Warwick Britton:** Conceptualization; Funding acquisition; Writing-review & editing. **Bernadette M Saunders:** Conceptualization; Funding acquisition; Methodology; Supervision.

CONFLICT OF INTEREST

The authors declare no conlict of interest.

DATA AVAILABILITY STATEMENT

Raw data can be made available upon request.

REFERENCES

1. Lacey DC, Achuthan A, Fleetwood AJ, *et al.* Defining GM-CSF- and macrophage-CSF dependent macrophage responses by in vitro models. *J Immunol* 2012; **188**: 5752–5765.

2. Shapouri-Moghaddam A, Mohammadian S, Vazini H, *et al.* Macrophage plasticity, polarization, and function in health and disease. *J Cell Physiol* 2018; **233**: 6425–6440.

3. Mantovani A, Biswas SK, Galdiero MR, Sica A, Locati M. Macrophage plasticity and polarization in tissue repair and remodelling. *J Pathol* 2013; **229**: 176–185.

4. Arora S, Dev K, Agarwal B, Das P, Syed MA. Macrophages: their role, activation and polarization in pulmonary diseases. *Immunobiology* 2018; **223**: 383–396.

5. Gosselin D, Link VM, Romanoski CE, *et al.* Environment drives selection and function of enhancers controlling tissue-specific macrophage identities. *Cell* 2014; **159**: 1327–1340.

6. Lavin Y, Winter D, Blecher-Gonen R, *et al.* Tissue-resident macrophage enhancer landscapes are shaped by the local microenvironment. *Cell* 2014; **159**: 1312–1326.

7. Okabe Y, Medzhitov R. Tissue-specific signals control reversible program of localization and functional polarization of macrophages. *Cell* 2014; **157**: 832–844.

8. Bellon T, Martinez V, Lucendo B, *et al.* Alternative activation of macrophages in human peritoneum: implications for peritoneal fibrosis. *Nephrol Dial Transplant* 2011; **26**: 2995–3005.

9. Mitsi E, Kamng'ona R, Rylance J, *et al.* Human alveolar macrophages predominately express combined classical M1 and M2 surface markers in steady state. *Respir Res* 2018; **19**: 66.

10. Bazzan E, Turato G, Tine M, *et al.* Dual polarization of human alveolar macrophages progressively increases with smoking and COPD severity. *Respir Res* 2017; **18**: 40.

11. Redente EF, Higgins DM, Dwyer-Nield LD, Orme IM, Gonzalez-Juarrero M, Malkinson AM. Differential polarization of alveolar macrophages and bone marrow-derived monocytes following chemically and pathogen-induced chronic lung inflammation. *J Leukoc Biol* 2010; **88**: 159–168.

12. Orecchioni M, Ghosheh Y, Pramod AB, Ley K. Macrophage polarization: different gene signatures in M1 (LPS+) vs. classically and M2(LPS-) vs. Alternatively activated macrophages. *Front Immunol* 2019; **10**: 1084.

13. Fleetwood AJ, Lawrence T, Hamilton JA, Cook AD. Granulocyte-macrophage colony-stimulating factor (CSF) and macrophage CSF-dependent macrophage phenotypes display differences in cytokine profiles and transcription factor activities: implications for CSF blockade in inflammation. *J Immunol* 2007; **178**: 5245–5252.

14. Witmer-Pack MD, Hughes DA, Schuler G, *et al.* Identification of macrophages and dendritic cells in the osteopetrotic (op/op) mouse. *J Cell Sci* 1993; **104**: 1021–1029.

15. Chamberlain LM, Holt-Casper D, Gonzalez-Juarrero M, Grainger DW. Extended culture of macrophages from different sources and maturation results in a common M2 phenotype. *J Biomed Mater Res Part A* 2015; **103**: 2864–2874.

16. Mauel J, Defendi V. Infection and transformation of mouse peritoneal macrophages by simian virus 40. *J Exp Med* 1971; **134**: 335–350.

17. Palleroni AV, Varesio L, Wright RB, Brunda MJ. Tumoricidal alveolar macrophage and tumor infiltrating macrophage cell lines. *Int J Cancer* 1991; **49**: 296–302.

18. Oliveira PM, Matos BN, Pereira PAT, *et al.* Microparticles prepared with 50–190 kDa chitosan as promising non-toxic carriers for pulmonary delivery of isoniazid. *Carbohyd. Polym.* 2017; **174**: 421–431.

19. Bai XY, Oberley-Deegan RE, Bai A, *et al.* Curcumin enhances human macrophage control of *Mycobacterium tuberculosis* infection. *Respirology* 2016; **21**: 951–957.

20. Woo M, Wood C, Kwon D, Park KHP, Fejer G, Delorme V. *Mycobacterium tuberculosis* infection and innate responses in a new model of lung alveolar macrophages. *Front Immunol* 2018; **9**: 438.

21. Huang L, Nazarova EV, Tan SM, Liu YC, Russell DG. Growth of *Mycobacterium tuberculosis in vivo* segregates with host macrophage metabolism and ontogeny. *J Exp Med* 2018; **215**: 1135–1152.

22. Guirado E, Rajaram MVS, Chawla A, *et al.* Deletion of PPARγ in lung macrophages provides an immunoprotective response against *M. tuberculosis* infection in mice. *Tuberculosis* 2018; **111**: 170–177.

23. O'Garra A, Redford PS, McNab FW, Bloom CI, Wilkinson RJ, Berry MPR. The immune response in tuberculosis. *Ann Rev Immunol* 2013; **31**: 475–527. In: Littman DR, Yokoyama WM (eds). Annual Review of Immunology. 31. Palo Alto: Annual Reviews.

24. Saukkonen JJ, Bazydlo B, Thomas M, Strieter RM, Keane J, Kornfeld H. β-chemokines are induced by *Mycobacterium tuberculosis* and Inhibit its growth. *Infect Immun* 2002; **70**: 1684–1693.

25. Ansari AW, Kamaruizaman A, Schmidt RE. Multifaceted impact of host C-C chemokine CCL2 in the immuno-pathogenesis of HIV-1/*M. tuberculosis* co-infection. *Front Immunol* 2013; **4**: 312.

26. Cambier CJ, O'Leary SM, O'Sullivan MP, Keane J, Ramakrishnan L. Phenolic glycolipid facilitates mycobacterial escape from microbicidal tissue-resident macrophages. *Immunity* 2017; **47**: 552–565.

27. East L, Isacke CM. The mannose receptor family. *Biochim Biophys Acta* 2002; **1572**: 364–386.

28. Killick KE, Cheallaigh CN, O'Farrelly C, Hokamp K, MacHugh DE, Harris J. Receptor-mediated recognition of mycobacterial pathogens. *Cell Microbiol* 2013; **15**: 1484–1495.

29. Chen CY, Gault A, Shen LJ, Nabavi N. Molecular cloning and expression of early T cell costimulatory molecule-1 and its characterization as B7–2 molecule. *J Immunol* 1994; **152**: 4929–4936.

30. Edwards JP, Zhang X, Frauwirth KA, Mosser DM. Biochemical and functional characterization of three activated macrophage populations. *J Leukoc Biol* 2006; **80**: 1298–1307.

SUPPORTING INFORMATION

Additional supporting information may be found online in the Supporting Information section at the end of the article.

Appendix 4

Supplementary data for Chapter 2 "Macrophages of different tissue origin

exhibit distinct inflammatory responses to mycobacterial infection"

Supplementary table 1. Fluorophore-tagged antibodies used for cell staining in preparation for flow cytometry.

Antigen	Fluorochrome	Clone	Catalogue #	Manufacturer
CD11b	BB515	M1/70	564455	BD Biosciences
CD11c	BV421	N418	565451	BD Biosciences
MHC-II	BV510	2G9	743871	BD Biosciences
Ly6C	BV605	AL-21	563011	BD Biosciences
CD64	BV650	X54-5/7.1	740622	BD Biosciences
Ly6G	BV786	1A8	740953	BD Biosciences
CD206	AF700	C068C2	141734	Biolegend
F4/80	APC eFluor780	BM8	47-4801-82	eBioscience
Siglec F	PE	E50-2440	562068	BD Biosciences
CD80	PE	16-10A1	561955	BD Biosciences
CD86	APC	GL1	558703	BD Biosciences
CD24	PE-CF594	M1/69	562477	BD Biosciences
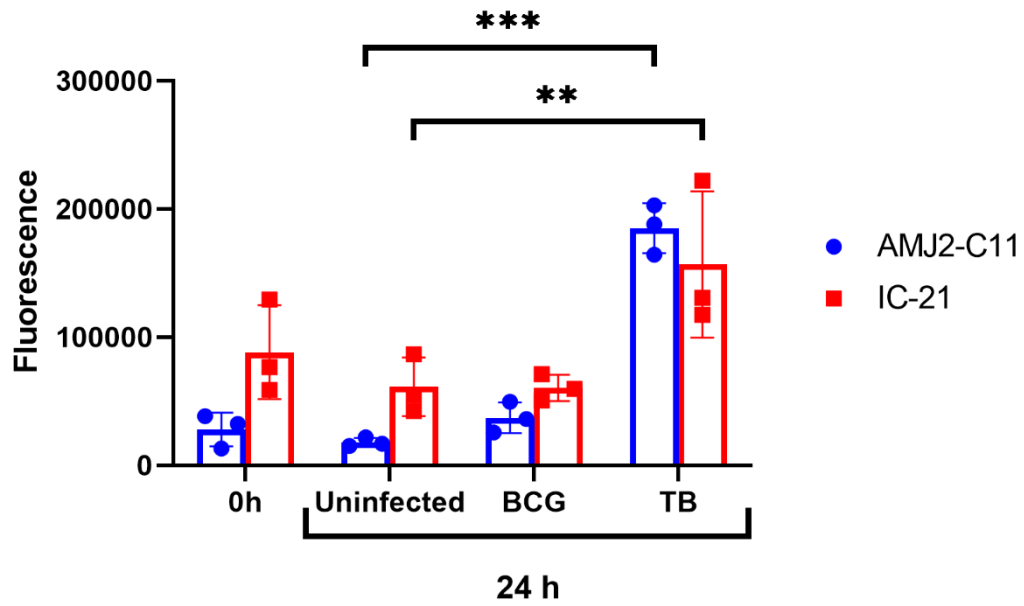
Supplementary figure 1. Mouse macrophage cell lines maintain viability 24 h after mycobacterial infection. Mitochondrial activity is not significantly different 24 h after BCG infection. TB infection causes significantly increased mitochondrial activity in AMJ2-C11 and IC-21 cells. Data are the mean ± SD of triplicate wells, with individual values shown. Asterisks represent significant difference in fluorescence by 2-way ANOVA with multiple comparisons post-test, Šidák method corrected. ** $P < 0.01$, *** $P < 0.001$.
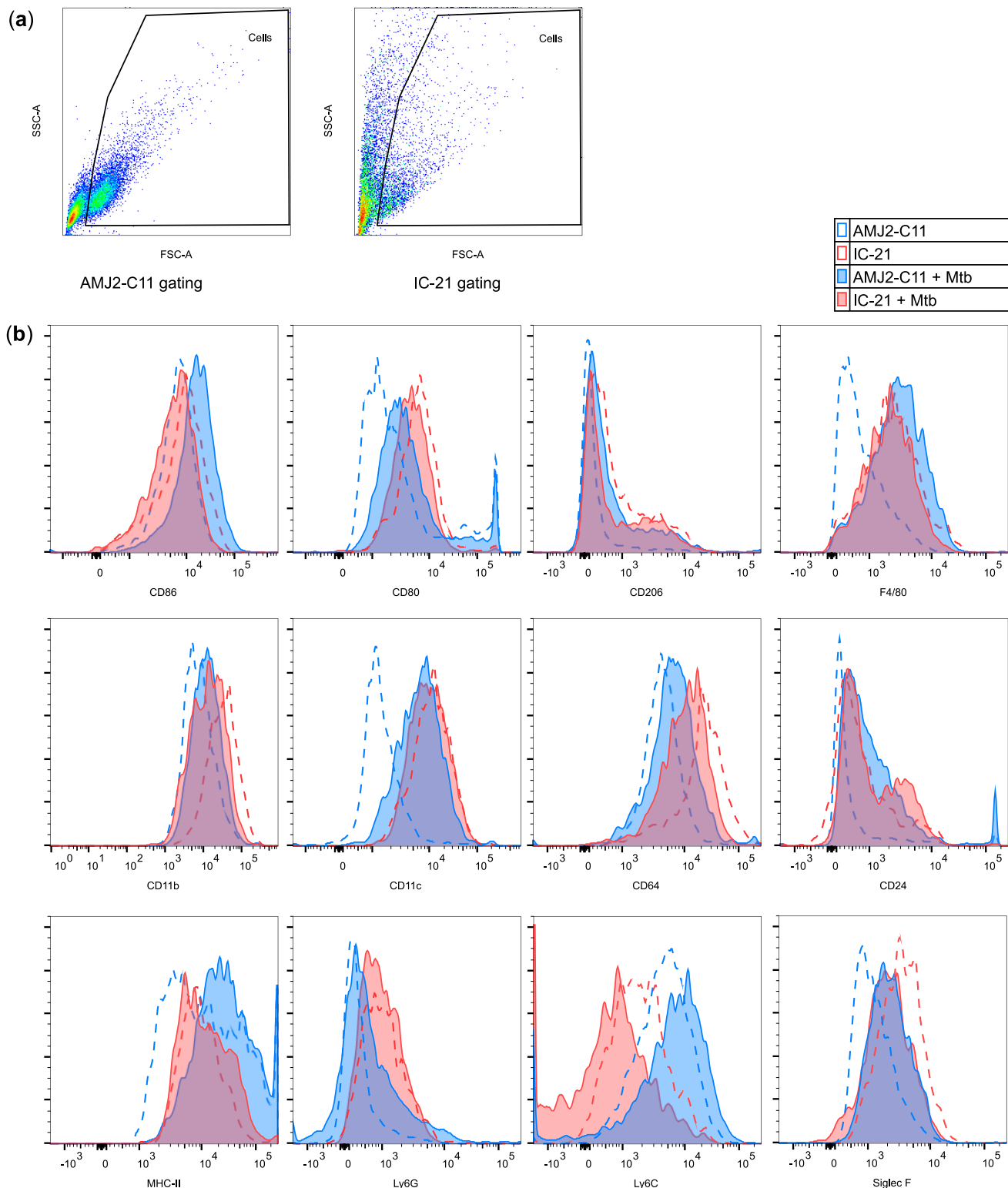
Supplementary figure 2. Example analysis of AMJ2-C11 and IC-21 cells by flow cytometry. (**a**) Forward and side scatter dot plots illustrating gating of AMJ2-C11 and IC-21 cell populations to exclude dead cells and debris, during flow cytometric analysis. IC-21 cells are adherent and were gently removed on ice and then by scrapping, which resulted in higher cell death. (**b**) Representative histograms illustrate expression of protein markers on the macrophage cell surface. Shown are AMJ2-C11 cells (blue) and IC-21 cells (red) 24 hours after infection with *M. tuberculosis*, overlayed on uninfected cells (dotted histograms).
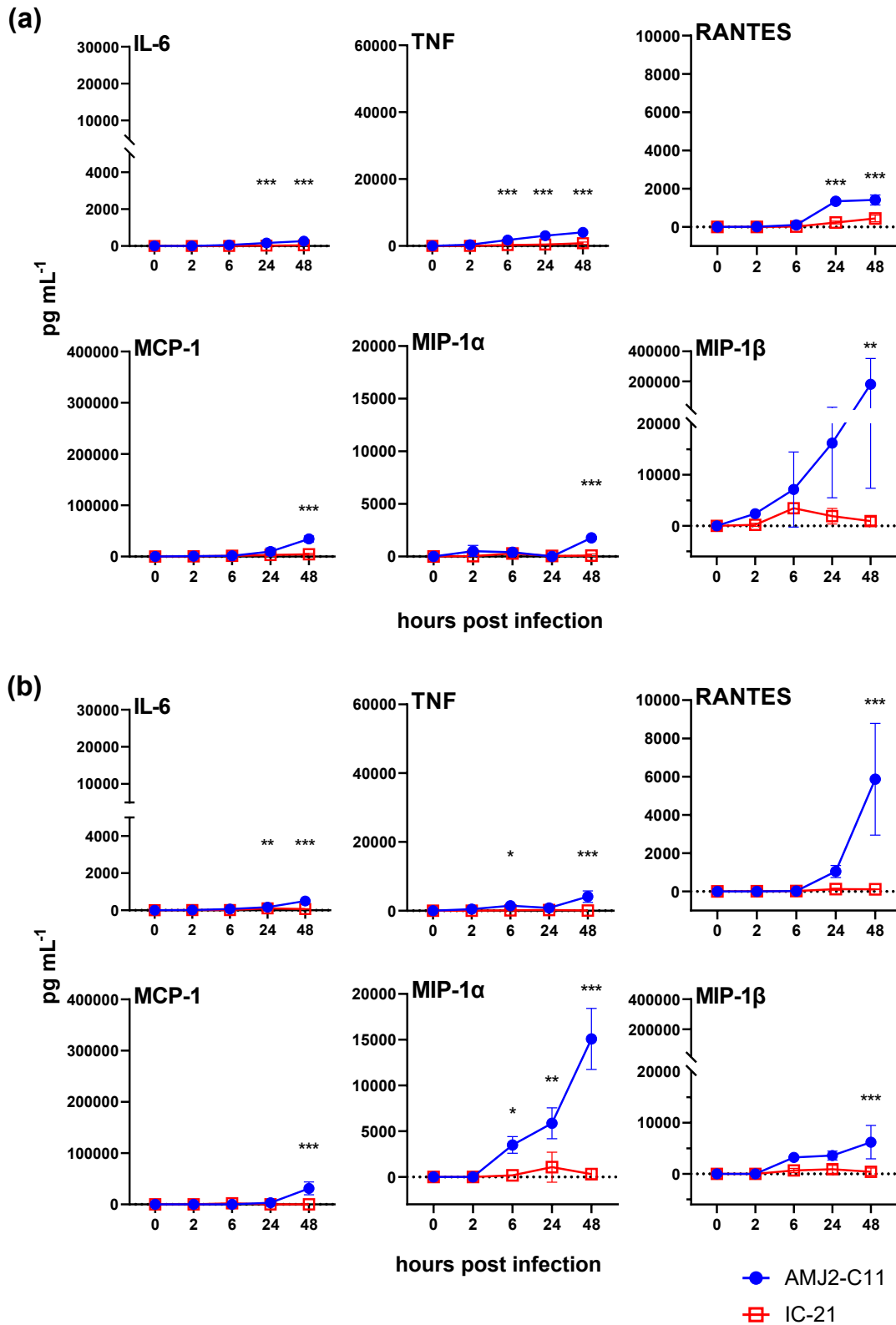
Supplementary figure 3. Supernatant cytokine concentrations from repeat (**a**) BCG and (**b**) *M. tuberculosis* infection experiment. Data are the mean ± SD of triplicate wells. Asterisks represent significant difference between AMJ2-C11 and IC-21 expression by 2-way ANOVA with multiple comparisons post-test, Šidák method corrected. * $P < 0.05$, ** $P < 0.01$, *** $P < 0.001$.
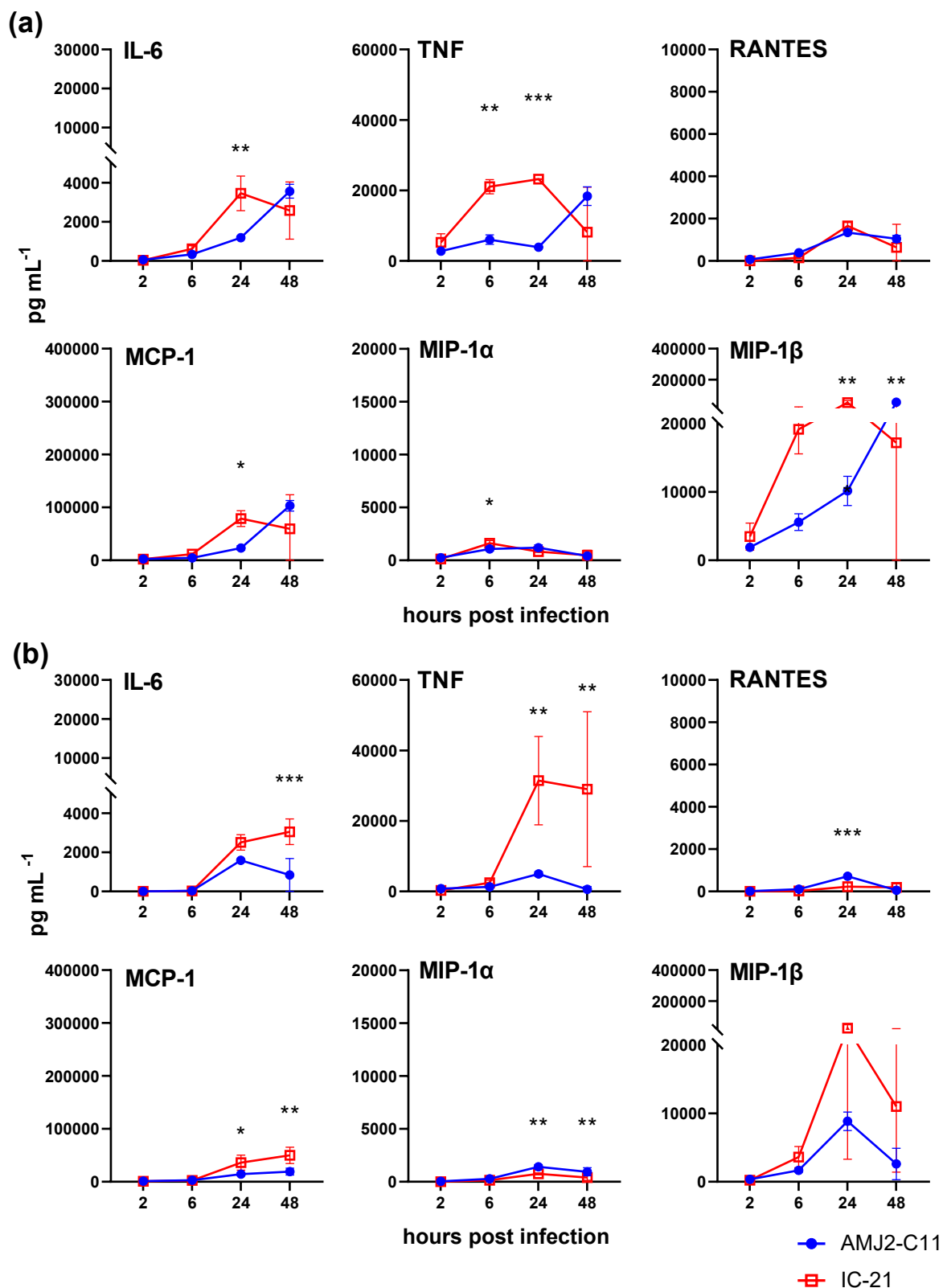
Supplementary figure 4. Supernatant cytokine concentrations from repeat (**a**) BCG and (**b**) *M. tuberculosis* infection experiment. Data are the mean ± SD of triplicate wells. Asterisks represent significant difference between AMJ2-C11 and IC-21 expression by 2-way ANOVA with multiple comparisons post-test, Šidák method corrected. * $P < 0.05$, ** $P < 0.01$, *** $P < 0.001$.

Appendix 5

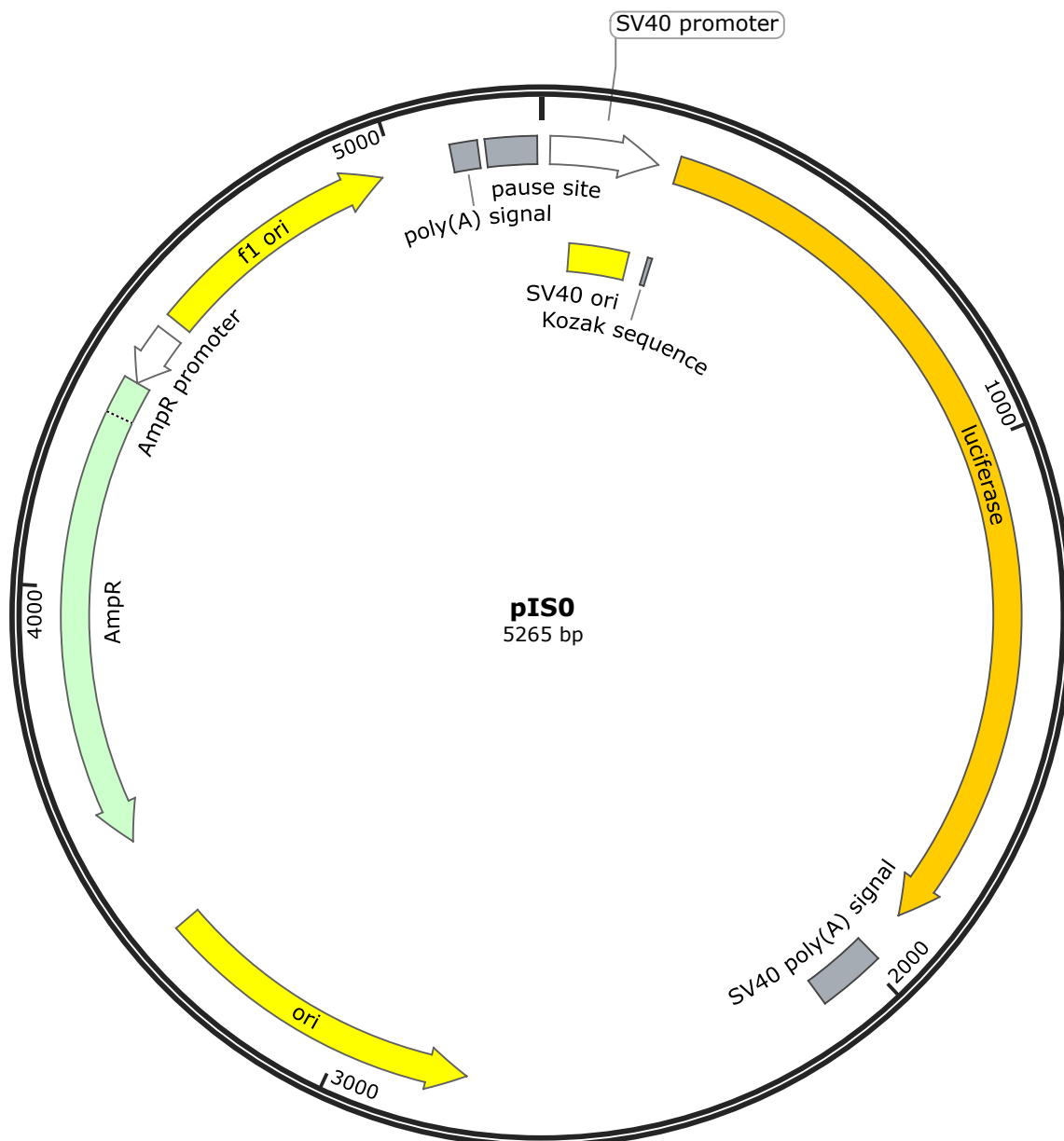pIS0 luciferase expression plasmid maps for transfection experiments

Figure A 1. pIS0 luciferase expression plasmid map. Firefly luciferase expressed under the SV40 promoter. Ampicillin resistance gene for cloning in bacteria.
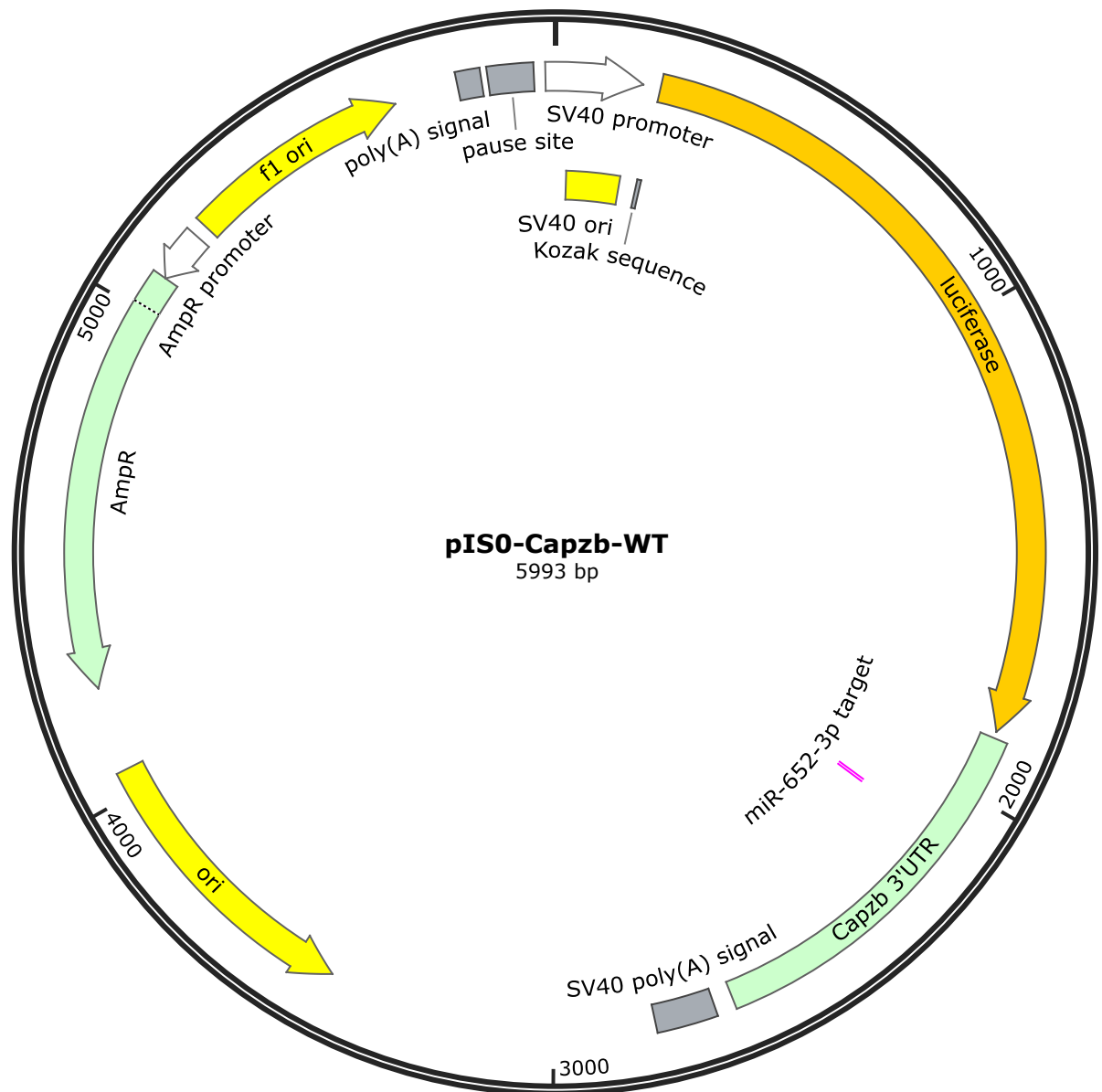
Figure A 2. pIS0-Capzb-WT luciferase reporter plasmid map. Firefly luciferase expressed under the SV40 promoter. Ampicillin resistance gene for cloning in bacteria. The wild type mouse *Capzb* 3' untranslated region was inserted at the luciferase 3' end, containing the predicted miR-652-3p target sequence.
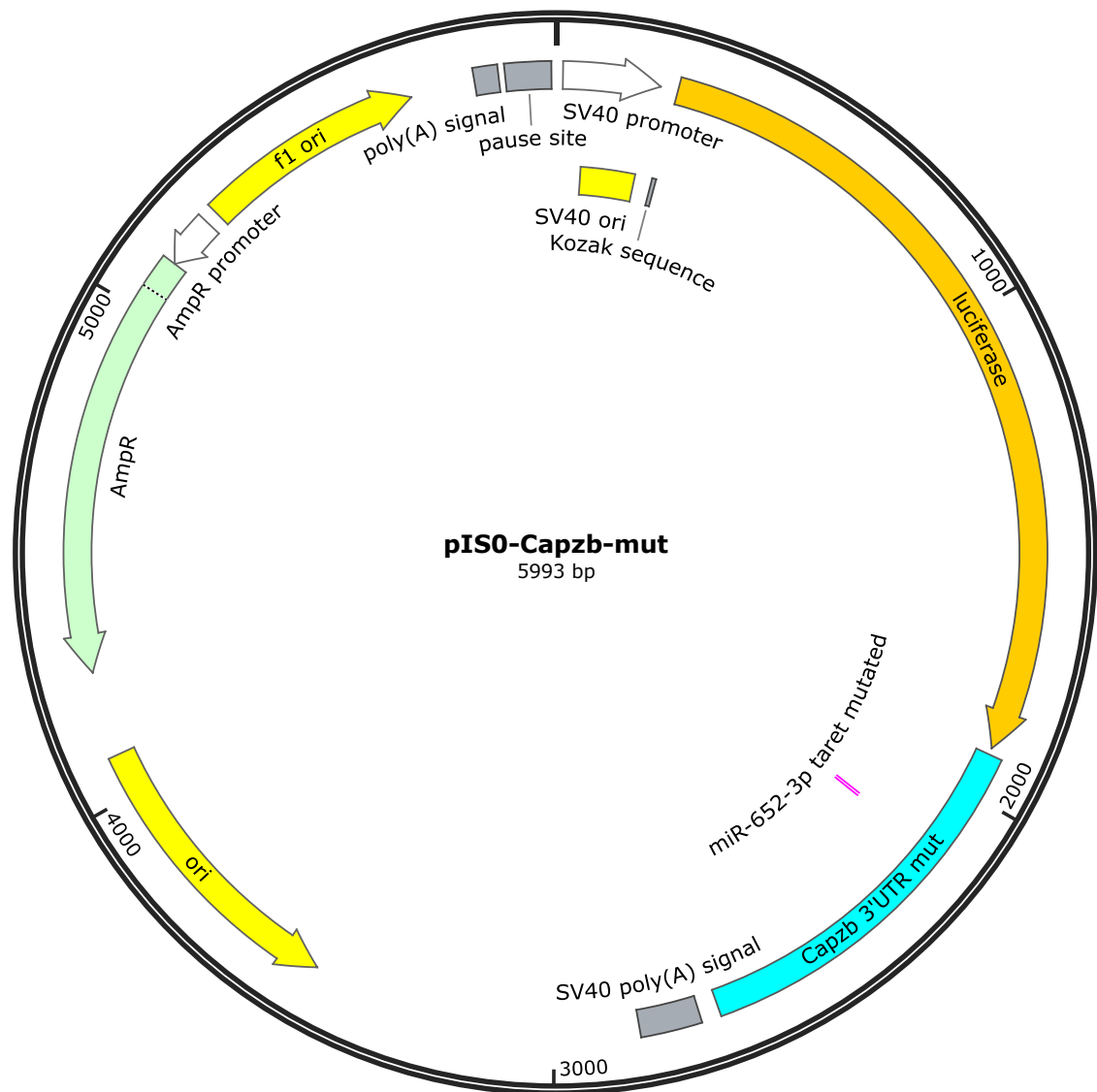
Figure A 3. pIS0-Capzb-mut luciferase reporter plasmid map. Firefly luciferase expressed under the SV40 promoter. Ampicillin resistance gene for cloning in bacteria. The mutated mouse *Capzb* 3' untranslated region was inserted at the luciferase 3' end, containing the inverted miR-652-3p target sequence.

Appendix 6

Supporting data for Chapter 4 - The impact of miR-652 during in mycobacterial infection
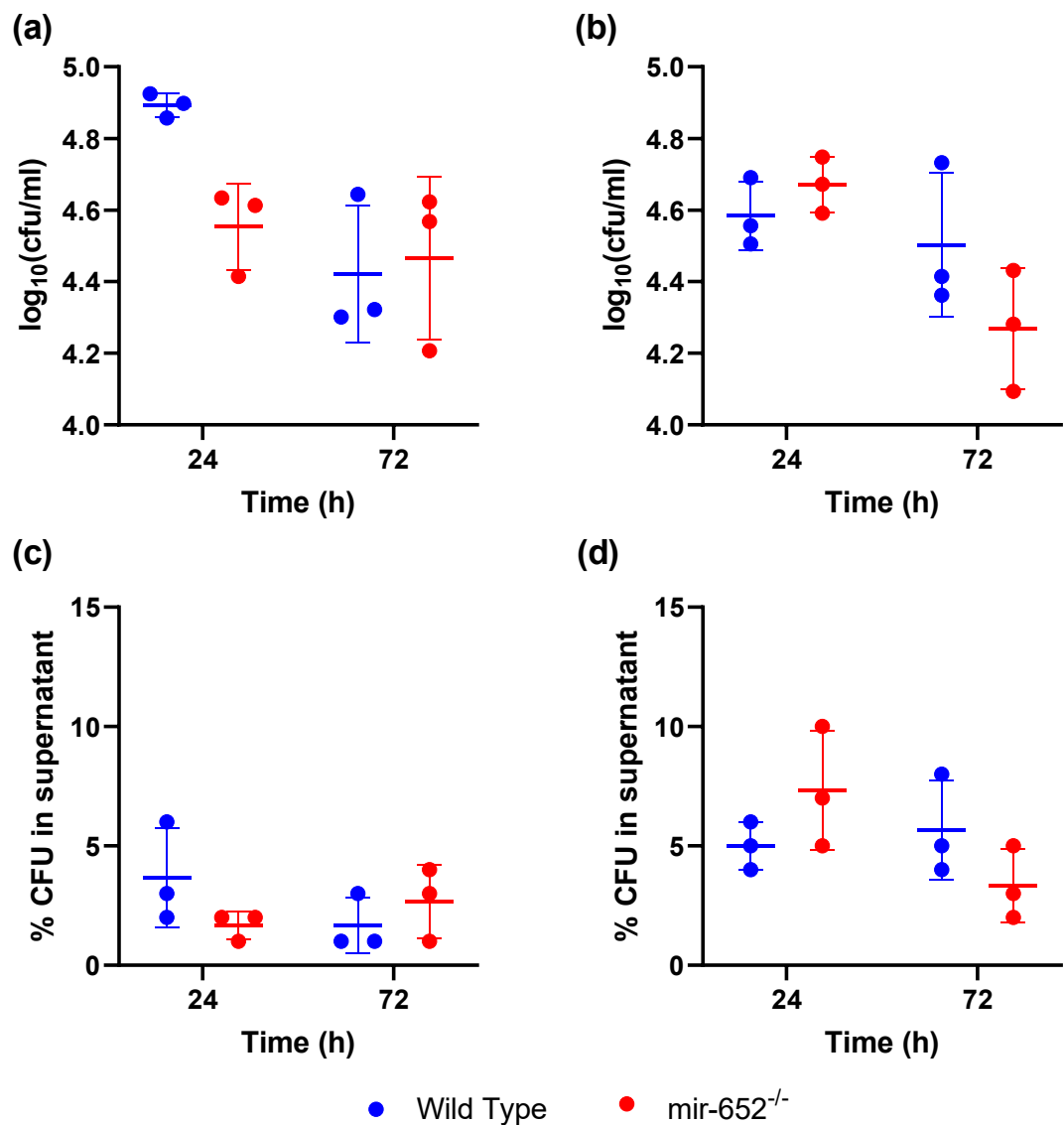
Figure A 4. A small minority of mycobacteria are removed in culture supernatant, leaving the majority internalised by macrophages, or adherent to the assay plate. Mouse BMDMs were infected as in Figure 1.3. Supernatant from mouse BMDMs infected with (a) *M. tuberculosis* or (b) *M. avium* was taken for enumeration of bacterial CFU in suspension. Supernatant bacterial load did not differ between wild type and miR-652^{-/-} cell wells. Less than 10% of (c) *M. tuberculosis* and (d) *M. avium* CFU were collected with supernatant. The percentage of bacterial CFU in supernatant was not significantly different between wild type and miR-652^{-/-} cell wells. Data are the mean ± SD of 3 biological replicates. Comparisons were made using 2-way ANOVA with multiple comparisons post-test.
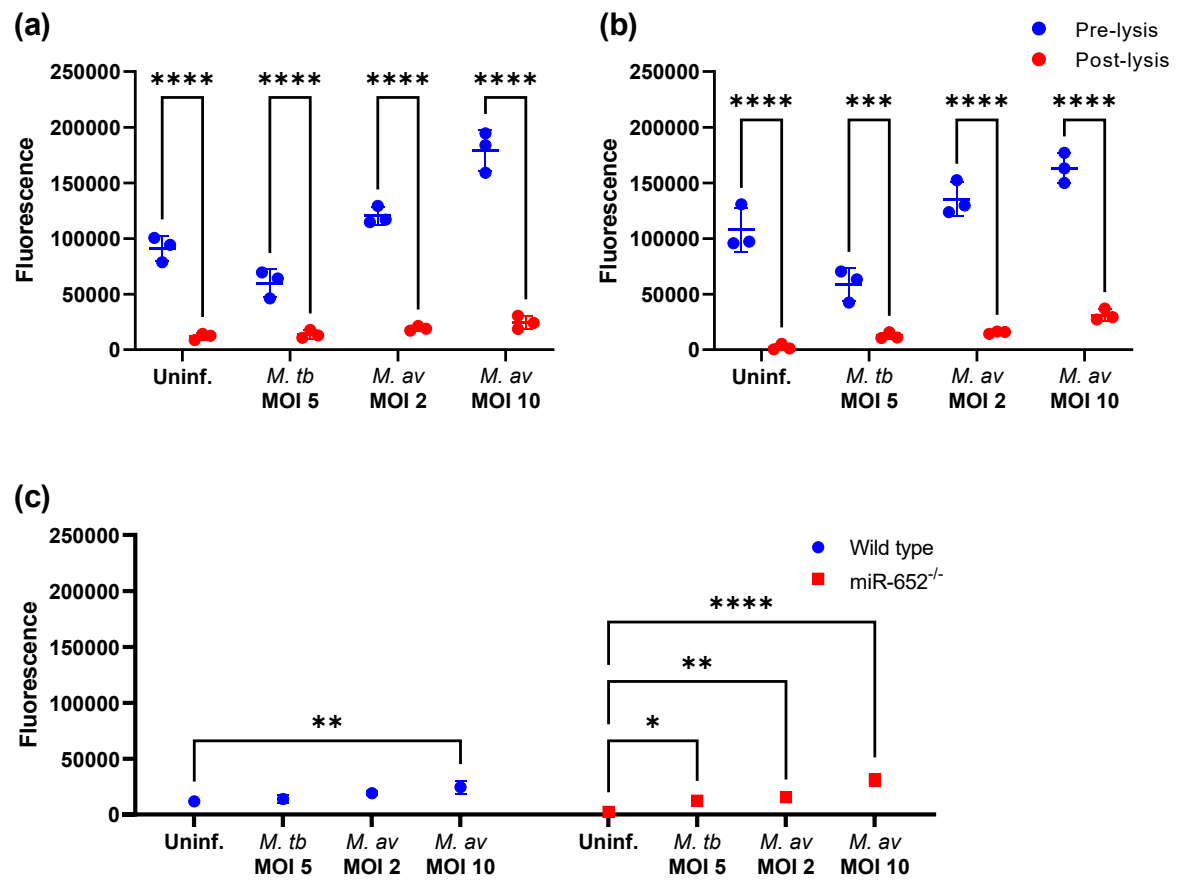
Figure A 5. Internalised mycobacteria have small effect on resazurin metabolic activity assay fluorescence readout 24 hours post-infection. The metabolic activity of mycobacteria infected (a) wild type and (b) miR-652$^{-/-}$ BMDMs was determined pre- and post-lysis with 0.1% Triton-X100. (c) The metabolic activity of the infecting mycobacteria post-lysis is only significantly different to that of lysed uninfected cells at high bacterial MOI. Data are mean ± SD of 3 biological replicates.